4

RESULTS AND DISCUSSION

4.0 INTRODUCTION

The results of the current investigation entitled "Corrosion monitoring of metal (Mild steel, Aluminium) /1M HCl interface in the presence of *Spathodea campanulata*, *Tecoma capensis* leaf and flower extracts –Chemical, Electrochemical and Theoretical studies**"** are discussed in the light of the objectives set forth under the following subdivisions

Module I : Characterisation of the selected inhibitors

Module II : Assessment of selected inhibitors as corrosion inhibitors for mild steel and aluminium – Experimental and Surface Analytical Techniques

Module III : Theoretical studies using Hyperchem 7.5

Module I : Characterisation of the selected inhibitors

4.1 Characterisation of selected plant extracts

The selected plant extracts are characterised using the following techniques

4.1.1 Phytochemical screening

4.1.2 GC-MS

4.1.3 FT-IR

4.1.4 UV

4.1.1 Phytochemical screening

Plants are packed with natural source of phytochemicals with diversified structural macromolecules that have impending chemical and biological significance. The use of screening tests has gained momentum in recent days as they provide swift means to evaluate the plant specimens for the presence of bioactive compounds that have the ability to mimic polar organic macro molecules that aid in mitigating corrosion process. **(Ncube *et al*, 2008)**

The investigated plant extracts are screened for the presence of flavonoids, alkaloids, terpenoids, saponins, tannins, reducing sugar, polyphenols, and anthraquinones using standard procedure **(Harborne, 1984)**.(Appendix-I)

***Spathodea Campanulata* leaves and flowers:**

The phytochemical characteristics of the extract of various parts of the investigated plant species are summarized in Table 4.1.The results confirm the presence of constituents

which are known to exhibit medicinal as well as physiological activities. The results indicate the presence of phytoconstituents like flavonoid, tannins, terpenoids, steroids and saponins in the leaves and moderate amount of flavonoids, terpenoids and anthroquinones in the flowers extract. Similar assertions are also made by **Ugbabe *et al*, 2010.**

Table 4.1. Preliminary phytochemical screening of the crude extracts of the investigated Plants

Phytochemical constituents	*Spathodea campanulata*		*Tecoma capensis*	
	Leaves	Flowers	Leaves	Flowers
Flavonoids	+++	+	+++	++
Alkaloids	+	-	-	-
Terpenoids	++	+	++	+
Saponins	+	++	+	++
Tannins	+	-	+	-
Reducing sugar	-	+	+	+
Polyphenols	+	+	+	+
Anthroquinones	-	+	-	+

+++, appreciable amount; ++, moderate amount; +, trace amount; -, not detected

***Tecoma capensis* leaves and flowers:**

Phytochemical screening of *Tecoma capensis* leaves and flowers extract indicate the presence of phytoconstituents like flavonoid, tannins, terpenoids, steroids and the saponins in the leaves and the occurrence of flavonoids ,terpenoids and polyphenols in the flowers extract. Phytochemical screening results are consistent with the literature survey. **(Elamaran Tamiljothi *et al*, 2011**)

4.1.2 GC-MS Analysis

4.1.2.1 GC-MS Analysis of SCL

The GC-MS spectrum of SCL is obtained from Thermofisher GC-MS-MS ITQ1100 spectrometer using electron ionization (EI) source. Ten peaks at retention time 15.52, 15.99, 16.27, 17.06, 17.28, 17.50, 17.85 and 18.44 are observed in GC.

In the MS spectrum of GC peak at 15.52, M^+ ion is noticed at m/z 429, and base peak is seen at m/z 209. The other significant m/z peaks are at 401, 355, 327, 281, 267,

225, 209, 193, 149, 135 and 73. The spectrum shows two (M-28) peaks at m/z 401 and at m/z 327 corresponding to the loss of 'CO' indicating the presence of two –CO groups.

(M-44) peak is detected at m/z 149 that is characteristic of the –COOH group. Along with (M-44), (M-46) peaks are also present at m/z 355 and at m/z 281, indicating the presence of ester function. (M-14) peaks are observed at m/z 267 and m/z at 135 reflects the presence of double bonds in the extract. The (M-18) peak at m/z 61 confirms the presence of –OH group in the extract.

4.1.2.2 GC-MS Analysis of SCF

The GC-MS spectrum of SCF showed seven peaks at retention time 15.73, 17.12, 17.83, 18.87, 19.12, 19.52 and 19.7. The GC-MS spectrum and peak fragmentation is shown in Figure 4.2 .

The mass spectrum of the fraction at retention time 15.73 reflects a series of M-14 peaks at m/e 185.21, 171.24, 157.22, 143.19, 129.17 and 115.14, 83.13 and 60.70 indicating the presence of $–CH_2$ units. Along with this, M-18 peak at 97.13 is noticed, indicating the presence of –OH group. The same M-14 and M-18 peaks are also observed in the MS spectrum of the fraction at the retention time 17.13, 19.1 and 17.83. Hence these compounds may be a straight chain compound with -OH functional group.

Two characteristic M-28 peaks at m/e 236.37 and 194.29 and M-14 peaks at m/e 180.31, 123.17, 83.15, 69.15 are noticed in the MS spectrum of the fraction at retention time 18.87 indicating the presence of–CO- groups along with $–CH_2$ units. The same is reflected in the MS spectrum of the fraction at retention time 19.77. Hence the compound may contain –CO- group with –OH- groups.

In the MS spectrum of SCF, at retention time 19.12 two M-28 peaks at m/e 213.3 and 157.2 are observed indicating the presence of –CO- group. A characteristic M-17 and M-18 peaks at m/e 281.21 and 111.15 for –OH groups are also present along with M-14 peaks at m/e 267.4, 241.3, 199.26, 185.25, 143.17, 129.15 and 97.13 showing the presence of a straight chain with OH and CO groups.

4.1.2.3 GC-MS Analysis of TCL

The GC-MS spectrum of TCL has been obtained from Jeol GC mate, Mass spectrometer using electron ionization (EI) source. Six peaks at retention time 12.23, 17.12, 17.88, 18.87, 19.55 and 27.97 are observed in the GC. The GC-MS spectrum and peak fragmentation is shown in Figure 4.13.

In the MS spectrum of GC peak at 12.23, two M-15 peaks at m/e151, and 131 are observed indicating the presence of methyl groups. Two three M-13 peaks at m/e 138.2, 111.21 and 91.13 are detected which shows the presence of –CH groups. The mass spectrum of the fraction at retention time 17.12 indicates continuous M-14 peaks at m/e 256.4, 213.35, 199.3, 185.29, 171.27, 157.25, 143.22, 129.2 and 115.16 reflecting the presence of $–CH_2$ groups. Along with this M-17 peak at 239.42 and M-18 peak at 97.17 are also observed indicating the presence of –OH group. Hence this may be a straight chain compound with -OH functional group. The same M-14 and M-18 peaks are also observed in the MS spectrum of the fraction at the retention time 17.88 and 18.87.

Two M-18 peaks at m/e 264.45 and 111.2, and four M-14 peaks at m/e 185.2, 97.18, 83.17, 69.17 are exhibited in the MS spectrum of the fraction at retention time 19.55 indicating the presence of –OH along with $–CH_2$ units. A characteristic M-28 peak at m/e 161.2 is noticed in the MS spectrum of the fraction at retention time 27.97 indicating the presence of –CO- group.

4.1.2.4 GC-MS Analysis of TCF

The GC-MS spectrum of TCF shows eight peaks at retention time 14.05, 15.73, 17.83, 18.9, 19.12, 19.52, 19.75 and 23.27. The GC-MS spectrum and peak fragmentation is shown in Figure 4.4

In the MS spectrum of GC peak at 14.05 characteristic M-18 and M-28 peaks are observed at m/e 140.1 and 112 showing the presence of –OH and –CO- group. In the mass spectrum of the fraction at retention time 15.73, a series of M-14 peaks at m/e 185.24, 171.22, 157.19, 143.17, 129.1, 115.12 and 101.1 are noticed indicating the presence of $–CH_2$ groups. Along with this, M-17 peak at 211.3 is observed indicating the presence of –OH group. M-14 and M-18 peaks are also identified in the MS spectrum of the fraction at the retention time 17.83 and 19.12. Hence these compounds may be a straight chain compound with -OH functional group

Two characteristic M-28 peaks at m/e 151.2 and 111.1, and an M-18 peak at m/e 264.41 are noted in the MS spectrum of the fraction at retention time 19.52, indicating the presence of –OH and –CO- groups. The same is displayed in the MS spectrum of the fraction at retention time 23.27. Hence the compound may contain –CO- group with –OH- groups.

4.1.3 FT-IR Analysis

Table – 4.2 FT-IR spectral data of crude SC/ TC extracts

Observed IR Frequency , (cm^{-1})				Assignment	Reference
SCL	SCF	TCL	TCF		
3950 3834 3395	3950 3842 3750 3395	3418 3387	3387	O–H stretch, H–bonded N-H stretch	**Odiongenyi *et al*, 2009**
2924	2924	2924	2924	C–H stretch	**Li *et al*,2012**
	2855	2855	2855	C=O stretch	**Bahrami *et al*, 2010**
2376	2376	2384		–C ≡ N stretch	**Taleb Ibrahim *et al*,2011**
1628	1628	1628	1628	C=O stretch	**Li *et al*,2012**
1520		1543		C-C in ring	**Taleb Ibrahim *et al*,2011**
1443	1427	1443	1443	C–O stretch	**Abboud *et al*, 2009**
1381 1319	1381 1327	1381 1327	1373	C–O-C stretch	**Li *et al*, 2009**
1265	1265	1250	1258	C-O stretch	**Eddy *et al*, 2009**
1072	1065 1026	1065	1072	C-O stretch	**Eddy *et al*, 2009**
779		883	818	O–H bend	**Abboud *et al*, 2009**
	772	772	772	O–H bend	**Eddy *et al*, 2009**
633 602	625	640	625	C-H “bend”	**Eddy *et al*, 2009**

4.1.3.1 FT-IR spectroscopic study of SCL

A transmission spectrum of SCL is depicted in Figure 4.1 and the observed frequencies are tabulated in Table 4.2. A strong band at 3395 cm^{-1} is attributed to N-H /OH stretching. An absorption band related to – CH_2 stretching is noticed at 2924 cm^{-1}.A strong band at 1628 cm^{-1} corresponds to C=O stretching. Peaks observed at 1520, 1072 indicate C=C stretching and C-O aromatic system. A peak at 633 cm^{-1} denotes C=C bending vibration of the aromatic ring system. Thus the FT IR spectrum implies the presence of O and N atom containing functional groups, that act as a prerequisite for a molecule to function as a corrosion inhibitor

4.1.3.2 FT-IR spectroscopic study of SCF

IR spectrum of SCF powder is represented in Figure 4.2 and the interpreted frequencies are listed in Table 4.2. A strong and broad band observed at 3395 cm^{-1} can be ascribed to N-H or O-H stretching frequencies. A small band at 2924 cm^{-1} is noticed due to C-H stretching vibration. A strong absorption peak at 1628 cm^{-1} can be attributed to C=C

and C=N stretching or N-H bending vibration. Peak at 1427 cm^{-1} corresponds to C-O stretching. Strong band obtained at 1381 cm^{-1} is related with CH_3 or C-H in plane bending vibration. There are 3 peaks found in the range of 1000 cm^{-1} to 1300 cm^{-1} which correspond to C-N or C-O stretching. The absorption peaks obtained below 1000 cm^{-1} are due to aliphatic and aromatic C-H functional groups. It can be concluded on the basis of FT-IR spectrum that SCF extract contains functional groups having C-N, C-O, O-H, N-H, C=N linkages as well as aromatic rings. **(Ji *et al*, 2013)**

4.1.3.3 FT-IR spectroscopic study of TCL

FT-IR spectrum of TCL is shown in Figure 4.3 and the spectral frequencies are listed in Table 4.2. A peak at 2924 cm^{-1} may be due to stretching mode of aliphatic and aromatic C–H groups, respectively. The peak at 1628 cm^{-1} correspond to the stretching modes of carbonyl groups in ester (R–CO–O–R) or aldehyde (R–CO–H) and ketones (R–CO–R) or organic acids (RCOOH). A peak for C–O stretching mode is noted at 1443 cm^{-1}. The peaks at 1381 and 1327 cm^{-1} imply the presence of C–O–C stretch and a peak pertaining to C-O stretch is noticed at 1250 cm^{-1}. A band at 1065 cm^{-1} is due to the stretching mode of C–O. This indicates that TCL extract contains mixture of compounds i.e. terpenoids, flavonoids etc., in it that are capable of mimicking synthetic organic compounds **(Satapathy *et al*, 2009)**

4.1.3.4 FT-IR spectroscopic study of TCF

Figure 4.4 depicts the FT-IR spectrum of the TCF powder and the corresponding data are listed in Table 4.2. A strong broad band at 3387 cm^{-1} may be attributed to O-H stretching. An absorption band at 2924 cm^{-1} is related to C-H stretching vibration , and a band at 1628 cm^{-1} corresponds to the C=O stretching vibration . The band at 1443 cm^{-1} is assigned to C-O stretching vibration. A peak at 1258 cm^{-1} is attributed to C-O stretching. A band at 1072 cm^{-1} indicates the stretching vibration of C–O. Hence, it can be inferred that TCF extract contains oxygen and nitrogen atoms in functional groups (O–H, N–H, C=O, C–N, C–O, C=C) and aromatic ring, which meets the general structural consideration of the corrosion inhibitors. **(Li *et al*, 2012)**

The assertions of FT-IR spectral data are well supported by Phytochemical screening analysis and GC-MS studies.

Figure 4.1 : Characterisation of SCL extract

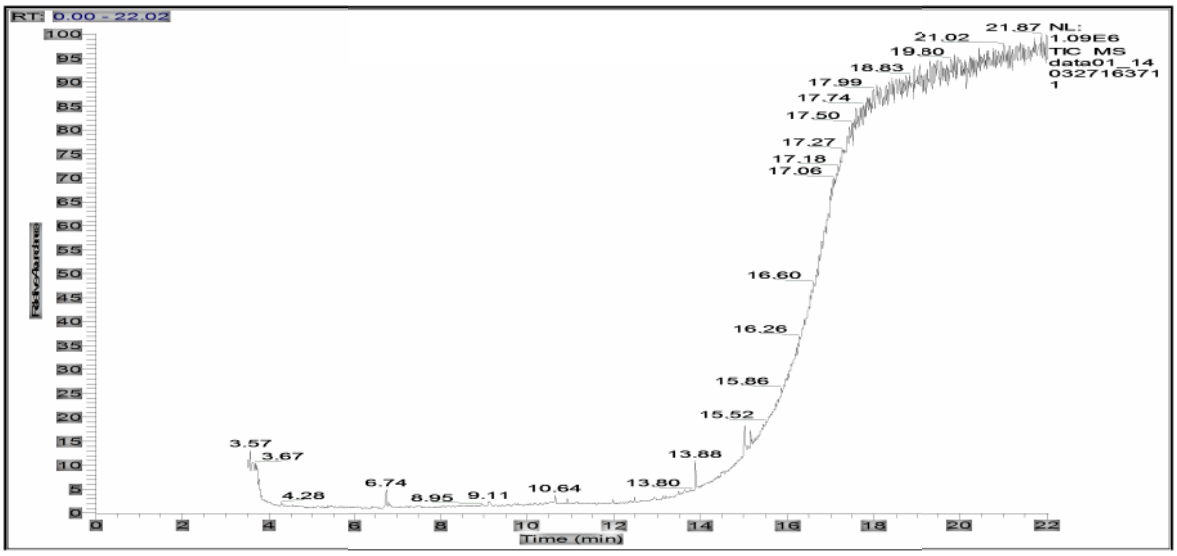

GC-MS

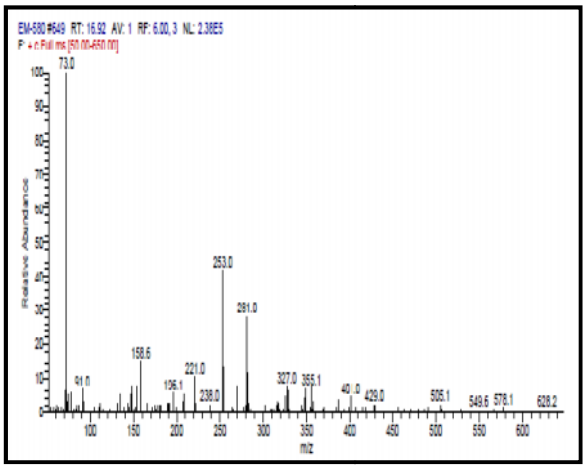

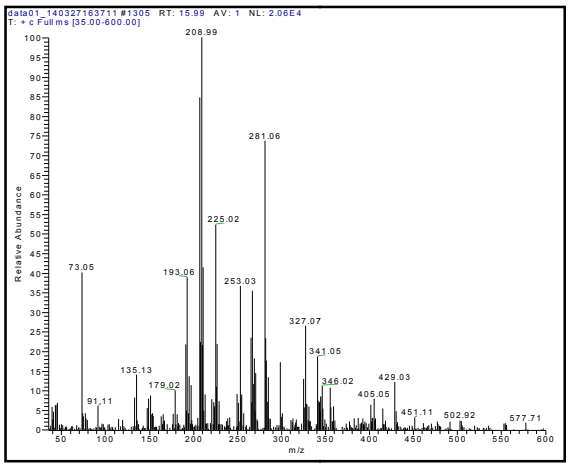

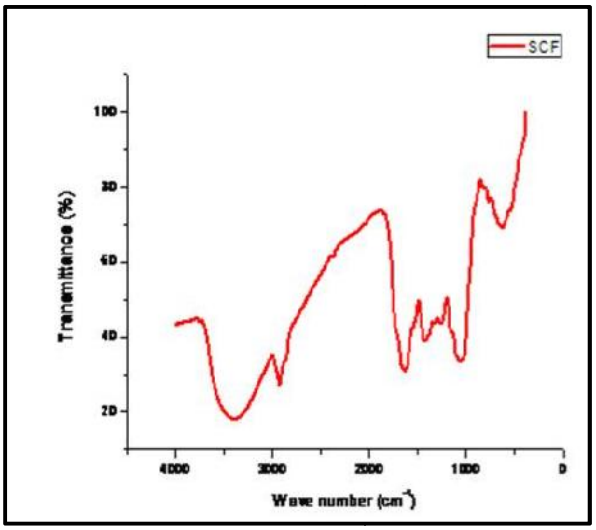

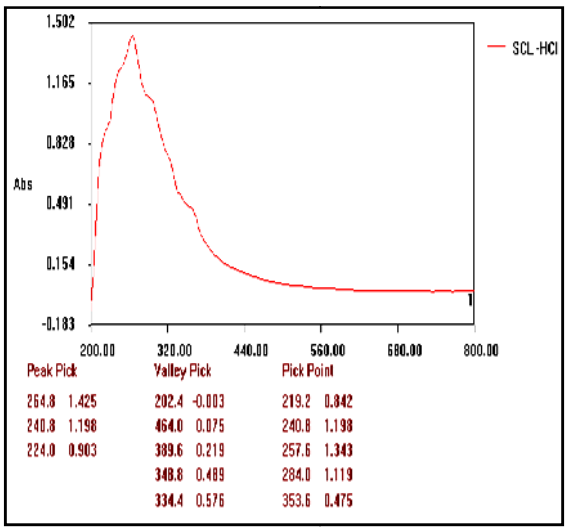

FT-IR

UV

Figure 4.2 : Characterisation of SCF extract

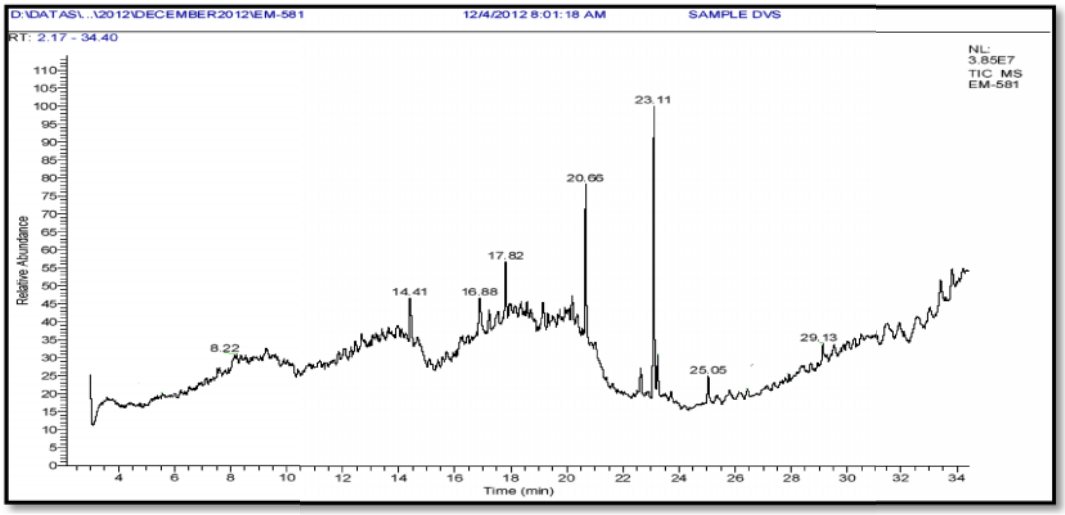

GC-MS

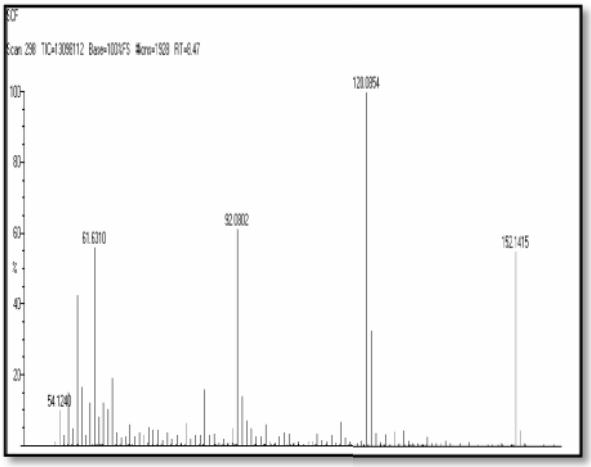

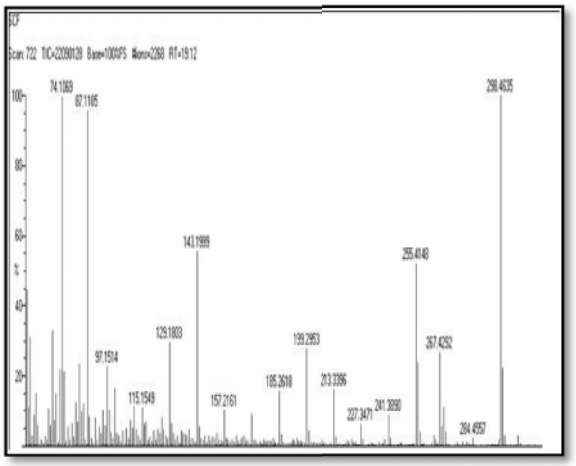

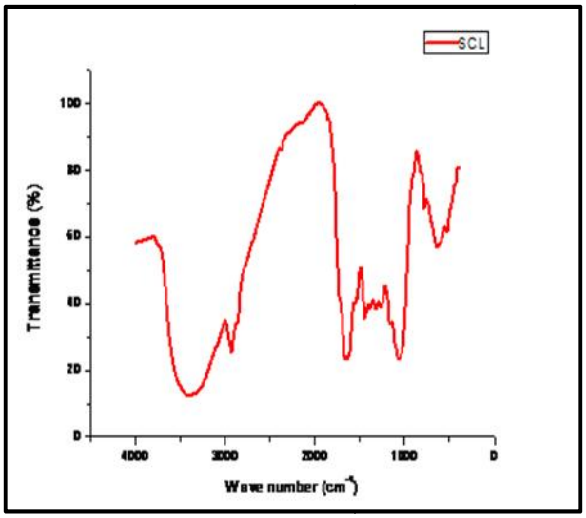

FT-IR

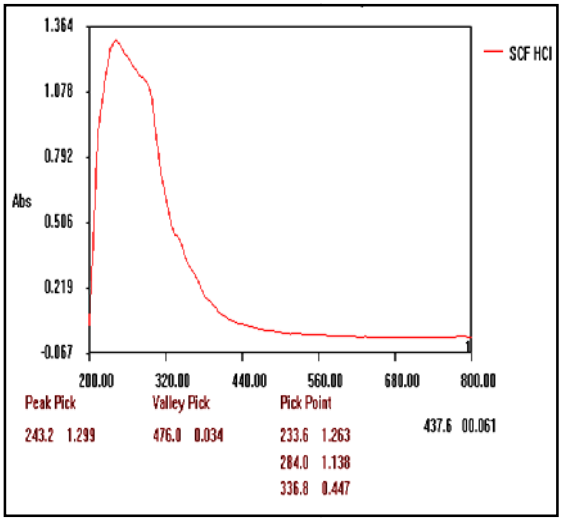

UV

Figure 4.3 : Characterisation of TCL extract

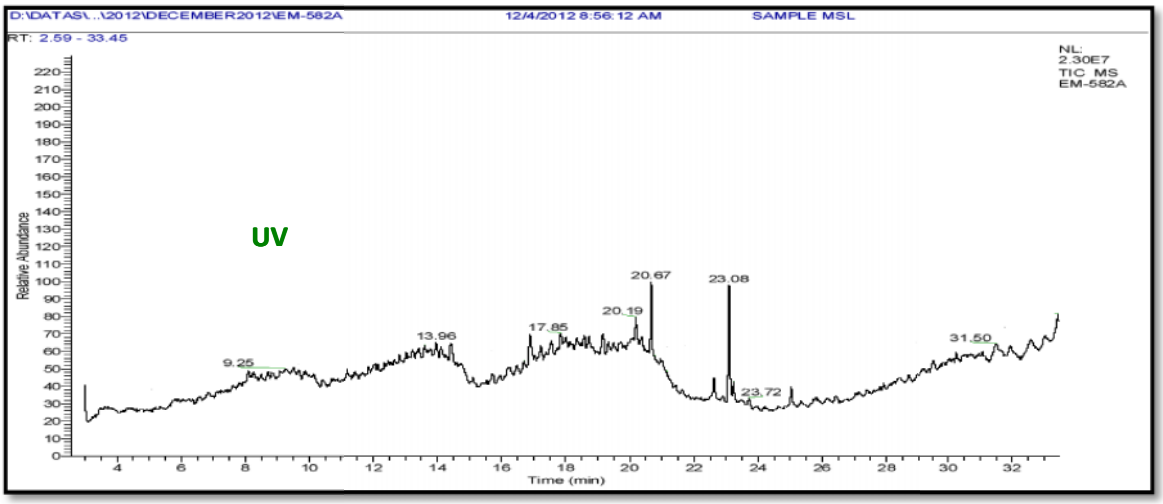

UV

GC-MS

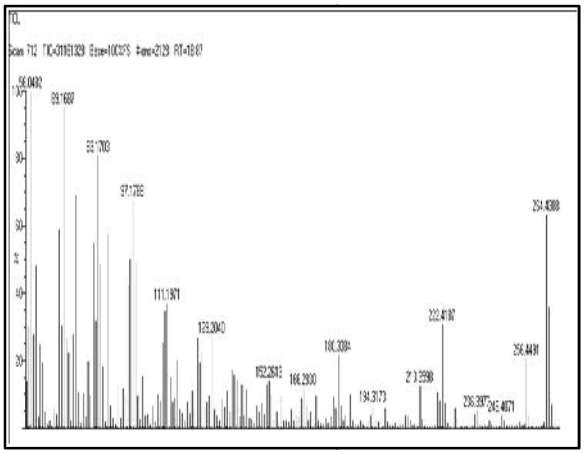

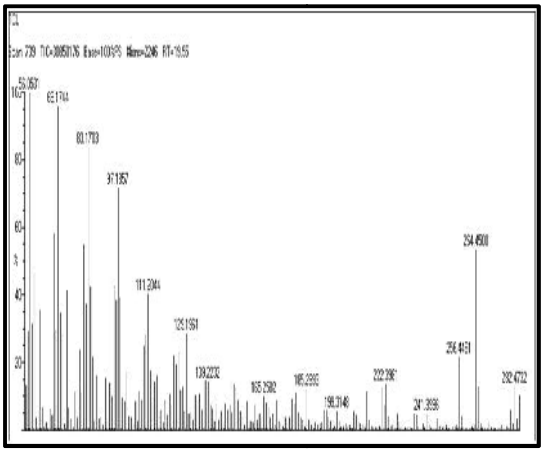

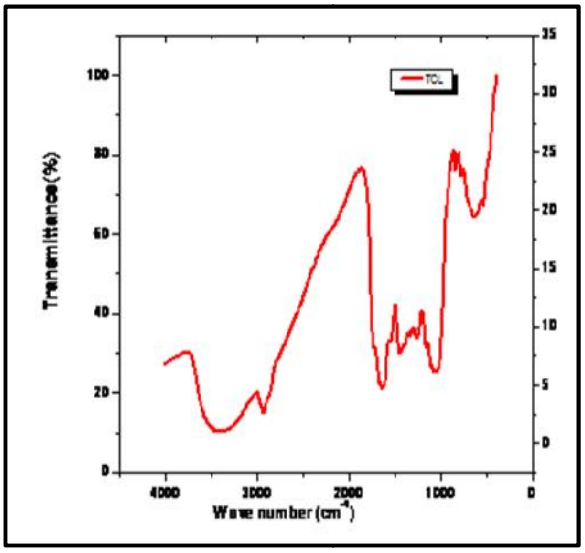

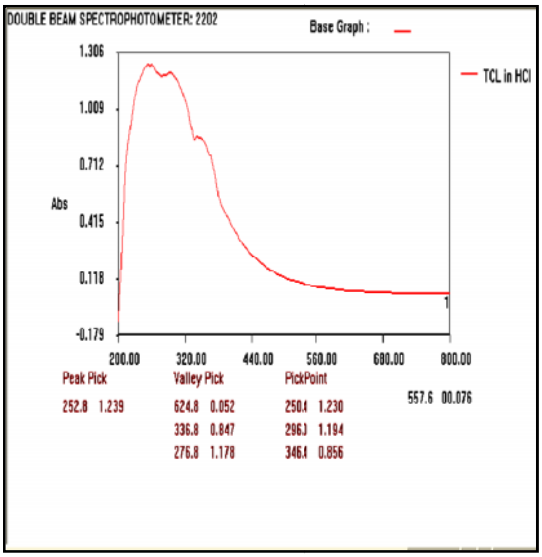

FT-IR

UV

Figure 4.4 : Characterisation of TCF extract

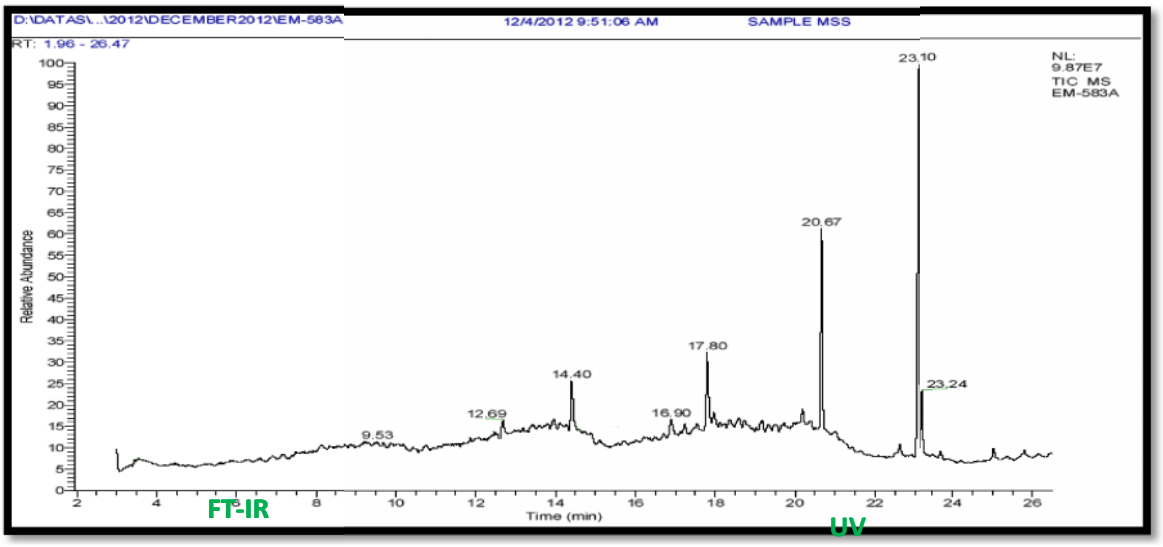

FT-IR

UV

GC-MS

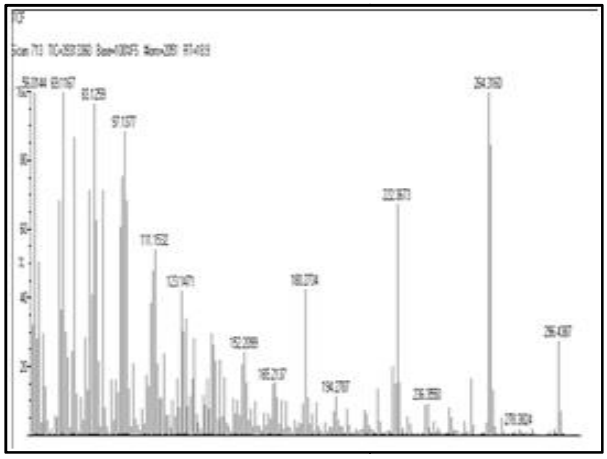

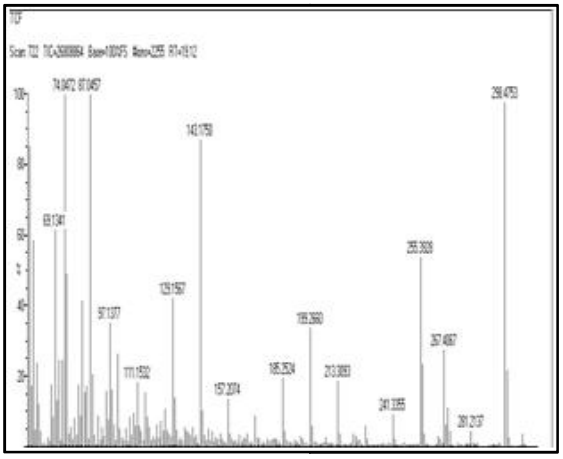

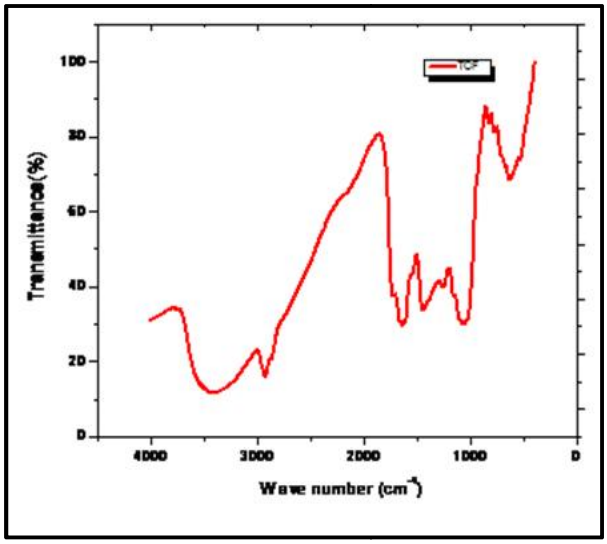

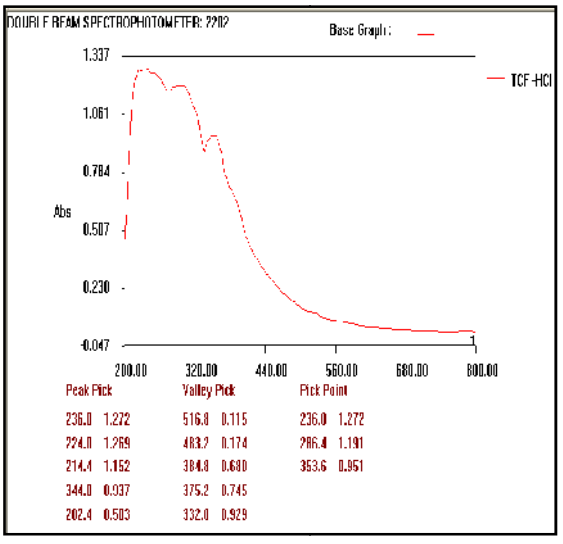

FT-IR

UV

4.1.4 UV analysis

4.1.4.1 UV spectrophotometric study of SCL

The UV-VIS profile of plant extract is taken at the 200 to 800 nm wavelength due to the sharpness of the peaks and proper baseline. The profile shows the peaks at 224 nm, 241 nm, 265 nm, 284 nm, 334 and 354 nm (Figure 4.1, and Table 4.3).This might be due to the presence of flavonoid type of compounds amongst other phytochemicals like terpenoids and iridoids.

4.1.4.2 UV spectrophotometric study of SCF

UV spectrum of SCF displays a prominent absorbance at 200-240 nm, while good absorbance at a range of 240-325 nm. The moderate absorbance is noted at the range of 310-340 nm (Figure 4.2). Qualitative investigation indicates the presence of flavonoids in the extract. The results show strong-to-moderate absorption of UV radiation along the whole range and this ability may be due to the presence of flavonoids**.(Patil *et al*, 2011)**

4.1.4.3 UV spectrophotometric study of TCL

Figure 4.3 depicts the UV spectrum of TCL .The UV spectrum of TCF exhibits a prominent peak at 253 nm and a shoulder peak at 346 nm. Generally UV of flavonoids are found to exhibit two characteristic absorption peaks at 300-400 nm (band I) and 240-280 nm (band II) **(Li *et al*, 2012)**. The spectral data in Table 4.3 indicates the presence of flavonoids and other compounds containing N or O atoms.

4.1.4.4 UV spectrophotometric study of TCF

Figure. 4.4 shows the UV absorption spectrum of crude extract of TCF and values of absorption bands are presented in Table 4.3. Figure 4.4 reveals major peaks at 236 nm and 286 nm. The bands at 224 nm and 236 nm could be connected with the transitions π-π* transition respectively. The presence of chromophores, amino group and carboxyl groups in the plant extract, makes it transparent in the UV-Visible region. Hence the plant might consist of flavonoid like structures.

Table: 4.3 UV spectral data of crude SCL / SCF / TCL / TCF extracts

Inhibitor	Absorption bands (nm)	Transitions
SCL	224,241, 265, 284,334,354	$n \rightarrow \pi^*$ $\pi \rightarrow \pi^*$ $n \rightarrow \sigma^*$
SCF	243, 284, 334, 337	
TCL	250,253,296 , 346	
TCF	236, 224, 286, 344,354	

IR and mass spectral results well support the UV visible spectral results.Characterisation of the investigated plant extracts by GC-MS, FT-IR and UV spectral studies confirm the presence of flavonoid, terpenoid, based compounds in the plant extracts.

Module II: Assessment of selected inhibitors as corrosion inhibitors for MS and AA1100 – Experimental and Surface Analytical Techniques

- **Electrochemical Measurements**
- **Mass loss Measurements**
  - **Adsorption isotherms**
  - **Activation Parameters for inhibition process**
  - **Thermodynamic adsorption parameters**
- **Surface Analytical Techniques**

4.2 ELECTROCHEMICAL MEASUREMENTS

4.2.1 POTENTIODYNAMIC POLARISATION STUDIES OF MS/AA1100/1MHCl

Polarisation measurements are very important for measurement of variety of electrochemical phenomena.The potentiodynamic polarisation studies for investigated metal specimens (MS and AA1100) are carried out in an attempt to envisage the electrochemical response of the metal electrodes in the presence of SC / TC green inhibitors in 1M HCl medium. The derived parameters are tabulated from the recorded curves obtained for all the investigated inhibitors and discussed.

- **Mild Steel as Working Electrode:**

4.2.1.1 Potentiodynamic polarisation studies of Mild steel (MS) in the presence of SCL in 1M HCl

The potentiodynamic polarisation curves reflect a slight change in the anodic (b_a) and cathodic (b_c) curves ie, 89±10 mV and 141±15 mv for anodic and cathodic Tafel slopes in the presence of various concentrations of SCL (Figure 4.5 and Table 4.4). This supports the view that the inhibitor is able to suppress both the anodic dissolution and cathodic hydrogen evolution. The results indicate a considerable reduction in the I_{corr} values in the presence of the inhibitor. Inspection of the data shows that I_{corr} values decrease from 0.0075 A/cm^2 to 0.0006 A/cm^2. This confirms the inhibitive nature of the extract and also the adsorption of the plant extract on the metal surface. **(Doner and Kardas, 2011)**The values of inhibition efficiency (IE) are found to be increasing with increase in concentration of inhibitor. A maximum of 92.0 percentage of inhibition is obtained with 0.7%

concentration. Addition of extract can be seen to shift E_{corr} toward more positive values, as well as reduce the current densities of the cathodic as well as anodic reactions, which correspond to a mixed-type mechanism.**(Bockris and Yang ,2012)**

The data in Table 4.4 clearly indicate that, R_p values increase with increasing concentration of SCL .The R_p values are found to vary from 4.2 Ohm/cm^2 for that of the uninhibited solution to 28.4 Ohm/cm^2 for the optimum concentration of the inhibitor (0.7% SCL) affording an efficiency of 85.2 percentage .This is indicative of the adsorption of the active constituents of SCL onto the metal surface which creates a physical barrier for mass and charge transfer thereby providing a high degree of protection for the metal surface. **(Gerengi and Sahin, 2011)**

4.2.1.2 Potentiodynamic polarisation measurements of MS in the presence of SCF in 1M HCl

The parameters derived from polarisation curves of MS (Figure 4.5) are tabulated in Table 4.4 .The introduction of SCF into the corrodent solution gives rise to parallel Tafel lines indicating that the inhibitor molecules retard the corrosion process without altering the corrosion mechanism.**(Rastogi, 2003)**.

Table 4.4: Potentiodynamic polarisation parameters for the corrosion of MS in the absence and presence of different concentrations of SCL / SCF in 1M HCl

S.No.	Conc. (%)	Tafel polarisation parameters					Linear polarisation resistance parameters	
		E_{corr} mV/ SCE	I_{corr} A/cm^2	b_a mV/ decade	b_c mV/ decade	IE (%)	R_p Ohm/cm^2	IE (%)
SCL								
1.	Blank	-496	0.0075	89	141	-	4.2	-
2.	0.1	-483	0.0040	97	112	46.7	4.8	12.5
3.	0.2	-487	0.0028	92	129	62.7	9.9	57.6
4.	0.3	-479	0.0010	99	129	86.7	22.4	75.9
5.	0.4	-480	0.001	89	131	86.7	22.6	81.3
6.	0.5	-485	0.0009	95	128	88.0	24.0	82.5
7.	0.6	-485	0.0007	85	130	90.7	28.0	85.0
8.	0.7	-498	0.0006	88	135	92.0	28.4	85.2
SCF								
1.	Blank	-496	0.0075	89	141	-	4.2	-
2.	0.1	-478	0.0040	87	117	46.7	8.5	50.6
3.	0.2	-487	0.0032	81	123	57.3	8.7	51.7
4.	0.3	-475	0.0025	96	143	66.7	10.0	58.0
5.	0.4	-476	0.0027	93	143	64.0	11.4	63.2
6.	0.5	-478	0.0024	94	149	68.0	12.9	67.4
7.	0.6	-475	0.0020	92	143	73.3	13.5	68.9
8.	0.7	-474	0.0016	82	154	78.7	14.4	70.8

The results infer the inhibitor molecules are capable of displacing the Tafel slopes in the range of 89±7 mV and 141±12 mV for anodic (b_a) and cathodic (b_c) Tafel slopes respectively suggesting the mixed nature of the inhibitor. The results also indicate the influence of inhibitor molecules on I_{corr} values.

With an increase in inhibitor concentration, the I_{corr} values decrease from 0075 A/cm^2 (blank) to 0.0016 A/cm^2 (0.6% SCF) resulting in a proportional increase of IE values. This behaviour indicates the protective nature of the extract.

A maximum of 78.7 percentage of inhibition is obtained with 0.7% concentration. No significant change in E_{corr} values are observed in the presence of SCF. Generally an inhibitor can be classified as a cathodic /anodic inhibitor if the shift is more than 85 mV with respect to that of blank. In the present case, the E_{corr} values record a minor shift of the magnitude of 22 mV from the blank value, demonstrating the mixed nature of the inhibitor**. (Satapathy *et al*, 2009)**

Linear Polarisation resistance values (R_p) show an increase in value from 4.2 ohm/cm^2 for that of blank to 14.4 ohm/cm^2 for the addition of the highest concentration of SCF. Increase in R_p with concentration infers that the active constituents of SCF inhibit corrosion of MS by adsorption process. Maximum increase in R_p values is noticed at 0.7% SCF with an efficiency of 70.8 percentage.

4.2.1.3 Potentiodynamic polarisation studies of TCL / MS / 1M HCl

Polarisation curves of MS in 1M HCl in the presence and absence of various concentration of TCL are given in Figure 4.5.Electrochemical parameters namely I_{corr}, E_{corr}, b_a and b_c at 303K for 1M HCl attained from polarisation curves are summarised in Table -4.5. The values of anodic (b_a) and cathodic (b_c) Tafel constants are calculated from the linear regions of the polarisation curves and the corrosion current (I_{corr}) densities are determined from the intersection of the extrapolated Tafel lines.

The data from the polarisation curves illustrate a deviation in the anodic (b_a) and cathodic (b_c) corrosion current density values in the range of 90± 24 mV and 152 ± 25 mv for anodic (b_a) and cathodic(b_c) Tafel slopes respectively . This supports the view that the inhibitor is able to suppress both the anodic dissolution and cathodic hydrogen evolution. The corrosion current (I_{corr}) decreases markedly in the presence of the inhibitor and the magnitude of such an effect increases with increasing concentration of the inhibitor. This decrease may be due to the adsorption of the inhibitor onto the metal surface. **(Hussin *et al*, 2011)**. I_{corr} values are found to reduce from 0.0035 A/cm^2 (blank) to 0.0006 A/cm^2 (0.7% TCL) to arrive at a maximum efficiency of 82.9 percentage at 0.7% concentration of

TCL. No marked changes in the E_{corr} values are noted. The results of tafel slopes and E_{corr} values demonstrate the mixed nature of the inhibitor under study.

Table 4.5: Potentiodynamic polarisation parameters for the corrosion of MS in the absence and presence of different concentrations of TCL / TCF in 1M HCl

S.No.	Conc. of inhibitor in (%)	Tafel polarisation parameters					Linear polarisation resistance parameters	
		E_{corr} mV/ SCE	I_{corr} A/cm^2	b_a mV/ decade	b_c mV/ decade	IE (%)	R_p Ohm/cm^2	IE (%)
TCL								
1.	Blank	-475	0.0035	90	152	-	85.5	-
2.	0.1	-473	0.0021	101	142	40.0	152.4	43.9
3.	0.2	-473	0.0018	114	130	48.6	178.9	52.2
4.	0.3	-462	0.0014	92	139	60.0	204.1	58.1
5.	0.4	-442	0.0013	98	143	62.9	224.4	61.9
6.	0.5	-435	0.0009	82	138	74.3	238.2	64.1
7.	0.6	-456	0.0008	93	114	77.1	267.1	68.0
8.	0.7	-458	0.0006	76	149	82.9	348.6	75.5
TCF								
1.	Blank	-475	0.0035	90	152	-	85.5	-
2.	0.1	-433	0.0030	98	108	14.3	102	16.2
3.	0.2	-514	0.0015	95	129	57.1	159	46.2
4.	0.3	-522	0.0013	99	134	62.9	168	49.1
5.	0.4	-499	0.0013	88	138	62.9	198	56.8
6.	0.5	-458	0.0013	94	127	62.9	278	69.2
7.	0.6	-470	0.0011	85	129	68.6	321	73.4
8.	0.7	-423	0.0010	84	128	71.4	386	77.9

Linear polarisation resistance (R_p) of MS in the absence and presence of TCL are listed in Table 4.5. R_p values infer that as the concentration of TCL increases, the R_p values also increase. Maximum inhibition efficiency is found to be 75.5 percentage.

4.2.1.4 Potentiodynamic polarisation studies of TCF / MS / 1M HCl

Figure 4.5 shows the anodic and cathodic polarisation curves of mild steel in 1 M HCl solution, without and with different concentration of TCF extract. It can be seen that both the cathodic and anodic curves reflect lower current density in the presence of TCF than those recorded in the solution without TCF. This indicates that TCF extract inhibits the corrosion process. The electrochemical parameters, that is, corrosion current density (I_{corr}), anodic (b_a) and cathodic (b_c) Tafel constants, and polarisation resistance (R_p), are given in Table 4.5.

The table divulges the fact that the addition of the inhibitor shifts the anodic (b_a) and cathodic (b_c) slope values in the scale of 90 ± 9 mV and 152- 44 mv for anodic (b_a) and cathodic (b_c) Tafel slopes respectively. This denotes the suppression of both the anodic dissolution and cathodic hydrogen evolution by the inhibitor

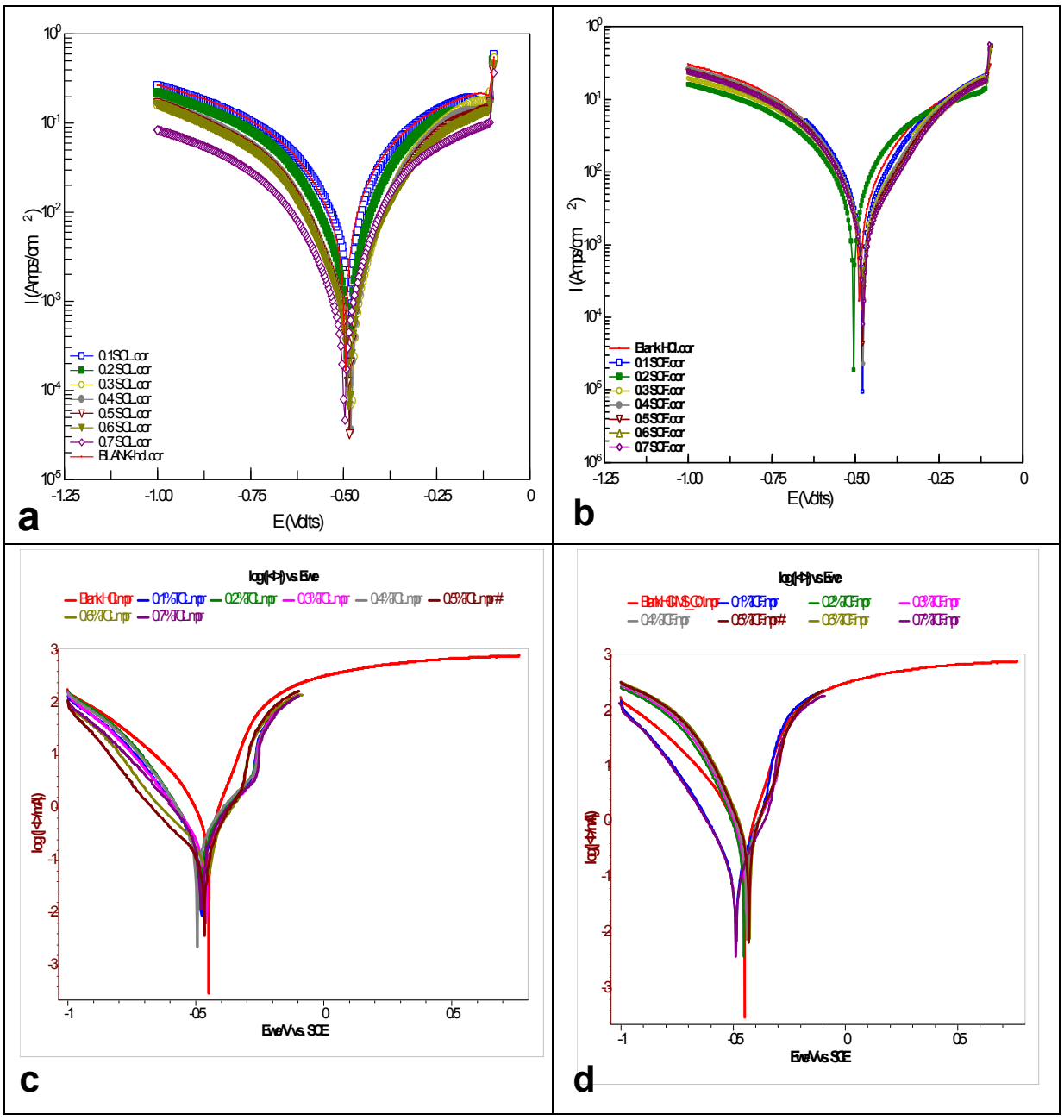

Figure 4.5 Potentiodynamic polarisation curves for MS in 1 M HCl in absence and presence of (a) SCL; (b) SCF; (c) TCL; (d) TCF extracts

Significant reduction in the I_{corr} values is noted in the presence of the inhibitor. The corrosion current decreases from 0.0035 A/cm^2 for that of the uninhibited solution to

0.0010 A/cm^2 at 0.7% TCF. The IE is found to increase with increase in concentration of the inhibitor affording a maximum efficiency of 71.4 percentage. The negligible shift in the E_{corr} values infers the mixed nature of the inhibitor under investigation **(Ashassi Sorakbi, 2006)**

It is evident from Table 4.5 that, the R_p values increase with increasing TCF concentration. Polarisation resistance values in the table with and without the addition of the inhibitor demonstrate that the values of R_p increases from 85.5 ohm/cm^2 (blank) to 386 ohm/cm^2 in the presence of 0.7% TCF. Inhibition performance of TCF is found to be 77.9 percentage.

The potentiodynamic polarisation results of studied inhibitors suggest that the inhibitors are first adsorbed onto the mild steel surface and impede the corrosion reaction by merely blocking the reaction sited of the electrode surface without affecting the anodic and cathodic reaction. **(Abd El-Rehim *et al*, 2001)**

4.2.1.5 Potentiodynamic polarisation studies of SCL / SCF / TCL / TCF / MS /1M HCl at higher temperatures

Temperature is an important condition in studies on metal dissolution. The corrosion rate in acid solutions, increases exponentially with increasing temperature because the hydrogen evolution over potential decreases.The effect of temperature on the rate of corrosion of MS is studied in 1 M HCl in the absence and presence of different concentration of SCL / SCF / TCL / TCF extracts. Polarisation curves for MS in 1 M HCl solution in the studied temperature range (303-333 K) are shown in Figure 4.6 and 4.7.The numerical values of corrosion current density (I_{corr}), corrosion potential (E_{corr}),anodic and cathodic Tafel slope (b_a and b_c), and polarisation resistance (R_p) are given in Tables 4.6 and 4.7. These values are calculated from the intersection of the anodic and cathodic Tafel lines of the polarisation curve at E_{corr}. Although the data (Tables 4.6 and 4.7) shows an increase in corrosion current density with rising temperature, the corrosion current density of inhibited solutions is always lower than the blank one.In the absence and presence of SCL / SCF / TCF extracts, the I_{corr} value decreases with increasing temperature till 323K and then increases at 333K.For TCL extract, the I_{corr} value decreases till 313K and then increases. It is also apparent that the SCL / SCF / TCL / TCF extracts have inhibiting properties at all the temperatures studied and that inhibition efficiency values increases with increasing temperature till 323K (for TCL till 313K). The maximum efficiencies noted at 323K for the investigated inhibitors at 0.7 % concentration are: 83.3 (for SCL); 71.4 percentage (for SCF); 81.4 percentage (for TCL at 313K) and 70.7 percentage (for TCF).

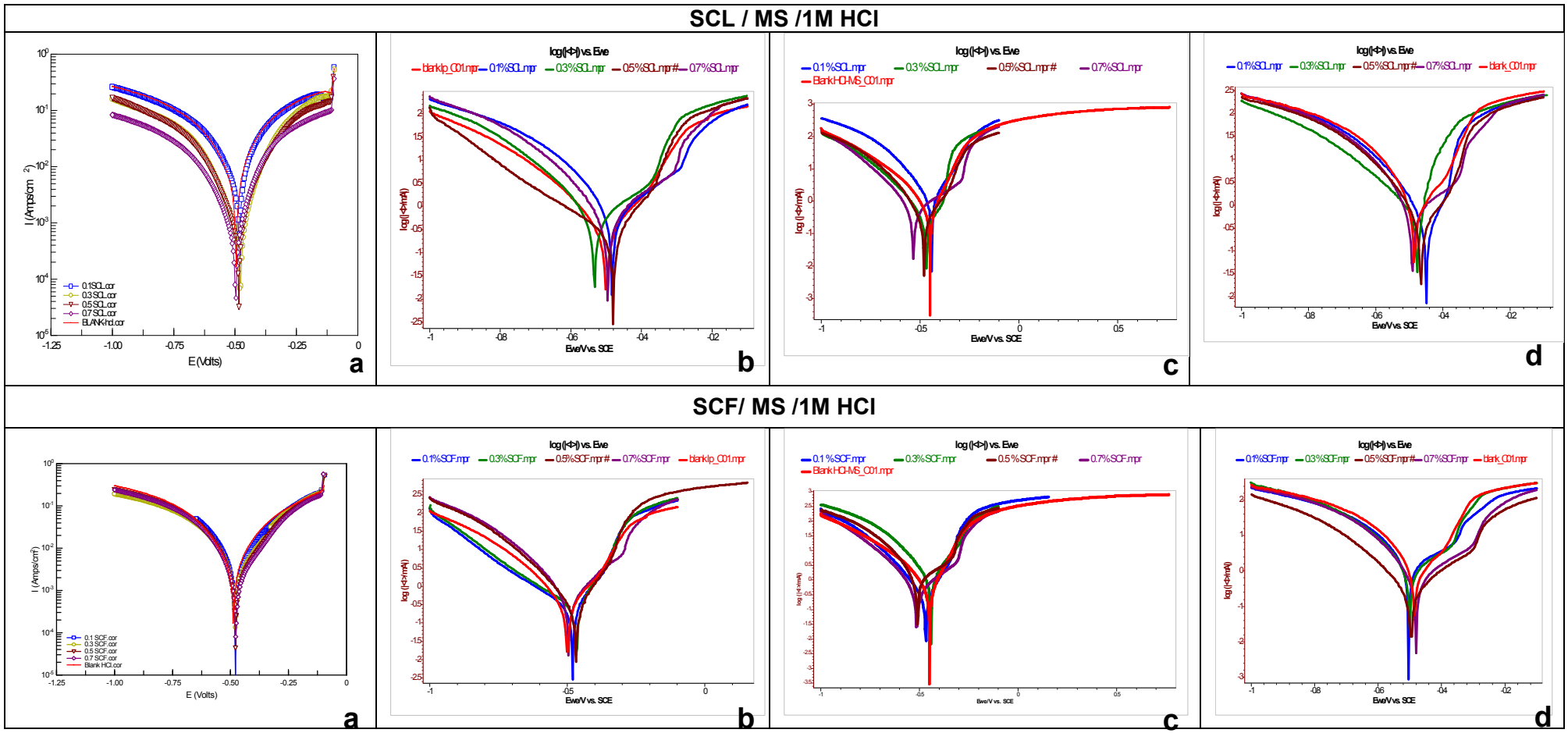

Figure 4.6 Potentiodynamic polarisation plots of MS in 1 M HCl in absence and presence of SCL and SCF at (a) 303K (b) 313K (c) 323K and (d) 333K

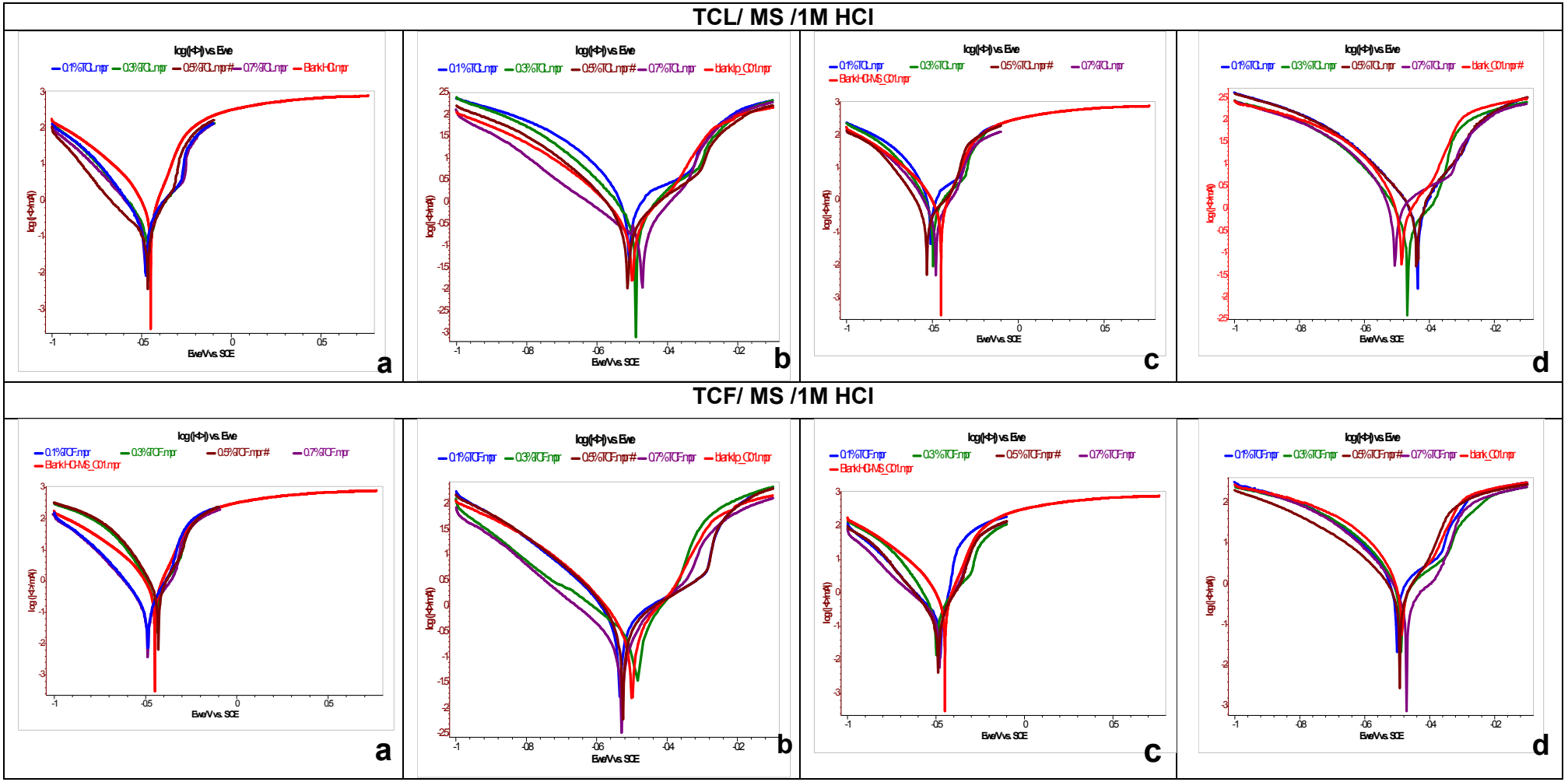

Figure 4.7 Potentiodynamic polarisation plots of MS in 1 M HCl in absence and presence of TCL and TCF at (a) 303K (b) 313K (c) 323K and (d) 333K

Table 4.6: Potentiodynamic polarisation parameters for corrosion of MS in the absence and presence of different concentrations of SCL / SCF in 1M HCl at room temperature and higher temperatures

Conc (%)	SCL							SCF						
	Tafel					Polarisation parameters		Tafel					Polarisation parameters	
	E_{corr} mV/ SCE	I_{corr} A/cm^2	b_a mV/ decade	b_c mV/ decade	IE (%)	R_p Ohm/cm^2	IE (%)	E_{corr} mV/ SCE	I_{corr} A/cm^2	b_a mV/ decade	b_c mV/ decade	IE (%)	R_p Ohm/cm^2	IE (%)
303K								**303K**						
Blank	-496	0.0075	89	141	-	4.2	-	-496	0.0075	89	141	-	4.2	-
0.1	-483	0.0040	97	112	46.7	4.8	12.5	-478	0.0040	87	117	46.7	8.5	50.6
0.3	-479	0.0010	99	129	86.7	22.4	75.9	-476	0.0027	93	143	66.7	11.4	58.0
0.5	-485	0.0009	95	128	88.0	24.0	82.5	-475	0.0020	92	143	68.0	13.5	67.4
0.7	-485	0.0007	85	130	92.0	24.0	85.2	-474	0.0016	82	154	78.7	14.4	70.8
313K								**313K**						
Blank	-449	0.0043	85	140	-	7.1	-	-449	0.0043	85	140	-	7.1	-
0.1	-469	0.0042	86	120	2.3	32.8	78.4	-446	0.0041	108	125	4.7	43.4	83.6
0.3	-485	0.0034	89	139	20.9	88.9	92.0	-449	0.0040	113	119	7.0	44.7	84.1
0.5	-473	0.0013	72	128	69.8	144.0	95.1	-445	0.0035	84	134	18.6	53.1	86.6
0.7	-477	0.0008	67	121	81.4	199.0	96.4	-452	0.0015	87	139	65.1	80.0	91.1
323K								**323K**						
Blank	-450	0.0042	85	131	-	4.2	-	-450	0.0042	85	131	-	4.2	-
0.1	-483	0.0036	77	125	14.3	44.5	90.6	-452	0.0039	112	122	7.1	50.4	91.7
0.3	-471	0.0034	109	133	19.0	64.8	93.5	-495	0.0031	101	140	26.2	55	92.4
0.5	-439	0.0017	60	134	59.5	88.7	95.3	-474	0.0013	73	134	69.0	62	93.2
0.7	-482	0.0007	71	116	83.3	159	97.4	-459	0.0012	65	119	71.4	87.7	95.2
333K								**333K**						
Blank	-458	0.0098	102	127	-	6.1	-	-458	0.0098	102.4	127	-	6.1	-
0.1	-468	0.0064	96	119	34.7	19.2	68.2	-468	0.0090	89	120	8.2	23.8	74.4
0.3	-463	0.0055	86	123	43.9	29.6	79.4	-501	0.0080	76.9	128	18.4	43.9	86.1
0.5	-481	0.0046	108	142	53.1	38.3	84.1	-448	0.0057	75.8	135	41.8	47.7	87.2
0.7	-441	0.0029	112	131	70.4	44.3	86.2	-447	0.0032	78.3	127	67.3	49.7	87.7

Table 4.7: Potentio dynamic polarisation parameters for corrosion of MS in the absence and presence of different concentrations of TCL / TCF in 1M HCl at room temperature and higher temperatures

Conc (%)	TCL							TCF						
	Tafel					Polarisation parameters		Tafel					Polarisation parameters	
	E_{corr} mV/ SCE	I_{corr} A/cm^2	b_a mV/ decade	b_c mV/ decade	IE (%)	R_p Ohm/cm^2	IE (%)	E_{corr} mV/ SCE	I_{corr} A/cm^2	b_a mV/ decade	b_c mV/ decade	IE (%)	R_p Ohm/cm^2	IE (%)
303K								**303K**						
Blank	-475	0.0035	90	152	-	85.5	-	-475	0.0035	90	152	-	85.5	-
0.1	-473	0.0021	101	142	40.0	152.4	43.9	-433	0.0030	98	108	14.3	102	16.2
0.3	-462	0.0014	92	139	60.0	204.1	58.1	-522	0.0013	99	134	62.9	168	49.1
0.5	-435	0.0009	82	138	74.3	238.2	64.1	-458	0.0013	94	127	62.9	278	69.2
0.7	-458	0.0006	76	149	82.9	348.6	75.5	-423	0.0010	84	128	71.4	386	77.9
313K								**313K**						
Blank	-449	0.0043	85	140	-	7.1	-	-449	0.0043	85	140	-	7.1	-
0.1	-523	0.0028	89	148	34.9	81.2	91.3	-431	0.0042	79	139	2.3	29.4	75.9
0.3	-471	0.0018	111	133	58.1	109.0	93.5	-456	0.0027	97	127	37.2	56.1	87.3
0.5	-468	0.0009	74	144	79.1	176.0	96.0	-494	0.0020	98	136	53.5	89.6	92.1
0.7	-477	0.0008	75	124	81.4	184.5	96.2	-441	0.0019	73	139	55.8	98.7	92.8
323K								**323K**						
Blank	-450	0.0042	85	131	-	4.2	-	-450	0.0041	85	131	-	4.2	-
0.1	-460	0.0018	111	134	57.1	64.2	93.5	-442	0.0038	88	134	7.3	64.2	93.5
0.3	-474	0.0013	71	142	69.0	86.9	95.2	-469	0.0037	115	142	9.8	86.9	95.2
0.5	-461	0.0012	93	134	71.4	104.0	96.0	-483	0.0023	115	134	43.9	104	96.0
0.7	-523	0.0011	107	130	73.8	151.0	97.2	-469	0.0012	82	130	70.7	151	97.2
333K								**333K**						
Blank	-458	0.0098	102	127	-	6.1	-	-458	0.0098	102	127	-	6.1	-
0.1	-422	0.0082	87	138	16.3	23.4	73.9	-431	0.0077	94	127	21.4	22.4	72.8
0.3	-460	0.0067	87	130	31.6	51.3	88.1	-440	0.0053	81	130	45.9	28.7	78.7
0.5	-431	0.0069	87	118	29.6	22.7	73.1	-472	0.0046	68	136	53.1	39.4	84.5
0.7	-450	0.0031	107	135	68.4	29.4	79.3	-458	0.0033	94	139	66.3	45.2	86.5

Further increase of temperature to 333K decreases the IE. However the results show that the IE increases on increasing the inhibitor concentration as highlighted by **Chauhan *et al*, 2007** and the efficiencies stabilise to 70.4 percentage (SCL); 67.3 percentage (SCF) ; 68.4 percentage (TCL) and 66.3 percentage (TCF) at optimum concentration of 0.7% at 333K. Similar trend is also noted in R_p values. The potentiodynamic polarisation curves reflect a slight change in the anodic and cathodic curves for the investigated inhibitors , ie, ± 10 mV for anodic curves and ± 15 mV for cathodic curves at room temperature. For the higher temperatures an average shift of ± 20 mV and ± 25 mV for anodic curves for cathodic curves are noticed. This reflects the mixed behaviour of the studied inhibitors at higher temperatures also **(Satapathy *et al*, 2009)**.The above results confirm the effectiveness of the inhibitor in the investigated temperature range.

4.2.2 ELECTROCHEMICAL IMPEDANCE MEASUREMENTS

The EIS technique has been one of the methods used to report the mechanism of corrosion and corrosion protection of metals and alloys in aggressive media. Impedance measurements provide an insight into the kinetics of interfacial mass transfer process **(Bentiss *et al*, 1999)** .The EIS technique is based on the response of an equivalent circuit for an electrode/solution interface. The response can be analysed by transfer functions due to an applied small-amplitude potential excitation at varying signals and sweep rates. In turn, a sine-wave perturbation of small amplitude is employed on a corroding system being modelled as an equivalent circuit for determining the corrosion mechanism.

4.2.2.1 Electrochemical Impedance spectroscopy Studies of MS in the Presence of different concentration of SCL & SCF in 1M HCl

i) SCL / MS / 1M HCl

Figure 4.8 exemplifies Nyquist and Bode representations of the impedance response after 1/2 h of immersion. The impedance profile in uninhibited acid (Figure -4.8) reflects a single capacitive semicircle. **(Oguzie *et al*, 2014)** .The observed capacitive loop arises from double layer capacitance-induced charge transfer processes, and its diameter is correlated to the charge transfer resistance (R_{ct}) at the interface. Analyses of the spectra also reveal that they are not perfect semicircle in nature. This anomalous behaviour may be attributed to surface roughness, distribution of the active sites or due to the adsorption of the inhibitor species**. (Titz *et al*, 1990)** The diameter of the semi circle increases with increase in concentration of the studied inhibitor and the shape of the semi circle does not change in the presence of the inhibitor implying that there is no change in the mechanism of MS dissolution in the presence of SCL. The results reflect that the R_{ct} values increase

(from 30.4 Ωcm^2 to 224.4 Ωcm^2) with increase in concentration of inhibitor (Table 4.8) to afford a maximum efficiency of 86.5 percentage.This might be due to the adsorption of the phytochemical constituents adsorbed onto the MS surface. The corresponding Bode plots show only one maximum phase reflecting one time constant. This is indicative of one step mechanism **(Khamis *et al*, 2007).**

The value of C_{dl} decreases with inhibitor concentration .This decrease in value C_{dl} which results from a decrease of dielectric constant and / or increase in thickness of double layer suggests that the inhibitor molecules function by adsorption at acid / metal interface **(McCafferty and Hackerman, 1972).**

ii) SCF / MS / 1M HCl

Nyquist plots / Bode plots / Bode plots in theta- frequency formats for MS in 1M HCl in the absence and presence of various concentration of SCF are depicted in Figure 4.7. The impedance spectral data of SCF derived from these figures are given in Table 4.8. It is evident from Figure 4.8 that the impedance spectra exhibits a single capacitive semi circle in the high frequency region corresponding to one time constant in the Bode plots **(Oguzie *et al*, 2010).** Analyses of the spectra also reflect the depressive nature of the Nyquist semicircle with centre under the real axis. This can be attributed to surface roughness, distribution of the active sites or due to the adsorption of the inhibitor species **(Titz *et al*, 1990**). The plots in Figure 4.8 further infer that the diameter of the semi circle is dependent on the concentration of the studied inhibitor. The R_{ct} values are found to increase with increase in inhibitor concentration and the C_{dl} values tend to decrease. It follows from the data in Table 4.8, that ,on addition of SCF extract, the R_{ct} values increases from 4.0 Ωcm^2 to 23.6 Ωcm^2 affording an efficiency of 83.1 percentage at 0.7% concentration. The decrease in C_{dl} values with the increase in inhibitor concentration is due to the adsorption of the SCF molecules replacing water at the metal–solution interface that leads to the decrease in local dielectric constant and / or an increase in the thickness of the electrical double layer **(Behpour *et al*,2009)** Hence, the change in C_{dl} values caused by the gradual displacement of water molecules by the adsorption of the SCF molecules at the metal–solution interface decreases the extent of the corrosion **(Benabdellah *et al*,2007).**

4.2.2.2 Electrochemical Impedance response of MS electrode in the presence of different concentrations of TCL & TCF extracts in 1M HCl

i) TCL / MS / 1M HCl

The impedance spectral data of TCL in 1M HCl are given in Table 4.9 and Figure 4.9.

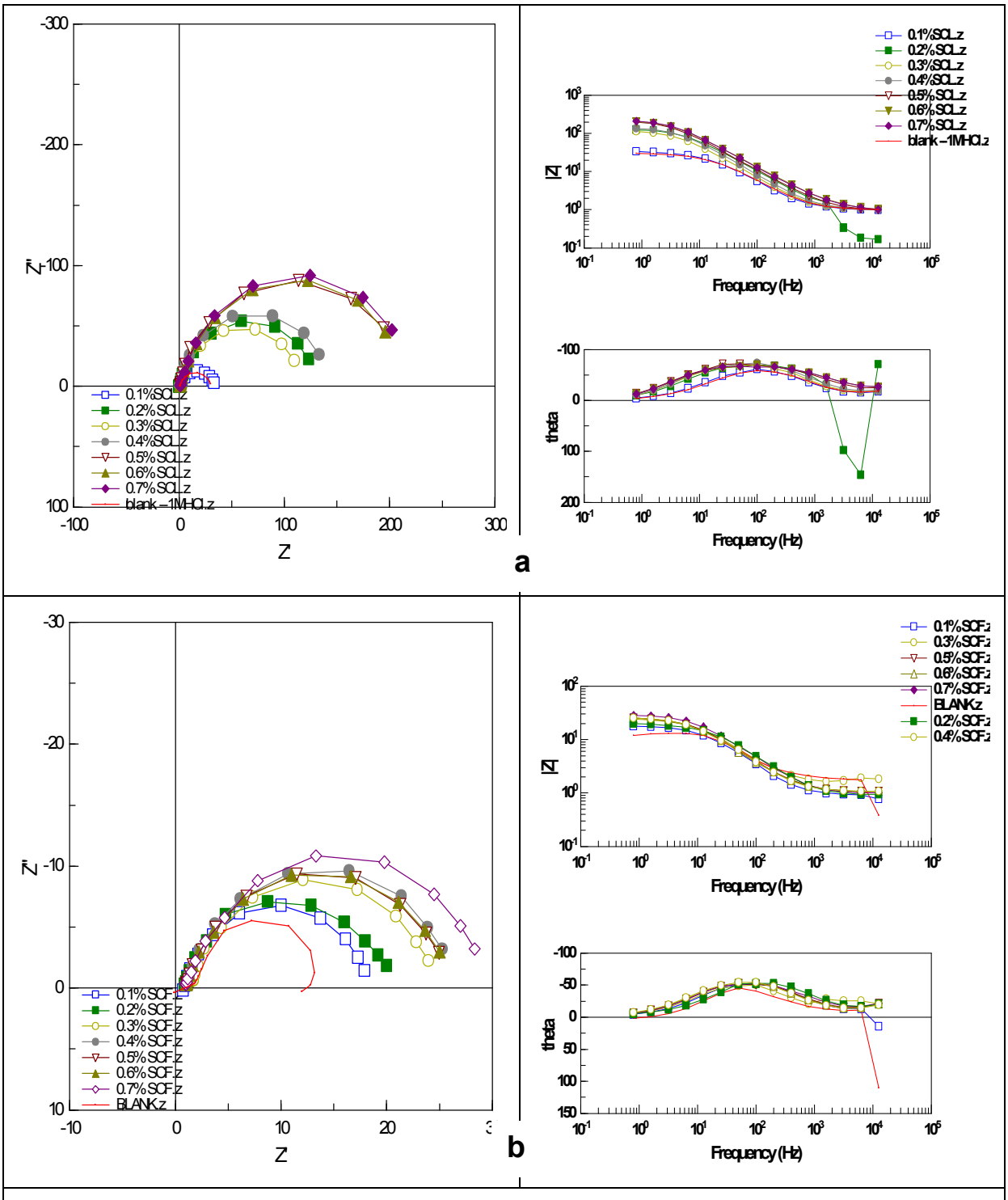

Figure 4.8 Nyquist and Bode diagrams for MS Electrode in 1M HCl in the absence and presence of (a)SCL (b) SCF

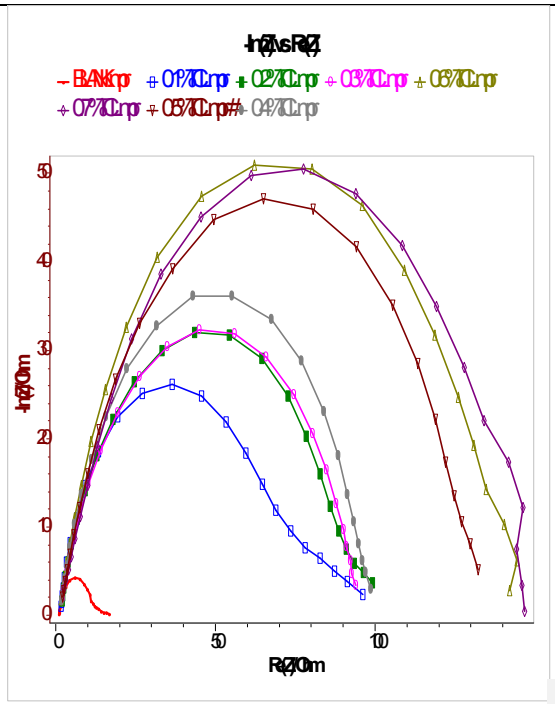

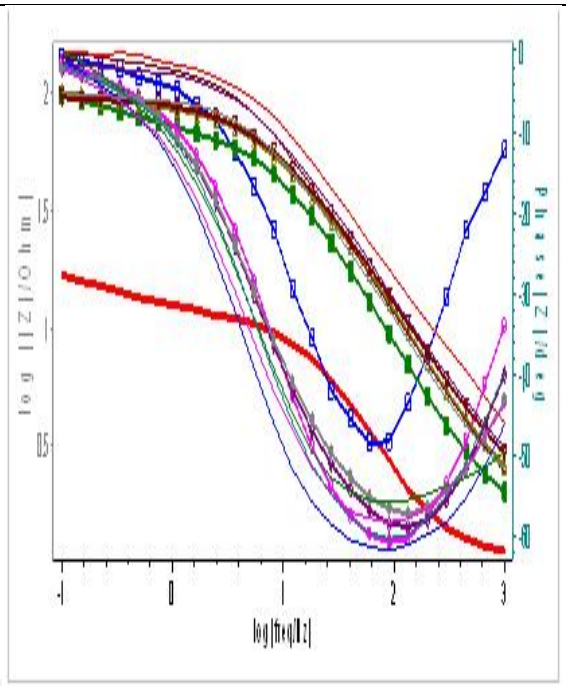

c

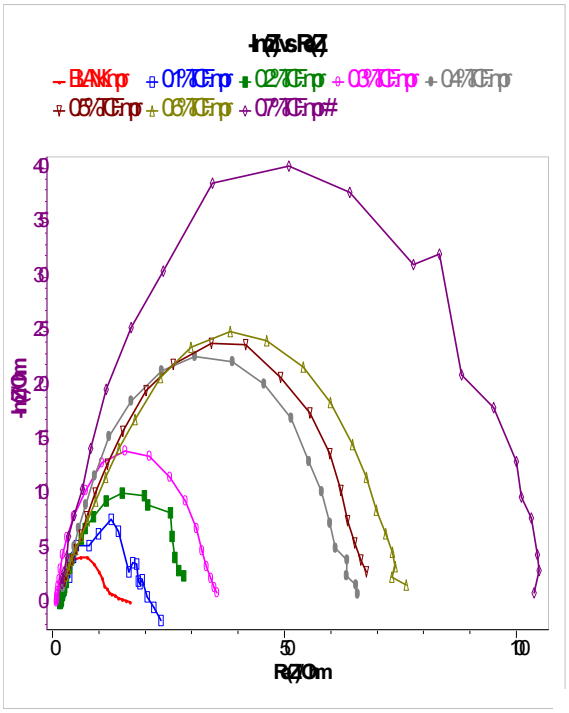

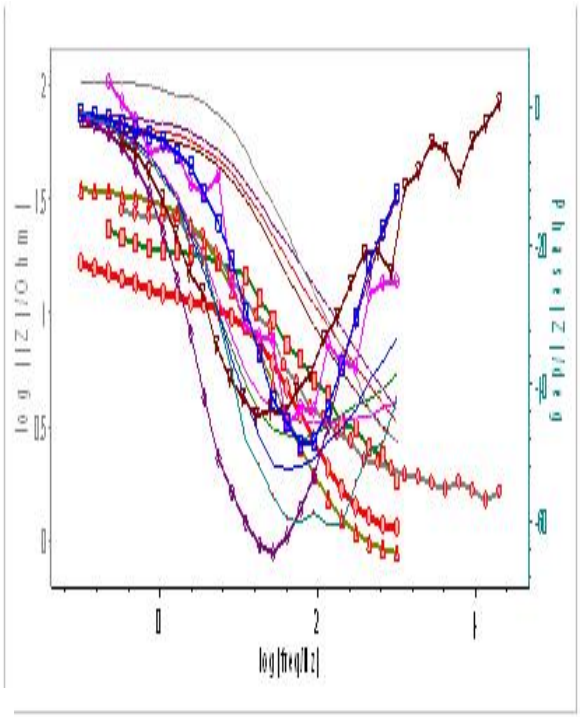

d

Figure 4.9 Nyquist and Bode plots of MS Electrode in 1M HCl in the absence and presence of (c) TCL; (d) TCF

From Figure 4.9, it can be seen that the semicircles obtained cut the real axis at higher and lower frequencies. At higher frequency end, the intercept corresponds to R_s and at lower frequency end the intercept corresponds to $R_s + R_{ct.}$, R_{ct} can be obtained by the difference between these two values .The figure demonstrates that the shapes of the impedance plots for inhibited systems are not substantially different from the uninhibited system, thereby suggesting an unaltered electrochemical characteristic of the solution with increased impedance. Surface heterogeneities / adsorption of the inhibitor species results in a depressed semi circular appearance of the impedance spectra. **(Naqvi *et al*, 2011)**. The results demonstrate the increase of charge transfer resistance (R_{ct}) values from 15.2 Ωcm^2 to 146.2 Ωcm^2 for TCL with increase in concentration of the inhibitor.A maximum efficiency of 89.6 percentage is noticed at 0.7% of TCL. The semicircle in all cases corresponds to a capacitive loop. The diameter of the capacitive loop increases with increase of inhibitor concentration, the increase being more pronounced at higher concentrations of TCL. This may be attributed to the adsorption of the active constituents of the inhibitor species on the metal/solution interface that possibly mitigates the corrosion of MS electrode **(Elyn Amyra *et al*, 2011)**. Bode plots confirm the presence of a single time constant.The decrease in C_{dl} values with increase in concentration of the inhibitor may be because of adsorption of the inhibitor molecules on the metal surface leading to the formation of a film on the metal surface **(Bentiss *et al*, 1999)**

ii) TCF / MS / 1M HCl

The impedance spectral data of MS / HCl / TCF obtained from Nyquist plots (Figure 4.9) in 1M HCl are given in Table 4.9 .As observed, the impedance spectra exhibits a single depressed semi circle whose diameter increases with increasing concentration of the inhibitor implying a charge transfer process for the corrosion inhibition mechanism. **(Hussin *et al*, 2011)** The figure also confirms the fact that the presence of the inhibitor did not modify the corrosion reaction of MS electrode in the presence of the inhibitor. The impedance parameters demonstrate the increase of charge transfer resistance (R_{ct}) values from 15.2 Ωcm^2 to 103.1 Ωcm^2 for TCF with increase in concentration of the inhibitor. A maximum of 82.9 percentage IE is obtained at 0.7% TCF. Single capacitive semicircle noted in the Nyquist plot corresponds to a single time constant in the Bode representation **(Oguzie *et al*, 2014).** The increase of absolute impedance at low frequencies in the Bode plots confirm the higher protection with increasing concentration of the inhibitor, which is related to the adsorption of the inhibitor on the MS surface.**(Mahdavian and Asshari, 2010)**

It is clear from the table that C_{dl} values tend to decrease with increase in inhibitor concentration. This behaviour is the result of increase in surface coverage by the inhibitor molecules of plant extract which leads to increase in IE **(Lecante *et al*, 2011)**

Analysis of Impedance Spectral data

The deviation of Nyquist plots (Figures.4.8 and 4.9) from perfect semicircles at high frequencies are often referred to as frequency dispersion of interfacial impedance. This anomalous phenomenon can be attributed to inhomogeneity of the electrode surface arising from surface roughness or interfacial phenomena. When a non-ideal frequency response is present, it is conventional to use distributed circuit elements in an equivalent circuit. The most widely used is the constant-phase element (CPE), which has a non-integer power dependence on the frequency **(Afia *et al*, 2012).**

For corrosion reactions which are strictly charge transfer controlled, impedance behaviour can be explained with the help of a simple and commonly used equivalent circuit composed of a double layer capacitance, charge transfer resistance (R_{ct}) and solution resistance (R_s). The resistor R_s is in series to the double layer capacitance and R_{ct}, while double layer capacitance is parallel to R_{ct}. The double layer capacitance is in parallel with the impedance due to the charge transfer reaction. This type of circuit is used to model the iron/acid interface (**Li *et al,* 2007**). The constant phase element (CPE) is introduced in the circuit instead of a pure double layer capacitance to give more accurate fit as shown in the Figure 4.10. **(Ross Macdonald *et al,* 1987).**

The impedance function of a CPE is defined by the mathematical expression given below:

$$Z_{CPE} = Y_o^{-1} (i\omega)^{-n} \qquad \textbf{(4.1)}$$

where Y_o is the CPE constant (in Ω^{-1} s^n cm^{-2}), ω is the sine wave modulation angular frequency (in rad s^{-1}), i^2 =-1 is the imaginary number, n=α/ (π/2) in which α is the phase angle of CPE and n is the CPE exponent (0 ≤ n≤ 1) which measures the deviation from the ideal capacitive behaviour and it represents the surface irregularity. The constant phase element (CPE) is used in the place of capacitor to compensate the non-homogeneity of the surface that causes a greater depression in Nyquist semicircle diagram. (**Havriliak *et al,* 1997; Cruz *et al*, 2008; Lopez *et al,* 2005**).

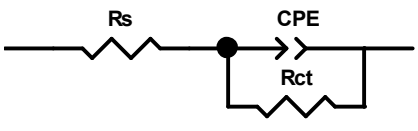

Figure 4.10 Proposed equivalent circuit model for MS / Inhibitors / 1M HCl

The values of double layer capacitance C_{dl} for a circuit including CPE are calculated according to the following equation

$$C_{dl} = (Y_o\ \omega_{max})^{n-1} \qquad \textbf{(4.2)}$$

Where ω_{max} is angular frequency ($\omega_{max} = 2\pi f_{max}$) at which the imaginary part of the impedance is maximal and f_{max} is AC frequency at maximum. **(Hasan *et al*, 2007)**

The CPE is considered to be a surface irregularity of the electrode causing a depression in the Nyquist semicircle diagram (**Garcia-Ochoa and Genesca, 2004**); thus, a conclusion cannot be drawn with regards to metal solution interface performing as a capacitor. If the electrode surface is considered as homogeneous and plane, the exponential value (n) becomes equal to 1.0 and the metal-solution interface acts as a capacitor with regular surface. The impedance parameters, namely charge-transfer resistance (R_{ct}), solution resistance (R_s), the constant phase element (Y_o) related to the capacity of the double layer and the exponent (n), relevant to the capacitive semicircle of the mild steel/ 1M HCl / SCL / SCF / TCL / TCF extracts are listed in Tables 4.8 and 4.9. These parameters are calculated from the non-linear least square fit of the equivalent circuit as depicted in Figure- 4. 10. Simulation of Nyquist plots with above model shows an excellent agreement with experimental data. It means that the suggested equivalent circuit model, presented in Figure-4.10, could reasonably represent the charge-transfer and metal/solution interface features related to the corrosion process of carbon steel in acidic solution containing investigated inhibitors.

In Tables 4.8 and 4.9, the double layer capacitance (C_{dl}) derived from the CPE are also presented, using the following equation (4.3)

$$C_{dl} = (Y_o\ Rct^{\ n-1})^{1/n} \qquad \textbf{(4.3)}$$

The CPE is attributed to the non-homogeneity of the electrode surface as well as due to the mass transport process. If the electrode surface is homogeneous and plane, the exponential value (n) is equal to 1 and the electrode surface can be treated as an ideal capacitance. The interface time constant (τ) and the double layer capacitance value (C_{dl}) of the CPE can be calculated by the following equations (4.4 and 4.5) (**Guo Gao *et al,* 2007**).

$$C_{dl} = (Y_o\ R_{ct}^{\ 1-n})^{\ 1/n} \qquad \textbf{(4.4)}$$

$$Y_o = \ \tau^n / R_{ct} \qquad \textbf{(4.5)}$$

The relaxation time (τ) of the surface, that is, the time required for attaining the charge distribution to equilibrium **(Toshima and Uchida, 1970)** is given by:

$$\tau = C_{dl} \times R_{ct} \qquad \textbf{(4.6)}$$

The adsorption of inhibitor needs some time to attain equilibrium. This time is very short, as shown in Tables 4.8 and 4.9. In 1M HCl containing different inhibitor concentration, τ increases with increase of inhibitor concentration which means slow adsorption process **(Mahdi nasibi *et al,* 2013)**.

The fit parameter, exponential factor n, is often related to the degree of heterogeneity of the interface and / or the surface film ie, larger the deviation from 1, the more heterogenous the surface layer **(Hosseini *et al*, 2003)**. Indeed, the lower n value for uninhibited solution (n =0.5, 0.84, 0.93) indicates a surface inhomogeneity resulting from surface metal roughening and/or formation on the surface of corrosion products. The values of n lies between 0.9 and 1.1 in the case of inhibited solutions. Addition of inhibitors increases n value indicating reduction of surface inhomogeneity due to the adsorption of investigated inhibitors on the most active adsorption sites at the mild steel surface. Experimentally determined values of n for the corroding metal electrode lies around 0.9 **(Hosseini *et al,* 2003)**; as can also been seen from Tables 4.8 and 4.9 in the present cases.

Also, the addition of investigated inhibitors to the corrosive solution decreases the double layer capacitance (C_{dl}) and it reflects the time constant (τ) value (Tables 4.8 and 4.9). For example, when the plant extract concentration increases to 0.7% in the corrosive medium (1M HCl), the interface (τ) parameter changes while the capacitance (C_{dl}) value decreases. This signifies that the charge and discharge rates to the metal–solution interface are greatly decreased. This shows that there is an agreement between the amount of charge that can be stored (i.e. capacitance) and the discharge velocity in the interface (τ).The double layer between the charged metal surface and the solution is considered as an electrical capacitor. The adsorption of investigated inhibitors on the mild steel surface decreases its electrical capacity because they displace the water molecules and other ions originally adsorbed on the surface. The decrease in this capacity with increase in investigated inhibitors concentration may be attributed to the formation of a protective layer on the electrode surface. The thickness of this protective layer increases with increase in inhibitor concentration, since more investigated inhibitors will electrostatically adsorb on the electrode surface, resulting in a noticeable decrease in C_{dl}. i.e. the inhibitor molecules may reduce the capacitance by increasing the double layer

thickness according to the Helmholtz model (**Oguzie *et al,* 2007**) given by the following equation (4.6).

$$C_{dl} = \varepsilon \varepsilon_o / d \quad \textbf{(4.7)}$$

where d is the thickness of the protective layer, ε is the dielectric constant of the protective layer and ε_o is the permittivity of free space (8.854×10^{-14} Fcm^{-1}).

Discussion on Bode Plots

Phase angle at higher frequencies provide a general idea of anti corrosion performance. As the phase angle tends to become more negative, the electrochemical behaviour is found to be more capacitive **(Mahdavian *et al*, 2006).** Charge transfer increment could raise current tendency to pass through the capacitor in the circuit. According to the appearance of θ vs phase diagrams; increasing concentration of the plant extracts results in more negative values of phase angles at higher frequencies indicating superior inhibitive behaviour at higher concentrations. Also depression of phase angle at relaxation frequency occurs with decreasing the concentration of the plant extracts which indicates the decrease of capacitive response with the decrease of inhibitor concentration.Such a phenomenon could be attributed to higher corrosion activity at lower concentration of the inhibitors. The increase of absolute impedance at low frequencies in Bode plot (Figures 4.8 and 4.9) confirms the higher protection with increasing concentration of the inhibitors, which is related to adsorption of inhibitors on MS surface.

After analyzing the impedance results (Tables 4.8 and 4.9), it is obvious that the charge-transfer resistance value, R_{ct}, increases with the concentration of SCL / SCF / TCL / TCF and reaches a maximum value at 0.7% in the case of studied inhibitors. A large charge-transfer resistance is associated with a slower corroding system, due to a decrease in the active surface necessary for the corrosion reaction. The increase of the n value after addition of inhibitors in the corrosive solution can corroborate this conclusion. As it can be seen from Tables 4.8 and 4.9, the R_{ct} values increases with the increasing the concentrations of the inhibitors. On the other hand, the values of C_{dl} decrease with an increase in the concentration of the inhibitors. This decrease in the C_{dl}, which can result from a decrease in local dielectric constant and/or an increase in the thickness of the electric double layer, suggests that the molecules function by adsorption at the metal /solution interface. Thus, the change in C_{dl} values is caused by to the gradual replacement of water molecules by the adsorption of the molecules on the metal surface, decreasing the extent of the metal dissolution **(Bentiss *et al,* 2005)**. The highest percentage inhibition efficiency is achieved at 0.7% concentration of SCL / SCF / TCL / TCF .The results drawn from Impedance and Polarisation measurements are quite comparable.

Table: 4.8 Electrochemical Impedance parameters for corrosion of MS in the absence and presence of different concentrations of SCL and SCF in 1M HCl

Conc (%)	SCL									SCF								
	R_S (Ωcm^2)	Y_0 ($\mu F/cm^2$)	n	R_{ct} (Ωcm^2)	IE (%)	f_{max} (μHz)	CPE/C_{dl} ($\mu F/cm^2$)	θ	τ (S^n)	R_S (Ωcm^2)	Y_0 ($\mu F/cm^2$)	n	R_{ct} (Ωcm^2)	IE (%)	f_{max} (μHz)	CPE/C_{dl} ($\mu F/cm^2$)	θ	τ (S^n)
Blank	0.861	5399	0.93	30.4	-	15.4	365		0.011	-0.63	40110	0.50	4.0	-	55.6	721.7		0.003
0.1	0.826	4901	0.96	33.9	10.6	12.87	341	0.07	0.012	0.95	10566	0.82	15.1	73.5	20.4	517.8	0.28	0.008
0.2	0.053	2458	0.97	64.9	53.2	7.6	323	0.12	0.037	1.00	9633	0.84	16.5	75.8	19.0	507	0.30	0.008
0.3	0.959	3115	1.13	118.4	74.4	4.287	314	0.14	0.037	1.77	8272	0.87	19.3	79.3	16.5	500	0.31	0.010
0.4	0.939	2817	1.14	142.7	78.7	4.353	256	0.3	0.046	1.15	7469	0.89	21.3	81.2	15.2	492	0.32	0.010
0.5	0.748	1233	1.17	217.6	86.0	3.428	213	0.41	0.042	1.15	7674	0.88	20.8	80.8	16.5	465	0.36	0.010
0.6	1.289	1123	1.16	218.5	86.1	3.796	192	0.47	0.043	1.16	7648	0.89	20.8	80.8	15.3	499	0.31	0.010
0.7	1.402	767	1.16	224.4	86.5	3.73	190	0.48	0.04	1.11	6756	0.89	23.6	83.1	19.3	350	0.52	0.008

Table: 4.9 Electrochemical Impedance parameters for corrosion of MS in the absence and presence of different concentrations of TCL and TCF in 1M HCl

Conc (%)	TCL									TCF								
	R_S (Ωcm^2)	Y_0 ($\mu F/cm^2$)	n	R_{ct} (Ωcm^2)	IE (%)	f_{max} (μHz)	CPE/C_{dl} ($\mu F/cm^2$)	θ	τ (S^n)	R_S (Ωcm^2)	Y_0 ($\mu F/cm^2$)	n	R_{ct} (Ωcm^2)	IE (%)	f_{max} (μHz)	CPE/C_{dl} ($\mu F/cm^2$)	θ	τ (S^n)
Blank	0.830	10476	0.84	15.2	-	13.3	789		0.012	0.830	10476	0.84	15.2	-	13.3	789		0.012
0.1	0.766	1788	1.06	89.1	82.9	8.2	218	0.72	0.019	-0.13	8208	0.88	19.4	21.6	13.0	631	0.20	0.012
0.2	1.550	1645	1.07	96.8	84.3	8.2	201	0.75	0.019	1.59	5812	0.95	27.4	44.5	9.4	617	0.22	0.017
0.3	0.631	1665	1.07	95.6	84.1	8.2	203	0.74	0.019	1.67	4855	0.98	32.8	53.7	8.9	548	0.31	0.018
0.4	1.384	1701	1.07	93.6	83.8	8.2	208	0.74	0.019	1.89	2572	1.06	61.9	75.4	6.3	411	0.48	0.025
0.5	1.803	1220	1.11	130.5	88.4	5.5	222	0.72	0.029	1.78	2435	1.05	65.4	76.8	7.6	320	0.59	0.021
0.6	0.836	1122	1.11	141.9	89.3	5.5	204	0.74	0.029	2.01	2036	1.06	78.2	80.6	7.7	265	0.66	0.021
0.7	1.916	1089	1.11	146.2	89.6	5.5	198	0.75	0.029	1.60	1544	1.08	103.1	82.9	7.1	219	0.72	0.023

4.2.2.3 Electrochemical Impedance spectroscopy Studies of MS/HCl in the Presence of different concentration of SCL / SCF / TCL /TCF at higher temperatures

To investigate the mechanism of inhibition, EIS measurements were taken for MS/HCl at various temperatures in the absence and presence of different concentrations of SCL / SCF / TCL / TCF. Figures 4.11 and 4.12 give the Nyquist plots of MS in the absence and presence of various concentrations (0.1, 0.3, 0.5 and 0.7%) of SCL / SCF / TCL / TCF at different temperatures. Corresponding data are given in Tables 4.10 and 4.11. In the studied temperature range (303 - 333 K), the values of R_{ct} increases with increasing temperature till 323K and at 333K a decrease is noticed. The values of inhibition efficiency of the inhibitors increase with increasing temperature till 323 K and then a slight decrease is noted. Furthermore, the increase in inhibitor concentration causes a decrease in C_{dl} and increase in R_{ct}. These results confirm that the plant extracts act as an efficient inhibitor in the temperature range studied. **(Hmamou *et al*, 2012) .**The findings are consistent with potentiodynamic polarisation curves experiments carried out at higher temperatures. The diameter of Nyquist plot increases on increasing the concentration of investigated inhibitors. This suggests that the formed inhibitive film is strengthened by the addition of plant extracts. **(Chauhan, 2006)**

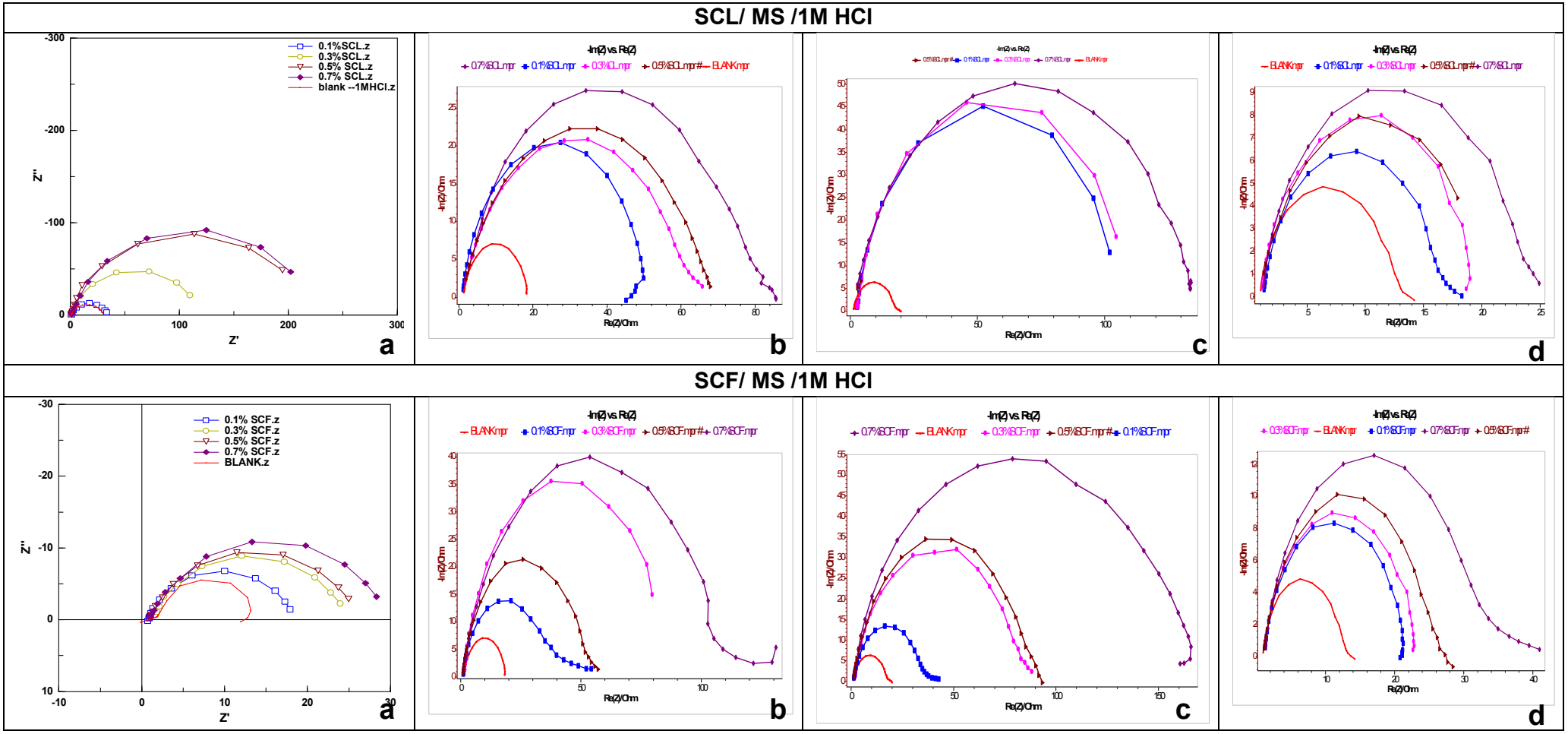

Figure 4.11 Impedance plots of MS in 1M HCl in the absence and presence of SCL and SCF at (a) 303K (b) 313K (c) 323K and (d) 333K

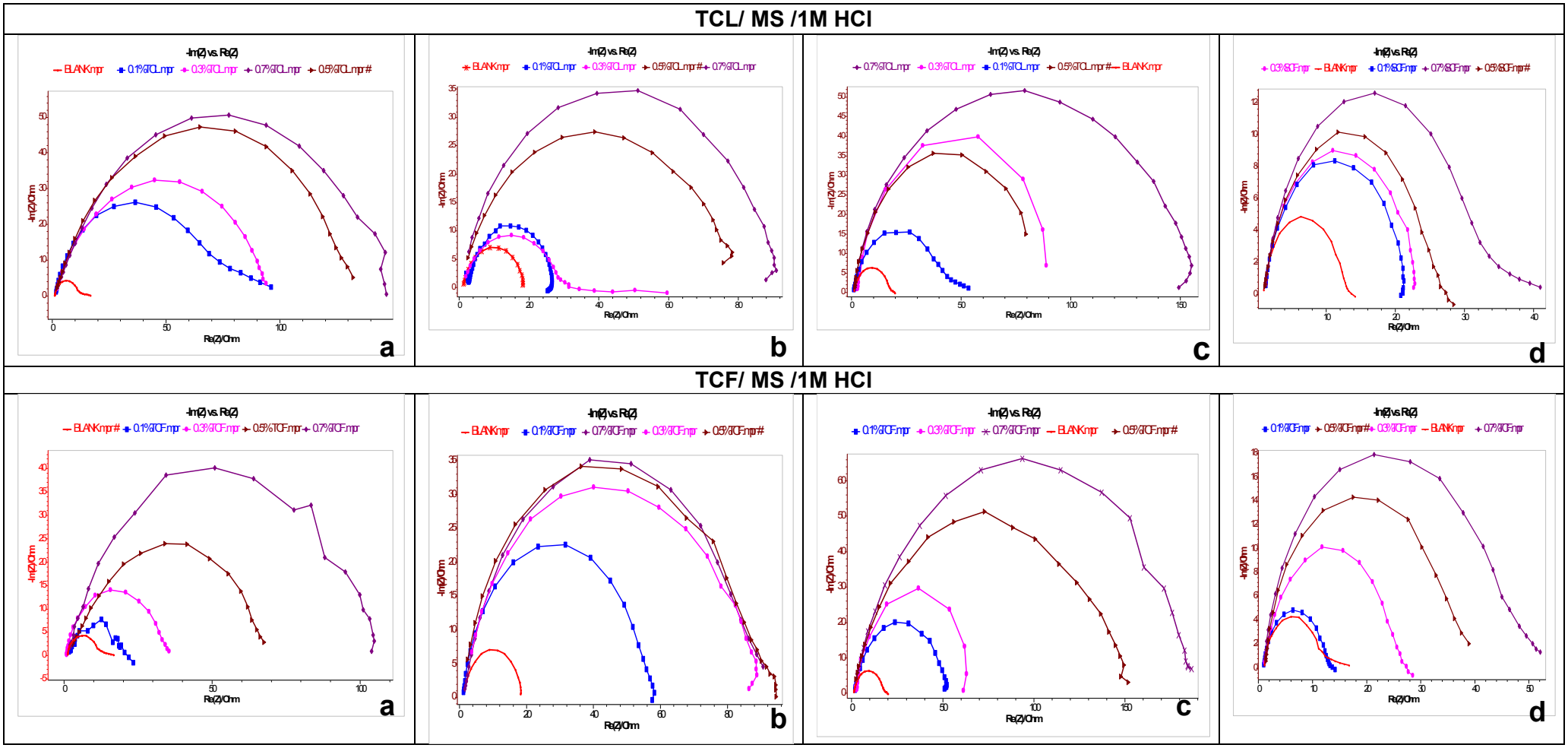

Figure 4.12 Impedance plots of MS in 1M HCl in the absence and presence of TCL and TCF at (a) 303K (b) 313K (c) 323K and (d) 333K

Table: 4.10 Electrochemical Impedance parameters for corrosion of MS in the absence and presence of different concentrations of SCL and SCF in 1M HCl at room temperature and higher temperatures

Conc (%)	SCL									SCF								
	R_S (Ωcm^2)	Y_0 ($\mu F/cm^2$)	n	R_{ct} (Ωcm^2)	IE (%)	f_{max} (μHz)	CPE/C_{dl} ($\mu F/cm^2$)	θ	τ (S^n)	R_S (Ωcm^2)	Y_0 ($\mu F/cm^2$)	n	R_{ct} (Ωcm^2)	IE (%)	f_{max} (μHz)	CPE/C_{dl} ($\mu F/cm^2$)	θ	τ (S^n)
303K										**303K**								
Blank	0.861	5399	0.93	30.4	-	15.4	365		0.011	-0.63	40110	0.50	4.0	-	55.6	721.7		0.003
0.1	0.826	4901	0.96	33.9	10.6	12.87	341	0.07	0.012	0.95	10566	0.82	15.1	73.5	20.4	517.8	0.28	0.008
0.3	0.959	3115	1.13	118.4	74.4	4.287	314	0.14	0.037	1.77	8272	0.87	19.3	79.3	16.5	500	0.31	0.010
0.5	0.748	1233	1.17	217.6	86.0	3.428	213	0.41	0.042	1.15	7674	0.88	20.8	80.8	16.5	465	0.36	0.010
0.7	1.402	767	1.16	224.4	86.5	3.73	190	0.48	0.04	1.11	6756	0.89	23.6	83.1	19.3	350	0.52	0.008
313K										**313K**								
Blank	1.2	9178	0.83	17.4	-	27.2	337.3	-	0.01	1.2	9178	0.83	17.4	-	27.2	337.3	-	0.006
0.1	1.6	3234	1.01	49.2	64.6	9.8	329.6	0.02	0.02	1.4	3324	0.99	47.9	63.7	12.2	271.7	0.19	0.013
0.3	1.4	1889	1.02	84.3	79.4	12.2	154.4	0.54	0.01	0.4	2504	1.01	63.6	72.6	12.2	204.7	0.39	0.013
0.5	2.3	1531	0.97	104.0	83.3	21.1	72.6	0.78	0.01	0.6	2365	1.02	67.3	74.1	12.2	193.3	0.43	0.013
0.7	3.1	1453	0.96	109.6	84.1	22.8	63.8	0.81	0.01	-0.9	1896	0.84	84.0	79.3	60.6	31.29	0.91	0.003
323K										**323K**								
Blank	0.9	8946	0.85	17.8	-	18.3	489.8	-	0.01	0.9	8945.8	0.85	17.8	-	18.3	489.8	-	0.009
0.1	0.6	4170	0.95	38.2	53.4	18.3	228.3	0.53	0.01	2.6	1543.0	1.09	103.2	82.8	6.3	244.0	0.50	0.025
0.3	2.4	2097	1.05	76.0	76.6	9.3	225.8	0.54	0.02	2.7	1485.4	1.09	107.2	83.4	6.3	234.9	0.52	0.025
0.5	0.9	1779	1.06	89.5	80.1	8.2	217.1	0.56	0.02	3.4	1529.6	0.92	104.1	82.9	32.1	47.7	0.90	0.005
0.7	-2.1	938	0.91	169.7	89.5	27.2	34.5	0.93	0.01	0.4	1177.8	0.93	135.2	86.8	27.2	43.3	0.91	0.006
333K										**333K**								
Blank	1.2	13823	0.78	11.5	-	16.4	844.7	-	0.01	1.2	13823	0.78	11.5	-	16.4	844.7	-	0.01
0.1	1.5	8740	0.86	18.2	36.8	16.8	521.6	0.38	0.01	1.7	10531	0.84	15.1	23.8	12.6	834.8	0.01	0.01
0.3	1.2	7942	0.87	20.1	42.8	18.3	434.9	0.49	0.01	1.2	8896	0.87	17.9	35.8	12.2	726.5	0.14	0.01
0.5	1.2	7284	0.88	21.9	47.5	18.3	398.9	0.53	0.01	1.4	9226	0.86	17.3	33.5	15.5	596.5	0.29	0.01
0.7	0.5	4346	0.97	36.6	68.6	12.2	355.3	0.58	0.01	1.7	7199	0.90	22.1	48.0	13.1	551.3	0.35	0.01

Table: 4.11 Electrochemical Impedance parameters for corrosion of MS in the absence and presence of different concentrations of TCL and TCF in 1M HCl at room temperature and higher temperatures

Conc (%)	TCL									TCF								
	R_S (Ωcm^2)	Y_0 ($\mu F/cm^2$)	n	R_{ct} (Ωcm^2)	IE (%)	f_{max} (μHz)	CPE/C_{dl} ($\mu F/cm^2$)	θ	τ (S^n)	R_S (Ωcm^2)	Y_0 ($\mu F/cm^2$)	n	R_{ct} (Ωcm^2)	IE (%)	f_{max} (μHz)	CPE/C_{dl} ($\mu F/cm^2$)	θ	τ (S^n)
303K										**303K**								
Blank	0.830	10476	0.84	15.2	-	13.3	789		0.012	0.83	10476	0.84	15.2	-	13.28	789		0.012
0.1	0.766	1788	1.06	89.1	82.9	8.2	218	0.72	0.019	-0.13	8208	0.88	19.4	21.6	13.0	631	0.20	0.012
0.3	0.631	1665	1.07	95.6	84.1	8.2	203	0.74	0.019	1.67	4855	0.98	32.8	53.7	8.9	548	0.31	0.018
0.5	1.803	1220	1.11	130.5	88.4	5.5	222	0.72	0.029	1.78	2435	1.05	65.4	76.8	7.6	320	0.59	0.021
0.7	1.916	1089	1.11	146.2	89.6	5.5	198	0.75	0.029	1.60	1544	1.08	103.1	82.9	7.1	219	0.72	0.023
313K										**313K**								
Blank	1.2	9178	0.83	17.4	-	27.2	337.3	-	0.006	1.2	9178	0.83	17.4	-	27.2	337.3	-	0.006
0.1	2.7	6039	0.87	26.4	34.1	35.9	168.3	0.50	0.004	1.4	3230	1.00	49.3	64.7	12.1	267.5	0.21	0.013
0.3	2.8	2654	0.87	60.0	71.0	53.0	50.1	0.85	0.003	2.3	1910	1.06	83.4	79.1	8.0	239.9	0.29	0.020
0.5	-0.4	1987	0.90	80.1	78.3	40.6	48.9	0.86	0.004	-0.2	1777	0.84	89.6	80.6	60.6	29.3	0.91	0.003
0.7	0.3	1758	0.89	90.6	80.8	40.6	43.3	0.87	0.004	-1.5	1682	0.83	94.7	81.6	60.6	27.8	0.92	0.003
323K										**323K**								
Blank	0.9	8946	0.85	17.8	-	18.3	489.8	-	0.01	0.9	8946	0.85	17.8	-	18.3	489.8	-	0.01
0.1	1.6	3916	1.00	40.7	56.3	9.1	428.9	0.12	0.02	1.6	3049	1.00	52.2	65.9	11.8	257.3	0.48	0.01
0.3	2.9	1802	1.09	88.4	79.9	6.3	285.0	0.42	0.03	3.1	2636	1.01	60.4	70.5	12.6	208.7	0.57	0.01
0.5	1.4	1889	1.02	84.3	78.9	12.2	154.4	0.68	0.01	-0.7	1046	1.02	152.2	88.3	12.2	85.5	0.83	0.01
0.7	-1.4	1010	0.92	157.7	88.7	27.2	37.1	0.92	0.01	4.2	981	0.96	162.3	89.0	19.5	50.2	0.90	0.01
333K										**333K**								
Blank	1.2	13823	0.78	11.5	-	16.4	844.7	-	0.01	1.2	13823	0.78	11.5	-	16.4	844.7	-	0.01
0.1	2.0	10497	0.82	15.2	24.3	23.5	446.8	0.47	0.01	0.7	11472	0.81	13.9	17.3	18.3	628.4	0.26	0.01
0.3	1.6	8846	0.85	18.0	36.1	22.2	399.0	0.53	0.01	1.4	9361	0.83	17.0	32.4	25.3	370.5	0.56	0.01
0.5	1.1	4814	0.96	33.1	65.3	12.2	393.6	0.53	0.01	1.5	6705	0.90	23.8	51.7	18.4	364.6	0.57	0.01
0.7	0.8	4559	0.96	34.9	67.0	12.2	372.6	0.56	0.01	1.5	4592	0.94	34.7	66.9	17.4	264.2	0.69	0.01

❖ **Aluminium alloy 1100 (AA1100) as Working Electrode:**

4.2.3 Potentiodynamic polarisation studies of AA1100 in the presence and absence of SCL/ 1M HCl

The surface dissolution characteristics of AA1100 in the presence and absence of various concentration of SCL are shown in Figure 4.13, while Table 4.12 demonstrates the corresponding electrochemical parameters.

Figure 4.13 demonstrates that the accumulation of the inhibitor to the HCl solution reduces both anodic metal dissolution and cathodic hydrogen evolution reactions, as expected in the presence of various concentrations of SCL. In addition, the anodic and cathodic Tafel slopes show a slight shift in b_a and b_c values in the range of ±15 mV for anodic Tafel slope and ± 50 mV for cathodic Tafel slopes (b_c) with the addition of SCL. This suggests that the inhibition occurred through simple blocking of the available active sites on the metal surface. Inspection of Table 4.12 reflects high I_{corr} values in 1.0 M HCl without inhibitor indicating strong corrosiveness on AA1100 in 1M HCl **(Li and Deng, 2012)**. The reduction in I_{corr} values are more pronounced with the increasing inhibitor concentration. The observed data reflects that I_{corr} values decrease from 0.0145 A/cm^2 for that of the blank to 0.0018 A/cm^2 in the presence of 0.7% SCL. This confirms the inhibitive nature of the extract and also the adsorption of the plant extract on metal surface. The dependence of IE on the inhibitor concentration is also tabulated (Table 4.12). The results imply the enhancement of IE with increasing concentration of the inhibitor. A maximum of 87.6 percentage of inhibition is obtained with 0.7 % SCL. No appreciable shift is recognised in the E_{corr} values in the presence of the inhibitor. This corresponds to a mixed-type mechanism.

Values of R_p increase appreciably with increasing concentration of SCL indicating the effectiveness of the inhibitor in minimising the corrosion of the metal under investigation **(Morad *et al*, 2008)**.The table indicates the shift in R_p values from 2.3 Ohm/cm^2 for the uninhibited solution to 33.5 Ohm/cm^2 for the optimum concentration of the inhibitor (0.7% SCL) . A maximum efficiency of 93.1 percentage is furnished at 0.7% of the extract.

4.2.3.1 Potentiodynamic polarisation measurements of AA 1100 in the presence of SCF / HCl

The potentiodynamic curves for AA1100 in 1M HCl on the presence and absence of SCF are depicted in Figure 4.13. The derived electrochemical parameters are tabulated in Table 4.12.From the data obtained for b_a and b_c values, it is clear that SCF acts as mixed type inhibitor as no remarkable change is noted in the b_a and b_c values. The

b_a and b_c values are found to vary from the blank in the range of ±15 mV for anodic Tafel slope (b_a) and ± 25 mV for cathodic Tafel slope (b_c) indicating the mixed nature of the inhibitor.The similarity in the shape of the anodic and cathodic Tafel curves for the blank and the inhibitor solutions reflects that there is no change in the mechanism of corrosion reaction and the inhibitor acts by simple adsorption mode. **(Fouda, 2012).**

It can be noticed from the table that the I_{corr} values decrease from 0.0141 A/cm^2 (blank) to 0.0017 A/cm^2 (0.7% SCF) and the percentage of IE increases from 9.2 at 0.1% SCF to a maximum of 87.9 at 0.7% SCF . The E_{corr} value doesn't show any reasonable change in the presence of the inhibitor. Thus SCF can be classified as mixed inhibitor. **(Jayaperumal, 2010)**

The data also indicates the fact that linear polarisation resistance values (R_p) increase from 1.5 ohm/cm^2 (blank) to 28.2 ohm/cm^2 in the presence of 0.7% concentration of SCF. This behaviour points out the inhibitory effect of the additive. The inhibitor is found to afford a maximum efficiency of 94.7 at 0.7% SCF.

Table 4.12 : Potentiodynamic polarisation parameters for the corrosion of AA1100 in the absence and presence of different concentrations of SCL / SCF in 1M HCl

S.No.	Conc. (%)	Tafel polarisation parameters					Linear polarisation resistance parameters	
		E_{corr} mV/ SCE	I_{corr} A/cm^2	b_a mV/ decade	b_c mV/ decade	IE (%)	R_p Ohm/cm^2	IE (%)
SCL								
1.	Blank	-904	0.0145	131	264	-	2.3	-
2.	0.1	-938	0.0140	117	247	3.4	2.6	11.5
3.	0.2	-945	0.0136	132	226	6.2	2.5	8.0
4.	0.3	-958	0.0122	121	230	15.9	4.6	50.0
5.	0.4	-918	0.0096	139	256	33.8	4.7	51.1
6.	0.5	-851	0.0079	136	223	45.5	4.5	48.9
7.	0.6	-1059	0.0043	130	205	70.3	14.9	84.6
8.	0.7	-1081	0.0018	117	227	87.6	33.5	93.1
SCF								
1.	Blank	-768	0.0141	123	222	-	1.5	-
2.	0.1	-773	0.0128	122	250	9.2	2.8	46.4
3.	0.2	-791	0.0112	128	229	20.6	3.1	51.6
4.	0.3	-801	0.0076	130	233	46.1	4.7	68.1
5.	0.4	-824	0.0064	126	256	54.6	6.1	75.4
6.	0.5	-1030	0.0055	115	215	61.0	8.7	82.8
7.	0.6	-832	0.0040	123	219	71.6	14.5	89.7
8.	0.7	-764	0.0017	117	247	87.9	28.2	94.7

4.2.3.2 Potentiodynamic polarisation studies of TCL on AA1100 / 1M HCl

Polarisation polarisation studies are carried out to ascertain the interaction between the electrode surface and the inhibitor species and the corresponding figures are depicted in Figure 4.13. The associated electrochemical parameter values namely I_{corr}, E_{corr}, b_a and b_c at 303K for AA1100 in 1M HCl are summarised in Table 4.13. The polarisation curves are presented in Figure 4.13.

The results indicate a shift in b_a and b_c values in the range of ±12 mV for anodic Tafel slope and ± 15 mV for cathodic Tafel slopes (b_c) in the presence of the inhibitor.The results of tafel slopes b_a and b_c and E_{corr} values demonstrate the mixed nature of the inhibitor under study. On comparison of the electrochemical parameters calculated from the polarisation curves of aluminium electrode in different concentrations of TCL with those of the blank values, it is apparent that the I_{corr} values reduce from 0.0141 A/cm^2 (blank) to 0.0030 A/cm^2 (0.7% TCL).A maximum efficiency of 78.7 percentage is obtained at 0.7% concentration of TCL. No drastic changes in the E_{corr} values are noted.

Table 4.13: Potentiodynamic polarisation parameters for the corrosion of AA1100 in the absence and presence of different concentrations of TCL / TCF in 1M HCl

S.No.	Conc. of inhibitor in (%)	Tafel polarisation parameters					Linear polarisation resistance parameters	
		E_{corr} mV/ SCE	I_{corr} A/cm^2	b_a mV/ decade	b_c mV/ decade	IE (%)	R_p Ohm/cm^2	IE (%)
TCL								
1.	Blank	-768	0.0141	123	222	-	1.5	-
2.	0.1	-796	0.0118	124	224	16.3	2.4	37.5
3.	0.2	-788	0.0116	123	234	17.7	2.6	42.3
4.	0.3	-776	0.0106	119	206	24.8	2.5	40.0
5.	0.4	-815	0.0105	120	232	25.5	2.2	31.8
6.	0.5	-809	0.0099	121	214	29.8	3.3	54.5
7.	0.6	-831	0.0079	136	223	44.0	11.5	87.0
8.	0.7	-827	0.0030	121	232	78.7	29.6	94.9
TCF								
1.	Blank	-768	0.0141	123	222	-	1.5	-
2.	0.1	-783	0.0124	98	228	12.1	1.8	16.7
3.	0.2	-781	0.0085	94	204	39.7	2.9	48.3
4.	0.3	-798	0.0082	101	218	41.8	3.5	57.1
5.	0.4	-802	0.0075	123	248	46.8	3.5	57.1
6.	0.5	-798	0.0073	105	212	48.2	12.4	87.9
7.	0.6	-808	0.0041	107	236	70.9	15.5	90.3
8.	0.7	-797	0.0034	90	207	75.9	28.2	94.7

Linear polarisation resistance (R_p) of AA1100 in the absence and presence of TCL are listed in Table 4.13. From R_p values, it can be inferred that as the concentration of TCL increases, the R_p values also increase. Maximum inhibition efficiency is found to be 94.9 percentage.

4.2.3.3 Potentiodynamic polarisation studies of AA1100 / TCF / 1M HCl

Potentiodynamic anodic and cathodic polarisation plots of AA1100 in 1M HCl in the presence and absence of various concentration of TCF are given in Figure 4.13 The respective kinetic parameters including corrosion current density (I_{corr}), corrosion potential (E_{corr}), cathodic Tafel slope (b_c) , anodic Tafel slope (b_a) and inhibition efficiency (IE%) at 303K for 1M HCl are tabulated in Table 4.13.

The nature of polarisation curves remains the same in the presence of the inhibitor .This led to the conclusion that the corrosion mechanism remains unchanged with the addition of the inhibitor. It is illustratedfrom the data of the table that the addition of the inhibitor shifted the anodic (b_a) and cathodic (b_c) slope values towards low corrosion current density. Anodic and cathodic Tafel slopes, b_a and b_c are found to shift in the range of ± 50 mV (b_a) and ± 20 mV (b_c). This reflects the mixed nature of the inhibitor.This indicated that the inhibitor is able to suppress both the anodic dissolution and cathodic hydrogen evolution. I_{corr} values are found to significantly reduce in the presence of the inhibitor. The corrosion current decreases from 0.0141 A/cm^2 for that of the uninhibited solution to 0.0034 A/cm^2 at 0.7% TCF. The IE is found to increase with increase in concentration of the inhibitor affording a maximum efficiency of 75.9 percentage. The negligible shift in the E_{corr} values indicates the mixed nature of the inhibitor under investigation **(Ashassi Sorakbi, 2006)**.

R_p increases with addition of inhibitor, which indicates that the electrode exhibits slower corrosion in the presence of inhibitor. Polarisation resistance values of the AA1100 / TCF / 1M HCl system depict that the values of R_p increases from 1.5 (blank) to 28.2 ohm/cm^2 in the presence of 0.7% TCF. Inhibition performance of TCF is found to be 94.7 percentage.

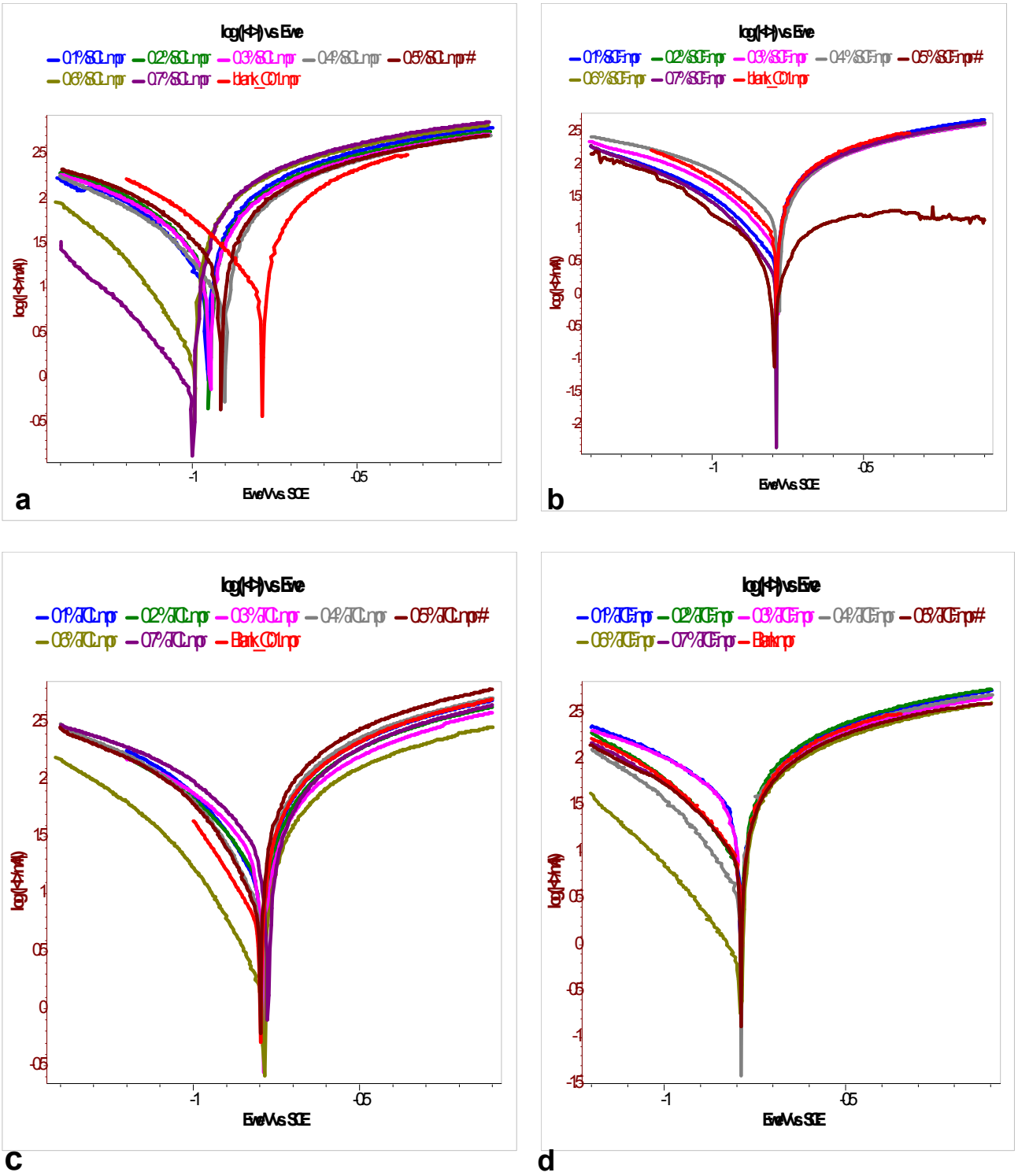

Figure 4.13 Potentiodynamic polarisation plots of AA1100 in 1M HCl in absence and presence of (a) SCL (b) SCF (c) TCL (d) TCF extracts

4.2.3.4 Potentiodynamic polarisation studies at higher temperatures on AA1100/HCl/ Inhibitors

To investigate the mechanism of inhibition and to calculate the activation energies of the corrosion process, polarisation measurements are obtained at different temperatures in the absence and presence of different concentrations of SCL / SCF /TCL / TCF. The results obtained from the polarisation curves (Figures 4.14 and 4.15) are tabulated in Tables 4.14 and 4.15 .The corrosion potential shifted ± 25mV anodically and ± 50 mV cathodically for all investigated temperatures compared to the blank indicating that the investigated extracts act as mixed inhibitors. In the studied temperature range (303K - 333K) the corrosion current density (I_{corr}) decrease and the polarisation resistance (R_p) increases with increasing temperature till 313K and then the corrosion current density (I_{corr}) increases and the polarisation resistance (R_p) decreases with increase of temperature. The corrosion current density of AA1100 increases more rapidly with temperature in the absence of the inhibitor. The inhibition efficiencies calculated from the polarisation resistance (R_p) show the same trend as those obtained from corrosion current ($I_{corr.}$)These results confirm that extracts of SCL / SCF / TCL / TCF act as efficient inhibitors in the range of temperature studied **(Benali *et al*, 2014)**. The decrease in inhibition efficiency at higher temperature reveals that the film formed on the metal surface is less protective at higher temperatures, since the desorption rate of the inhibitor is greater at higher temperatures (**Djeddi *et al*, 2014).**

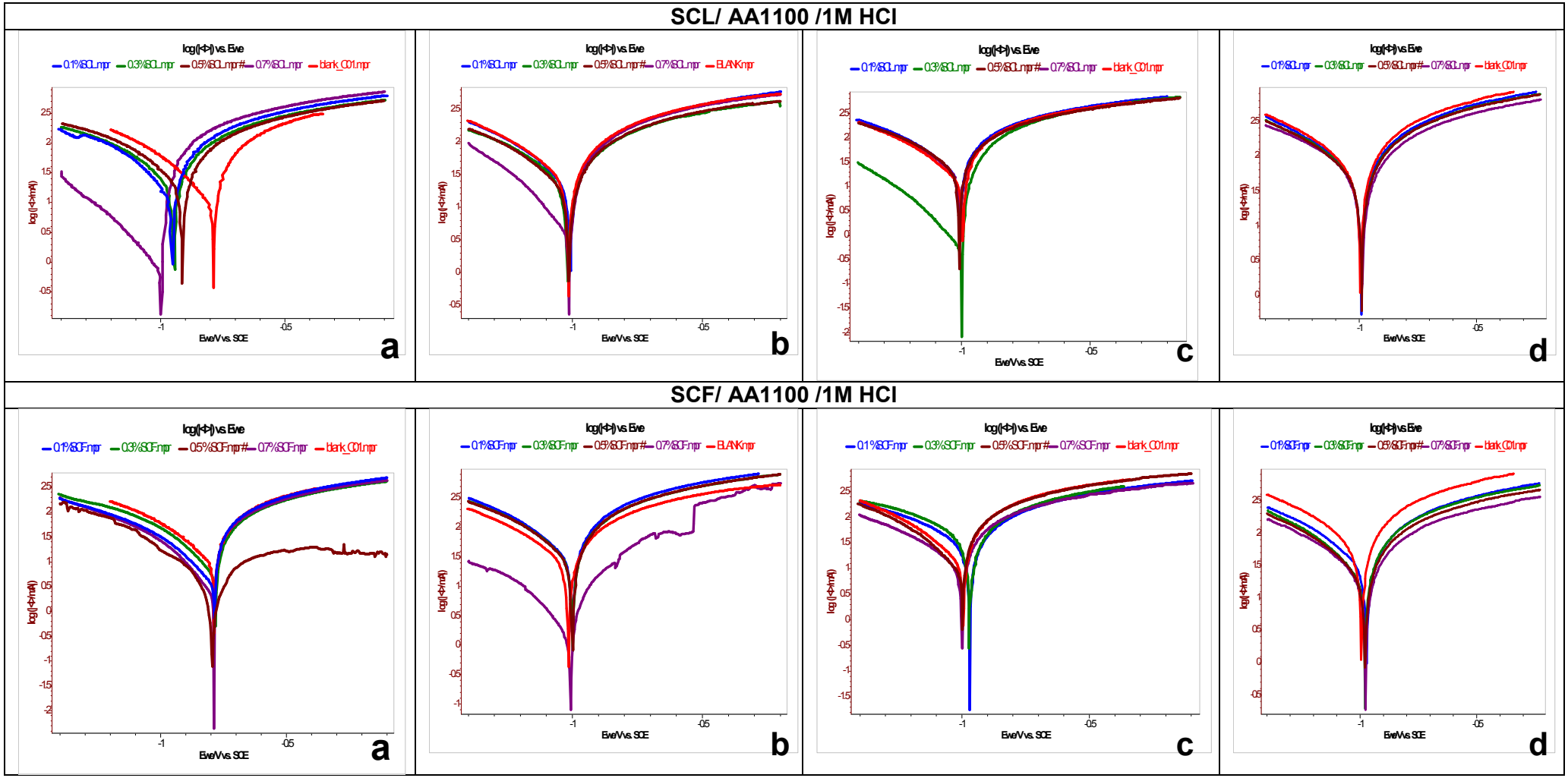

Figure 4.14 Potentiodynamic polarisation plots of AA1100 in 1M HCl in absence and presence of SCL and SCF at (a) 303K (b) 313K (c) 323K and (d) 333K

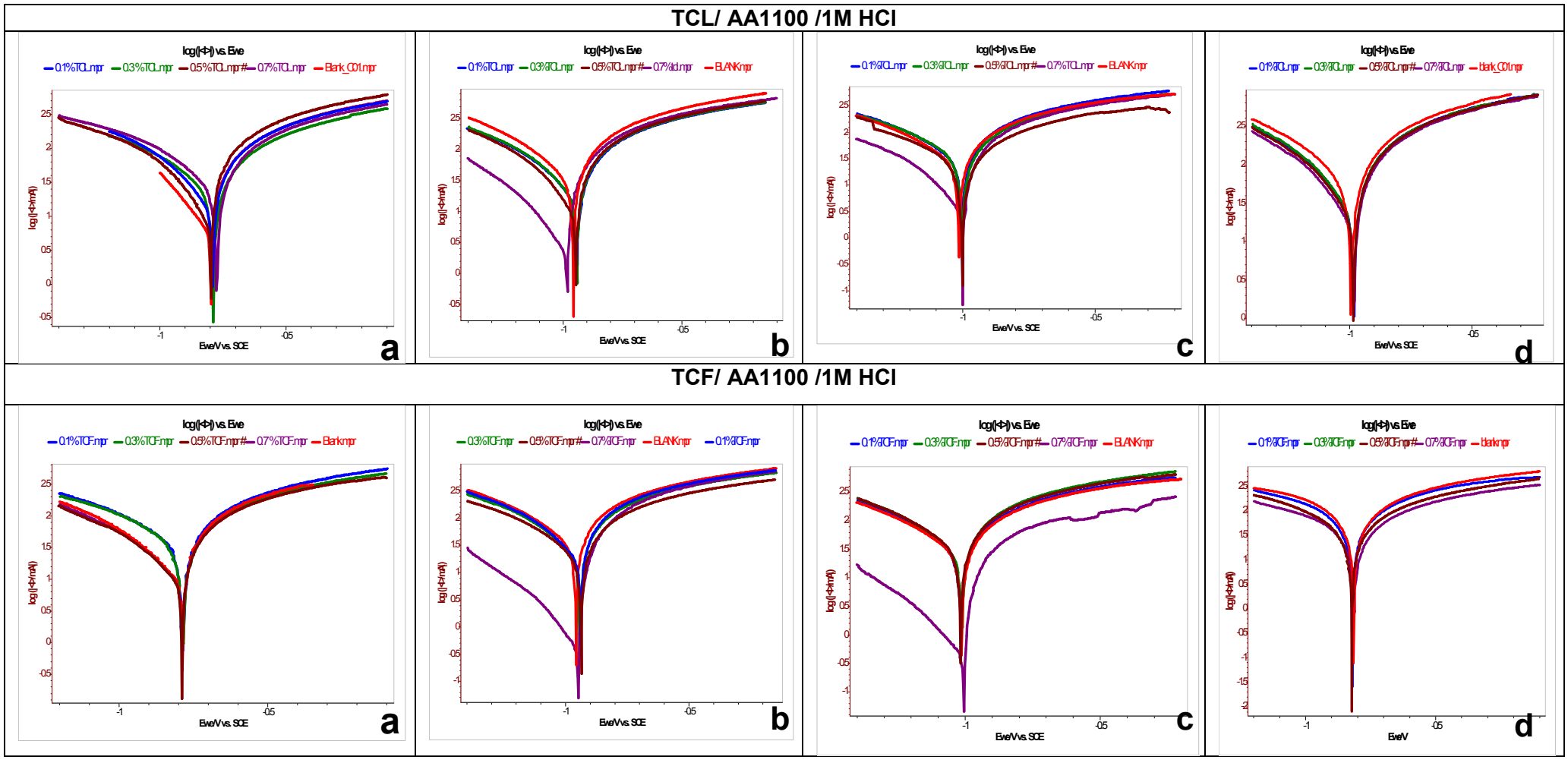

Figure 4.15 Potentiodynamic polarisation plots of AA1100 in 1M HCl in absence and presence of TCL and TCF at (a) 303K (b) 313K (c) 323K and (d) 333K

Table 4.14: Potentiodynamic polarisation parameters for corrosion of AA1100 in the absence and presence of different concentrations of SCL / SCF at room temperature and higher temperatures

Conc (%)	SCL							SCF						
	Tafel					Polarisation parameters		Tafel					Polarisation parameters	
	E_{corr} mV/ SCE	I_{corr} A/cm^2	b_a mV/ decade	b_c mV/ decade	IE (%)	R_p Ohm/cm^2	IE (%)	E_{corr} mV/ SCE	I_{corr} A/cm^2	b_a mV/ decade	b_c mV/ decade	IE (%)	R_p Ohm/cm^2	IE (%)
303K								**303K**						
Blank	-904	0.0145	131	264	-	2.3	-	-768	0.0141	123	222	-	1.5	-
0.1	-938	0.0140	117	247	3.4	2.6	11.5	-773	0.0128	122	250	9.2	2.8	46.4
0.3	-958	0.0122	121	230	15.9	4.6	50.0	-801	0.0076	130	233	46.1	4.7	68.1
0.5	-851	0.0079	136	223	45.5	4.5	48.9	-1030	0.0055	115	215	61.0	8.7	82.8
0.7	-1081	0.0018	117	227	87.6	33.5	93.1	-764	0.0017	117	247	87.9	28.2	94.7
313K								**313K**						
Blank	-1000	0.0165	118	267	-	1.2	-	-989	0.0172	115	182	-	1.1	-
0.1	-999	0.0141	115	241	14.5	2.3	47.8	-998	0.0147	88	130	14.5	1.7	35.3
0.3	-1000	0.0118	109	252	28.5	2.7	55.6	-1001	0.0167	117	153	2.9	1.9	42.1
0.5	-1009	0.0118	123	219	28.5	3.9	69.2	-1002	0.0135	101	127	21.5	1.9	42.1
0.7	-1048	0.0066	143	274	60.0	5.8	79.3	-1028	0.0016	134	178	90.7	9.7	88.7
323K								**323K**						
Blank	-994	0.0142	121	147	-	2.1	-	-780	0.0119	136	223	-	1.6	-
0.1	-958	0.0113	104	209	20.4	3.6	41.7	-814	0.0075	137	206	37.0	2.2	27.3
0.3	-965	0.0105	103	133	26.1	5.1	58.8	-820	0.0052	101	212	56.3	2.1	23.8
0.5	-1021	0.0096	131	196	32.4	7.1	70.4	-790	0.0021	74	167	82.4	9.8	83.7
0.7	-1002	0.0059	81	139	58.5	12.0	82.5	-778	0.0018	126	199	84.9	14.3	88.8
333K								**333K**						
Blank	-985	0.0283	120	238	-	0.8	-	-985	0.0283	120	238	-	0.8	-
0.1	-984	0.0233	128	221	17.7	1.3	38.5	-977	0.0118	109	128	58.3	2.1	61.9
0.3	-984	0.0197	126	183	30.4	1.4	42.9	-982	0.0103	103	140	63.6	2.6	69.2
0.5	-988	0.0185	125	166	34.6	1.5	46.7	-982	0.0098	111	148	65.4	3.4	76.5
0.7	-977	0.0172	126	194	39.2	1.7	52.9	-977	0.0088	119	159	68.9	5.1	84.3

Table 4.15: Potentiodynamic polarisation parameters for corrosion of AA1100 in the absence and presence of different concentrations of TCL / TCF at room temperature and higher temperatures

Conc (%)	TCL							TCF						
	Tafel					Polarisation parameters		Tafel					Polarisation parameters	
	E_{corr} mV/ SCE	I_{corr} A/cm^2	b_a mV/ decade	b_c mV/ decade	IE (%)	R_p Ohm/cm^2	IE (%)	E_{corr} mV/ SCE	I_{corr} A/cm^2	b_a mV/ decade	b_c mV/decade	IE (%)	R_p Ohm/cm^2	IE (%)
303K								**303K**						
Blank	-768	0.0141	123	222	-	1.5	-	-768	0.0141	123	222	-	1.5	-
0.1	-796	0.0118	124	224	16.3	2.4	37.5	-783	0.0124	98	128	12.1	1.8	16.7
0.3	-776	0.0106	119	206	24.8	2.5	40.0	-798	0.0082	99	118	41.8	3.5	57.1
0.5	-809	0.0099	121	214	29.8	3.3	54.5	-798	0.0073	95	112	48.2	12.4	87.9
0.7	-827	0.0030	121	232	78.7	29.6	94.9	-797	0.0034	90	107	75.9	28.2	94.7
313K								**313K**						
Blank	-1000	0.0165	118	267	-	1.2	-	-1000	0.0165	118	267	-	1.2	-
0.1	-1007	0.0117	118	131	29.1	2.0	40.0	-1013	0.0134	100	131	18.8	2.1	42.9
0.3	-1002	0.0111	117	141	32.7	1.4	14.3	-1017	0.0109	94	138	33.9	2.2	45.5
0.5	-1000	0.0115	108	132	30.3	2.9	58.6	-1016	0.0074	101	138	55.2	2.1	42.9
0.7	-1015	0.0017	81	146	89.7	7.3	83.6	-1049	0.0032	90	149	80.6	44.0	97.3
323K								**323K**						
Blank	-994	0.0142	121	148	-	2.1	-	-994	0.0145	121	148	-	2.1	-
0.1	-945	0.0093	91	132	34.5	2.7	22.2	-944	0.0140	99	161	3.4	2.2	4.5
0.3	-944	0.0088	88	126	38.0	2.6	19.2	-943	0.0136	95	145	6.2	2.3	8.7
0.5	-960	0.0079	99	133	44.4	3.3	36.4	-939	0.0102	91	127	29.7	5.8	63.8
0.7	-1014	0.0028	79	156	80.3	10.0	79.0	-1013	0.0056	67	172	61.4	30.2	93.0
333K								**333K**						
Blank	-985	0.0283	120	238	-	0.8	-	-812	0.0165	113	143	-	1.1	-
0.1	-991	0.0161	110	139	43.1	1.0	20.0	-813	0.0132	98	139	20.0	1.5	26.7
0.3	-984	0.0141	84	131	50.2	1.6	50.0	-816	0.0116	107	132	29.7	1.3	15.4
0.5	-989	0.0137	89	143	51.6	1.8	55.6	-819	0.0100	116	139	39.4	1.7	35.3
0.7	-987	0.0124	95	156	56.2	2.0	60.0	-810	0.0081	98	131	50.9	2.6	57.7

4.2.4 Electrochemical Impedance spectroscopy of AA1100

4.2.4.1 Electrochemical Impedance spectroscopy Studies in the Presence of different concentration of SCL & SCF on AA1100/1M HCl

i) SCL / AA1100 / 1M HCl

Typical Nyquist and Bode plots obtained when an AA1100 sample is immersed in 1M HCl solution in the presence and absence of various concentrations of SCL are depicted in Figure 4.16 and tabulated in Table 4.16. The figures reflect that the impedance spectra consists of a large capacitive loop at high frequency (HF) followed by a large inductive one at low frequency values. Several authors have noticed a small inductive loop at low frequency (LF) for aluminium in hydrochloric acid **(Yurt *et al*, 2006; Zhang *et al*, 2010)** with lesser diameter compared to that of the capacitive loop. In the present case,it can be seen that the impedance spectra yield an elliptical shape and a broad peak is observed in the Bode format. Similar impedance plots have been reported of aluminium **(Garrigues *et al*, 1996)** and aluminium alloy **(Noor *et al*, 2009)** in HCl media either without or with organic compounds. The addition of the inhibitor onto the corrodent solution did not produce any discerning effect on the shape of the Nyquist plots. This indicates a similar corrosion mechanism in the presence of the inhibitor also.

A considerable increase in the size of the capacitive and inductive loops is noted with increase in inhibitor concentration. This suggests the increase of impedance with addition of SCL lowers the corrosion of AA1100. The high frequency loops are not perfect semicircle in appearance. This might be attributed to the frequency dispersion as a result of the roughness and inhomogeneous of electrode surface .R_{ct} values are found to vary from 5.9 Ωcm^2 for that of the blank to 131.9 Ωcm^2 to that of the inhibitor. A maximum of 95.5 percentage IE is afforded by 0.7% of the inhibitor. C_{dl} decreases from 124 $\mu F/cm^2$ (blank solution) to 20.8 $\mu F/cm^2$ (0.7% SCL) .This might be due to the decrease in local dielectric constant and/or an increase in the thickness of the electrical double layer, suggesting that the inhibitor molecules function by adsorption at the metal / solution interface. **(Li *et al*, 2012)**

ii) SCF / AA1100/ 1M HCl

The Nyquist diagrams for AA1100 in 1.0 M HCl without and with various concentrations of SCF are presented in Figure 4.16 and the corresponding parameters are tabulated in Table 4.17. The impedance spectra consist of a large capacitive loop at high frequency (HF) followed by a large inductive one at low frequency values. Impedance plots of similar nature have been reported for aluminium **(Garrigues *et al*, 1996; Ge *et al*, 2008)**

and aluminium alloy **(Noor, 2009; Pinto *et al*, 2011)** in HCl media either without or with organic compounds. The shape of the impedance spectra is the same even after the addition of the inhibitor, indicating that there is almost no change in the corrosion mechanism due to the addition of the inhibitor. The sizes of both capacitive and inductive loops increase significantly with an increase in inhibitor concentration. This suggests that the impedance of inhibited substrate increases with concentration, which in turn leads to lower corrosion of AA1100. **(Deng and Li, 2012).** Noticeably, these high frequency loops are not perfect semicircles which can be attributed to the frequency dispersion as a result of the roughness and inhomogeneous of electrode surface. **(Lebrini *et al*, 2007)**. R_{ct} values increase with increasing concentration of the inhibitor (Table 4.17). IE increases with the concentration of SCF and the maximum IE reaches up to 98.6 %, which further confirm that SCF exhibits good inhibitive performance for AA1100 in 1.0 M HCl .The decrease in C_{dl} values on the addition of the inhibitor can result from a decrease in local dielectric constant and/or an increase in the thickness of the electrical double layer, suggesting that the inhibitor molecules function by adsorption at the metal / solution interface **(Lorenz *et al*, 1981; Lagrene *et al*,2002)**

4.2.4.2 Electrochemical Impedance response of AA1100 electrode in the presence of different concentrations of TCL & TCF extracts

i) TCL/AA1100/ 1M HCl

Nyquist plots for the uninhibited and inhibited solutions containing various concentrations of TCL in 1M HCl are depicted in Figure 4.17 and the corresponding parameters are collected in Table 4.18 .A high frequency capacitive loop and a low frequency inductive loop are noted in the impedance spectra. R_s values are very small indicating that the IR drop could be small.

Bode plots confirm the presence of a single time constant. A comparison between the result of R_{ct} at uninhibited solution and inhibited solution shows an increase in R_{ct} values with increasing concentration of the inhibitor. The R_{ct} values increase from 1.6 Ωcm^2 to 42.2 Ωcm^2 affording an efficiency of 96.1 percentage at 0.7% concentration The C_{dl} values decrease with addition of the inhibitor from 195 $\mu F/cm^2$ (blank solution) to 33 $\mu F/cm^2$ (0.7% SCF) that might be due a decrease in local dielectric constant and/or an increase in the thickness of the electrical double layer. This indicates that the inhibitor molecules function by adsorption of phytochemical constituents of the extract onto the metal surface at the metal / solution interface. **(Li *et al*, 2012)**

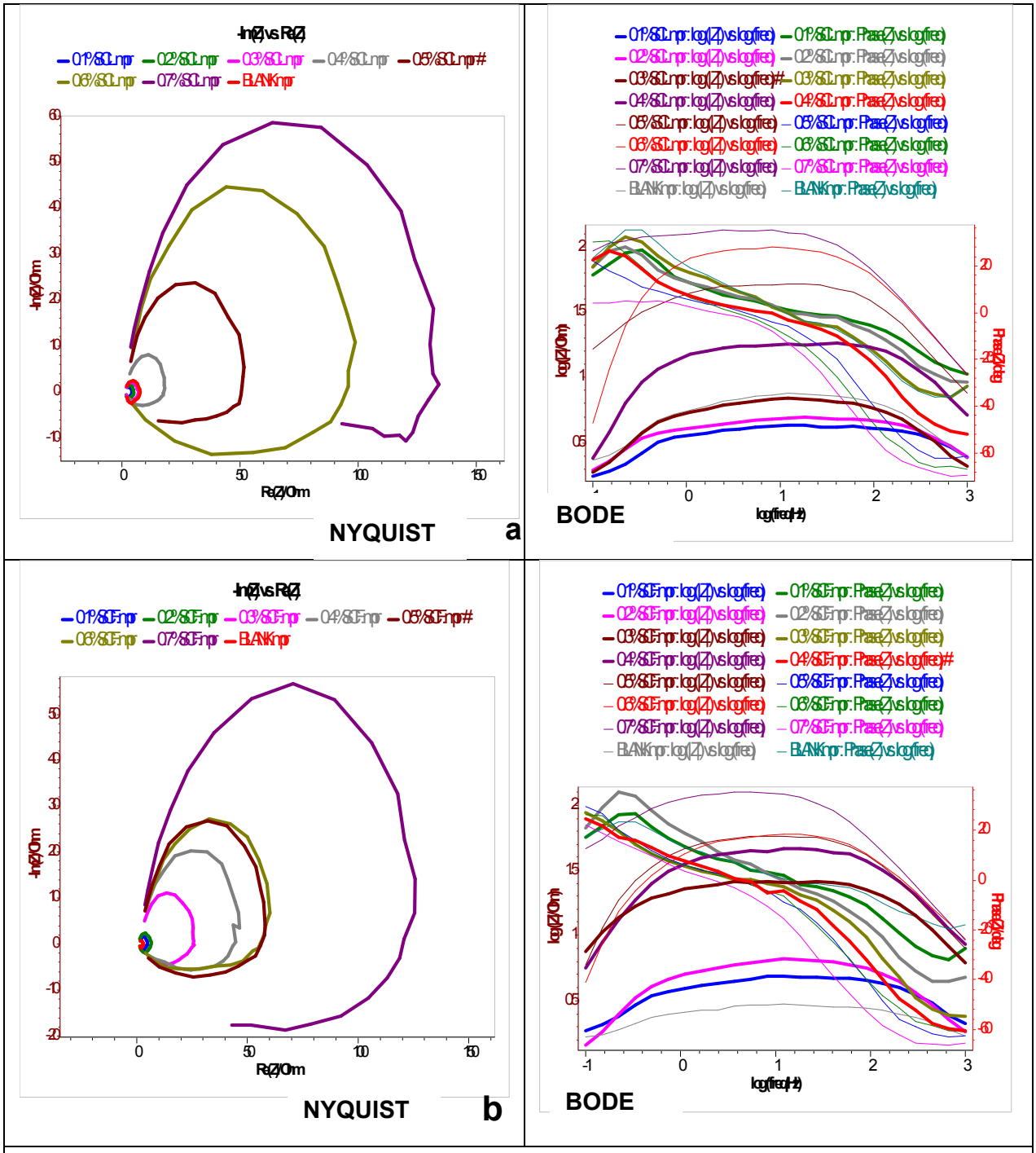

Figure 4.16 Impedance response of AA1100 Electrode in the absence and presence of (a) SCL (b) SCF in Nyquist and Bode format

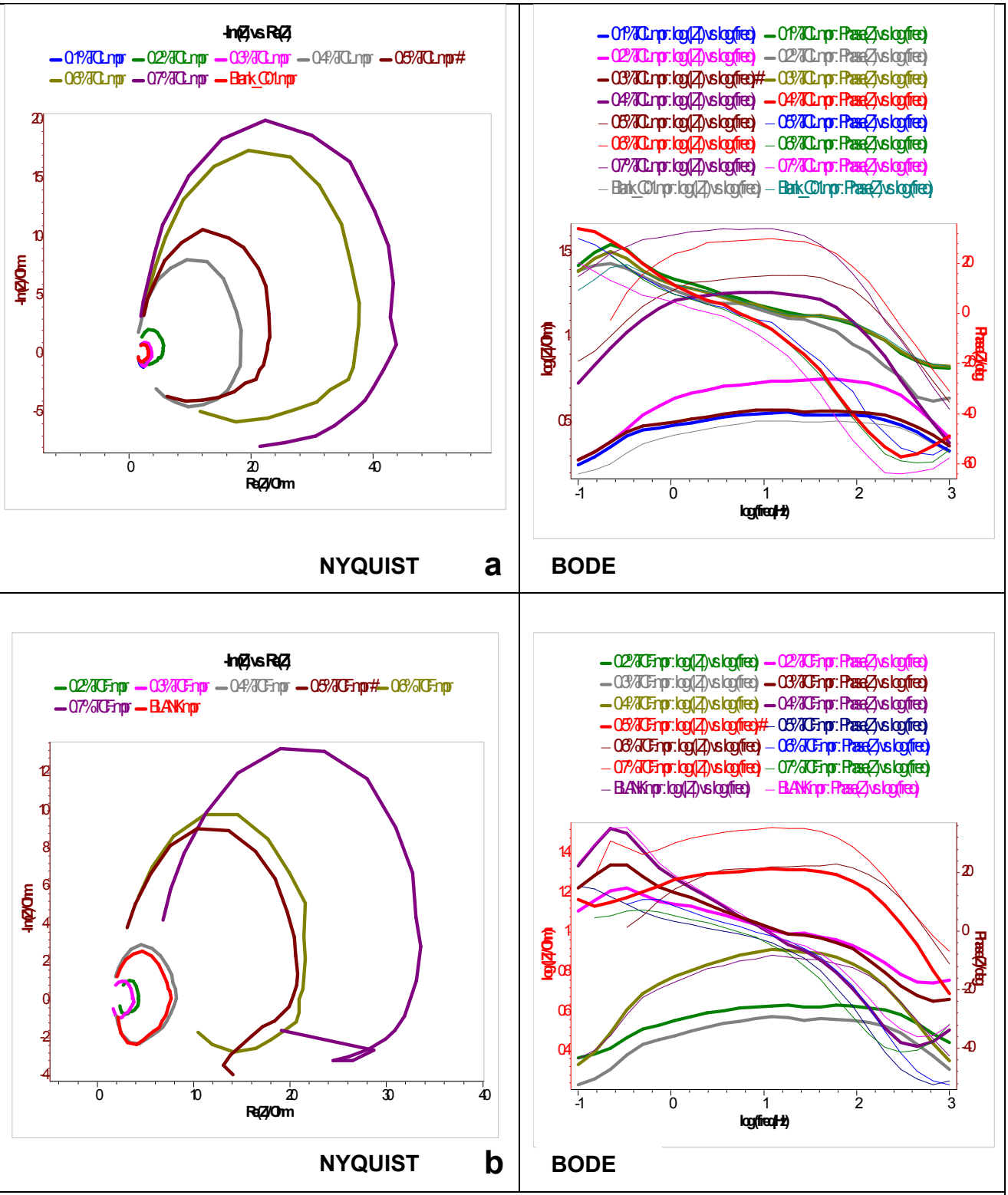

Figure 4.17 Nyquist and Bode plots of AA1100 Electrode in the absence and presence of (a) TCL (b) TCF

Table 4.16: Electrochemical Impedance parameters for corrosion of AA1100 in the absence and presence of different concentrations of SCL in 1M HCl

Conc (%)	R_S (Ωcm^2)	Y_0 ($\mu F/cm^2$)	n	R_{ct} (Ωcm^2)	IE (%)	f_{max} (μHz)	CPE/C_{dl} ($\mu F/cm^2$)	θ	τ (S^n)	L	RL
Blank	1.6	26998	0.56	5.9	-	218	124.0	-	0.0007	1.0	0.4
0.1	0.3	26812	0.50	6.0	1.7	302	26.1	0.79	0.0005	1.9	3.3
0.2	1.0	26659	0.49	6.1	3.3	663	20.4	0.84	0.0002	2.9	5.6
0.3	0.5	24555	0.52	6.5	9.2	755	28.7	0.77	0.0002	1.9	1.7
0.4	0.4	8457	0.69	18.8	68.6	264	31.9	0.74	0.0006	5.6	4.4
0.5	3.2	3103	0.77	51.3	88.5	119	32.5	0.74	0.0013	18.4	22.5
0.6	2.3	1581	0.80	100.7	94.1	76	30.2	0.76	0.0021	17.3	7.7
0.7	1.1	1207	0.81	131.9	95.5	59	20.8	0.83	0.0027	252.9	391.3

Table 4.17 Electrochemical Impedance parameters for corrosion of AA1100 in the absence and presence of different concentrations of SCF in 1M HCl

Conc (%)	R_S (Ωcm^2)	Y_0 ($\mu F/cm^2$)	n	R_{ct} (Ωcm^2)	IE (%)	f_{max} (μHz)	CPE/C_{dl} ($\mu F/cm^2$)	θ	τ (S^n)	L	RL
Blank	1.02	83108	0.25	1.9	-	533	156.0	-	0.0003	0.7	0.4
0.1	0.19	22712	0.60	7.0	72.9	205	111.0	0.29	0.0008	1.2	2.7
0.2	0.08	31463	0.51	5.1	54.2	511	61.6	0.61	0.0003	1.5	1.7
0.3	3.47	7141	0.72	22.3	91.5	202	35.3	0.77	0.0008	9.6	1.5
0.4	5.70	2913	0.81	54.7	97.3	90	32.3	0.79	0.0018	11.4	15.8
0.5	-3.42	2625	0.79	60.7	97.5	100	26.2	0.83	0.0016	11.7	3.5
0.6	4.27	2604	0.79	61.1	97.5	101	25.7	0.84	0.0016	12.6	3.3
0.7	0.10	1180	0.84	135.0	98.6	47	25.1	0.84	0.0034	63.0	58.4

Table 4.18 Electrochemical Impedance parameters for corrosion of AA1100 in the absence and presence of different concentrations of TCL in 1M HCl

Conc (%)	R_S (Ωcm^2)	Y_0 ($\mu F/cm^2$)	n	R_{ct} (Ωcm^2)	IE (%)	f_{max} (μHz)	CPE/C_{dl} ($\mu F/cm^2$)	θ	τ (S^n)	L	RL
Blank	1.6	97871	0.19	1.6	-	502	195.0	-	0.0003	0.28	0.0045
0.1	1.6	86967	0.23	1.8	11.1	547	159.0	0.18	0.0003	0.78	0.17
0.2	2.1	48562	0.42	3.3	50.4	342	142.0	0.27	0.0005	0.68	0.24
0.3	0.4	47392	0.42	3.4	51.6	482	98.4	0.50	0.0003	1.25	2.32
0.4	0.6	8359	0.74	19.1	91.5	146	57.1	0.71	0.0011	6.95	4.61
0.5	1.6	7030	0.76	22.7	92.8	131	53.5	0.73	0.0012	6.19	7.11
0.6	1.1	4103	0.81	38.8	95.8	91	44.9	0.77	0.0017	10.97	18.72
0.7	1.5	3775	0.79	42.2	96.1	114	33.0	0.83	0.0014	49.82	17.54

Table 4.19: Electrochemical Impedance parameters for corrosion of AA1100 in the absence and presence of different concentrations of TCF in 1M HCl

Conc (%)	R_S (Ωcm^2)	Y_0 ($\mu F/cm^2$)	n	R_{ct} (Ωcm^2)	IE (%)	f_{max} (μHz)	CPE/C_{dl} ($\mu F/cm^2$)	θ	τ (S^n)	L	RL
Blank	1.6	67587	0.32	2.4	-	545	124.0	-	0.0003	1.0	0.4
0.1	0.7	67160	0.32	2.5	0.6	564	119.0	0.04	0.0003	1.5	1.3
0.2	1.9	49360	0.41	3.2	27.0	499	99.0	0.20	0.0003	0.6	0.5
0.3	0.4	26998	0.53	5.9	60.1	552	48.9	0.61	0.0003	1.2	2.1
0.4	1.4	24456	0.54	6.5	63.8	549	44.6	0.64	0.0003	1.5	1.8
0.5	0.8	7806	0.73	20.4	88.5	176	44.4	0.64	0.0009	16.9	22.2
0.6	1.3	7455	0.72	21.4	89.0	200	37.2	0.70	0.0008	3.7	21.4
0.7	5.8	5326	0.72	29.9	92.1	209	25.5	0.79	0.0008	5.1	42.0

ii) TCF/AA1100/ 1M HCl

Important mechanistic and kinetic information can be obtained from EIS technique for an electrochemical system under evaluation. Nyquist impedance plots for AA1100 electrode in 1M HCl in the presence and absence of different concentrations of TCF extract are given in Figure 4.17 and the data obtained from these plots are tabulated in Table 4.19. As can be observed from the figure, the impedance diagrams show semicircles, indicating that the corrosion process is mainly charge transfer controlled. The impedance spectra consists of a capacitive loop at high frequencies (HF) and an inductive loop at low frequencies (LF). It is worth noting that similar Nyquist profiles are also observed the system containing various concentration of the inhibitor .This signifies that the corrosion mechanism remains the same in the presence of the inhibitor also. The high frequency capacitive loop could be assigned to the charge transfer of the corrosion process and to the formation of oxide layer particularly, the reaction of aluminium oxidation at the metal/ oxide / electrolyte interface. The LF inductive loop may be related to the relaxation process obtained by adsorption and incorporation of sulfate ions, oxide ions and charged intermediates on and into the oxide film. **(Pinto *et al*, 2011).** As the inhibitor concentration increases, the R_{ct} values also increase while the C_{dl} values decrease. The presence of TCF extract increases the R_{ct} values from 2.4 Ωcm^2 to 29.9 Ωcm^2 affording an efficiency of 92.1 percentage at 0.7% concentration.The decrease in C_{dl} values with increase in concentration of the inhibitor ie from 124 $\mu F/cm^2$ (blank solution) to 25.5 $\mu F/cm^2$ (0.7% TCF) reflects that the metal surface is efficiently covered by the adsorbed inhibitor and thus obtained protection from the acid corrosion.

Analysis of Impedance Spectral data for AA1100 / SCL / SCF / TCL / TCF systems

The capacitive loop at HF could be assigned to the formation of oxide layer on Al. According to **Mansfeld *et al* , 1987; Bessone *et al* ,1983; Wit and Lenderink ,1996 and Brett 1992** , an oxide free Al surface is very difficult to produce. Even if producing such a surface, it repassivates very fast by O_2 to form the oxide layer **(Burstein *et al*, 1992)**. The capacitive loop at HF corresponded to the interfacial reactions, particularly, the reaction of aluminium oxidation at the metal/ oxide / electrolyte interface **(Bret *et al*, 1992)**. In the present system, formation of Al^+ ions at the metal/oxide interface occurs due to the dissolution of the oxide layer in the presence of 1.0 M HCl .Migration of Al^+ occurs through the oxide/solution interface wherein they are further oxidized to Al^{3+}. The complex of [metal-oxide-hydroxide-inhibitor]$_{ads}$ could also be formed in the presence of inhibitor **(Metlkoš-Hukovic´ ,1998)**. All the above said processes are represented by only one loop that could be attributed either to the overlapping of the loops of processes, or to the assumption that one process dominates and, therefore, excludes the other processes **(de Wit 1996)**.

The presence of the large inductive loop at low frequency might be due to the relaxation of adsorbed charged intermediates **(Amin *et al*, 2009)**. This is found to be more pronounced when the intermediates such as H_{ads}^{+} **(Lenderink, 1993)**, Cl^-, O^{2-} ion or inhibitor species **(Quraishi *et al*, 2010)** are strongly adsorbed onto the electrode surface. It might be also attributed to the re-dissolution of the oxide layer surface or Al-dissolution at low frequencies **(Bessone *et al*, 1992)**.

Impedance analysis is a powerful tool for the mechanistic analysis of interfacial processes **(Girija *et al*, 2006)**.The impedance spectra obtained from Nyquist plots are analysed by fitting into the equivalent circuit model in Figure 4.18 that is used elsewhere to describe aluminium / acid interface.**(Li *et al*, 2013)**. Rs, R_{ct} and RL reflect the solution resistance, charge transfer resistance and inductive resistance, respectively connected with the capacitive loop. L is the inductance that is correlated with the inductive loop. Inductive elements are commonly observed for aluminium impedance behaviour in acid solution **(Yurt *et al* ,2006 ; Metikos *et al*, 2002)** . The impedance values of CPE are calculated by

$$Z_{CPE} = 1/Y_0 (j\omega)^n \qquad \textbf{(4.8)}$$

where Y_o is the CPE constant (in Ω^{-1} s^n cm^{-2}), ω is the angular frequency (in rad s^{-1}),j is the imaginary root and n the exponential term.

In general, the impedance loops measured are often depressed semi circles with centres below the real axis. This kind of phenomena is known as dispersing effect. Considering that the impedance of a double layer does not behave as an ideal capacitor in the presence of a dispersing effect, a CPE is used as a substituent for a capacitor to fit more accurately the impedance behaviour of the electrical double layer. **(Li *et al*, 1999)** The impedance parameters, namely charge-transfer resistance (R_{ct}),inductive resistance RL, the constant phase element (Y_o) related to the capacity of the double layer and the exponent (n), relevant to the capacitive and inductive loops of the AA1100/ 1M HCl/ inhibitor system are given in Tables 4.16 - 4.19. These parameters are calculated from the non-linear least square fit combined with randomisation at 5000 iterations of the equivalent circuit shown in Figure 4.18

Simulation of Nyquist plots with above model indicats excellent agreement with experimental data .It means that the suggested equivalent circuit model, presented in Figure 4.18 , could reasonably represent the charge-transfer and metal / solution interface features related to the corrosion process of in acidic solution containing SCL / SCF / TCL / TCF extracts.

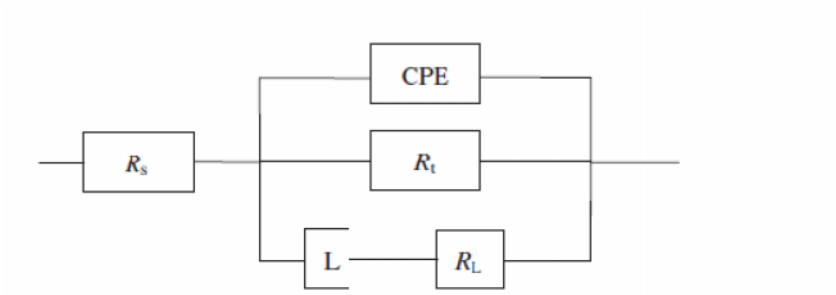

Figure 4.18 Proposed equivalent circuit model for AA1100 /Inhibitors / 1M HCl (Li *et al*, 2012)

With the help of the equivalent circuit, the polarisation resistance (Rp) can be calculated as follows

$$Rp = \frac{R_{ct} x RL}{R_{ct} + RL} \qquad \textbf{(4.9)}$$

The interface time constant (τ) and the double layer capacitance value (C_{dl}) of the CPE can be calculated by the following equations (**Guo Gao *et al*, 2007).**

$$C_{dl} = (Y_o R_{ct}^{1-n})^{1/n} \qquad \textbf{(4.10)}$$

$$Y_o = \frac{\tau^n}{R_{ct}} \qquad \textbf{(4.11)}$$

After analyzing the impedance results (Tables 4.16-4.19), it is obvious that the charge-transfer resistance value, Rct, increases with the concentration of SCL / SCF / TCL / TCF and reaches a maximum value at 0.7%. A large charge-transfer resistance is associated with a slower corroding system, due to a decrease in the active surface necessary for the corrosion reaction. The increase of the n value after addition of in the corrosive solution can corroborate this conclusion. Indeed, the lower n value for uninhibited solution (n = 0.78) indicates a surface inhomogeneity resulting from surface metal roughening and / or formation on the surface of corrosion products. The values of n lies between 0.9-1.1 in the case of inhibited solutions. Addition of SCL / SCF / TCL / TCF increases n value indicating reduction of surface inhomogeneity due to the adsorption of molecules on the most active adsorption sites at the AA1100 surface. Also, the addition of the inhibitors to the corrosive solution decreases the double layer capacitance (C_{dl}) and it increases the time constant (τ) value (Tables 4.16-4.19). For example, when the concentration increases to 0.7% in the corrosive medium (1M HCl), the interface (τ) parameter increases while the capacitance (C_{dl}) value decreases signifying that the charge and discharge rates to the metal–solution interface greatly decreases. This shows that there is agreement between the amount of charge that can be stored (i.e. capacitance) and the discharge velocity in the interface (τ). The double layer between the charged metal surface and the solution is considered as an electrical capacitor. The adsorption of the inhibitor molecules on the AA1100 surface decreases its electrical capacity because they displace the water molecules and other ions originally adsorbed on the surface. The decrease in this capacity with increase in concentration may be attributed to the formation of a protective layer on the electrode surface. The thickness of this protective layer increases with increase in inhibitor concentration, since more of the inhibitor species will electrostatically adsorb on the electrode surface, resulting in a noticeable decrease in C_{dl}. This trend is in accordance with Helmholtz model, given by the following equation

$$C_{dl} = \frac{\varepsilon \, \varepsilon_o}{d} \qquad \textbf{(4.12)}$$

where d is the thickness of the protective layer, ε is the dielectric constant of the protective layer and ε_o is the permittivity of free space (8.854×10^{-14} Fcm^{-1}).

The shape of the Bode plots is related to the thickness and the dielectric properties of the film formed on the AA1100 electrode. In the high-frequency region the phase angle approaches 0° while in the middle frequency region the capacitive behavior of the system is

evident for all concentrations, determined by the dielectric properties of the formed film. Also, depression of phase angle at relaxation frequency occurs at lower concentration of SCL / SCF / TCL / TCF resulting in decrease of capacitive response with the decrease of inhibitor concentration. Such a phenomenon could be attributed to higher corrosion activity at low concentrations of inhibitors. The increase of absolute impedance at low frequencies in Bode plot confirms the higher protection with increasing the concentration of inhibitors, which is related to adsorption of inhibitors on the AA1100 surface. **(Mahdavian and Attar, 2006)**

As it can be seen from Tables 4.16 - 4.19, the R_{ct} values increase with the increasing the concentration of the inhibitors. On the other hand, the values of C_{dl} decrease with an increase in the inhibitors concentration. This decrease in the C_{dl}, which can result from a decrease in local dielectric constant and/or an increase in the thickness of the electric double layer, suggests that the molecules function by adsorption at the metal /solution interface. Thus, the change in C_{dl} values is due to gradual replacement of water molecules by the adsorption of the molecules on the metal surface, decreasing the extent of the metal dissolution **(Bentiss *et al,* 2005)**

4.2.4.3 Electrochemical Impedance spectroscopy Studies in the Presence of different concentration of SCL / SCF / TCL / TCF at higher temperatures on AA1100 / 1M HCl corrosion

Figures 4.19 - 4.20 demonstrate the Nyquist and Bode representations of the impedance response after 1/2 h of immersion. The impedance profile in uninhibited acid reflects a single capacitive semicircle **(Oguzie *et al*, 2014)** .The observed capacitive loop arises from double layer capacitance-induced charge transfer processes, and its diameter is correlated to the charge transfer resistance (R_{ct}) at the interface(Figures 4.19,4.20). Analyses of the spectra also reveal that they are not perfect semicircle in nature. This anomalous behaviour may be attributed to surface roughness, distribution of the active sites or due to the adsorption of the inhibitor species. The diameter of the semi circle increases with increase in concentration of the studied inhibitor and the shape of the semi circle does not change in the presence of the inhibitor implying that there is no change in the mechanism of AA1100 dissolution in the presence of SCL / SCF / TCL /TCF. The results reflect that the R_{ct} values increases with increase in concentration of inhibitor (Tables 4.20 and 4.21).This might be due to the adsorption of the phytochemical constituents adsorbed onto the AA1100 surface. The value of C_{dl} decreases with an increase in the inhibitor concentration. This situation is the result of an increase in the surface coverage by the inhibitors, which led to an increase in IE.

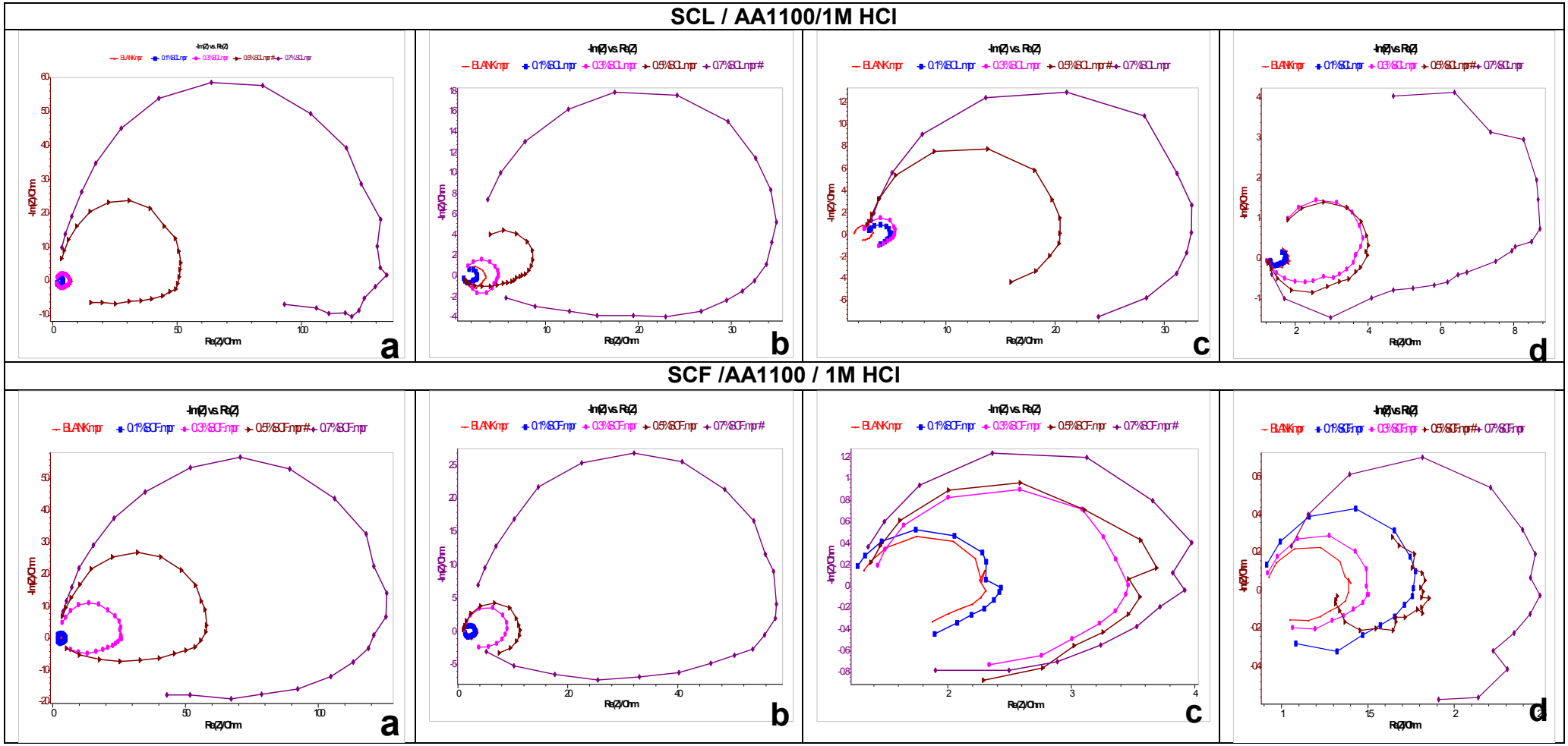

Figure 4.19 Impedance plots of AA1100 in 1 M HCl in absence and presence of SCL and SCF at (a) 303K (b) 313K (c) 323K and (d) 333K

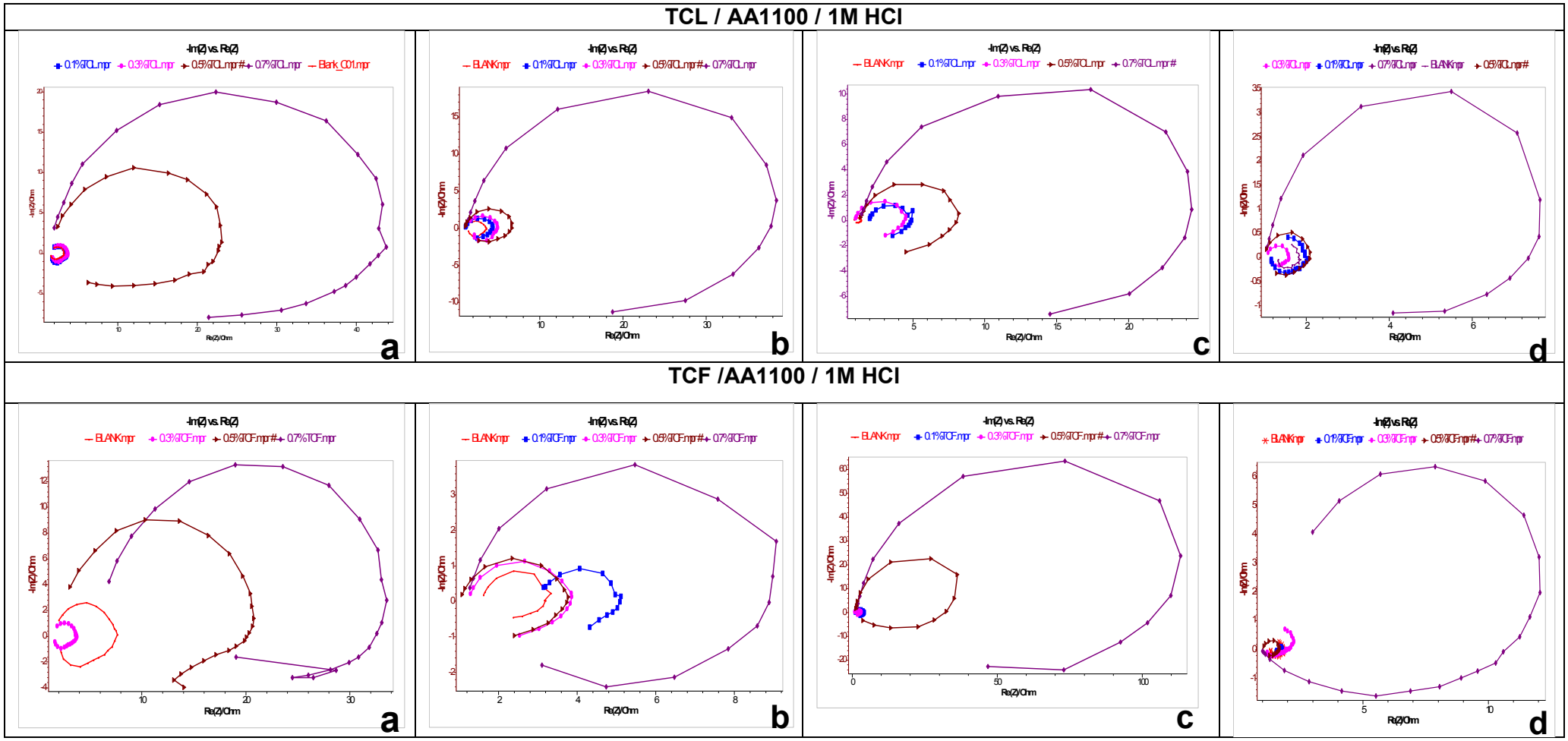

Figure 4.20 Impedance plots of AA1100 in 1 M HCl in absence and presence of TCL and TCF at (a) 303K (b) 313K (c) 323K and (d) 333K

Table 4.20: Electrochemical Impedance parameters for corrosion of AA1100 in the absence and presence of SCL / SCF in 1M HCl at room and higher temperatures

(a)SCL / AA1100 / 1M HCl

Conc (%)	R_S (Ωcm^2)	Y_0 ($\mu F/cm^2$)	N	R_{ct} (Ωcm^2)	IE (%)	f_{max} (μHz)	CPE/C_{dl} ($\mu F/cm^2$)	θ	τ (S^n)	L	RL
303 K											
Blank	1.6	26998	0.56	5.9	-	217.7	124.00	-	0.0007	1.0	0.4
0.1	-0.3	26812	0.55	5.9	0.7	302.4	26.05	0.29	0.0005	1.9	3.3
0.3	0.5	24555	0.53	6.5	9.1	754.6	28.7	0.74	0.0002	1.9	1.7
0.5	3.2	3103	0.77	51.3	88.5	119.1	32.5	0.79	0.0013	18.4	22.5
0.7	1.1	1207	0.81	131.9	95.5	59.2	20.8	0.84	0.0027	252.9	391.3
313K											
Blank	1.42	73347	0.29	2.2	-	427.2	171.7	-	0.0004	0.37	0.05
0.1	0.92	58264	0.36	2.7	20.6	698.3	83.4	0.51	0.0002	0.39	0.39
0.3	0.857	48845	0.40	3.3	33.4	843.6	57.9	0.66	0.0002	0.15	1.08
0.5	0.89	21119	0.53	7.5	71.2	939.9	22.5	0.87	0.0002	0.52	0.92
0.7	1.008	4404	0.72	36.2	94.0	203.5	21.6	0.87	0.0008	3.61	10.5
323K											
Blank	1.60	88366	0.23	1.8	-	637.6	138.6	-	0.0002	0.09	1.01
0.1	2.80	68993	0.31	2.3	21.9	735.5	93.8	0.32	0.0002	0.33	1.05
0.3	2.49	53256	0.38	3.0	39.7	847.5	62.8	0.55	0.0002	0.16	2.23
0.5	2.82	8951	0.68	17.8	89.9	277.9	32.2	0.77	0.0006	5.75	20.4
0.7	2.88	5374	0.68	29.6	93.9	295.4	18.2	0.87	0.0005	9.87	26.3
333K											
Blank	0.94	386494	0.05	0.4	-	2941.4	131.4	-	0.0001	0.02	0.11
0.1	1.31	373968	0.05	0.4	3.2	3917.1	95.5	0.27	0.0000	0.03	0.03
0.3	1.37	239416	0.19	0.7	38.1	2805.4	85.3	0.35	0.0001	0.09	0.29
0.5	0.77	50777	0.39	3.1	86.9	659.8	77.0	0.41	0.0002	0.18	0.68
0.7	0.19	46958	0.39	3.4	87.9	1654.6	28.4	0.78	0.0001	0.04	5.37

(b)SCF / AA1100 / 1M HCl

Conc (%)	R_S (Ωcm^2)	Y_0 ($\mu F/cm^2$)	N	R_{ct} (Ωcm^2)	IE (%)	f_{max} (μHz)	CPE/C_{dl} ($\mu F/cm^2$)	θ	τ (S^n)	L	RL
303 K											
Blank	1.02	83108	0.25	1.9	-	533	156.0	-	0.0003	0.7	0.4
0.1	0.19	22712	0.60	7.0	72.9	205	111.0	0.29	0.0008	1.2	2.7
0.3	3.47	7141	0.72	22.3	91.5	202	35.3	0.77	0.0008	9.6	1.5
0.5	-3.42	2625	0.79	60.7	97.5	100	26.2	0.83	0.0016	11.7	3.5
0.7	0.10	1180	0.84	135.0	98.6	47	25.1	0.84	0.0034	63.0	58.4
313K											
Blank	1.43	73347	0.29	2.2	-	427.2	171.7	-	0.0004	0.376	0.05
0.1	0.69	63491	0.33	2.5	13.4	803.9	79.0	0.54	0.0002	0.446	0.80
0.3	1.01	18714	0.62	8.5	74.5	280.4	66.7	0.61	0.0006	0.619	2.44
0.5	1.03	15122	0.65	10.5	79.4	230.8	65.5	0.62	0.0007	2.616	5.55
0.7	3.44	3373	0.65	47.2	95.4	300.6	11.2	0.93	0.0005	0.316	7.45
323K											
Blank	1.37	175331	0.04	0.9	-	1234.7	142.0	-	0.0001	0.16	0.35
0.1	2.08	53345	0.39	3.0	69.6	453.2	117.7	0.17	0.0004	0.10	3.96
0.3	0.94	41641	0.45	3.8	76.3	431.5	96.5	0.32	0.0004	0.43	2.34
0.5	1.29	23978	0.57	6.6	86.3	344.1	69.7	0.51	0.0005	1.04	1.76
0.7	1.05	6773	0.73	23.5	96.1	191.4	35.4	0.75	0.0008	4.74	11.7
333K											
Blank	0.94	386494	-0.47	0.4	-	2941.4	131.4	-	0.0001	0.03	0.1
0.1	0.89	300275	-0.32	0.5	22.3	2322.3	129.3	0.02	0.0001	0.02	0.2
0.3	0.87	187911	-0.07	0.8	51.4	2592.2	72.5	0.45	0.0001	0.06	0.2
0.5	0.75	198326	-0.10	0.8	48.7	3070.5	64.6	0.51	0.0001	0.04	0.5
0.7	-0.10	37805	0.42	4.2	90.2	1846.0	20.5	0.84	0.0001	0.57	2.1

Table 4.21: Electrochemical Impedance parameters for corrosion of AA1100 in the absence and presence of different concentrations of TCL / TCF in 1M HCl at room and higher temperatures

(a)TCL / AA1100 / 1M HCl

Conc (%)	R_S (Ωcm^2)	Y_0 ($\mu F/cm^2$)	N	R_{ct} (Ωcm^2)	IE (%)	f_{max} (μHz)	CPE/C_{dl} ($\mu F/cm^2$)	θ	τ (S^n)	L	RL
303 K											
Blank	1.6	97871	0.19	1.6	-	501.9	195.0	-	0.0003	0.28	0.0045
0.1	1.6	86967	0.23	1.8	11.1	547.0	159.0	0.18	0.0003	0.78	0.17
0.3	0.4	47392	0.42	3.4	51.6	481.6	98.4	0.50	0.0003	1.25	2.32
0.5	1.6	7030	0.76	22.7	92.8	131.4	53.5	0.73	0.0012	6.19	7.11
0.7	1.5	3775	0.79	42.2	96.1	114.3	33.0	0.83	0.0014	49.82	17.54
313K											
Blank	1.43	73347	0.29	2.2	-	427.2	171.7	-	0.0004	0.38	0.05
0.1	1.17	49162	0.40	3.2	33.0	603.4	81.5	0.53	0.0003	0.34	0.79
0.3	0.78	38305	0.47	4.2	47.8	414.3	92.5	0.46	0.0004	0.43	1.20
0.5	0.97	27370	0.53	5.8	62.7	473.8	57.8	0.66	0.0003	1.49	1.27
0.7	1.09	4257	0.67	37.4	94.2	283.7	15.0	0.91	0.0006	5.87	8.76
323K											
Blank	1.60	88366	0.23	1.8	-	637.6	138.6	-	0.0002	0.09	1.01
0.1	3.06	78986	0.26	2.0	10.6	804.2	98.2	0.29	0.0002	0.38	0.89
0.3	1.33	61150	0.34	2.6	30.8	727.2	84.1	0.39	0.0002	0.29	0.90
0.5	1.06	55990	0.37	2.8	36.6	651.0	86.0	0.38	0.0002	0.27	1.28
0.7	1.30	18120	0.61	8.8	79.5	329.4	55.0	0.60	0.0005	0.40	1.83
333K											
Blank	0.94	386494	-0.47	0.4	-	2941.4	131.4	-	0.0001	0.03	0.11
0.1	0.98	168682	-0.03	0.9	56.4	1323.0	127.5	0.03	0.0001	0.14	0.20
0.3	0.40	112853	0.14	1.4	70.8	943.6	119.6	0.09	0.0002	0.54	2.56
0.5	0.02	72347	0.29	2.2	81.3	958.4	75.5	0.43	0.0002	0.17	2.74
0.7	0.90	59416	0.35	2.7	84.6	942.8	63.0	0.52	0.0002	0.86	3.76

(b)TCF / AA1100 / 1M HCl

Conc (%)	R_S (Ωcm^2)	Y_0 ($\mu F/cm^2$)	N	R_{ct} (Ωcm^2)	IE (%)	f_{max} (μHz)	CPE/C_{dl} ($\mu F/cm^2$)	θ	τ (S^n)	L	RL
303K											
Blank	1.6	67587	0.32	2.4	-	545.1	124.0	-	0.0003	1.0	0.4
0.1	0.7	67160	0.32	2.4	0.6	564.4	119.0	0.04	0.0003	1.5	1.3
0.3	0.4	26998	0.53	5.9	60.1	552.3	48.9	0.61	0.0003	1.2	2.1
0.5	0.8	7806	0.73	20.4	88.5	175.6	44.4	0.64	0.0009	16.9	22.2
0.7	5.8	5326	0.72	29.9	92.1	208.9	25.5	0.79	0.0008	5.1	42.0
313K											
Blank	1.43	73347	0.29	2.2	-	427.2	171.7	-	0.0004	0.38	0.05
0.1	1.26	60870	0.35	2.6	17.0	523.4	116.3	0.32	0.0003	0.44	0.10
0.3	1.02	50696	0.40	3.1	30.9	485.6	104.4	0.39	0.0003	0.22	0.60
0.5	0.90	23838	0.57	6.7	67.5	378.3	63.0	0.63	0.0004	0.86	3.76
0.7	0.93	3954	0.71	40.3	94.6	212.6	18.6	0.89	0.0007	0.98	1.82
323K											
Blank	1.37	175331	-0.04	0.9	-	1234.7	142.0	-	0.0001	0.161	0.36
0.1	1.08	112217	0.14	1.4	36.0	1428.4	78.6	0.45	0.0001	0.196	0.84
0.3	1.13	66710	0.31	2.4	62.0	1253.0	53.2	0.63	0.0001	0.299	1.22
0.5	1.07	55735	0.36	2.9	68.2	873.6	63.8	0.55	0.0002	0.174	1.40
0.7	0.62	12873	0.66	12.4	92.7	282.2	45.6	0.68	0.0006	0.345	1.57
333K											
Blank	0.94	386494	-0.47	0.4	-	2941.4	131.4	-	0.0001	0.03	0.11
0.1	3.16	176732	-0.05	0.9	54.3	1469.1	120.3	0.08	0.0001	0.32	0.70
0.3	1.38	126478	0.10	1.3	67.3	1491.1	84.8	0.35	0.0001	0.17	0.79
0.5	0.42	92633	0.21	1.7	76.0	2264.3	40.9	0.69	0.0001	0.08	1.64
0.7	0.90	48711	0.38	3.3	87.4	1546.4	31.5	0.76	0.0001	0.14	1.27

4.3 MASS LOSS METHOD

Mass loss method is a means of evaluating corrosion rates of metals in corrosive environments and it forms a baseline method of measurement in many corrosion monitoring programmes. Mass loss is one of the most frequently used methods as it is simple and reliable **(Cang *et al*, 2012).**

- **Mass loss experiments for MS / 1M HCl / SCL / SCF / TCL / TCF**

4.3.1 Effect of concentration and Immersion time

4.3.1.1 Effect of concentration and Immersion time of SCL on MS / 1M HCl

The effect of SCL extract on the corrosion inhibition of MS is tested by mass loss measurements. Table 4.22 and Figure 4.21 shows the variation of corrosion rate and inhibition efficiency with increase in concentration of the inhibitor. It can be seen from the table and Figure 4.21 that the corrosion rate decreases with increasing concentration of the inhibitor. The IE of the inhibitor increases from 54.9 percentage at 0.1% SCL to 88.4 percentage at 0.7 % of SCL.

Table-4.22 Inhibition efficiency as a function of immersion time and concentration of SCL /SCF in 1M HCl

Conc. %	1/2 h		1h		3h		6h		12h		24h	
	CR (mpy)	IE (%)	CR (mpy)	IE (%)	CR (mpy)	IE (%)	CR (mpy)	IE (%)	CR (mpy)	IE (%)	CR (mpy)	IE (%)
SCL												
Blank	1032		1190		1238		2197		1561		1209	
0.1	465	54.9	290	75.6	246	80.1	147	93.3	422	73.0	595	50.8
0.2	432	58.1	188	84.2	182	85.3	120	94.5	202	87.1	311	74.3
0.3	380	63.2	166	86	133	89.2	117	94.7	137	91.2	278	77.0
0.4	300	70.9	154	87.1	107	91.4	70	96.8	134	91.4	232	80.8
0.5	245	76.3	149	87.5	84	93.2	57	97.4	124	92.0	149	87.7
0.6	182	82.4	128	89.2	60	95.2	48	97.8	69	95.6	135	88.8
0.7	120	88.4	107	91	40	96.8	43	98.0	24	98.5	76	93.7
SCF												
Blank	1032		1190		1238		2197		1561		1209	
0.1	321	68.9	563	52.7	223	82.0	439	80.0	337	78.4	515	57.4
0.2	295	71.4	495	58.4	202	83.7	198	91.0	229	85.3	491	59.4
0.3	269	73.9	450	62.2	181	85.4	165	92.5	200	87.2	480	60.3
0.4	251	75.7	279	76.6	137	88.9	110	95.0	156	90.0	466	61.4
0.5	213	79.4	182	84.7	126	89.8	105	95.2	147	90.6	310	74.4
0.6	168	83.7	145	87.8	87	93.0	97	95.6	117	92.5	238	80.3
0.7	136	86.8	139	88.3	67	94.6	92	95.8	97	93.8	193	84.0

An insight into the stability of SCL extract with time may be gained by studying the effect of the extract on MS specimen for various time of immersion. The results evaluated for the variation of mass loss with exposure time for the MS specimen immersed in 1M HCl with and without inhibitors are presented in Table 4.22. From the table, it can be seen that a maximum IE of 98.5 percentage is maintained till 12 h and thereafter a slight decline is observed and the efficiency stabilises to 93.7 percentage at 24h for the extract.

4.3.1.2 Effect of concentration and Immersion time of SCF on MS/1M HCl

Table 4.22 and Figure 4.21 presents the corrosion rate of MS in the presence of different concentrations of SCF.A significant reduction in the mass loss is noticed in the presence of the inhibitor. It has been observed that the corrosion rate decreases with the increase in concentration of SCF and percentage inhibition efficiency is found to increase with the concentration of inhibitor. It can be seen from the table that the maximum inhibition efficiency is 86.8 percentage at 0.7% extract.

The mass loss of MS coupons are evaluated for a period of ½ h, 1 h 3 h, 6 h, 12 h and 24 h of immersion in 1 M HCl in the absence and presence of inhibitor. Inspection of Table 4.22 reveals that the inhibition efficiency of studied inhibitor increases markedly with an increase of the exposure time. The results show that corrosion rate increases with increase in time to some extent and then decreases for the studied inhibitor.From the table, it can be seen that a maximum IE of 95.8 percentage is maintained till 6 h and thereafter a slight decline is observed. But the inhibition efficiency is found to stabilise at 24h to afford an efficiency of 84 percentage demonstrating the effectiveness of the inhibitor at longer periods of immersion.

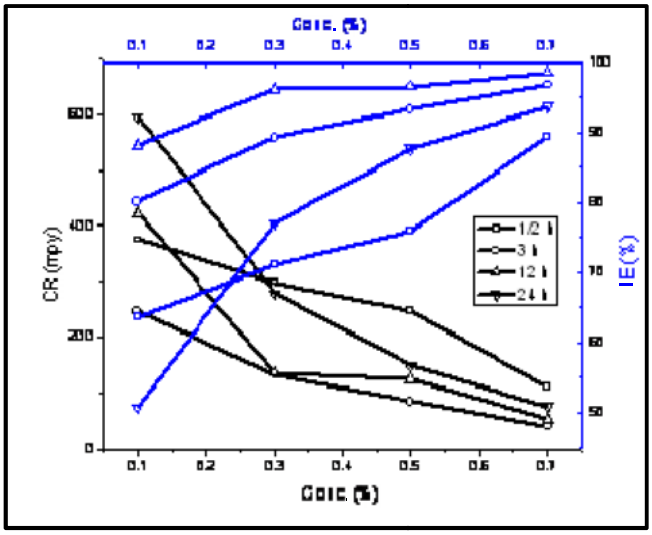

MS/ SCL/ 1M HCl

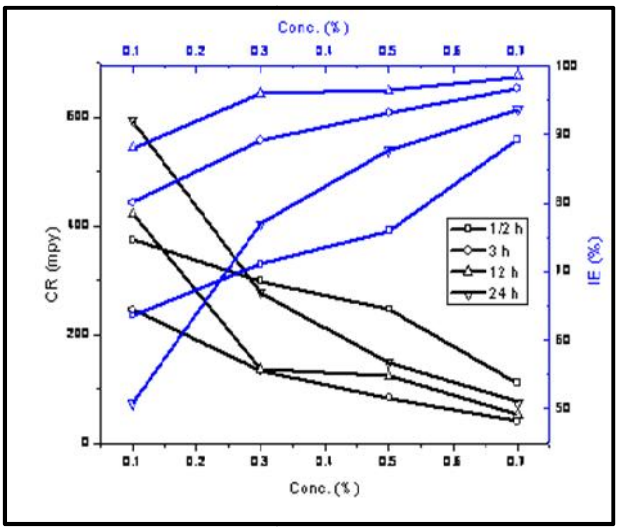

MS /SCF/1M HCl

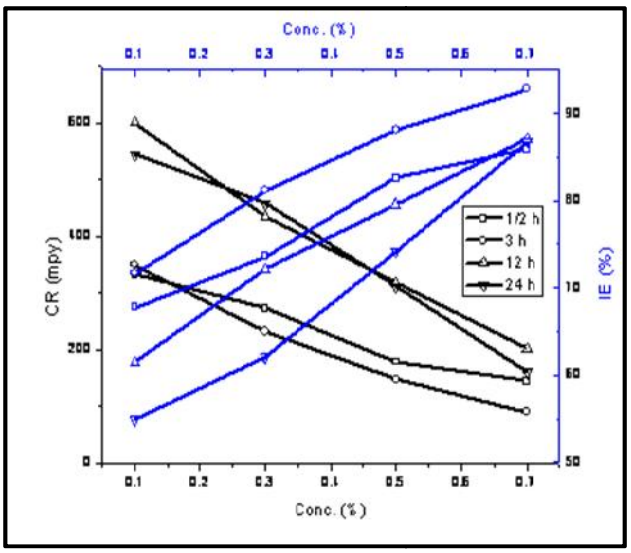

MS /TCL /1MHCl

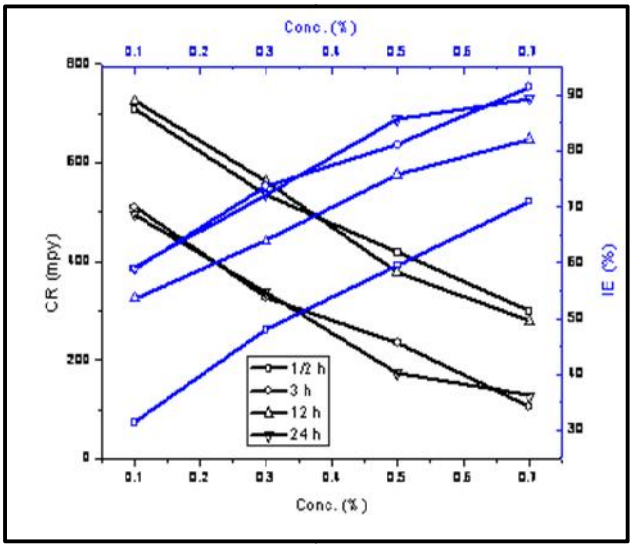

MS /TCF /1MHCl

Figure 4.21: Inhibition efficiency as a function of time and concentration of SCL /SCF/ TCL/ TCF extracts on MS in 1M HCl

4.3.1.3 Effect of concentration and Immersion time of TCL on MS/1M HCl

The Inhibition efficiency of MS exposed to 1M HCl at room temperature as a function of different concentration of TCL has been evaluated by mass loss measurements. Table `4.23 and Figure 4.21 shows the dependance of inhibition efficiency with change in concentration of the inhibitor .The results indicate a sharp increase in IE from 63.7 percentage (0.1 % TCL) to 89.2 percentage at 0.7% concentration. Further increase in concentration did not cause any appreciable change in the inhibitor performance (**Li *et al*, 2012**). It can be seen from the table that the maximum inhibition efficiency is 89.2 percentage at ½ hr of immersion period.

Immersion time is an important parameter that needs to be assessed to check the stability of the inhibitive nature of the inhibitor under study. Hence attempts are made to analyse the stability of extract with time. The results evaluated for the variation of weight loss with exposure time for the MS specimen immersed in 1M HCl with and without inhibitors are presented in Table 4.23. The mass loss for the MS in 1M HCl containing different concentration of the studied inhibitor as a function of time is represented in Figure 4.21. From the table, it can be seen that a maximum IE of 96.1 percentage for TCL is attained at 6 h and thereafter a slight decline is noticed. However the efficiency stabilises to 89.4 percentage at 24h.

4.3.1.4 Effect of concentration and Immersion time of TCF on MS/1M HCl

The influence of TCF extract on the corrosion inhibition of MS has been assessed by mass loss measurements. Table 4.23 shows the variation of inhibition efficiency with increase in concentration of the inhibitor. Inspection of Figure 4.21 reveals that the addition of TCF markedly decreases the corrosion rate of MS. This result indicates the inhibitive nature of the inhibitor on MS corrosion in 1M HCl medium. (**Dong *et al*, 2011**).It is clear from the results that the IE increases steadily from 67.8 percentage at 0.1% concentration to 85.9 percentage at 0.7% concentration.

The corrosion rate and inhibition efficiency of MS electrode exposed to various concentration of TCF extract in 1M HCl solution for various time intervals are tabulated in Table 4.23. From the table, it is noted that a maximum IE of 94.8 percentage for TCF is maintained till 6 h and thereafter a slight decline is observed and the efficiency stabilises to 86.8 percentage (TCF) at 24h.

Table-4.23 Inhibition efficiency as a function of immersion time and concentration for TCL / TCF / MS / 1M HCl systems

Conc. %	1/2 h		1h		3h		6h		12h		24h	
	CR (mpy)	IE (%)	CR (mpy)	IE (%)	CR (mpy)	IE (%)	CR (mpy)	IE (%)	CR (mpy)	IE (%)	CR (mpy)	IE (%)
TCL												
Blank	1032		1190		1238		2197		1561		1209	
0.1	375	63.7	444	62.7	510	58.8	427	80.6	725	53.6	495	59.1
0.2	367	64.4	380	68.1	455	63.3	316	85.6	626	59.9	458	62.1
0.3	299	71.0	328	72.4	326	73.7	215	90.2	564	63.9	337	72.1
0.4	273	73.6	260	78.1	279	77.5	186	91.6	448	71.3	241	80.1
0.5	247	76.1	162	86.4	235	81.1	161	92.7	378	75.8	173	85.7
0.6	188	81.8	145	87.8	168	86.4	126	94.3	354	77.3	144	88.1
0.7	111	89.2	132	88.9	105	91.5	86	96.1	279	82.1	128	89.4
TCF												
Blank	1032		1190		1238		2197		1561		1209	
0.1	333	67.8	260	78.1	350	71.7	625	71.6	601	61.5	545	54.9
0.2	307	70.3	226	81	264	78.6	426	80.6	474	69.8	495	59.1
0.3	273	73.5	200	83.2	233	81.2	315	85.7	435	72.1	458	62.1
0.4	196	81	162	86.4	166	86.6	226	89.7	342	78.1	377	68.8
0.5	179	82.7	145	87.8	148	88.0	200	90.9	318	79.6	312	74.2
0.6	154	85.1	128	89.2	135	89.1	143	93.5	279	82.2	241	80.1
0.7	146	85.9	102	91.4	90	92.7	114	94.8	202	87.1	160	86.8

REASON FOR HIGH IE AT HIGHER CONCENTRATION OF THE INHIBITORS:

Analysis of the tables indicate that IE increases with increasing concentration of the inhibitors.This indicates the dependance of inhibiting effect on the concentration of inhibitor molecules .Enhanced efficiency at higher concentration may be ascribed to the increase in coverage of MS surface by the inhibitor molecules at higher concentration of the extract leading to a compact and coherent film on the surface of MS. Further increase in concentration of the inhibitor did not show an increase in inhibition efficiency .This might be possibly due to the total coverage of the metal surface by the inhibitor. **(Singh and Quraishi 2010)**

REASON FOR LOW IE AT LONGER PERIOD OF IMMERSION:

The IE of the studied extracts increase with increasing time of immersion upto 6h (12h for SCL) and then decrease to finally stabilise at 24h to afford 84- 93 percentage.This behaviour can be discussed on the basis that prolonged immersion of MS in acid solution **(Zakvi and Mehta, 1987)**.

a) allows the cathodic or hydrogen evolution kinetics to increase presumably or more cathodic or carbon containing sites are exposed by the corrosion process.

b) increase the concentration of ferrous ions which decrease the corrosive nature of the acid.

4.3.2 Effect of temperature:

Interaction between the metal electrode and the corrodent acidic medium is alters significantly in the presence of inhibitors. To assess the impact of temperature on corrosion and corrosion inhibition process, mass loss measurements are carried out in the range of 303 to 353K **(Edouk *et al*, 2010)** .The collected results are tabulated and discussed.

4.3.2.1 Role of temperature on SCL and SCF

The stability and mechanism of adsorption of the investigated extracts on the surface of MS has been evaluated by means of mass loss experiments in the temperature range 303 to 353 K and the results pertaining to it are discussed.

Table 4.24 presents the variation of the inhibitor efficiency of SCL and SCF with temperature in 1M HCl. It can be seen that, the presence of SCL and SCF in 1M HCl, decreases the corrosion rate of MS at any given temperature with increase in inhibitor concentration. In contrast at constant inhibitor concentration, the corrosion rate increases with a rise in temperature. Analysing the temperature effect of SCL and SCF, the IE increases with increase in temperature up to 323K giving rise to 94.1 percentage for SCL and 93.1 percentage for SCF and then a slight decrease is noted at 333 to 343K which then stabilises to 87.4 percentage for SCL and 82.2 percentage for SCF at 353K.

Table 4.24: Relationship between Inhibition efficiency and concentration for SCL / SCF / MS / 1M HCl systems at various temperatures

CONC. %	TEMPERATURE (K)											
	303		313		323		333		343		353	
	CR (mpy)	IE (%)	CR (mpy)	IE (%)	CR (mpy)	IE (%)	CR (mpy)	IE (%)	CR (mpy)	IE (%)	CR (mpy)	IE (%)
SCL												
Blank	1032		2755		6252		8146		9971		18091	
0.1	465	54.9	995	63.9	2244	64.1	3284	59.7	4785	52.0	8180	54.8
0.2	432	58.1	798	71	1638	73.8	2491	69.4	4606	53.8	6491	64.1
0.3	380	63.2	696	74.7	1413	77.4	2158	73.5	3813	61.8	6141	66.1
0.4	300	70.9	517	81.2	988	84.2	1757	78.4	2849	71.4	5297	70.7
0.5	245	76.3	457	83.4	819	86.9	1390	82.9	2311	76.8	4359	75.9
0.6	182	82.4	355	87.1	600	90.4	1041	87.2	1655	83.4	3403	81.2
0.7	120	88.4	201	92.7	369	**94.1**	887	89.1	1100	89.0	2279	87.4
SCF												
Blank	1032		2755		6252		8146		9971		18091	
0.1	321	68.9	601	78.2	913	85.4	1605	80.3	4188	58.0	6676	63.1
0.2	295	71.4	568	79.4	625	90.0	1287	84.2	3829	61.6	4432	75.5
0.3	269	73.9	518	81.2	606	90.3	1246	84.7	3470	65.2	4233	76.6
0.4	251	75.7	449	83.7	556	91.1	1214	85.1	3121	68.7	4179	76.9
0.5	213	79.4	394	85.7	544	91.3	1165	85.7	2353	76.4	3672	79.7
0.6	168	83.7	320	88.4	469	92.5	1035	87.3	1924	80.7	3600	80.1
0.7	136	86.8	270	90.2	431	**93.1**	937	88.5	1585	84.1	3220	82.2

4.3.2.2 Impact of temperature on IE of on TCL / TCF /MS / 1M HCl

The Kinetic and mechanistic aspects of corrosion may be gained by studying the effect of temperature on the corrosion of MS in the presence and absence of the inhibitor. It can be noted from Table 4.25 that the maximum IE obtained is 90.7 percentage (for TCL) and 93.8 percentage (for TCF) in 1M HCl .The values reflect that the IE increases up to 323K affording an efficiency of 90.7 percentage (for TCL) and 93.8 percentage (for TCF) and then a slight decrease is observed after that and at 353K it is found to be at 84.2 percentage (for TCL) and 83.2 percentage (for TCF) respectively.

Table 4.25: Relationship between Inhibition efficiency and concentration for TCL / TCF/ MS / 1M HCl systems at various temperatures

CONC %	TEMPERATURE (K)											
	303		313		323		333		343		353	
	CR (mpy)	IE (%)	CR (mpy)	IE (%)	CR (mpy)	IE (%)	CR (mpy)	IE (%)	CR (mpy)	IE (%)	CR (mpy)	IE (%)
TCL												
Blank	1032		2755		6252		8146		9971		18091	
0.1	375	63.7	1126	59.1	2243	64.0	4922	60.0	4231	57.6	7480	58.7
0.2	367	64.4	955	65.3	1825	70.8	2235	72.6	3736	62.5	6465	64.3
0.3	299	71.0	657	76.2	1586	74.6	2149	73.6	2943	70.5	6116	66.2
0.4	273	73.6	623	77.4	1365	78.2	1800	77.9	2422	75.7	5084	71.9
0.5	247	76.1	554	79.9	810	87.0	1476	81.9	1945	80.5	4376	75.8
0.6	188	81.8	520	81.1	699	88.8	1186	85.4	1604	83.9	3651	79.8
0.7	111	89.2	281	89.8	580	**90.7**	904	88.9	1348	86.5	2857	84.2
TCF												
Blank	1032		2755		6252		8146		9971		18091	
0.1	333	67.8	967	64.9	1307	79.1	2077	74.5	4188	58.0	7634	57.8
0.2	307	70.3	628	77.2	982	84.3	1750	78.5	3833	61.6	5174	71.4
0.3	273	73.5	540	80.4	757	87.9	1352	83.4	3490	65.0	4378	75.8
0.4	196	81	507	81.6	569	90.9	1238	84.8	3091	69.0	4125	77.2
0.5	179	82.7	479	82.6	539	91.4	1149	85.9	2353	76.4	3636	79.9
0.6	154	85.1	410	85.1	469	92.5	1075	86.8	1894	81.0	3383	81.3
0.7	146	85.9	386	86.0	388	**93.8**	863	89.4	1595	84.0	3039	83.2

REASON FOR LOW IE AT HIGHER TEMPERATURES:

According to **Putilova, 1960** the decrease in the inhibition efficiency of the inhibitors with increase in temperature might be due to adsorption and desorption. Adsorption and desorption of inhibitor molecules continuously occur at the metal surface and an equilibrium exists between these two processes at a particular temperature. With the increase of temperature the equilibrium between adsorption and desorption processes is shifted leading to a higher desorption rate than adsorption until equilibrium is again established at a different value of equilibrium constant.

This is due to increased effect of temperature on the dissolution process of MS and partial desorption of the inhibitor from the metal surface **(Ashish Kumar Singh *et al*, 2009).**

4.3.3 Effect of concentration and Immersion time –AA1100 /1M HCl.

4.3.3.1 Effect of concentration and Immersion time of SCL / AA1100 / 1M HCl

The corrosion behaviour of aluminum alloy in 1M HCl solution containing various concentrations of SCL extract is tested by mass loss measurements. The data obtained is presented in Table 4.26. The table indicates that the amount of material loss decreases significantly with increasing concentration of SCL extract. The addition of the extract results in noticeable reduction in the amount of metal loss from the AA1100 surface in comparison with that of control (1M HCl) at 303K. This indicates that the inhibitor impedes the corrosion of aluminum in 1M HCl solution. Table 4.26 reflects that the inhibition efficiency increases with increasing extract concentration and the percentage inhibition efficiency is relatively high ie, 89 % at 0.7% of extract concentration.

Table 4.26 Inhibition efficiency as a function of immersion time and concentration of SCL / SCF on AA1100/1M HCl

conc. %	1/2 h		1h		3h		6h		12h		24h	
	CR (mpy)	IE (%)	CR (mpy)	IE (%)	CR (mpy)	IE (%)	CR (mpy)	IE (%)	CR (mpy)	IE (%)	CR (mpy)	IE (%)
SCL												
Blank	1434		2159		4027		5943		3267		1572	
0.1	248	82.7	378	82.5	882	78.1	1349	77.3	771	76.4	453	71.2
0.2	212	85.2	311	85.6	838	79.2	1165	80.4	663	79.7	412	73.8
0.3	204	85.8	190	91.2	789	80.4	1129	81.0	640	80.4	365	76.8
0.4	199	86.1	123	94.3	677	83.2	1016	82.9	591	81.9	324	79.4
0.5	195	86.4	99	95.4	580	85.6	975	83.6	549	83.2	302	80.8
0.6	184	87.2	84	96.1	447	88.9	886	85.1	516	84.2	288	81.7
0.7	158	89.0	69	96.8	399	90.1	807	86.4	467	85.7	277	82.4
SCF												
Blank	1434		2159		4027		5943		3267		1572	
0.1	215	85.0	339	84.3	793	80.3	1236	79.2	709	78.3	406	74.2
0.2	191	86.7	272	87.4	749	81.4	1082	81.8	631	80.7	347	77.9
0.3	174	87.9	166	92.3	660	83.6	957	83.9	583	82.2	340	78.4
0.4	166	88.4	106	95.1	576	85.7	868	85.4	502	84.6	300	80.9
0.5	157	89.1	80	96.3	519	87.1	814	86.3	481	85.3	294	81.3
0.6	141	90.2	69	96.8	387	90.4	689	88.4	418	87.2	248	84.2
0.7	133	90.7	56	97.4	250	93.8	612	89.7	379	88.4	190	87.9

Table 4.26 represents the variation of mass loss against time for AA1100 corrosion in 1 M HCl without and with different concentrations (0.1–0.7 %) of the extract. Inspection

of the table also reflects that mass loss of AA1100 decreases with increase in immersion time in the presence of the extract. From the table, it can be deduced that a maximum IE of 96.8 percentage is maintained till 1 h and thereafter a slight decline is observed and the efficiency stabilises to 82.4 percentage at 24h for the extract.

4.3.3.2 Effect of concentration and Immersion time of SCF / AA1100 / 1M HCl

The effect of SCF on the corrosion inhibition of AA1100 in 1 M HCl has been studied using mass loss technique. The results obtained are presented in Table 4.26. The extent of mass loss in the presence of the extract is found to be concentration dependent, decreasing as concentration of the extract increased. Decrease in corrosion rate of AA1100 on addition of the extract to the corrosive medium is an indication that the extract is exerting inhibitive effect and retarding the acid-induced corrosion of AA1100 coupons. The effectiveness of the extract in retarding the corrosion of AA1100 in 1 M HCl is obtained by comparing the corrosion rates of the metal in the presence and the absence of the extract is expressed in terms of the inhibition efficiency (% IE). The inhibition efficiency values are listed in Table 4.26. Results in the Table show that inhibition efficiency increases as the concentration of the extract increases reaching a maximum value of 90.7 at higher concentration (0.7% SCF) of the extract studied.

It also reflects that the inhibition efficiency of studied inhibitor increases markedly with an increase of the exposure time till 1h and then decreases for the studied inhibitor. From the Table, it can be seen that a maximum IE of 97.4 percentage is maintained till 1h and thereafter a slight decline is observed and the efficiency stabilises to 87.9 percentage at 24h for the extract in HCl medium.

4.3.3.3 Effect of concentration and Immersion time of TCL

The mass loss results for AA1100 in 1 M HCl with and without addition of different concentrations of TCL are summarized in Table 4.27 . From Table 4.27 it can be seen that the extent of corrosion in 1 M HCl solution containing TCL decreases as the concentration of inhibitor increases. This is because the amount adsorbed and coverage of the AA1100 surface by inhibitor increases with inhibitor concentration. A highest inhibition efficiency of 89.6 percentage is obtained at 0.7% TCL. No appreciable change in the inhibitor performance is noticed with further increase in concentration **(Li *et al*, 2012).**

The results evaluated for the variation of weight loss with exposure time for the AA1100 specimen immersed in 1M HCl with and without inhibitors are presented in Table 4.27. From the table, it can be seen that a maximum IE of 96.4 percentage for TCL is

maintained till 1h and thereafter a slight decline is observed and the efficiency stabilises to 84.3 percentage at 24h.

4.3.3.4 Effect of concentration and Immersion time of TCF

The impact of TCF extract on the corrosion inhibition of AA1100 has been evaluated by mass loss measurements. Table 4.27 reflects that the corrosion rate values (in mpy) decrease as the inhibitor concentrations increase, i.e. the corrosion inhibition enhances with the inhibitor concentration. This result may be due to the fact that the addition of TCF markedly decreased the corrosion rate of AA1100. This result indicates the inhibitive nature of the inhibitor on AA1100 corrosion in 1M HCl medium**.(Dong *et al*, 2011**) .Further analysis of the results indicates that the IE increases steadily from 83.2 percentage at 0.1% concentration to 90.2 percentage at 0.7% concentration.

The corrosion rate and inhibition efficiency of AA1100 electrode exposed to various concentration of TCF extract in 1M HCl solution for various time intervals are tabulated in Table 4.27. From the table, it is noted that a maximum IE of 97.1 percentage for TCF is maintained till 1h and thereafter a slight decline is observed and the efficiency stabilises to 85.1 percentage (TCF) at 24h.

Table 4.27 Inhibition efficiency as a function of immersion time and concentration of TCL / TCF on AA1100/1M HCl

CONC. %	1/2 h		1h		3h		6h		12h		24h	
	CR (mpy)	IE (%)	CR (mpy)	IE (%)	CR (mpy)	IE (%)	CR (mpy)	IE (%)	CR (mpy)	IE (%)	CR (mpy)	IE (%)
TCL												
Blank	1434		2159		4027		5943		3267		1572	
0.1	257	82.1	402	81.4	830	79.4	1284	78.4	732	77.6	468	70.2
0.2	249	82.6	348	83.9	729	81.9	1159	80.5	640	80.4	429	72.7
0.3	232	83.8	268	87.6	604	85.0	1117	81.2	585	82.1	395	74.9
0.4	224	84.4	233	89.2	548	86.4	998	83.2	568	82.6	338	78.5
0.5	199	86.1	184	91.5	515	87.2	856	85.6	533	83.7	311	80.2
0.6	166	88.4	114	94.7	439	89.1	826	86.1	487	85.1	289	81.6
0.7	149	89.6	77	96.4	395	90.2	755	87.3	451	86.2	247	84.3
TCF												
Blank	1434		2159		4027		5943		3267		1572	
0.1	240	83.2	391	81.9	797	80.2	1313	77.9	706	78.4	399	74.6
0.2	224	84.4	358	83.4	705	82.5	1135	80.9	634	80.6	380	75.8
0.3	191	86.7	283	86.9	616	84.7	975	83.6	516	84.2	340	78.4
0.4	182	87.3	186	91.4	576	85.7	939	84.2	487	85.1	294	81.3
0.5	157	89.1	142	93.4	467	88.4	874	85.3	461	85.9	269	82.9
0.6	149	89.6	110	94.9	407	89.9	749	87.4	451	86.2	241	84.7
0.7	141	90.2	63	97.1	350	91.3	707	88.1	395	87.9	234	85.1

REASON FOR HIGH IE AT HIGHER CONCENTRATION OF THE INHIBITORS

The inhibition properties of the inhibitors may be due to the presence of the organic compounds in the extract. Organic compounds that contain O, S or N/or combination of the atoms have been reported as corrosion inhibitors for metals in alkaline or acid solutions **(Nnanna *et al*, 2010)**. The adsorption of these compounds on the metal surface reduces the surface area that is available for the attack of the aggressive HCl solution.It has been pointed out that the increase in inhibition efficiency with increase in extract concentration is an indication of an increase in the number of components of the extract adsorbed over the AA1100 surface blocking the active sites, in which direct acid attacks proceed and protect the metal from corrosion, while the increase in inhibition efficiency with immersion time rise is suggestive of strong adsorption of the phytoconstituents of the extract on the AA1100 surface forming a protective layer and shielding the metal from corrosion **(Ekanem *et al*, 2010).**

REASON FOR LOW IE AT LONGER PERIOD OF IMMERSION

The IE of the studied extracts increase with increasing time of immersion upto 1h and then decrease to finally stabilise at 24h.This behaviour can be discussed on the basis that the adsorptive film of inhibitors are dependent on the immersion time **(Obot *et al*, 2010)**. Initially, the adsorptive film becomes more compact and uniform with the increase of immersion time (0.5–1 h). However, along with prolonging of immersion time, the adsorptive film is not more uniform **(Shukla and Quraishi, 2010)** or the desorption of adsorbed inhibitors from metal surface owing to the aggressive corrosion of acid media **(Li and Deng, 2012)**.

4.3.4 Effect of temperature

The influence of temperature on the inhibited acid-metal reaction is very complex according to **Bentiss *et al* ,2005** as many changes occur on the metal surface such as rapid etching,desorption of inhibitor and the inhibitor itself may undergo decomposition. The dependance of percentage inhibition efficiency on temperature is studied by conducting mass loss measurements in the range of 303 to 353K **(Edouk *et al*, 2010)** .The collected results are tabulated and discussed.

4.3.4.1 Role of temperature on SCL and SCF on AA1100/1M HCl

The inhibition efficiency for different extract concentrations in 1.0 M HCl solution over the temperature range 303–353 K is presented in Figure. 4.22 It is observed that the inhibition efficiency increases with increasing concentration of SCL and SCF. This indicates

that phytochemical components of the extracts are absorbed onto the Al surface, resulting in blockage of reaction sites and protection of the metal surface from attack by corrosion-active ions in the acid medium. IE increases from 303 – 313K and decreases as the temperature increases to 323K. At SCL concentration of 0.7%, the maximum IE in 1.0 M HCl is 89 percentage at 303 K, 89.3 percentage at 313 K, 86.5 percentage at 323 K, and 85.5 percentage at 333 K and then stabilises at 353K to afford an efficiency of 74.2 percentage. At SCF concentration of 0.7%, the maximum IE in 1.0 M HCl is 90.7 percentage at 303 K, 96.4 percentage at 313 K, 95.8 percentage at 323 K, and 89.9 percentage at 333 K and then decreases to 78.1 percentage at 353K. These results indicate that both extracts are good inhibitors for AA1100 in 1.0 M HCl solution **(Djeddi *et al*, 2014).**

Table 4.28 Relationship between Inhibition efficiency and concentration of SCL and SCF at various temperatures on AA1100 / 1M HCl

CONC. %	TEMPERATURE (K)											
	303		313		323		333		343		353	
	CR (mpy)	IE (%)	CR (mpy)	IE (%)	CR (mpy)	IE (%)	CR (mpy)	IE (%)	CR (mpy)	IE (%)	CR (mpy)	IE (%)
SCL												
Blank	1434		7269		19146		29399		44972		69365	
0.1	248	82.7	1318	81.9	4641	75.8	7879	73.2	17359	61.4	31492	54.6
0.2	212	85.2	1268	82.6	3829	80.0	7320	75.1	16325	63.7	26914	61.2
0.3	204	85.8	1210	83.4	3531	81.6	6909	76.5	14346	68.1	25318	63.5
0.4	199	86.1	1160	84.0	3382	82.3	5939	79.8	13402	70.2	22127	68.1
0.5	195	86.4	1028	85.9	3232	83.1	5262	82.1	11333	74.8	20879	69.9
0.6	184	87.2	912	87.5	3017	84.2	4880	83.4	11153	75.2	19075	72.5
0.7	158	89.0	779	89.3	2586	86.5	4263	85.5	10478	76.7	17896	74.2
SCF												
Blank	1434		7269		19146		29399		44972		69365	
0.1	215	85.0	1343	81.5	5445	71.6	16455	44.0	16730	62.8	29549	57.4
0.2	191	86.7	1160	84.0	3370	82.4	13774	53.1	16460	63.4	28093	59.5
0.3	174	87.9	928	87.2	2393	87.5	11281	61.6	14796	67.1	24347	64.9
0.4	166	88.4	812	88.8	1838	90.4	10970	62.7	12952	71.2	19769	71.5
0.5	157	89.1	655	91.0	1398	92.7	10159	65.4	11378	74.7	17480	74.8
0.6	141	90.2	406	94.4	1015	94.7	9100	69.0	9264	79.4	15330	77.9
0.7	133	90.7	265	96.4	796	95.8	6295	78.6	9039	79.9	15191	78.1

4.3.4.2 Impact of temperature on IE of TCL and TCF on AA1100/1M HCl

The effect of temperature on the corrosion rate of AA1100 in 1M HCl solution in absence and presence of different concentrations of TCL and TCF are tabulated in Table 4.29. It can be noted from Figure 4.22 and Table 4.29, that the maximum I.E. obtained is 89.6 percentage (for TCL) and 90.2 percentage (for TCF) in 1M HCl. Experiments performed with 1M HCl at higher temperatures reveals that a maximum I.E. of percent is

noticed at 303 K for TCL and 323 K for TCF extracts .The values reflect that the IE is highest at 303K for TCL and 323K for TCF having an efficiency of 89.6 percentage (for TCL) and 91.5 percentage(for TCF) and then a slight decrease is observed after that and at 353K it is found to be at 74.7 percentage (for TCL) and 75.6 percentage (for TCF) respectively.

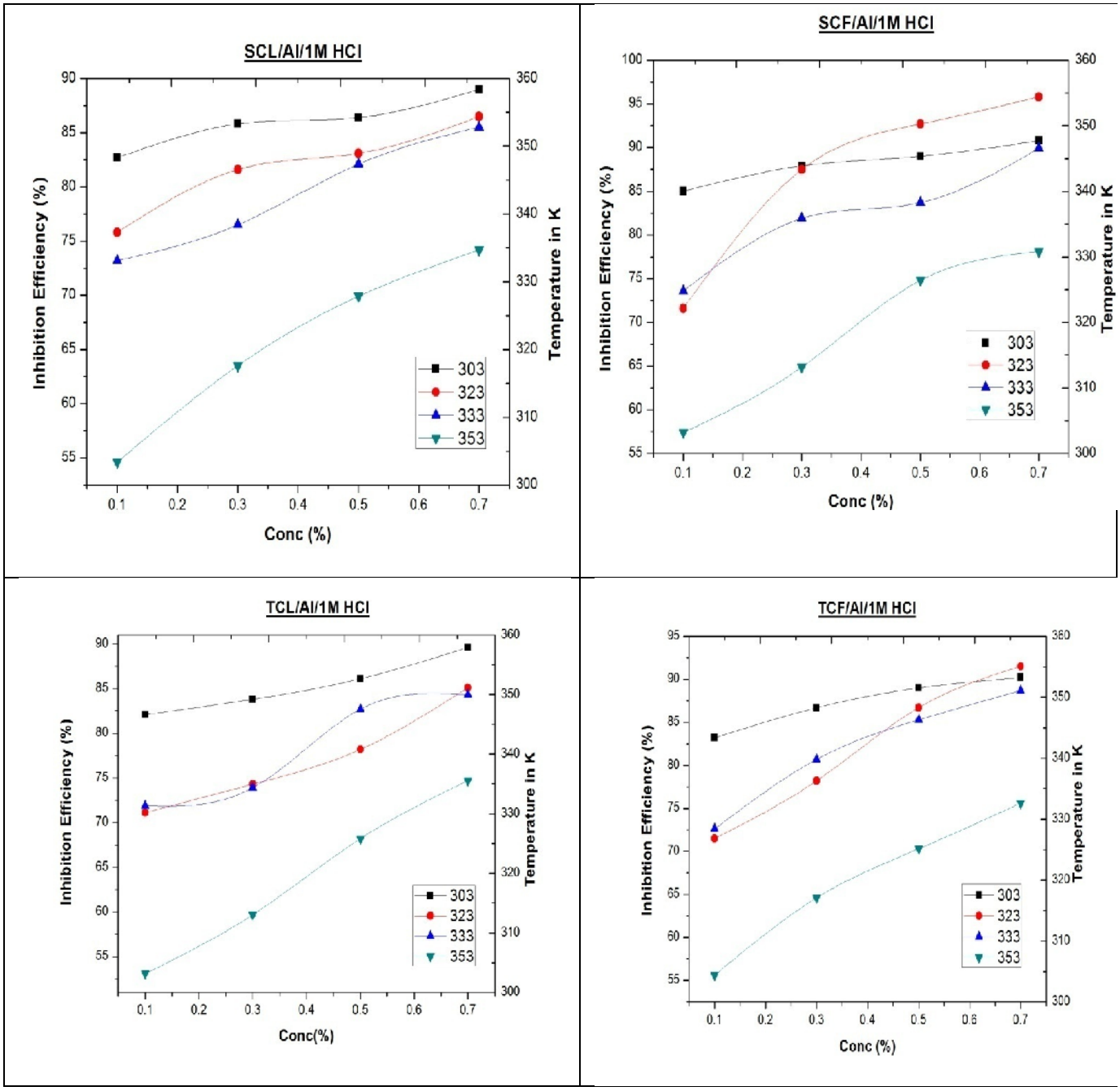

Figure 4.22 Impact of temperature on the corrosion inhibition of SCL /SCF/ TCL/ TCF extracts on AA1100 in 1M HCl

Table 4.29 IE as a function of temperature in the presence and absence of different concentration of TCL / TCF extracts on AA1100 in 1M HCl

CONC. %	TEMPERATURE (K)											
	303		313		323		333		343		353	
	CR (mpy)	IE (%)	CR (mpy)	IE (%)	CR (mpy)	IE (%)	CR (mpy)	IE (%)	CR (mpy)	IE (%)	CR (mpy)	IE (%)
TCL												
Blank	1434		7269		19146		29399		44972		69365	
0.1	257	82.1	1508	79.2	5527	71.1	8261	71.9	18079	59.8	32532	53.1
0.2	249	82.6	1351	81.4	5342	72.1	7585	74.2	17449	61.2	30313	56.3
0.3	232	83.8	1293	82.2	4921	74.3	7673	73.9	15695	65.1	27954	59.7
0.4	224	84.4	1194	83.6	4710	75.4	6350	78.4	14301	68.2	24416	64.8
0.5	199	86.1	1202	83.5	4174	78.2	5086	82.7	12817	71.5	22058	68.2
0.6	166	88.4	1169	83.9	3599	81.2	4939	83.2	12412	72.4	18590	73.2
0.7	149	89.6	1069	85.3	2853	85.1	4616	84.3	10748	76.1	17549	74.7
TCF												
Blank	1434		7269		19146		29399		44972		69365	
0.1	240	83.2	1343	81.5	5457	71.5	8055	72.6	17944	60.1	30798	55.6
0.2	224	84.4	1326	81.8	4863	74.6	6997	76.2	16235	63.9	28232	59.3
0.3	191	86.7	1227	83.1	4174	78.2	5674	80.7	14301	68.2	24555	64.6
0.4	182	87.3	1119	84.6	3599	81.4	5527	81.2	12907	71.3	22058	68.2
0.5	157	89.1	1218	83.2	2546	86.7	4322	85.3	12232	72.8	20601	70.3
0.6	149	89.6	945	87.0	1781	90.7	4057	86.2	9939	77.9	17619	74.6
0.7	141	90.2	622	91.4	1627	91.5	3322	88.7	9669	78.5	16925	75.6

REASON FOR LOW IE AT HIGHER TEMPERATURES

The tables reflect that IE afforded by the plant extracts decrease with increase in temperature. Similar results involving plant extracts used as corrosion inhibitor for aluminium in acid media have been reported by various investigators (**Obi-Egbedi, 2010 b).** It has been pointed out that the increase in inhibition efficiency with increase in extract concentration is an indication of an increase in the number of components of the extract adsorbed over the aluminium surface blocking the active sites, in which direct acid attacks proceed and protect the metal from corrosion, while the decrease in inhibition efficiency with temperature rise is suggestive of electrostatic interaction (physical adsorption) of the phytoconstituents of the extract on aluminium surface forming a protective layer and shielding the metal from corrosion **(Oguzie, 2007)**.

4.3.4.3 Comparison of IE of studied inhibitors using mass loss and electrochemical techniques on MS / AAA1100 / 1M HCl / SCL / SCF

Performance evaluation graph of investigated inhibitors using different techniques reveal that all the investigated inhibitors have quite comparable efficiency. Mass loss method furnishes significant raise in IE compared to other techniques (Figures 4.23 (a) and

4.24 (b)). This difference may be attributed to the fact that mass loss methods give average corrosion rates, whereas electrochemical methods give instantaneous corrosion rates. This difference may also be expected to arise because of the difference in the time required to form an absorbed layer of the organic compound which can bring down corrosion (**Muralidharan *et al,* 1995**).

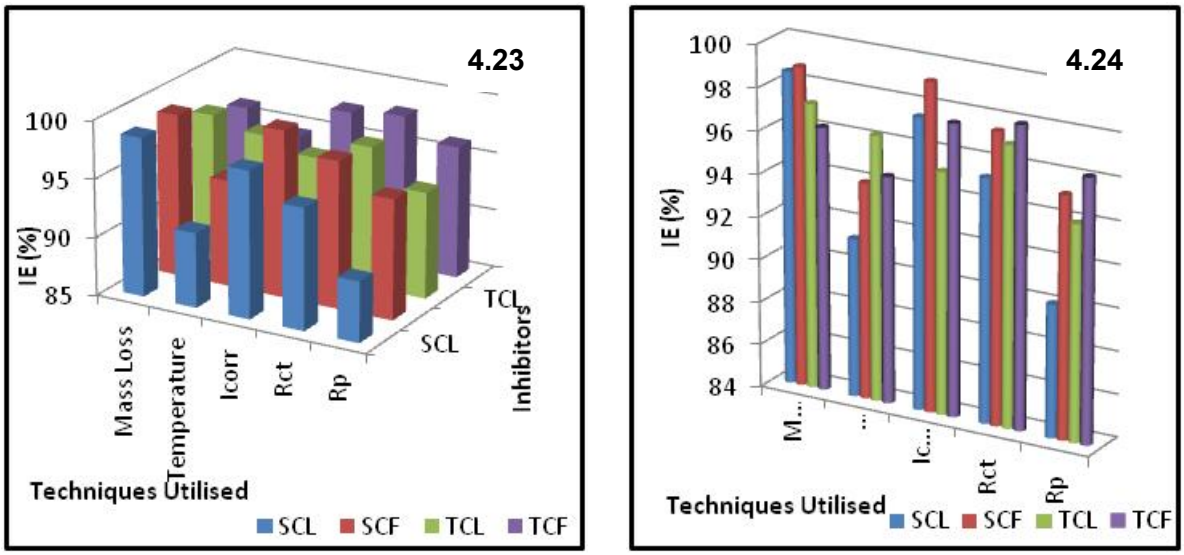

Figures 4.23 and 4.24 Comparison of IE of studied inhibitors using mass loss and electrochemical techniques for SCL /SCF /TCL /TCF / MS and AA 1100 / 1M HCl

The results obtained from mass loss, potentiodynamic polarisation and impedance techniques indicate that SCL/SCF/TCL/TCF extracts exhibit significant corrosion inhibition properties in 1M HCl. It is worth noting that the percentage inhibition efficiencies obtained from impedance measurements are comparable and run parallel with those obtained from mass loss and potentiodynamic polarisation measurements.

Comparing the IE of plant extracts, it is seen that there is no significant difference between the investigated inhibitors. Neverthless, in the case of SCL (for MS) and SCF (for AA1100), there is an increase of IE in the range of 1- 2% above other investigated inhibitors within the limit of the investigated concentration and temperature range. The results obtained from all investigated methods are in good agreement.

4.3.4.4 Synergistic aspects of plant extracts with reference to selected phytochemicals

The Bignoniaceac family plants utilised for the present investigation are usually found to be abundant in terpenoids, flavonoids alkaloids etc **(Cipriani *et al*,2007)**. Hence attempts have been made to extract flavonoid and total terpenoids from these plants by

simple procedure prescribed (**Laghari *et al*, 2011**) and confirmed using phytochemical screening methods. Extracted flavonoid and total terpenoid from the investigated plant extracts are represented as SCL-F, SCL-T, SCF-F, SCF-T, TCL-F, TCL-T, TCF-F, and TCF-T. Synthetically available flavonoids in our laboratory namely rutin and quercetin are also utilised for the present investigation. Mass loss measurements for a period of 3 hours have been carried out using the extracted and synthetically available Phytochemical of 0.7% concentration each for MS / AA1100 in 1M HCl and the results pertaining to the studies are presented and discussed below.

Table 4.30: Comparison of Corrosion rate and IE of extracted and synthetic phytochemicals for MS and AA1100 with the investigated inhibitors

SYSTEM	MS		AA1100	
	CR (mpy)	IE (%)	CR (mpy)	IE (%)
BLANK HCl	1238	-	4027	
SCL-F	210	83.0	750	81.4
SCL-T	220	82.2	816	79.7
SCF-F	214	82.7	725	82.0
SCF-T	207	83.3	600	85.1
TCL-F	187	84.9	560	86.1
TCL-T	175	85.9	590	85.3
TCF-F	216	82.6	612	84.8
TCF-T	201	83.8	607	84.9
Quercetin	235	81.0	700	82.6
Rutin	236	80.9	718	82.2

To confirm the inherent potential of the plant extracts, extracted and selected synthetic phytochemicals are tested for their corrosion inhibition potentials. Visualizing the results, it is clear that the IE is around 79-86% only for the extracted and selected synthetic phytochemicals.The investigated plant extracts furnish around 85-90% inhibition efficiency which might be due to the presence of large number of phytochemicals in the plant extract.The presence of other phytocomponents besides the crude flavonoid and terpenoid extracts may have been involved in the corrosion inhibition process or synergistically enhance the adsorption of plant extracts over the metal surface **(Bothi Raja,2013)**.

The findings infer that extraction of flavonoid and terpenoids incurring the expenditure of solvent, time and laborious lab procedure and the utilisation of costly synthetic phytochemical may not be essential as far as our present investigation is concerned.

4.3.5 Shelf life performance of SC/TC extracts at room temperature

For industrial purpose the extracts can be prepared in large scale and can be stored for a period of 3 years. This process may help to minimize the labour of the workers. Bearing this in mind, efforts have been taken to prepare the extracts in large scale and portion of it is kept in the room temperature. Mass loss method is best suited method to analyze the inhibitive action of these extracts. Experiments are conducted by selecting an optimum concentration, in the present case 0.7% concentration of SC / TC by mass loss measurements for a period of 3h immersion. Results pertaining to these studies are pictorially represented in Figure 4.25 a and b.

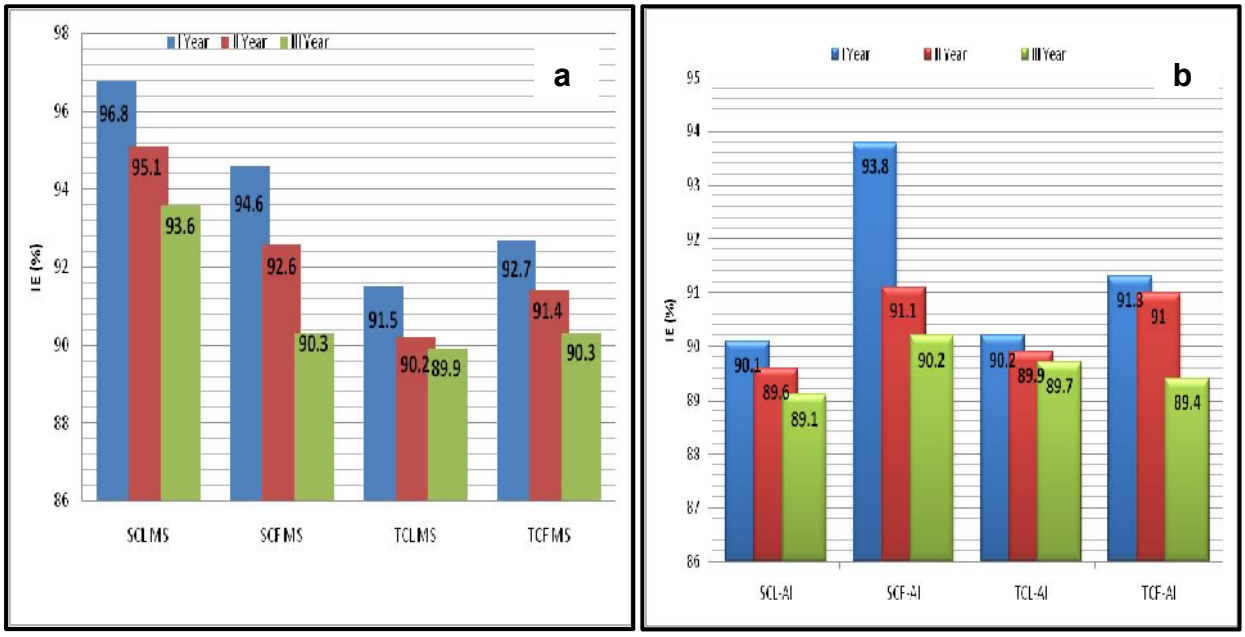

Figure: 4.25 Pictorial representation of durability of investigated inhibitors

a) MS / SCL / SCF / TCL / TCF / 1M HCl b) AA1100 / SCL / SCF / TCL / TCF / 1M HCl at room temperature for a period of 3 years

Analysis of data reveals that inhibition efficiency (%) is quite comparable for the all the tested inhibitors during the 3 years study period. This test confirms the long lasting inhibitive nature of the investigated inhibitors. Results obtained also infer the strong inhibitive action of the inhibitors kept at room temperature for the 3 years. It is up to the interest of industrialist to utilize the inhibitors at room temperature. Visual examination of the investigated plant extracts during storage reflects that the extracts are resistant towards

fungal and bacterial attack **(El-Etre *et al,* 2005)**. There is no unpleasant odour or evolution of gas during storage. The phytochemicals present in these extracts induce the antioxidant characteristics as reflected by very little change of viscosity after two years when stored in room temperature **(Das *et al,* 2004).** The inhibition efficiency for all the investigated inhibitors is about 85 percentage in the 3rd year. Thus these extracts prove to be good performers for 3 years. Thus they can be said to have appreciable shelf life.

4.4 Adsorption isotherm

In acid corrosion, generally, it is assumed that inhibitors act through a process of adsorption on the metal surface. The establishment of isotherms that describe the adsorptive behaviour of a corrosion inhibitor is an important part of its study, as they can provide important clues to the nature of the metal inhibitor interaction.

Adsorption isotherms impart a basic insight onto the interaction between the metal surface and the inhibitor species. Interpretation of the performance of the adsorbent type of inhibitor can be substantiated by fitting the data in one of the known adsorption isotherm.

Goodness of Fit:

Data are tested graphically by fitting to various isotherms. Statistical estimation of correlation for the curve fitting of isotherms are used to investigate the goodness of fit of the isotherms **(Schulthess *et al*, 1996).**

A measure of the goodness of fit is the square of correlation coefficient R^2 which shows that the % of the total variation of the dependent variables can be explained by the independent variable Y. Symbolically

$$R^2 = \frac{\Sigma Y_1^2}{\Sigma Y_1} = \frac{\text{Explained variation}}{\text{Total variation}} \qquad \textbf{(4.13)}$$

The value of R^2 generally lies between 0 and 1 ($0 \leq R^2 \leq 1$). The closer the value of R^2 lies to 1, the better is the regression line to data and vice versa.

To test the overall significance of regression model, the technology of ANOVA is used, which is defined by the F value.

$$F = \frac{\text{Explained sum of square/degrees of freedom}}{\text{Residual sum of squares/ degrees of freedom}} \qquad \textbf{(4.14)}$$

A large F value will be evidence against the null hypothesis, the explanatory variable have no effect of Y.

It is well recognized that the first step in inhibition of metallic corrosion is the adsorption of organic inhibitor molecules at the metal/solution interface. Furthermore, the adsorption depends on the molecules chemical composition, the temperature and the electrochemical potential at the metal/solution interface. So the adsorption of organic inhibitor molecules from the aqueous solution can be regarded as a quasi-substitution process between the organic compounds in the aqueous phase [$Org_{(sol)}$] and water molecules at the electrode surface [$H_2O_{(ads)}$].

$$Org_{(sol)} + x\ H_2O_{(ads)} \longleftrightarrow Org_{(ads)} + x\ H_2O_{(sol)} \qquad \textbf{(4.15)}$$

where x is the size ratio, that is, the number of water molecules replaced by one organic inhibitor. (**Noor *et al,* 2008**).

Attempts are made to fit θ values (obtained from mass loss values of MS and AA 1100 at different temperatures for ½ h immersion time) to various isotherms including Langmuir, Temkin, Freundlich, Frumkin, Flory-Huggins, El-Awady kinetic thermodynamic and Bockris-Swinkel's adsorption isotherms.

Langmuir adsorption isotherm can be obtained according to equation (4.16) **(Langmuir *et al,* 1917).**

$$\log (C/\theta) = \log C - \log K \qquad \textbf{(4.16)}$$

where K is the equilibrium constant, C is the concentration of inhibitor and θ is the degree of surface coverage of the inhibitors.

Temkin adsorption isotherm can be represented according to equation (4.17) **(Temkin *et al,* 1940)**

$$\exp (-2a\theta) = KC \qquad \textbf{(4.17)}$$

where 'a' is molecular interaction parameters, θ is the degree of surface coverage, K is the equilibrium constant of adsorption process and C is the concentration of the inhibitors.

Frumkin adsorption isotherm can be deduced according to equation (4.18) **(Frumkin *et al*, 1964)**

$$\ln [\theta / C (1- \theta)] = \ln K + 2a\ \theta \qquad \textbf{(4.18)}$$

where 'a' is the lateral interaction term describing the molecular interaction in the adsorbed layer, θ is the degree of surface coverage, K is the equilibrium constant of adsorption process and C is the concentration of inhibitors.

Freundlich adsorption isotherm can be written according to equation (4.19) **(Freundlich *et al,* 1907).**

$$\theta = K C^{1/n} \quad \textbf{(4.19)}$$

where n is the adsorption intensity, C is the inhibitor's concentration and K is the equilibrium constant of adsorption reaction.

Flory-Huggins adsorption isotherm can be explained according to equation (4.20) **(Flory, 1941; Huggins, 1941).**

$$\log (\theta/C) = \log K + x \log (1-\theta) \quad \textbf{(4.20)}$$

where θ is the degree of surface coverage, C is the concentration of the system studied x is the number of water molecule replaced by one inhibitor molecule and K is the equilibrium constant for the adsorption process.

El-Awady kinetic thermodynamic adsorption isotherm can be described according to equation (4.21) **(El-Awady *et al,* 1985)**

$$\log [\theta / (1- \theta)] = \log K' + y \log C \quad \textbf{(4.21)}$$

where C is the concentration of the adsorbate θ is the degree of surface coverage and 1/y is the number of inhibitor molecules occupying one active sites.

Bockris-Swinkel's adsorption isotherm can be arrived at using equation (4.22) **(Bockris *et al,* 1964)**

$$[\theta / (1-\theta)^x]^{[\theta + x (1- \theta) x-1]} / X^x = KC \quad \textbf{(4.22)}$$

Where θ is the degree of surface coverage, x is the number of water molecules substituted by one molecule of organic adsorbate and K is the equilibrium constant of the adsorption process.

A particular model which has highest value of R^2 can be considered as the best model to explain the changes in performance of the investigated extracts adsorbent-type inhibitors. Similarly, the effect of the level of concentration on the IE can be estimated by coefficient of the equation and can be tested against the hypothesis. The model used takes the following form $\ln y = \alpha + \beta x$, where 'y' is the surface coverage, α is the intercept, β is the slope and 'x' is the concentration. The same model is applied for the seven adsorption isotherms to identify the most suitable model for the problem under study using **Statistical Software Package SPSS 17.**

4.4.1 Adsorption isotherm behaviour of investigated inhibitors in acidic meda

Values of adsorption parameters deduced from various adsorption isotherm and the estimated coefficients of studied inhibitors in 1M HCl for MS and AA1100 are enlisted in Tables 4.31 - 4.38.

Table 4.31 Adsorption parameters deduced from various adsorption isotherms –MS / 1M HCl / SCL

Adsorption isotherms	Temp	Slope	t	intercept	R^2	F
Langmuir	303K	0.749	2.130** (0.077)	0.039	0.990	497.069** [0.000]
	313K	0.815	2.533** (0.044)	0.018	0.999	4083.267** [0.000]
	323K	0.807	0.513** (0.627)	0.002	1.000	12086.143** [0.000]
	333K	0.794	5.236** (0.002)	0.019	1.000	14065.680** [0.000]
	343K	0.705	1.185** (0.281)	0.026	0.984	312.368** [0.000]
	353K	0.776	3.805** (0.009)	0.045	0.996	1287.613** [0.000]
Temkin	303K	0.173	25.709** (0.000)	0.893	0.886	38.967** [0.002]
	313K	0.142	57.055** (0.000)	0.945	0.958	115.238** [0.000]
	323K	0.150	88.568** (0.000)	0.977	0.983	293.676** [0.000]
	333K	0.152	93.975** (0.000)	0.936	0.987	365.948** [0.000]
	343K	0.198	23.399** (0.000)	0.912	0.891	40.803** [0.001]
	353K	0.155	35.713** (0.000)	0.882	0.925	61.918** [0.001]
Frumkin	303K	0.163	2.585** (0.041)	1.926	0.005	0.025** [0.881]
	313K	-0.185	2.890** (0.028)	2.671	0.005	0.025** [0.879]
	323K	0.510	2.743** (0.034)	2.286	0.048	0.251** [0.638]
	333K	-0.720	5.744** (0.001)	2.943	0.193	1.195** [0.324]
	343K	0.709	2.4** (0.053)	1.523	0.112	0.628** [0.464]
	353K	-0.699	3.451** (0.014)	2.566	0.084	0.461** [0.527]
Freundlich	303K	0.251	-2.130** (0.077)	-0.090	0.918	55.611** [0.001]
	313K	0.185	-2.533** (0.044)	-0.041	0.977	209.184** [0.044]
	323K	0.193	-0.153** (0.627)	-0.005	0.993	689.273** [0.000]
	333K	0.206	-5.236** (0.002)	-0.044	0.995	946.525** [0.000]

Adsorption isotherms	Temp	Slope	t	intercept	R^2	F
Freundlich	343K	0.295	-1.185** (0.281)	-0.059	0.916	54.557** [0.001]
	353K	0.224	-3.805** (0.009)	-0.103	0.995	107.356** [0.000]
Flory-Huggins	303K	0.867	5.181** (0.002)	0.811	0.693	11.294** [0.020]
	313K	0.921	6.496** (0.001)	1.039	0.794	19.236** [0.007]
	323K	0.820	7.198** (0.000)	1.030	0.649	28.141** [0.003]
	333K	1.097	9.957 (0.000)	1.103	0.908	49.14 [0.001]
	343K	0.739	5.427** (0.002)	0.727	0.694	11.343** [0.020]
	353K	1.068	5.714** (0.001)	0.936	0.755	15.404** [0.11]
El-Awady kinetic thermodynamic	303K	0.887	8.271** (0.000)	0.834	0.822	23.079** [0.005]
	313K	0.899	11.871** (0.000)	1.049	0.860	30.841** [0.003]
	323K	1.035	13.846** (0.000)	1.189	0.896	43.846** [0.000]
	333K	0.866	18.872** (0.000)	0.974	0.944	83.834** [0.000]
	343K	1.008	25.576** (0.004)	0.880	0.836	25.576** [0.004]
	353K	0.791	10.037** (0.000)	0.799	0.855	29.424** [0.003]
3Bockris-Swinkles	303K	0.789	6.518** (0.001)	0.696	0.765	16.252** [0.010]
	313K	0.897	93341** (0.000)	0.941	0.825	23.571** [0.005]
	323K	1.050	10.921** (0.000)	1.050	0.867	32.721** [0.002]
	333K	0.829	13.572** (0.000)	0.851	0.912	52.072** [0.001]
	343K	0.877	6.442** (0.001)	0.736	0.778	17.554** [0.009]
	353K	0.705	70496** (0.000)	0.660	0.792	19.048** [0.007]

Figure within ( ) give t values; F Figure within [ ] give F ratio.

** - 1% level of significance, * - 5% level of significance.

Table 4.32. Adsorption parameters deduced from various adsorption isotherms –MS / 1M HCl / SCF

Adsorption isotherms	Temp	Slope	t	intercept	R^2	F
Langmuir	303K	0.885	5.864** (0.001)	0.060	0.998	2232.462** [0.000]
	313K	0.926	6.619** (0.001)	0.042	0.999	6294.933** [0.000]
	323K	0.960	8.599** (0.000)	0.025	1.000	33232.85** [0.000]
	333K	0.956	17.756** (0.000)	0.050	1.000	34839.53** [0.000]
	343K	0.804	4.110** (0.006)	0.062	0.994	843.208** [0.000]
	353K	0.880	5.699** (0.001)	0.062	0.997	1922.135** [0.000]
Temkin	303K	0.088	43.756** (0.000)	0.867	0.863	31.416** [0.002]
	313K	0.062	70.260** (0.000)	0.906	0.880	36.606** [0.002]
	323K	0.035	164.346** (0.000)	0.944	0.923	59.695** [0.001]
	333K	0.037	162.917** (0.000)	0.891	0.934	71.186** [0.002]
	343K	0.136	30.635** (0.000)	0.854	0.883	37.732** [0.002]
	353K	0.087	51.060** (0.000)	0.857	0.872	42.032** [0.001]
Frumkin	303K	-3.722	3.458** (0.014)	5.206	0.422	3.657** [0.114]
	313K	-6.419	3.747** (0.010)	8.147	0.551	6.141** [0.056]
	323K	-15.474	6.090** (0.001)	17.377	0.828	24.119** [0.004]
	333K	-17.743	6.833** (0.000)	17.941	0.869	33.105** [0.002]
	343K	-1.382	3.522** (0.012)	2.986	0.212	1.348** [0.298]
	353K	-5.211	5.497** (0.002)	6.252	0.711	12.290** [0.017]
Freundlich	303K	0.115	-5.864* (0.001)	-0.138	0.883	37.839** [0.002]
	313K	0.074	-6.619** (0.001)	-0.097	0.868	40.574** [0.001]
	323K	0.040	-8.599** (0.000)	-0.547	0.919	56.410** [0.001]
	333K	0.044	-17.756** (0.000)	-0.114	0.923	72.450** [0.000]
Freundlich	343K	0.196	-4.110** (0.006)	-0.143	0.910	50.297** [0.001]
	353K	0.120	-5.699** (0.001)	-0.144	0.852	35.561** [0.002]
Flory-Huggins	303K	1.677	4.934** (0.003)	1.459	0.742	14.398** [0.013]
	313K	1.888	5.464** (0.002)	1.918	0.794	19.267** [0.007]
	323K	2.630	9.883** (0.000)	3.150	0.936	73.601** [0.000]
	333K	3.669	8.001** (0.000)	3.456	0.910	50.367** [0.001]
	343K	1.297	5.353** (0.002)	1.038	0.748	14.819** [0.012]
	353K	2.446	8.275** (0.000)	1.909	0.903	46.533** [0.001]
El-Awady kinetic thermodynamic	303K	0.518	12.701** (0.000)	0.787	0.806	20.701** [0.000]
	313K	0.469	18.280** (0.000)	0.961	0.795	24.206** [0.004]
	323K	0.382	50.085** (0.000)	1.172	0.941	79.545** [0.000]
	333K	0.282	44.320** (0.000)	0.895	0.920	57.870** [0.001]
	343K	0.680	10.034** (0.000)	0.722	0.842	26.582** [0.004]
	353K	0.450	22.369** (0.000)	0.729	0.919	56.661** [0.001]
Bockris-Swinkles	303K	0.511	10.154** (0.000)	0.669	0.782	17.909** [0.008]
	313K	0.497	14.999** (0.000)	0.852	0.820	22.802** [0.005]
	323K	0.418	43.015** (0.000)	1.097	0.941	80.081** [0.000]
	333K	0.300	36.165** (0.000)	0.792	0.918	55.819** [0.001]
	343K	0.603	7.979** (0.000)	0.587	0.760	20.038** [0.007]
	353K	0.416	21.668** (0.000)	0.598	0.931	67.677** [0.001]

Figure within ( ) give t values; F Figure within [ ] give F ratio.
** - 1% level of significance, * - 5% level of significance.

Table 4.33. Adsorption parameters deduced from various adsorption isotherms –MS / 1M HCl / TCL

Adsorption isotherms	Temp	Slope	t	intercept	R^2	F
Langmuir	303K	0.835	3.318** (0.016)	0.054	0.994	780.317** [0.000]
	313K	0.799	2.847** (0.029)	0.031	0.996	1649.106** [0.000]
	323K	0.814	1.862** (0.112)	0.017	0.998	2424.652** [0.000]
	333K	0.812	3.379** (0.015)	0.027	0.998	3121.029** [0.000]
	343K	0.779	4.012** (0.007)	0.032	0.998	2882.833** [0.000]
	353K	0.818	5.940** (0.001)	0.063	0.997	1782.919** [0.000]
Temkin	303K	0.122	28.070** (0.000)	0.875	0.829	24.070** [0.000]
	313K	0.145	44.574** (0.000)	0.913	0.929	79.513** [0.000]
	323K	0.143	48.690** (0.000)	0.947	0.945	85.399** [0.000]
	333K	0.139	67.021** (0.000)	0.922	0.970	160.030** [0.000]
	343K	0.156	56.162** (0.000)	0.908	0.967	147.372** [0.000]
	353K	0.127	41.257** (0.000)	0.853	0.923	59.582** [0.000]
Frumkin	303K	-0.884	2.285** (0.062)	2.864	0.053	0.278** [0.621]
	313K	-0.834	3.696** (0.010)	2.915	0.115	0.648** [0.457]
	323K	-0.216	3.341** (0.016)	2.694	0.009	0.046** [0.839]
	333K	-1.290	5.621** (0.001)	3.369	0.359	2.797** [0.155]
	343K	-0.915	5.725** (0.001)	2.867	0.271	1.857** [0.231]
	353K	-0.231	15.186** (0.000)	2.765	0.312	31.122** [0.003]
Freundlich	303K	0.165	-3.318* (0.016)	-0.125	0.860	30.610** [0.003]
	313K	0.201	-2.847** (0.029)	-0.070	0.955	105.014** [0.000]
	323K	0.186	-1.862** (0.112)	-0.039	0.962	127.303** [0.000]
	333K	0.188	-3.379** (0.015)	-0.062	0.971	168.330** [0.000]

Adsorption isotherms	Temp	Slope	t	intercept	R^2	F
Freundlich	343K	0.221	-4.012** (0.007)	-0.073	0.979	231.364** [0.000]
	353K	0.182	-5.940** (0.001)	-0.145	0.946	87.781** [0.000]
Flory-Huggins	303K	1.056	4.194** (0.006)	0.993	0.622	8.219** [0.035]
	313K	1.082	6.268** (0.001)	1.045	0.792	18.986** [0.007]
	323K	0.976	7.243** (0.000)	1.078	0.832	24.751** [0.004]
	333K	0.989	7.871** (0.000)	1.076	0.857	30.078** [0.003]
	343K	1.184	9.094** (0.000)	1.065	0.893	41.821** [0.001]
	353K	0.544	-15.753** (0.000)	-0.742	0.805	20.658** [0.006]
El-Awady kinetic thermodynamic	303K	0.686	8.107** (0.000)	0.811	0.737	14.016** [0.013]
	313K	0.799	11.887** (0.000)	0.898	0.870	33.318** [0.002]
	323K	0.893	13.522** (0.000)	1.045	0.888	39.735** [0.001]
	333K	0.783	17.954** (0.000)	0.929	0.932	68.297** [0.000]
	343K	0.816	16.875** (0.000)	0.865	0.938	75.454** [0.001]
	353K	0.638	12.364** (0.000)	0.719	0.878	35.849** [0.002]
Bockris-Swinkles	303K	0.655	6.469** (0.001)	0.689	0.693	11.263** [0.020]
	313K	0.748	9.086** (0.000)	0.768	0.823	23.300** [0.005]
	323K	0.889	10.784** (0.000)	0.937	0.862	31.157** [0.003]
	333K	0.748	13.387** (0.000)	0.804	0.902	46.172** [0.001]
	343K	0.744	12.532** (0.000)	0.729	0.907	48.774** [0.001]
	353K	0.570	9.447** (0.000)	0.584	0.835	25.375** [0.004]

Figure within ( ) give t values; F Figure within [ ] give F ratio.
** - 1% level of significance, * - 5% level of significance.

Table 4.34 Adsorption parameters deduced from various adsorption isotherms – MS / 1M HCl / TCF

Adsorption isotherms	Temp	Slope	t	intercept	R^2	F
Langmuir	303K	0.864	5.087** (0.002)	0.045	0.998	2779.585** [0.000]
	313K	0.866	3731** (0.010)	0.037	0.998	2251.553** [0.000]
	323K	0.912	5.075** (0.02)	0.012	1.000	44720.112** [0.000]
	333K	0.909	12.152** (0.000)	0.037	1.000	26615.518** [0.000]
	343K	0.804	4.112** (0.006)	0.062	0.994	843.306** [0.000]
	353K	0.825	3.893** (0.008)	0.044	0.997	1603.114** [0.000]
Temkin	303K	0.104	53.551** (0.000)	0.893	0.924	61.051** [0.000]
	313K	0.101	60.014** (0.000)	0.906	0.934	70.389** [0.000]
	323K	0.076	229.818** (0.000)	0.968	0.990	515.335** [0.000]
	333K	0.074	156.026** (0.002)	0.914	0.981	254.845** [0.000]
	343K	0.136	30.635** (0.000)	0.854	0.883	37.732** [0.002]
	353K	0.123	60.635** (0.000)	0.886	0.957	111.958** [0.000]
Frumkin	303K	-3.075	5.018** (0.002)	4.796	0.559	6.350** [0.053]
	313K	-3.660	7.465** (0.000)	5.409	0.765	16.316** [0.010]
	323K	-3.769	12.280** (0.000)	6.549	0.887	39.280** [0.002]
	343K	-6.220	9.999** (0.000)	7.914	0.896	43.028** [0.001]
	353K	-1.382	3.522** (0.012)	2.986	0.212	1.348** [0.298]
	303K	-2.792	9.966** (0.000)	4.334	0.825	23.598** [0.005]
Freundlich	303K	0.136	-5.081** (0.002)	-0.105	0.932	68.345** [0.000]
	313K	0.134	-3.738** (0.010)	-0.086	0.915	53.930** [0.001]
	323K	0.088	-5.074** (0.002)	-0.028	0.988	417.049** [0.000]
	333K	0.091	-12.094** (0.000)	-0.085	0.982	267.010** [0.000]

Adsorption isotherms	Temp	Slope	t	intercept	R^2	F
Freundlich	343K	0.196	-4.110** (0.006)	-0.143	0.910	50.297** [0.001]
	353K	0.175	-3.896** (0.008)	-0.101	0.936	72.564** [0.000]
Flory-Huggins	303K	1.643	7.531** (0.000)	1.477	0.871	33.637** [0.002]
	313K	1.892	13.729** (0.000)	1.717	0.960	119.339** [0.000]
	323K	1.438	19.12** (0.000)	1.823	0.978	224.043** [0.000]
	333K	2.042	12.279 (0.000)	2.014	0.952	100.110 [0.000]
	343K	1.297	15.353** (0.003)	1.038	0.748	14.819** [0.002]
	353K	1.811	18.650** (0.000)	1.477	0.977	212.463** [0.000]
El-Awady kinetic thermodynamic	303K	0.601	18.098** (0.000)	0.853	0.906	48.411** [0.001]
	313K	0.577	33.370** (0.000)	0.883	0.966	141.585** [0.000]
	323K	0.708	55.589** (0.000)	1.257	0.983	291.980** [0.000]
	333K	0.516	39.463** (0.000)	0.958	0.964	134.587** [0.000]
	343K	0.680	10.034** (0.000)	0.722	0.842	26.582** [0.004]
	353K	0.624	37.118 (0.000)	0.793	0.981	253.893** [0.000]
3Bockris-Swinkles	303K	0.591	14.905** (0.000)	0.735	0.895	42.905** [0.001]
	313K	0.561	34.878** (0.000)	0.762	0.975	196.396** [0.000]
	323K	0.765	45.628** (0.000)	1.188	0.981	257.240** [0.000]
	333K	0.538	31.339** (0.000)	0.856	0.958	115.355** [0.000]
	343K	0.603	7.979** (0.000)	0.587	0.800	20.038** [0.007]
	353K	0.561	47.997** (0.000)	0.653	0.990	505.407** [0.000]

Table 4.35 Adsorption parameters deduced from various adsorption isotherms – AA1100 / 1M HCl / SCL

Adsorption isotherms	Temp	Slope	t	intercept	R^2	F
Langmuir	303K	0.835	3.311** (0.016)	0.054	0.994	777.513** [0.000]
	313K	0.798	2.846** (0.029)	0.030	0.997	1653.463** [0.000]
	323K	0.814	1.861** (0.112)	0.017	0.998	2419.562** [0.000]
	333K	0.812	3.390** (0.015)	0.027	0.998	3143.645** [0.000]
	343K	0.779	4.016** (0.007)	0.032	0.998	2890.884** [0.000]
	353K	0.818	5.933** (0.001)	0.063	0.997	1781.507** [0.000]
Temkin	303K	0.122	28.069** (0.000)	0.875	0.829	24.172** [0.004]
	313K	0.145	44.567** (0.000)	0.913	0.941	79.487** [0.000]
	323K	0.143	48.694** (0.000)	0.947	0.945	85.411** [0.000]
	333K	0.139	67.027** (0.000)	0.922	0.970	160.058** [0.000]
	343K	0.156	56.159** (0.000)	0.908	0.967	147.353** [0.000]
	353K	0.127	41.257** (0.000)	0.853	0.923	59.580** [0.001]
Frumkin	303K	-0.884	2.285** (0.062)	2.864	0.053	0.278** [0.621]
	313K	-0.834	3.696** (0.010)	2.915	0.115	0.648** [0.457]
	323K	-0.216	3.341** (0.016)	2.694	0.009	0.046** [0.839]
	333K	-1.290	5.621** (0.001)	3.369	0.359	2.797** [0.155]
	343K	-0.915	5.725** (0.001)	2.867	0.271	1.858** [0.231]
	353K	-2.133	4.460** (0.004)	3.574	0.424	3.677** [0.113]
Freundlich	303K	0.165	-3.319** (0.016)	-0.125	0.860	30.643** [0.003]
	313K	0.201	-2.846** (0.029)	-0.070	0.955	104.892** [0.000]
	323K	0.186	-1.864** (0.112)	-0.139	0.962	127.501** [0.000]
	333K	0.188	-3.379** (0.015)	-0.062	0.971	168.180** [0.000]
Freundlich	343K	0.221	-4.009** (0.007)	-0.073	0.979	230.947** [0.000]
	353K	0.182	-5.939** (0.001)	-0.145	0.946	87.723** [0.000]
Flory-Huggins	303K	1.056	4.193** (0.006)	0.993	0.622	8.215** [0.035]
	313K	1.082	6.268** (0.001)	1.042	0.792	18.984** [0.007]
	323K	0.976	7.241** (0.000)	1.078	0.832	24.741** [0.004]
	333K	1.225	8.850** (0.000)	1.183	0.891	40.809** [0.001]
	343K	1.184	9.098** (0.000)	1.065	0.893	41.864** [0.001]
	353K	1.481	6.121** (0.001)	1.162	0.805	20.678** [0.006]
El-Awady kinetic thermodynamic	303K	0.686	8.106** (0.000)	0.811	0.737	14.012** [0.000]
	313K	0.799	11.885** (0.000)	0.898	0.869	33.305** [0.002]
	323K	0.893	13.525** (0.000)	1.045	0.888	39.746** [0.001]
	333K	0.783	17.950** (0.000)	0.929	0.932	68.260** [0.000]
	343K	0.816	16.874** (0.000)	0.865	0.938	75.437** [0.000]
	353K	0.638	12.360** (0.000)	0.719	0.878	35.831** [0.002]
Bockris-Swinkles	303K	0.655	6.469** (0.001)	0.689	0.693	11.265** [0.020]
	313K	0.748	9.086** (0.000)	0.768	0.823	23.292** [0.005]
	323K	0.889	10.785** (0.000)	0.937	0.862	31.165** [0.003]
	333K	0.748	13.383** (0.000)	0.804	0.902	46.138** [0.001]
	343K	0.744	12.535** (0.000)	0.729	0.907	48.798** [0.001]
	353K	0.570	9.452** (0.000)	0.584	0.836	25.397** [0.004]

Figure within ( ) give t values; F Figure within [ ] give F ratio.
** - 1% level of significance, * - 5% level of significance.

Table 4.36. Adsorption parameters deduced from various adsorption isotherms – AA1100 / 1M HCl / SCF

Adsorption isotherms	Temp	Slope	t	intercept	R^2	F
Langmuir	303K	0.967	34.996** (0.000)	0.039	1.000	227052.142** [0.000]
	313K	0.915	2.037** (0.088)	0.011	0.999	8833.691** [0.000]
	323K	0.852	-2.104** (0.080)	-0.012	0.999	7120.795** [0.000]
	333K	0.908	8.414** (0.000)	0.043	0.999	9363.710** [0.000]
	343K	0.863	6.891** (0.000)	0.085	0.997	1469.397** [0.000]
	353K	0.820	6.905** (0.000)	0.078	0.997	1557.108** [0.000]
Temkin	303K	0.029	385.980** (0.000)	0.914	0.979	233.546** [0.000]
	313K	0.075	82.106** (0.000)	0.972	0.927	63.637** [0.000]
	323K	0.124	132.063** (0.000)	1.031	0.988	410.270** [0.000]
	333K	0.074	84.617** (0.002)	0.901	0.938	76.298** [0.000]
	343K	0.097	38.554** (0.000)	0.817	0.868	32.894** [0.002]
	353K	0.121	43.487** (0.000)	0.823	0.928	64.486** [0.000]
Frumkin	303K	-24.445	11.265** (0.000)	24.694	0.951	96.950** [0.000]
	313K	-0.564	1.664** (0.147)	3.811	0.010	0.048** [0.835]
	323K	0.804	4.910** (0.003)	2.550	0.272	1.867** [0.003]
	333K	-5.675	4.897** (0.003)	7.306	0.662	9.790** [0.026]
	343K	-3.976	4.146** (0.006)	4.845	0.542	5.922** [0.059]
	353K	-2.974	5.719** (0.001)	3.975	0.639	8.869** [0.031]
Freundlich	303K	0.165	-3.319** (0.016)	-0.125	0.860	30.643** [0.003]
	313K	0.201	--2.846** (0.029)	0.201	0.955	104.892** [0.000]
	323K	0.186	-1.864** (0.112)	-0.039	0.962	127.501** [0.000]
	333K	0.188	-3.379** (0.015)	-0.062	0.971	168.180** [0.000]
Freundlich	343K	0.221	-4.009** (0.007)	-0.073	0.979	230.947** [0.000]
	353K	0.182	-5.939** (0.001)	-0.145	0.946	87.723** [0.000]
Flory-Huggins	303K	3.844	11.034** (0.000)	4.015	0.952	98.296** [0.000]
	313K	0.935	5.607** (0.001)	1.371	0.761	15.935** [0.010]
	323K	0.857	20.594** (0.000)	1.271	0.976	207.435** [0.000]
	333K	1.852	6.235** (0.001)	1.800	0.831	24.654** [0.004]
	343K	2.046	5.379** (0.002)	1.453	0.784	18.145** [0.008]
	353K	1.887	7.390** (0.000)	1.299	0.869	33.229** [0.002]
El-Awady kinetic thermodynamic	303K	0.272	72.207** (0.000)	1.010	0.958	112.917** [0.000]
	313K	0.839	13.252** (0.000)	1.361	0.799	19.875** [0.007]
	323K	1.115	39.244** (0.000)	1.469	0.981	264.350** [0.000]
	333K	0.503	19.267** (0.000)	0.915	0.870	33.446** [0.002]
	343K	0.478	12.623** (0.000)	0.629	0.846	27.417** [0.003]
	353K	0.565	15.111** (0.000)	0.628	0.917	55.031** [0.001]
3Bockris-Swinkles	303K	0.297	59.277** (0.000)	0.920	0.956	108.929** [0.000]
	313K	0.912	11.534** (0.000)	1.302	0.795	19.426** [0.007]
	323K	1.186	30.910** (0.000)	1.411	0.976	200.853** [0.000]
	333K	0.521	15.345** (0.000)	0.809	0.853	29.059** [0.003]
	343K	0.427	10.340** (0.000)	0.498	0.824	23.437** [0.005]
	353K	0.476	12.394** (0.000)	0.488	0.897	43.594** [0.001]

Figure within ( ) give t values; F Figure within [ ] give F ratio.
** - 1% level of significance, * - 5% level of significance.

Table 4.37 Adsorption parameters deduced from various adsorption isotherms – AA1100 / 1M HCl / TCL

Adsorption isotherms	Temp	Slope	t	intercept	R^2	F
Langmuir	303K	0.956	9.446** (0.000)	0.048	1.000	10336.311** [0.000]
	313K	0.965	43.460** (0.000)	0.066	1.000	119723.14** [0.000]
	323K	0.914	7.650** (0.000)	0.075	0.998	2575.568** [0.000]
	333K	0.911	7.469** (0.000)	0.065	0.998	3277.300** [0.000]
	343K	0.874	12.907** (0.000)	0.111	0.998	3069.931** [0.000]
	353K	0.815	9.371** (0.000)	0.108	0.997	1489.577** [0.000]
Temkin	303K	0.038	86.318** (0.000)	0.894	0.807	20.841** [0.000]
	313K	0.028	291.034** (0.000)	0.858	0.967	145.776** [0.000]
	323K	0.066	45.467** (0.000)	0.839	0.801	20.134** [0.006]
	333K	0.069	53.614** (0.000)	0.858	0.854	29.239** [0.003]
	343K	0.084	53.137** (0.000)	0.769	0.915	53.584** [0.000]
	353K	0.116	39.391** (0.000)	0.769	0.918	55.884** [0.001]
Frumkin	303K	-13.065	3.366** (0.015)	14.006	0.589	7.180** [0.44]
	313K	-27.246	10.539** (0.000)	25.198	0.947	88.922** [0.000]
	323K	-6.193	3.204** (0.019)	7.056	0.483	4.679** [0.083]
	333K	-6.412	4.014** (0.007)	7.420	0.597	7.415** [0.042]
	343K	-6.223	5.787** (0.001)	6.056	0.766	16.345** [0.010]
	353K	-3.473	5.430** (0.002)	3.922	0.660	9.693** [0.0261]
Freundlich	303K	0.044	-9.452* (0.000)	-0.112	0.814	21.901** [0.005]
	313K	0.035	-43.441** (0.000)	-0.152	0.968	152.907** [0.000]
	323K	0.086	-7.642** (0.000)	-0.173	0.819	22.562** [0.005]
	333K	0.093	-7.476** (0.000)	-0.149	0.861	30.961** [0.003]
Freundlich	343K	0.126	-12.928** (0.000)	-.0.256	0.928	64.200** [0.000]
	353K	0.185	-9.379** (0.000)	-0.249	0.939	76.466** [0.000]
Flory-Huggins	303K	2.717	4.406** (0.005)	2.685	0.739	14.175** [0.013]
	313K	5.767	10.861** (0.000)	4.801	0.952	99.976** [0.000]
	323K	2.203	4.153** (0.006)	1.774	0.693	11.268** [0.020]
	333K	2.321	5.435** (0.002)	1.933	0.799	19.847** [0.007]
	343K	2.913	6.462** (0.001)	1.752	0.854	29.333** [0.003]
	353K	2.146	6.321** (0.001)	1.258	0.836	25.411** [0.004]
El-Awady kinetic thermodynamic	303K	0.307	22.114** (0.000)	0.916	0.766	16.402** [0.010]
	313K	0.194	78.028** (0.000)	0.774	0.958	114.079** [0.000]
	323K	0.382	13.252** (0.000)	0.708	0.752	15.182** [0.011]
	333K	0.408	17.284** (0.000)	0.761	0.836	25.579** [0.004]
	343K	0.387	16.036** (0.000)	0.510	0.898	44.038** [0.001]
	353K	0.510	12.175** (0.000)	0.503	0.901	45.428** [0.001]
Bockris-Swinkles	303K	0.330	18.097** (0.000)	0.816	0.762	15.984** [0.010]
	313K	0.203	62.064** (0.000)	0.661	0.956	107.895** [0.000]
	323K	0.377	10.584** (0.000)	0.589	0.732	13.656** [0.014]
	333K	0.407	14.222** (0.000)	0.644	0.828	24.127** [0.000]
	343K	0.321	12.746** (0.000)	0.380	0.874	34.619** [0.002]
	353K	0.390	9.508** (0.000)	0.364	0.861	30.950** [0.003]

Figure within ( ) give t values; F Figure within [ ] give F ratio.
** - 1% level of significance, * - 5% level of significance.

Table 4.38 : Adsorption parameters deduced from various adsorption isotherms – AA1100 / 1M HCl / TCF

Adsorption isotherms	Temp	Slope	t	intercept	R^2	F
Langmuir	303K	0.956	19.038** (0.000)	0.039	1.000	64641.648** [0.000]
	313K	0.953	5.629** (0.001)	0.051	0.999	3360.448** [0.000]
	323K	0.865	2.635** (0.000)	0.024	0.0998	2748.485** [0.000]
	333K	0.897	9.810** (0.002)	0.041	1.000	13636.179** [0.000]
	343K	0.858	13.989** (0.000)	0.087	0.999	5623.241** [0.000]
	353K	0.834	15.491** (0.000)	0.099	0.999	5081.380** [0.000]
Temkin	303K	0.038	213.810** (0.000)	0.913	0.961	123.359** [0.000]
	313K	0.040	49.101** (0.000)	0.890	0.605	7.664** [0.039]
	323K	0.109	50.164** (0.000)	0.939	0.915	53.824** [0.001]
	333K	0.082	103.027** (0.000)	0.905	0.965	137.906** [0.000]
	343K	0.098	67.958** (0.000)	0.810	0.955	106.227** [0.000]
	353K	0.108	67.420** (0.000)	0.786	0.964	134.993** [0.000]
Frumkin	303K	-16.623	8.247** (0.000)	17.517	0.903	46.608** [0.000]
	313K	-6.297	1.681** (0.144)	8.153	0.195	1.210** [0.322]
	323K	-1.063	2.936** (0.026)	3.569	0.094	0.519** [0.503]
	333K	1.000	NaN	0.000	1.000	
	343K	-4.940	17.340** (0.000)	5.446	0.816	22.132** [0.005]
	353K	-4.421	8.470** (0.000)	4.761	0.848	27.971** [0.003]
Freundlich	303K	0.044	-18.979** (0.000)	-0.090	0.964	133.979** [0.000]
	313K	0.047	-5.630** (0.001)	-0.116	0.617	8.052** [0.036]
	323K	0.135	-2.639** (0.000)	-0.055	0.931	67.257** [0.000]
	333K	0.102	-9.800** (0.002)	-0.095	0.972	176.795** [0.000]

Adsorption isotherms	Temp	Slope	t	intercept	R^2	F
Freundlich	343K	0.142	9.815** (0.000)	-0.201	0.969	154.342** [0.000]
	353K	0.166	2.802** (0.031)	-0.228	0.976	202.095** [0.000]
Flory-Huggins	303K	3.121	9.815** (0.000)	3.222	0.937	73.913** [0.000]
	313K	1.683	2.802** (0.031)	1.790	0.491	4.828** [0.079]
	323K	1.099	6.209** (0.001)	1.249	0.97	19.620** [0.007]
	333K	1.869	8.655** (0.000)	1.787	0.905	47.625** [0.001]
	343K	2.388	8.080** (0.000)	1.603	0.896	43.298** [0.001]
	353K	2.421	9.150** (0.000)	1.479	0.917	55.601 ** [0.001]
El-Awady kinetic thermodynamic	303K	0.331	50.825** (0.000)	0.997	0.944	84.911** [0.000]
	313K	0.336	12.096** (0.000)	0.912	0.541	5.903** [0.059]
	323K	0.775	13.375** (0.000)	1.065	0.850	28.226** [0.003]
	333K	0.539	25.208** (0.004)	0.917	0.929	65.500** [0.000]
	343K	0.467	19.818** (0.000)	0.604	0.933	69.910** [0.000]
	353K	0.487	20.119** (0.000)	0.541	0.951	96.847** [0.000]
3Bockris-Swinkles	303K	0.331	50.825** (0.000)	0.997	0.944	84.911** [0.000]
	313K	0.336	12.096** (0.000)	0.912	0.541	5.903** [0.059]
	323K	0.775	13.375** (0.000)	1.065	0.850	28.226** [0.003]
	333K	0.539	25.208** (0.004)	0.917	0.929	65.500** [0.000]
	343K	0.467	19.818** (0.000)	0.604	0.933	69.910** [0.000]
	353K	0.487	20.119** (0.000)	0.541	0.951	96.847** [0.000]

Figure within ( ) give t values; F Figure within [ ] give F ratio.
** - 1% level of significance, * - 5% level of significance.

Analysing the values of F, the following Table has been arrived at and the adsorption models followed by the studied inhibitors are represented in Table.4.39. The highest values of F are also highlighted in Table 4.39

Table 4.39 The results of Statistical SPSS 17 package on adsorption isotherms and the various adsorption models obeyed by the investigated inhibitors and their highest F values

Inhibitors	MS			AA1100		
	Adsorption Models	Highest F values	R^2	Adsorption Models	Highest F values	R^2
SCL	Langmuir	14066	1	Langmuir	3144	0.998
SCF	Langmuir	34840	1	Langmuir	227052	1
TCL	Langmuir	3121	0.998	Langmuir	119723	1
TCF	Langmuir	440720	1	Langmuir	64642	1

4.4.2 Langmuir Adsorption model for investigated inhibitors:

Langmuir Adsorption Isotherm

Langmuir adsorption equation relates degree of surface coverage to concentration of inhibitor according to equation (4.23).

$$\text{Log } (C/\theta) = \log C - \log K \qquad \textbf{(4.23)}$$

A plot of log (θ/1-θ) versus log C from mass loss data obtained for studied inhibitors yields straight lines as represented in Figure 4.26. The slope deviates from unity. This deviation may be explained on the basis of the interaction among adsorbed species on the metal surface. It has been postulated in the derivation of Langmuir adsorption isotherm equation that adsorbed molecules do not interact with one another, but this is not the case of large organic molecules having polar atoms (or) groups which can adsorbed on the cathodic and anodic sites of the metal surface such adsorbed species interact by mutual repulsion or attraction **(Eddy *et al,* 2010, Solomon *et al,* 2010).** It is also possible that the inhibitor studied can be adsorbed on the anodic and cathodic sites resulting in deviation from unit gradient.

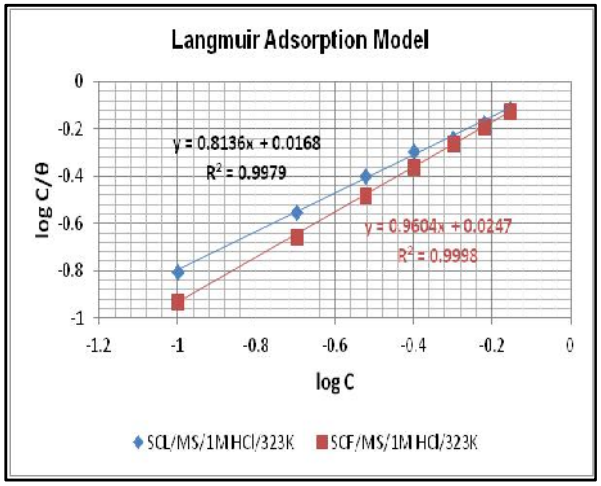

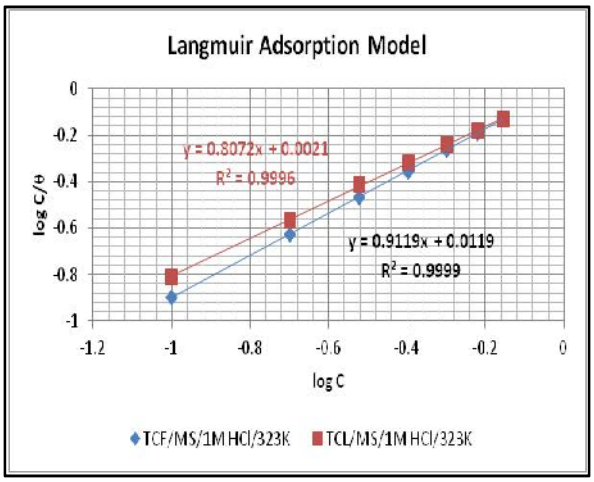

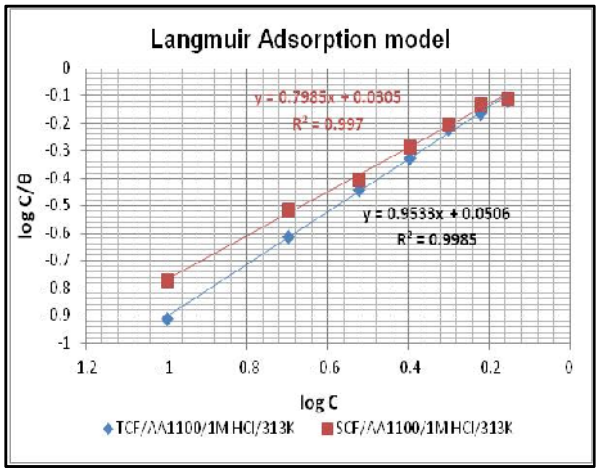

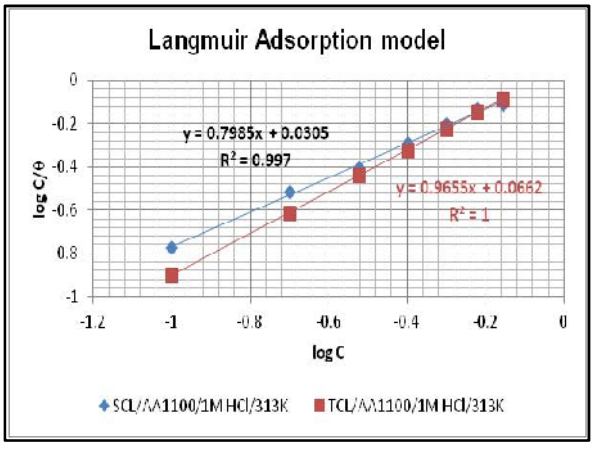

Figure 4.26 Langmuir Adsorption Isotherms for MS, AA1100 / SCL / SCF / TCL / TCF / 1M HCl systems

4.5 Kinetic parameters for inhibition process

4.5.1 Energy of Activation

Temperature has a great effect on the rate of metal electrochemical corrosion. **Popova *et al*, 2003; Obi-Egbedi and Obot, 2010 c** reflected that for corrosion in a neutral solution (oxygen depolarisation) the increase in temperature has a favourable effect on the over potential of oxygen depolarisation and the rate of oxygen diffusion but leads to a decrease of oxygen solubility, whereas for corrosion in acidic medium (hydrogen depolarisation), the corrosion rate increases exponentially with increase of temperature because the hydrogen evolution overpotential decreases.

Effect of temperature on the corrosion and inhibition process of MS / AA1100 in 1M HCl in the absence and presence of different concentrations of the SCL / SCF / TCL / TCF extracts after 1/2 h of immersion is studied at 303 - 353 K using mass loss measurements.

The dependence of corrosion rate on temperature can be regarded as an Arrhenius – type process, the rate of which is given by

$$\log \mathrm{CR} = \log \mathrm{A} - \mathrm{E_a}/2.303\mathrm{RT} \quad \textbf{(4.24)}$$

where CR is the corrosion rate of MS / AA1100, A is Arrhenius or pre-exponential constant, E_a is the activation energy for the corrosion of MS / AA1100, R is the gas constant and T is the temperature.

Figures 4.27 and 4.28 depict Arrhenius plot as log of corrosion rate (log CR) against the reciprocal of temperature (1/T) for MS / AA1100 in 1M HCl in the free acid solution and the acid containing different concentrations of SCL / SCF / TCL / TCF extracts.

The apparent activation energy for the corrosion of **MS/AA 1100** in 1M HCl is calculated from the Arrhenius plot of log CR against 1/T in the absence and presence of different concentrations of SCL / SCF / TCL / TCF. The E_a values are deduced from the slopes of these lines and the values of E_a for various concentrations of the inhibitors are tabulated in Table 4.40

It can be seen in the table that E_a is higher in the presence of the inhibitors than in their absence. The modification in the values of E_a may be attributed to the geometric blocking effect of adsorbed inhibitive species on the metal surface **(Tebbji *et al*, 2007)**. This observation further supports the proposed physisorption mechanism as reports **(Fu *et al*, 2010; Solomon *et al*, 2010; Ahamad *et al*, 2010)** show that lower values of E_a in the presence of inhibitors in comparison to the free acid solution are indicative of chemical adsorption mechanism, whereas the opposite suggests a physical adsorption mechanism.

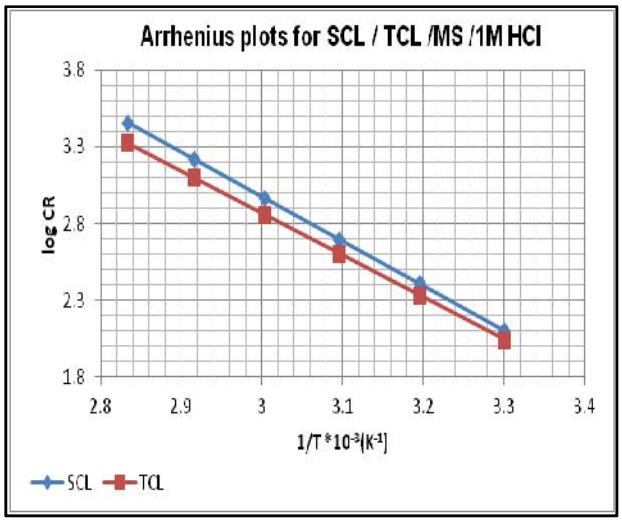

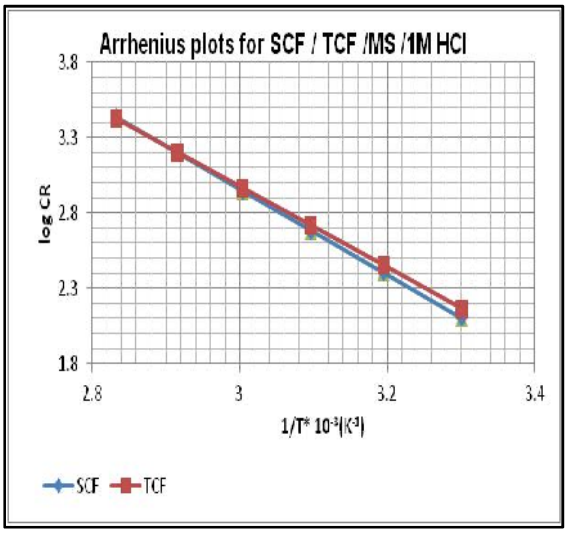

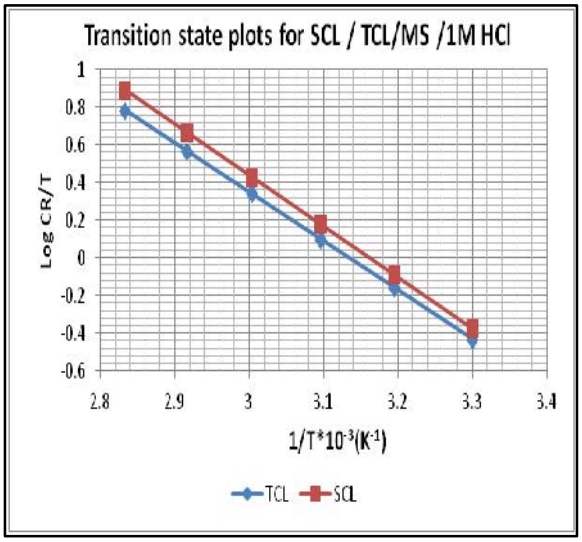

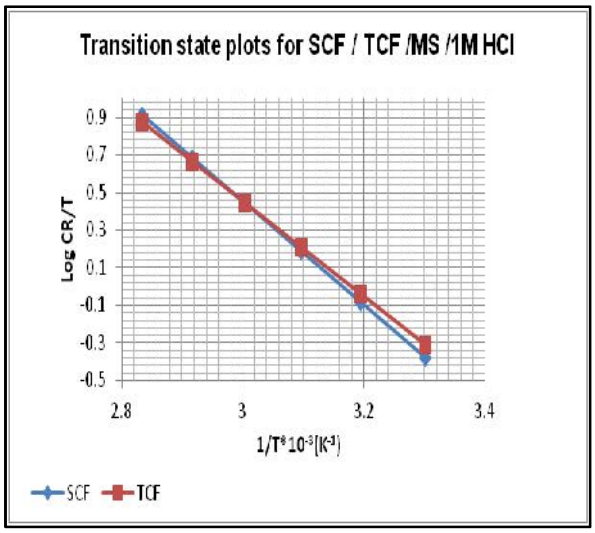

Figure 4.27 Arrhenius plots and Transition state plots for MS / SCL / SCF / TCL / TCF /1M HCl systems

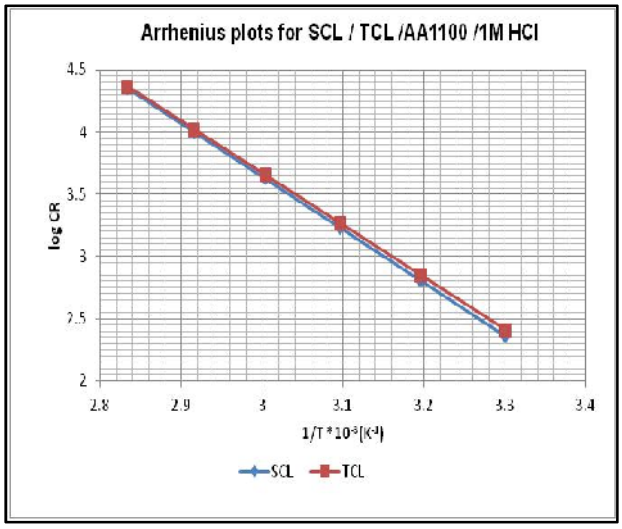

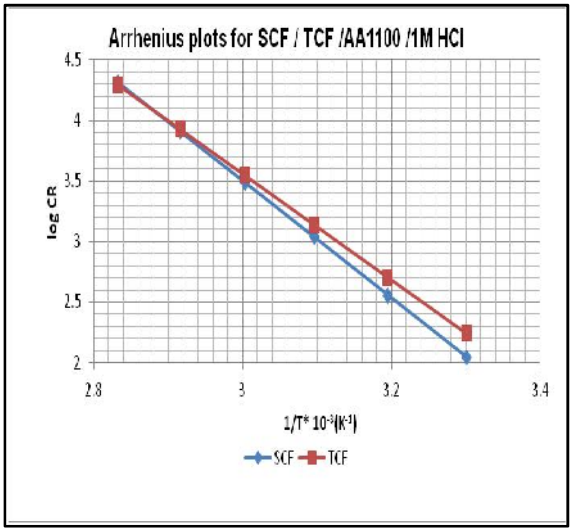

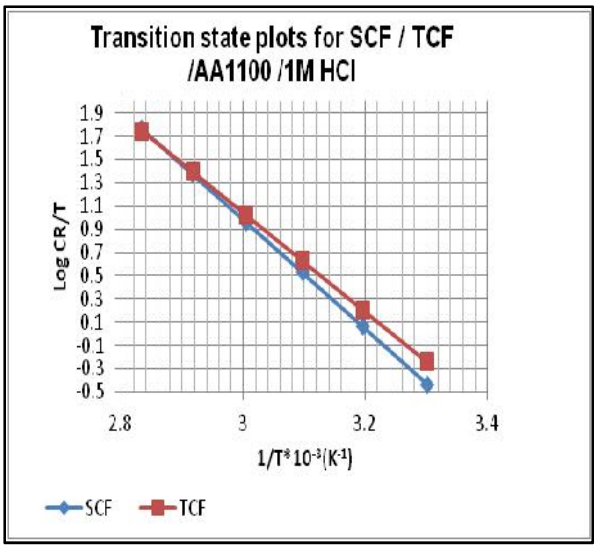

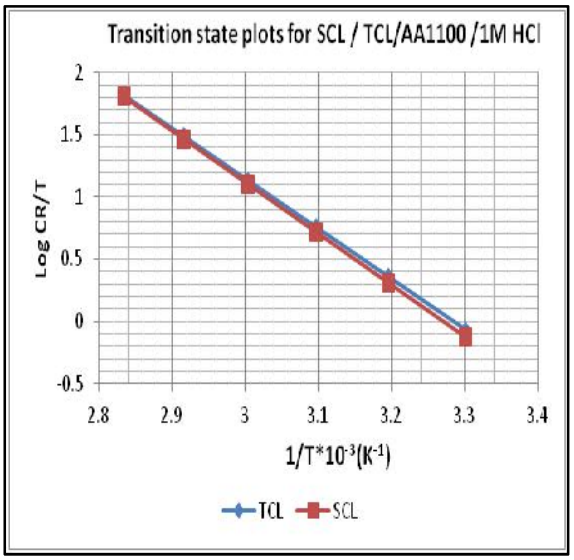

Figure 4.28 Arrhenius plots and Transition state plots for AA1100 / SCL / SCF/ TCL / TCF /1M HCl systems

Further evidence regarding the kinetic and mechanistic process of the corrosion mechanism can be realised from the values of apparent activation energy **(Ivanov, 1986)**. Inspection of Table 4.40 also reveals that E_a increases with increase in SCL / SCF / TCL / TCF extracts. Activation energy values for the investigated inhibitors are found to be higher than the blank values, implying the increase of energy barrier for the corrosion process in the presence of the additives. This emphasizes the electrostatic nature of the adsorbed inhibitors on the **MS / AA1100** surface. Similar observation are also noted by **Singh *et al*, 2010a** in their studies of the inhibition of corrosion of mild steel in hydrochloric acid solution by the extract of Kalmegh (A. paniculata) leaves extract. It is logical to assume that in this case the electrostatic adsorption is responsible for the good protective properties of the inhibitors. However, the adsorption phenomenon of an organic molecule is not considered only as a physical or as chemical adsorption phenomenon, but a wide spectrum of conditions, ranging from the dominance of chemisorption or electrostatic effects may arise due to the complex nature of the corrosion inhibiting process **(Solmaz *et al*, 2008b)**.

Table 4.40 –Activation parameters for MS / AA1100 corrosion in 1 M HCl in the absence and presence of different concentrations of SCL / SCF / TCL / TCF

Conc (%)	E_a (kJ/mol)							
	SCL		SCF		TCL		TCF	
	MS	AA1100	MS	AA1100	MS	AA1100	MS	AA1100
Blank	47	65	47	65	47	65	47	65
0.1	50	83	55	86	51	82	52	83
0.2	49	83	51	88	48	82	51	82
0.3	49	83	51	89	51	82	51	82
0.4	51	81	52	87	48	80	54	81
0.5	50	80	52	87	48	79	52	81
0.6	50	80	54	90	48	80	53	81
0.7	53	82	56	93	55	80	51	84
Average	50	82	53	88	50	81	52.2	82

4.5.2 Entropy of Activation and Enthalpy of Activation

In order to calculate the enthalpy, ΔH_a and entropy, ΔS_a of activation for the corrosion process, the alternative formulation of Arrhenius equation, also called transition state equation , is used:

$$\frac{CR}{T} = \frac{R}{Nh} \exp\left(\frac{\Delta Sa}{R}\right) \exp\left(\frac{\Delta Ha}{RT}\right) \quad \textbf{(4.25)}$$

where h is the Planck's constant, N is the Avogadro's number, ΔS_a is the entropy of activation, T is the absolute temperature and R is the universal gas constant.

The relationship between log (CR/T) versus 1/T for **MS / AA1100** corrosion in 1M HCl in the absence and presence of different concentrations of SCL / SCF / TCL / TCF extracts is shown in Figure 4.28. Straight lines are obtained with slope of ($-\Delta H_a/2.303R$) and an intercept of (log R/Nh + $\Delta S_a/2.303R$) from which the values of ΔH_a and ΔS_a respectively are computed and listed in Table 4.41.

Table 4.41 Average values of activation parameters for MS / AA1100 corrosion in 1 M HCl in the absence and presence of different concentrations of SCL/SCF/TCL/TCF

Inhibitor	E_a (kJ/mol)		ΔH_a (kJ/mol)		ΔS_a (J/mol K^{-1})	
	MS	AA1100	MS	AA1100	MS	AA1100
Blank	47	65	44.6	62.4	-37.9	25.5
SCL	50	82	47.2	76.8	-40.8	58.1
SCF	53	88	49.5	82.8	-35.5	75.6
TCL	50.0	81	46.9	76.1	-43.01	56.6
TCF	52.2	82	49.5	77.3	-36.8	59.3

The Table reflects that E_a and ΔH_a are close to each other as expected from transition state theory concept and they are also found to vary in a similar manner in the presence of the inhibitors. It is also seen in Table 4.41 that E_a and ΔH_a vary in the same manner but however, the values of ΔH_a are lower than that of E_a. This has been reported **(Ekanem *et al*, 2010; Noor, 2007)** to indicate that the corrosion process must involve a gaseous reaction, simply hydrogen evolution reaction associated with decrease in total reaction volume .The positive values of ΔH_a both in the absence and presence of additives reflect the endothermic nature of the steel dissolution process and it indicates that the dissolution of **MS / AA 1100** is difficult **(Zerga *et al*, 2010)**.

The values of ΔS_a in the absence and presence of the extracts are negative for **MS** (Table 4.41). This implies the inhibitor molecules, freely moving in the bulk solution are adsorbed in an orderly fashion onto the **MS** surface. This infers that the activation complex in the rate determining step represents as association rather than a dissolution step, meaning that a decrease in disordering takes place on going from reactants to the activated complex. Similar observations have been reported in the literature for mild steel dissolution in the absence and presence of inhibitors. **(Zerga *et al*, 2010; Noor and Al-Moubaraki, 2008).**

In the case of **AA1100**, the entropy of activation (ΔS_a) is found to be positive in the absence and presence of SCL / SCF / TCL / TCF implying that the rate-determining step for the activated complex is dissociation step rather than association. In other words, the adsorption process is accompanied by an increase in entropy, which is the driving force for the adsorption of inhibitor onto the AA1100 surface **(Obi-Egbedi and Obot, 2010b)**.

4.6 Thermodynamic Adsorption Parameters

Thermodynamic model is very useful to explain the adsorption phenomenon of inhibitor molecule. A plot of ΔG^{o}_{ads} versus T is linear (Figures 4.29 and 4.30) for MS /AA1100 acid corrosion in the presence of various concentrations of investigated extracts in both acid media. The slopes of the straight lines are equal to ΔS^{o}_{ads} and intercept equal to ΔH^{o}_{ads}. Figures 4.29 and 4.30 clearly shows the dependence of ΔG^{o}_{ads} on T, indicating good correlation among thermodynamic parameters

Table 4.42–Thermodynamic adsorption parameters for MS / AA1100 corrosion in 1 M HCl in the absence and presence of different concentrations of SCL/SCF/TCL/TCF

Inhibitor	Free energy of adsorption ΔG^{o}_{ads} (kJ/mol)						ΔS^{o}_{ads} J/mol	ΔH^{o}_{ads} kJ/mol
	303K	313K	323K	333K	343K	353K		
MS								
SCL	-15.9	-18.0	-19.2	-17.9	-18.4	-18.2	-26.7	-9.2
SCF	-15.7	-17.1	-18.7	-17.7	-17.2	-16.8	-13.0	-12.95
TCL	-16.3	-17.0	-17.8	-17.8	-17.7	-17.2	-18.6	-11.2
TCF	-15.5	-16.1	-19.0	-18.0	-17.2	-17.0	-27.5	-8.1
AA1100								
SCL	-16.3	-16.9	-16.7	-17.0	-15.8	-15.5	19.5	-22.8
SCF	-16.7	-17.1	-20.1	-18.1	-16.4	-16.1	21.8	-24.6
TCL	-16.4	-15.9	-16.4	-16.7	-15.7	-15.5	13.3	-20.5
TCF	-16.6	-17.5	-18.1	-17.8	-16.1	-15.7	25.8	-25.4

4.6.1 ΔG^{o}_{ads}

The calculated mean values of ΔG^{o}_{ads}, ΔH^{o}_{ads}, ΔS^{o}_{ads} at all the investigated temperatures (303-353K) using equation (3.20 and 3.21) for different concentration of SCL / SCF / TCL / TCF extracts are represented in Table 4.42

Figure 4.30 clearly shows the dependence of ΔG^{o}_{ads} on T, indicating the good correlation among thermodynamic parameters. The large and negative values of ΔG^{o}_{ads} ensure the spontaneity of the adsorption process and stability of the adsorbed layer on the steel surface (**Bentiss *et al,* 2005**).

Figure 4.29 Best fit curves of $-\Delta G°_{ads}$ Vs T for MS / SCL/ SCF/TCL/TCF /1M HCl

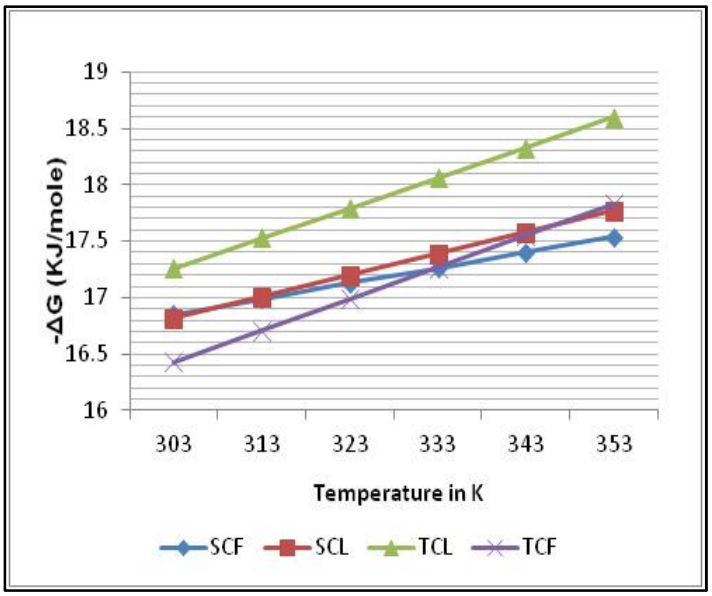

Figure 4.30 Best fit curves of $-\Delta G°_{ads}$ Vs T for AA1100 / SCL/ SCF/TCL/TCF /1M HCl

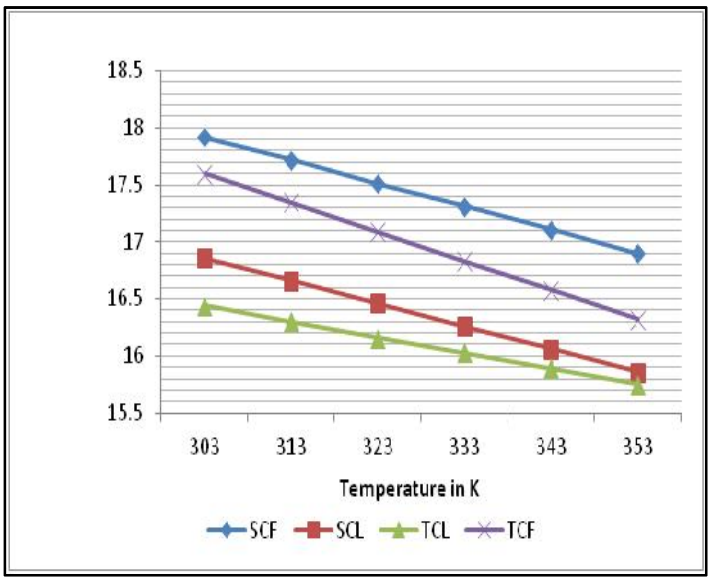

The calculated value of ΔG^{o}_{ads} presented in Table 4.42, are negative which indicate that the adsorption of inhibitor molecules on the metal surface is a spontaneous process. As, observed, the studied inhibitors obey the general rule that the effectiveness of corrosion inhibition increases with increasing the negative value of ΔG^{o}_{ads} Generally, values of ΔG^{o}_{ads} around -20 $kJmol^{-1}$ or lower are consistent with the electrostatic interaction between the charged molecules and the charged metal (physisorption); those around -40 $kJmol^{-1}$ or higher involve charge sharing or transfer from organic molecules to the metal surface to form a coordinate type of bond (chemisorption) (**Donahue and Nobe, 1965; Khamis *et al,* 1994**). In the present work, the calculated ΔG^{o}_{ads} values are almost slightly less negative than -20 $kJmol^{-1}$ ranging from -15 to -19 $kJmol^{-1}$. Hence it may be assumed that the adsorption of the inhibitor molecules is obeying physical adsorption however chemical adsorption may not be excluded due to the complex nature of the corrosion inhibiting process (**Ahamad *et al,* 2010).**

4.6.2 ΔH^{o}_{ads} and ΔS^{o}_{ads}

The positive sign of ΔH^{o}_{ads} for all the studied inhibitors - SCL / SCF / TCL / TCF extracts in 1M HCl reflects the endothermic nature of dissolution which suggests the slow dissolution of MS / AA1100. This behaviour can be explained as a result of the replacement process of water molecules during adsorption of inhibitors on the MS / AA1100 surface. (**Moretti *et al,* 2004**).

The entropy of adsorption ΔS^{o}_{ads} for the system SCL / SCF / TCL / TCF in 1M HCl obtained from equation (3.22) are negative because the inhibitor molecules freely moving in the bulk solution, are adsorbed in an orderly fashion onto the mild steel surface, resulting in a decrease in entropy **(Obi-Egbedi *et al,* 2010).** The negative values of entropy of adsorption (ΔS^{o}_{ads}) in the presence of all the studied inhibitors are attributed to the adsorption process which is accompanied by an increase in order of the system due to the adsorption of the studied inhibitor on the metal surface **(Gomma and Wahdan, 1994).** Inspection of table reveals that decrease in enthalpy and entropy is the driving force for the adsorption of SCL / SCF / TCL / TCF in 1M HCl on the MS / AA1100 surface **(Umoren *et al,* 2007b).**

4.7 Surface Analytical Techniques

In the present investigation, surface analysis of MS / AA1100 specimens exposed to the uninhibited and inhibited solutions are undertaken to corroborate the results obtained by mass loss and electrochemical measurements. The following surface analytical

techniques are used to study the surface of MS / AA1100 in the presence and absence of optimum concentration of SCL / SCF / TCL / TCF.

- **UV Visible spectral Analysis (UV)**
- **FT-IR Spectral studies (FT-IR)**
- **Scanning Electron Microscopic studies (SEM)**
- **Energy dispersive X-ray analysis (EDX)**
- **X-ray diffraction Analysis (XRD)**
- **3D optical profilometry**

One of the main criticisms of the use of the plant extracts as corrosion inhibitors is their inability to pinpoint the major active component that is responsible for the inhibiting action owing to the complex chemical composition of the crude extract. However further investigations and the use of surface analytical techniques will enable the characterization of the active materials in the adsorbed layer and assist in identifying the most active ingredients in the extract of plant materials. **(Ekanem *et al*, 2010).**

4.7.1 UV Visible spectral Analysis

A substantial evidence for the formation of metal complexes is often obtained by UV-visible spectroscopic investigation **(Quraishi *et al,* 2012)**. Since there is often a certain quantity of metal cation in the solution that is first dissolved from the metal surface, such procedures are conducted in the present work to confirm the possibility of the formation of complexes as described by **Obi- Egbedi *et al,* 2010.** Furthermore, it has been reported that change in position of the absorbance maximum and change in the value of absorbance indicate the formation of a complex between two species in solution. **(Abboud *et al,* 2007)**

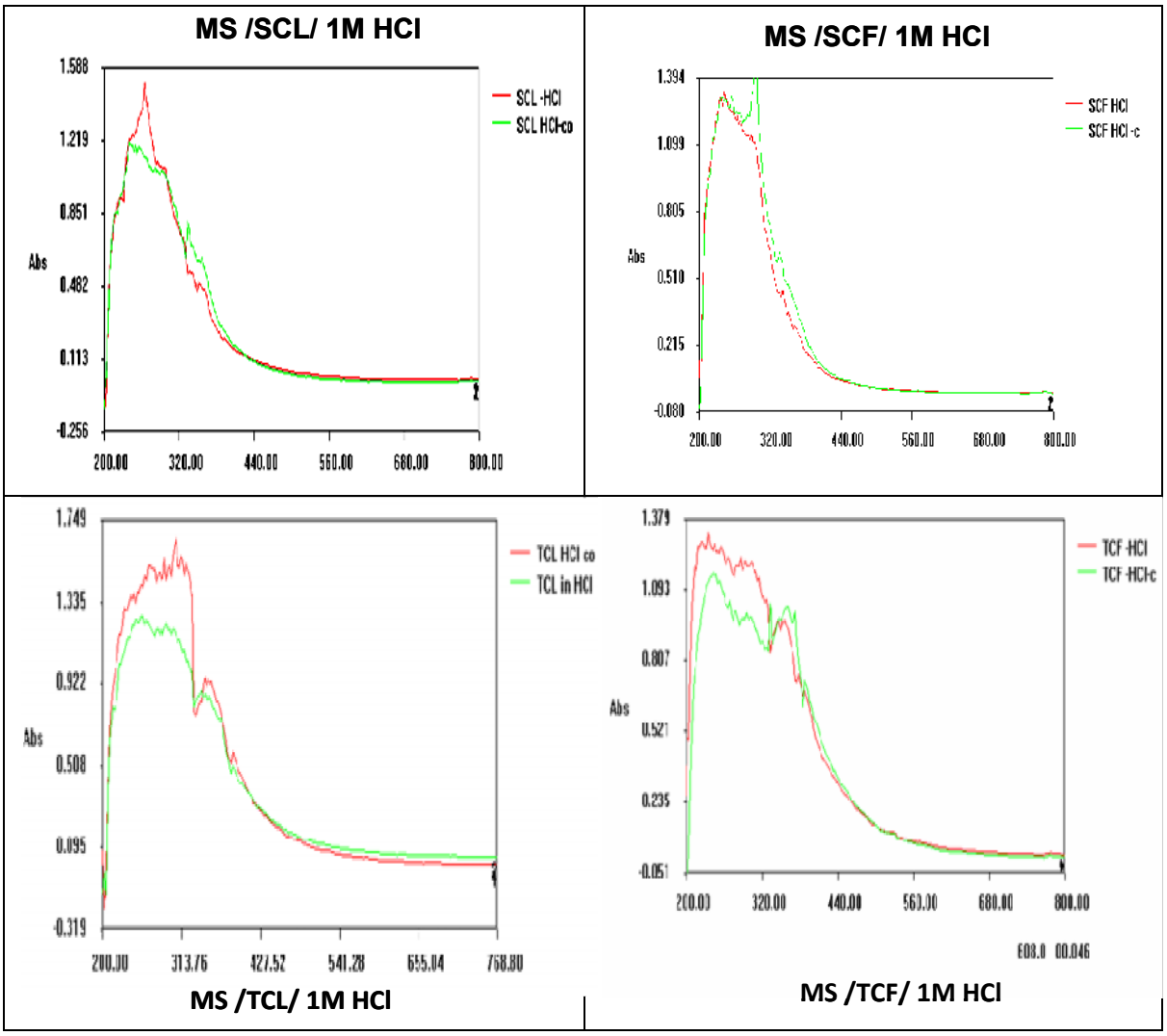

Figure 4.31 : UV spectra for crude plant extracts SCL /SCF /TCL /TCF and corrodent solution on MS in 1 M HCl

Table 4.43 : UV spectral details for crude plant extract and corrodent solution on MS in 1 M HCl

Inhibitor	Absorption bands (nm)		
	Crude plant extract	MS+1M HCl+ inhibitors	Transitions
SCL	224, 241, 265, 284, 334, 354	219, 243, 296, 339, 358	$n \rightarrow \pi^*$, $\pi \rightarrow \pi^*$
SCF	243, 284, 334, 337	245, 298, 300, 361	
TCL	250, 253, 296 , 346	269, 305, 351	
TCF	236, 224, 286, 344, 354	243, 294, 332, 361, 392	

❖ **SCL/SCF/TCL/TCF /MS/1M HCl systems**

To establish the possibility of the formation of Fe- inhibitor complex, UV–Visible absorption spectra is acquired for 0.7 % extracts of SCL/SCF/TCL/TCF in 1 M HCl solution before and after 3h of MS immersion .The spectra are collected in Figure 4.31 a-d . The electronic absorption spectra of SCL / SCF / TCL / TCF in 1M HCl before the immersion of MS reflect two bands in the UV region. These bands are noted due to $\pi \rightarrow \pi^*$ and $n \rightarrow \pi^*$ transitions. After 3h of immersion, the change in the position of the absorption maximum indicates the formation of a complex between the phytochemical constituents of the plant extracts and the MS electrode. Similar assertions are reported by **Singh *et al*, 2012**.

Table 4.44: UV spectral details for crude plant extract, corrodent solution on AA1100 in 1 M HCl

Inhibitor	Absorption bands (nm)		
	Crude plant extract	AA1100 +1M HCl+ inhibitors	Transitions
SCL	224, 241, 265, 284, 334, 354	250,270,320,332	$n \rightarrow \pi^*$, $\pi \rightarrow \pi^*$
SCF	243, 284, 334, 337	258,296,339,370	
TCL	250, 253, 296 , 346	260,330,356	
TCF	236, 224, 286, 344,354	265,322,356,378	

❖ **SCL / SCF / TCL / TCF / AA1100 / 1M HCl systems**

The UV visible spectrum of the corrosion product on the surface of AA1100 in the absence and presence of SCL / SCF / TCL / TCF extracts in 1M HCl are listed in Figure 4.32 and the details are given in Table 4.44. On comparing both these spectra, it may be noted that the bands observed for crude plant extracts shifts to higher wavelength region (Bathochromic shift or red shift) viz 360nm. The observed results conclude the co-ordination between the hetero atoms (oxygen and nitrogen) present in the inhibitor and surface of the metal ion. **(Petchiammal *et al*,2013)**

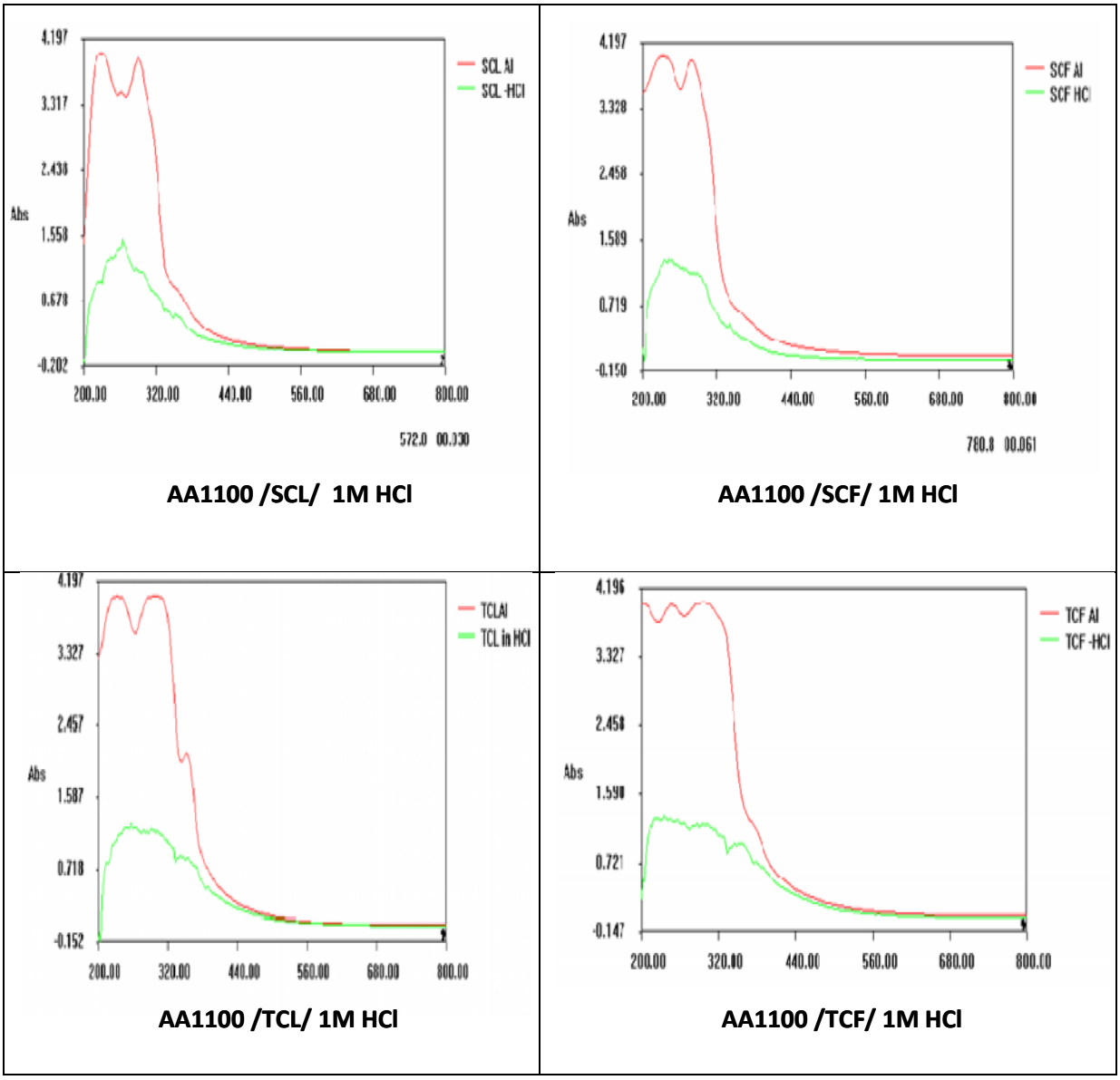

Figure 4.32: UV spectra for crude plant extracts SCL /SCF /TCL /TCF, corrodent solution on AA1100 in 1 M HCl

.4.7.2 FT-IR Spectral studies

It is well established that FTIR spectrophotometer is a powerful tool that can be used to identify the type of bonding. The functional groups pertaining to adsorption can be deduced from the FT –IR spectra. FTIR analyses of metal surface can be useful for predicting whether the phytochemical constituents of the plant extracts, that are organic in nature, are adsorbed or not adsorbed on the metal surface **(Singh et al, 2010 a)**

4.7.2.1 FT-IR analysis for SCL / SCF extract with MS as the electrode

i) SCL/ MS/1M HCl

The frequencies and peaks of IR adsorption deduced from the spectra (Figure 4.33 a) are recorded in Table 4.45. The FT-IR spectrum of SCL powder indicates a strong band at 3395 cm^{-1} that is attributed to N-H /OH stretching. An absorption band related to – CH_2 stretching is noticed at 2924 cm^{-1}.A strong band at 1628 cm^{-1} corresponds to C=O stretching. Peaks observed at 1519 cm^{-1}, 1381 cm^{-1} , 1072 cm^{-1} indicates C=C stretching C-O-C stretching and C-O stretching. A peak at 633 cm^{-1} denotes C=C bending vibration of the aromatic ring system. Thus the FT IR spectrum implies the presence of O and N atom containing functional groups, that act as a prerequisite for a molecule to function as a corrosion inhibitor. This shows that this plant extract contained a mixture of compounds, i.e., alkaloids, flavonoids and organic acids **(Satapathy *et al*, 2009)**.

Table 4.45: FT-IR spectral details of SC for crude plant extract and corrosion product on MS in 1 M HCl

Observed IR Frequency , (cm^{-1}) and Peak assignment					
SCL			SCF		
Crude plant extract	Corrosion product/ /Mildsteel/1M HCl	Frequency Assignment	Crude plant extract	Corrosion product/ /Mildsteel/1M HCl	Frequency Assignment
3950	3842	O-H stretch	3950	3981	O-H stretch
3395	3603	N-H / O-H stretc	3395	3318	N-H / O-H stretc
2924	3117	C-H stretch	2376	2376	C ≡N stretch
2376	2315	C ≡ N stretch			
1628	1636	C=O stretch	1628	1628	C=Ostretch
1520	1520	C-C in ring Aromatics	1427	1520	C-O stretch
1381	-	C-O-C stretch	1381	-	C-O-C stretch
1072	1057	C-O stretch	1265	1211	C-O stretch
633		C=C bending”	1065		Aromatics
	702	γ-Fe_2O_3	772	826	OH bend

The FT- IR spectrum of the corrosion product after 3h of immersion in 1M HCl in the presence of the inhibitor is depicted in Figure 4.33 a and tabulated in Table 4.45. The band observed at 3394 cm^{-1} (for that of the SCL extract) is shifted to 3603 cm^{-1} and the –CH_2 asymmetric band at 2924 cm^{-1} is shifted to 3117 cm^{-1}. A band at 2376 cm^{-1} attributed to C ≡ N stretching observed in the plant spectra shifts to 2315 cm^{-1} in the corrosion

product. The absorption band at 1628 cm^{-1} (C=O stretching) diminishes and shifts to 1636 cm^{-1}. A peak noticed for C-O stretching at 1072 cm^{-1} shifts to 1057 cm^{-1} The shift in the absorption frequencies of the inhibitor on the metal surface strongly supports the interaction between the phytochemical compounds of the inhibitor and metal surface. Bands at 450 cm^{-1} to 700 cm^{-1} probably originates mainly from γ -Fe_2O_3 (702 cm^{-1}). Some bonds are missing in the spectrum of the corrosion product indicating that these bonds might have been involved in bonding .This indicates that there is interaction (Fe-SCL complex formation) between the leaves extract of SCL and the surface of MS. This fact is also substantiated by UV spectral studies.**(Ebenso, 2010)**

ii) SCF / MS / 1M HCl

Fig. 4.33 (b) depicts the IR spectrum of the SCF extract and that of the protective film formed on the surface of the metal after immersion in the solution containing 0.7% SCF extract .Various adsorption modes of the SCF extract and that of the protective film formed on the surface of the metal after immersion in the solution containing 0.7 % SCF extract and their corresponding frequencies are tabulated in Table 4.45.

Analysis of the IR spectral data reflects that a band noticed at 3950 cm^{-1} shifts to 3981 cm^{-1} in the corrosion product. Bands at 2376 cm^{-1} and 1628 cm^{-1} pertaining to C≡N stretching and C=O stretching are noticed in the corrosion product also. Also a shift from 1427 cm^{-1} to 1520 cm^{-1} is noted for C-H bending .Some bonds, for example 1381 cm^{-1} corresponding to C-O-C stretching disappears in the corrosion product. A band for C-O stretching assigned to 1265 cm^{-1} is downshifted to 1211 cm^{-1} in the corrosion product and a band at 1065 cm^{-1} identified as a C-O stretching vibration disappears in the corrosion product. A band pertaining to OH bending noted at 772 cm^{-1} is shifted to 826 cm^{-1} in the corrosion product.

These progressive shifts in the wavelength are indicative of the interaction between the SCF and metal surface. Therefore, it can be proposed that the adsorption of the inhibitor took place via –OH stretching, C–O stretching for SCF extract. **(Umoren *et al*, 2011).**

4.7.2.2 FT-IR results for TCL / TCF / MS / 1M HCl systems

i) TCL / MS / 1M HCl

The FT-IR spectrum of TCL crude plant extract and that of the corrosion product is depicted in Figure 4.33 c.The functional groups responsible for absorption can be deduced

in Table 4.46. The original absorption at 3418 cm^{-1} is shifted to 3433 cm^{-1} by the strong stretching mode of O-H vibration. A peak, which can be attributed to aliphatic C-H stretching vibration, observed for the plant extract at 2924 cm^{-1} shifts to 3024 cm^{-1}. Peaks at 1628 cm^{-1} corresponding to C=O stretching is shifted to 1697cm^{-1}. Peaks shifting from 1543 cm^{-1} to 1528 cm^{-1} , and 1443 cm^{-1} to 1427 cm^{-1} reflects the presence of C-C ring in aromatics and C-H bending vibrations. (**Eddy and Ebenso, 2010**). A peak identified at 772 cm^{-1} pertaining to OH bending shifts to 748 cm^{-1} in the corrosion product. The shift in the characteristic frequencies pertaining to the functional groups present in the plant extract with reference to the corrosion product on the MS surface confirm the formation of Fe-TCL complex on MS surface.The formation of Fe-TCL complex is also corroborated from UV spectral studies.

Table 4.46 - Observed IR Frequency , (cm^{-1}) and Peak assignment for TCl and TCF

Observed IR Frequency , (cm^{-1}) and Peak assignment					
TCL			TCF		
Crude plant extract	Corrosion product/ /Mildsteel/1M HCl	Frequency Assignment	Crude plant extract	Corrosion product/ /Mildsteel/1M HCl	Frequency Assignment
3418	3433	O-H stretch	3387	3472	O-H stretch
2924	3024	C-H stretch	2924	3086	C-H stretch
			2855	3024	C-H stretch / C=O stretch
				2315	C ≡N stretch
1628	1698	C=O stretch	1628	1736	C=O stretch
1543	1528	C-C in ring Aromatics	1443	1427	C-O stretch
1443	1427	C-O stretch	1373	1366	C-O-C stretch
772	748	O–H bend	1258	1219	C-O stretch
640		C-H “oop”	1072	1049	C-O stretch
	702	γ-Fe_2O_3	772	748	O–H bend

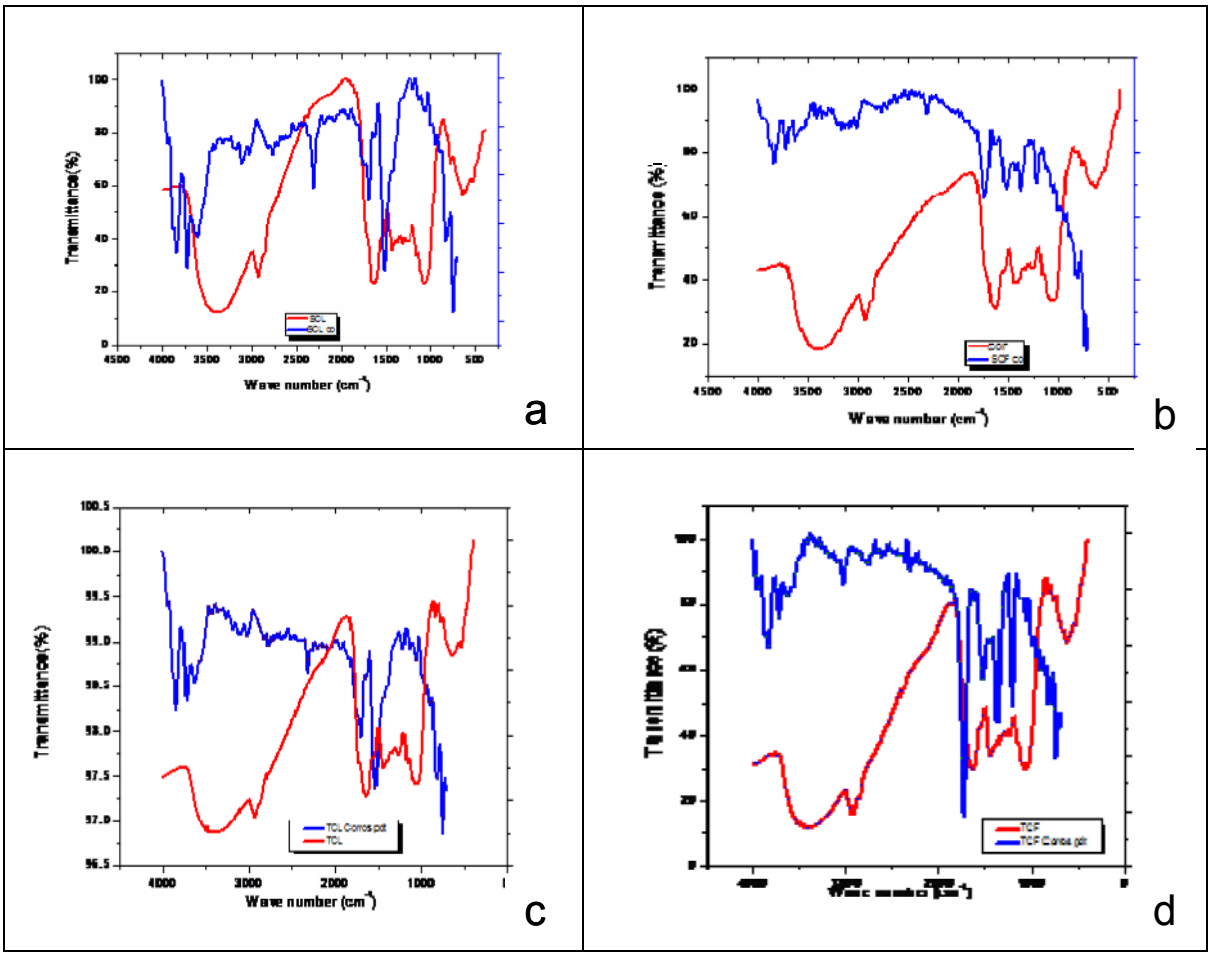

Figure 4.33 FT-IR Spectrum of (a) SCL and corrosion products in the presence of SCL (b) SCF and corrosion products in the presence of SCF (c) TCL and corrosion products in the presence of TCL (d) TCF and corrosion products in the presence of TCF.

ii) TCF/ MS / 1M HCl

Figure 4.33 d illustrates the FT-IR spectrum of crude extract of TCF and the corrosion product of MS. The frequencies and peaks of IR absorption deduced from the spectra are recorded in Table 4.46. From the results obtained, it may be noticed that O-H stretching at 3387 cm^{-1} (for TCF extract) shifts to 3418 cm^{-1}. The aliphatic and aromatic C-H stretching observed in crude plant extract at 2924 $cm^{-1,}$ 2855 cm^{-1} shifts to 3086 cm^{-1}, 3024 cm^{-1} respectively. A peak at 2315 cm^{-1} is noticed only in corrosion product which corresponds to C ≡N stretching vibration. A peak at 1628 cm^{-1} corresponding to C=O stretching vibration is shifted to 1736 cm^{-1} in the corrosion product. Peaks that are shifted from (1443 cm^{-1} to1427 cm^{-1}), and (1373 cm^{-1} to 1366 cm^{-1}), (1258 cm^{-1} to 1219 cm^{-1}) and (1072 cm^{-1} to1049 cm^{-1}) indicates the presence of C-O stretching and C-O-C stretching

groups (**Eddy *et al,* 2010**). The shift in the absorption frequencies of the TCF extract on the metal surface supports the interaction between the inhibitor and the metal surface. Also, some new bonds are noted in the spectrum of the corrosion product. This includes the C ≡N stretch at 2315 cm^{-1}. This also indicates that some new bonds are also formed through these functional groups. (**Eddy and Ebenso, 2010**). This emphasises the fact that the inhibitive nature of the extract is due to the formation of Fe-TCF complex on MS surface. This fact is also substantiated by UV spectral studies.

4.7.2.3 FT-IR results for SCL/SCF in the presence of AA1100 electrode

i) SCL /AA1100/1M HCl

The FT-IR spectra of crude plant extract and the corrosion product of SCL in AA1100 surface immersed in 1M HCl with 0.7% SCL is depicted in Figure 4.34 a. The respective FT-IR peaks of crude plant extract and corrosion product are tabulated in Table 4.47.

Table 4.47 Observed IR Frequency , (cm^{-1}) and Peak assignment for SCL / SCF / 1M HCl / AA1100

Observed IR Frequency , (cm^{-1}) and Peak assignment					
SCL			SCF		
Crude plant extract	Corrosion product/ /AA1100/1M HCl	Frequency Assignment	Crude plant extract	Corrosion product/ /AA1100/1M HCl	Frequency Assignment
3950	3935	O-H stretch	3950	3942	O-H stretch
1628	1589	C=Ostretch	3395	3341	N-H / O-H stretc
1520	-	C-C in ring Aromatics	2376	2307	C ≡N stretch
1381	-	C-O-C stretch			
1265	1258	C-O stretch	1628	1589	C=O stretch
1072	1018	C-O stretch	1265	-	C-O stretch
779	818	OH bend	1065	-	C-O stretch

A peak at 3950 cm^{-1} assigned to the presence of stretching mode of an O–H and/or N–H groups in the crude plant extract shifts to 3935 cm^{-1}. A decrease in intensity of the band corresponding to C=O from 1627 cm^{-1} to1589 cm^{-1} strongly suggests the interaction of the metal with the inhibitor. The peak pertaining to C-C in ring aromatic at 1520 cm^{-1} disappears in the corrosion product. The following peaks in crude plant extract corresponding to functional groups C-O stretching, C-O stretching and –O-H bending are shifted from 1265 cm^{-1} to 1258 cm^{-1}, 1072 cm^{-1} to 1018 cm^{-1}, 779 cm^{-1} to 818 cm^{-1} in the

corrosion product. A band assigned to C-O-C stretching at 1381 cm^{-1} disappears in the corrosion product. The change in the absorption frequencies of IR spectra supports the interaction between functional group of inhibitor with the surface of metal (**Rajappa *et al,* 2008**). Phytochemical screening results are supported by the IR spectral data.

ii) SCF /AA1100 / 1M HCl

The infrared spectra of crude extract and the product of SCF adsorption between extract and corrosion product are illustrated in Figure. 4.34 b. From the spectra, it can be observed that the OH stretching frequency of carboxylic acid shifts from 3950 cm^{-1} to 3943 cm^{-1} (Table 4.47).

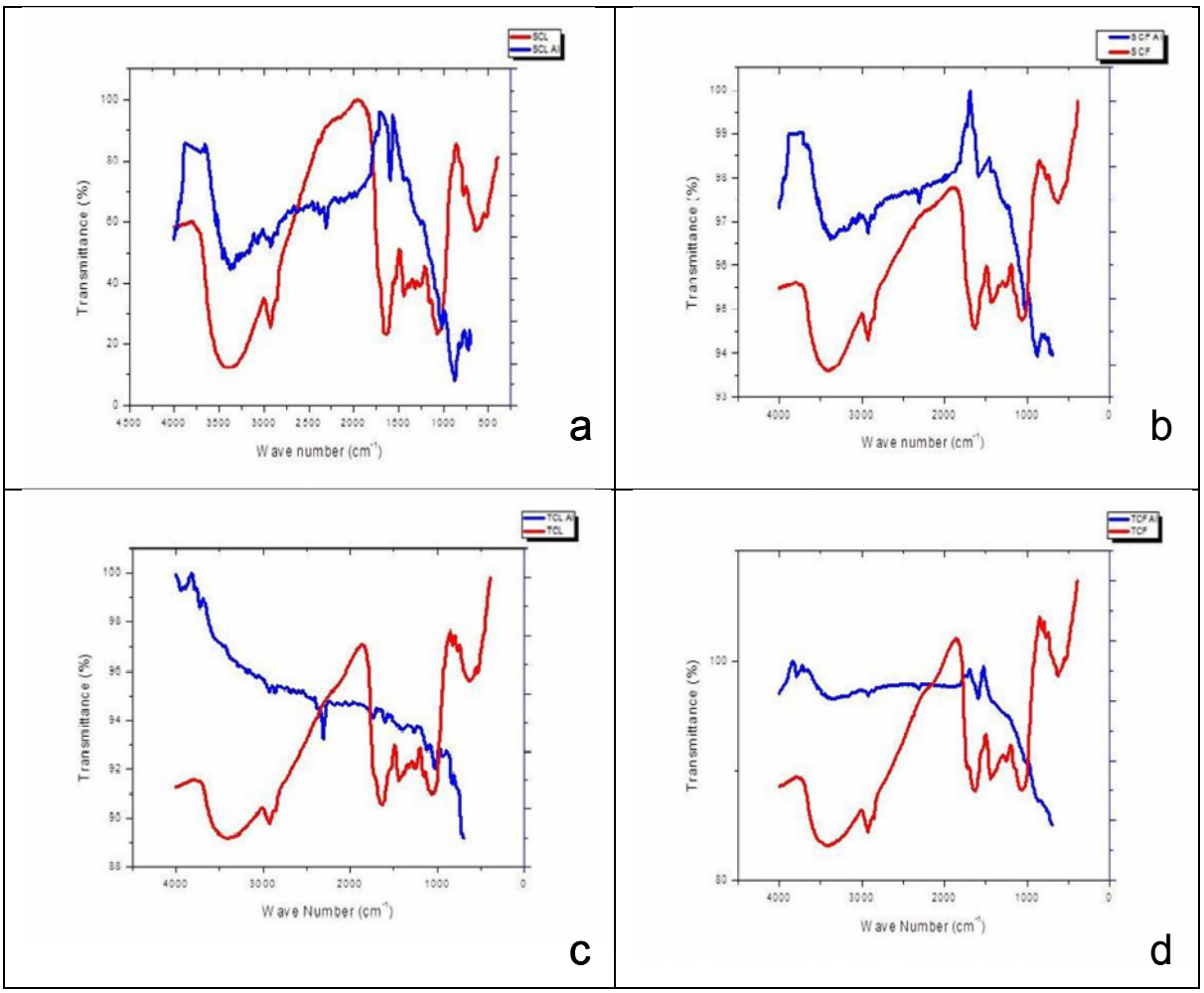

Figure 4.34 FT-IR Spectrum of (a) SCL and SCL / AA1100 (b) SCF and SCF / AA1100 (c)TCL and TCL / AA1100 (d) TCF and TCF / AA1100 in 1M HCl

The carbonyl (C=O) group frequency shifts from 1628 cm^{-1} to 1589 cm^{-1} which might be due to the interaction between the functional group and the metal. The C≡N

stretching frequency noted at 2376 cm^{-1} for crude plant extract shifts to 2307 cm^{-1} in the corrosion product. The C–O stretching frequency of carboxylic acid group noticed at 1265 cm^{-1}, 1065 cm^{-1} is found to disappear in the corrosion product. These group frequency changes for the functional groups of organic molecules of SCF confirm the adsorption on the metal surface, which is responsible for inhibiting corrosion (**Vinod Kumar *et al,* 2011**).

This reflects the formation of SCF- Al complex on AA1100 surface that is instrumental in minimising the corrosion of AA1100 in the acid medium. (**Kamal and Sethuraman, 2012; Gopiraman *et al,* 2012**).

4.7.2.4 FT-IR results for TCL/TCF in the presence of AA1100 electrode

i) TCL / AA1100 / 1M HCl

FT-IR spectral details of crude plant extract and corrosion product of AA1100 surface immersed in 1M HCl with 0.7% TCL (Figure 4.34 c) are tabulated and presented in Table 4.48.

Table 4.48 FT-IR spectral details of TC for crude plant extract, corrosion product on AA1100 in 1 M HCl

Observed IR Frequency , (cm^{-1}) and Peak assignment					
TCL			TCF		
Crude plant extract	Corrosion product/ /AA1100/1M HCl	Frequency Assignment	Crude plant extract	Corrosion product/ /AA1100/1M HCl	Frequency Assignment
2924	2924	C-H stretch	3387	3341	O-H stretch
2384	2307	C ≡N stretch	2924	3047	C-H stretch
1628	1736	C=O stretch	1628	1589	C=O stretch
1543	1597	C-C in ring Aromatics	1373	-	C-O-C stretch
1250	1265	C-O stretch	1072	1018	C-O stretch
1064	1118	C-O stretch			

The peak at 2924 cm^{-1} assigned to the presence of stretching mode of aliphatic and aromatic C–H groups (from plant extract) is also present in the corrosion product. A peak at 2384 cm^{-1} corresponding to C≡N stretching diminishes to 2307 cm^{-1} in the corrosion

product. The peaks at 1627 cm^{-1} and 1543 cm^{-1} reflecting the C=O and C-C in ring aromatics shifts to 1736 cm^{-1} and 1597 cm^{-1} . The following peaks in crude plant extracts corresponding to C-O stretching shifts from 1250 cm^{-1} to 1265 cm^{-1}, 1065 cm^{-1} to 1119 cm^{-1} in the corrosion product. The change in the absorption frequencies of IR spectra supports the interaction between functional group of inhibitor with the surface of metal (**Rajappa *et al,* 2008**).This finding highlights the formation of insoluble Al-TCL complex on the AA 1100 surface.

ii) TCF /AA1100/1M HCl

The infrared spectra of crude extract and the product of TCF adsorption between extract and corrosion product - TCF / AA1100 / 1M HCl are given in Figure. 4.34 d. From the spectra, it is noted that the OH stretching frequency of carboxylic acid shifts from 3387 cm^{-1} to 3341 cm^{-1} (Table 4.48). The carbonyl (C=O) group frequency shifts from 1628 cm^{-1} to 1589 cm^{-1} reflecting the interaction between the functional group and the metal. C-O-C frequency also vanishes from 1373 cm^{-1}. The C–O stretching frequency of carboxylic acid group downshifted from 1072 cm^{-1} to 1018 cm^{-1}. These group frequency changes for the functional groups of organic molecules of TCF confirm the adsorption on the metal surface, which is responsible for inhibiting corrosion (**Vinod Kumar *et al,* 2011**).

This highlights the formation of Al-TCF complex on AA1100 surface thereby inhibiting corrosion of AA1100.

4.7.3 Scanning Electron Microscopic studies (SEM)

The formation of a surface protective film by the investigated eco friendly inhibitors on the MS / AA1100 surface is confirmed by SEM observations. In the present investigation, SEM micrograph of MS/AA1100 specimens exposed to the uninhibited and inhibited solutions has been under taken and the findings are discussed.

4.7.3.1 Scanning electron micrograph of MS in the presence of SCL / SCF Extracts in 1M HCl

Scanning electron microscope images of the surface of the **SCL / SCF / MS/1M HCl** samples are taken to study the morphology before and after the inhibition process. Cleaned MS sample surfaces show few defects and sub micrometer cracks over the surface as shown in Figure 4.35 a. Deep corrosion and considerable loss of the surface material is noticed when the MS sample is treated in 1M HCl as shown in Figure 4.35 b. **(Ji *et al*, 2011)**. However, a significant decrease in the loss of surface material is observed

in presence of inhibitor (0.7% SCL and SCF) for same time period. It can be noted that the corrosion is tangibly suppressed resulting in a smoother surface similar to that of the original specimen (Figure 4.35 c,d) This enhancement of surface morphology indicates the formation of a good protective film of SCl/SCF on MS surface that is responsible for inhibition **(Mourya *et al*, 2014)**.

4.7.3.2 Scanning electron micrograph of MS in the presence of TCL/TCF Extracts in 1M HCl

Surface morphology of the MS samples immersed in HCl with and without **TCL/TCF** is shown in Figure 4.35 e, f and 4.35 b. Fig. 4.35a indicates the finely polished characteristic surface of MS with some scratches that had arisen during polishing. Fig.4.35 b reveals that the immersed specimens are drastically damaged in the presence of 1.0 M HCl, due to the direct attack of aggressive acid. Figure 4.35 e, f reflects the drastic change in morphology of MS surface in the inhibited solutions containing 0.7% TCL and TCF extracts which corresponds to the inhibition of corrosion in acid medium. The micrographs (Fig 4.35 a) also indicate that the scratches formed during metal polishing are also covered well by the inhibitors. Hence, the inhibitors protect MS in 1.0 M HCl solution. The smooth surface of MS in inhibited solution may be due to the phytochemical constituents present in TCL and TCF that hinder the dissolution of iron by forming protective film on MS surface and thereby reducing the corrosion rate **(Mayakrishnan *et al*, 2011).**

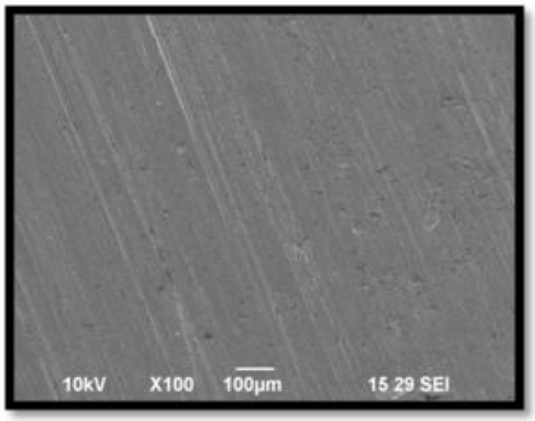

a.Plain Mild steel

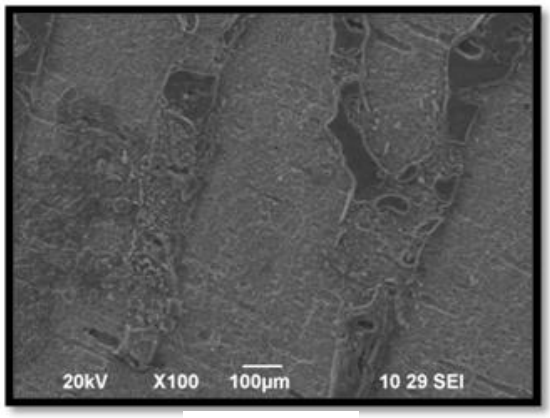

b.Blank

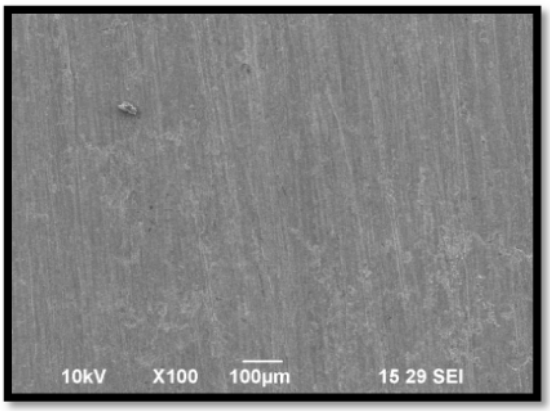

c. MS /SCL/ 1M HCl

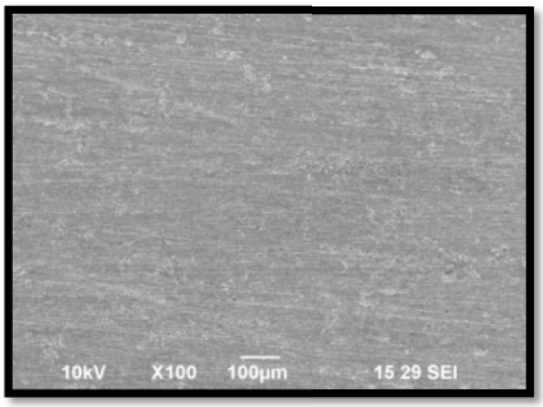

d. MS /SCF / 1M HCl

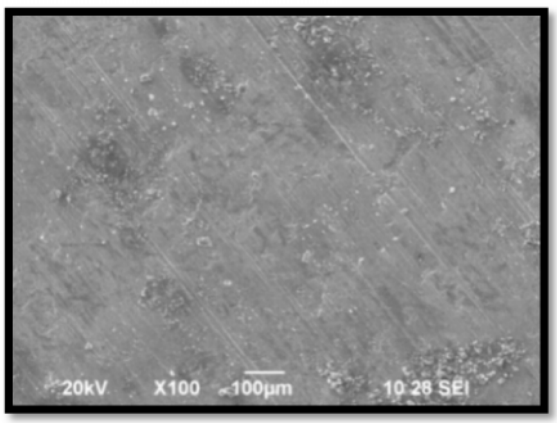

e. MS /TCL/ 1M HCl

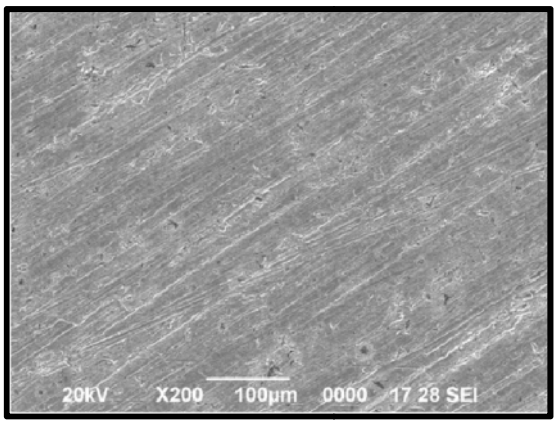

f.MS/TCF/1M HCl

Figure 4.35 : SEM images of MS corrosion in absence and presence of (c) SCL (d) SCF (e) TCL (f) TCF in 1M HCl

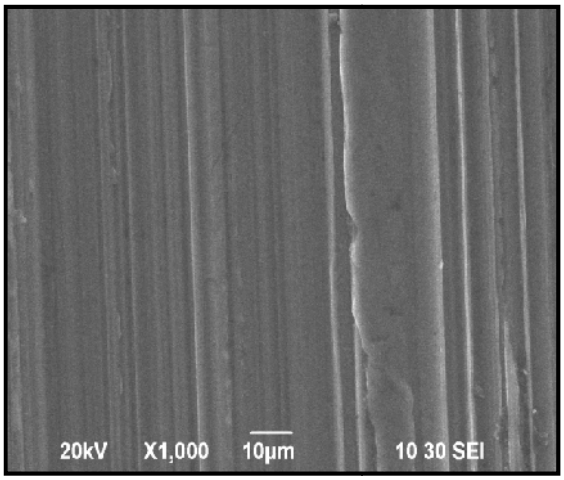

a. Plain AA1100

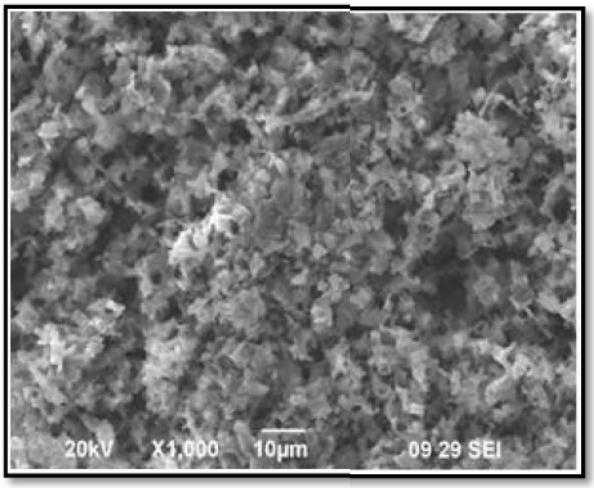

b. AA1100 in 1M HCl

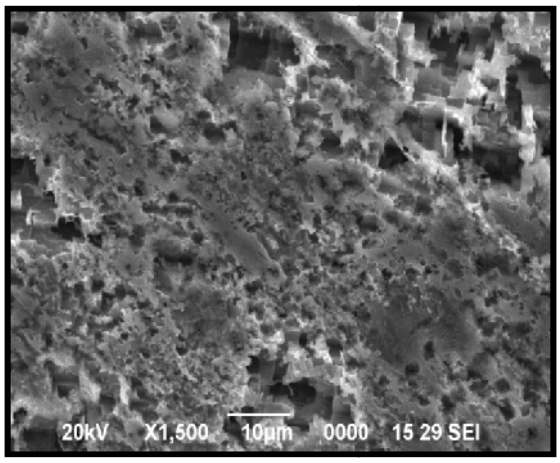

c. AA1100 /SCL/ 1M HCl

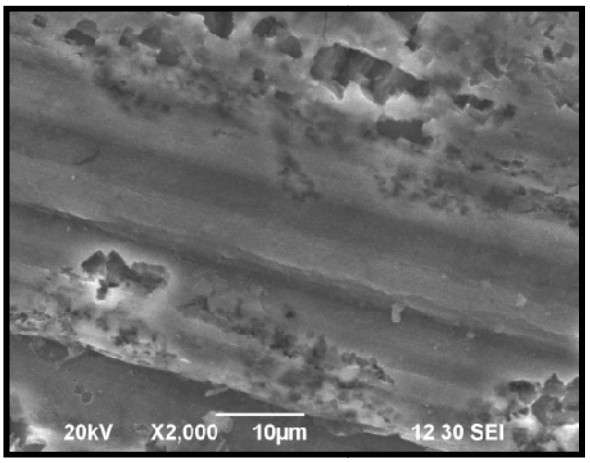

d. AA1100 /SCF / 1M HCl

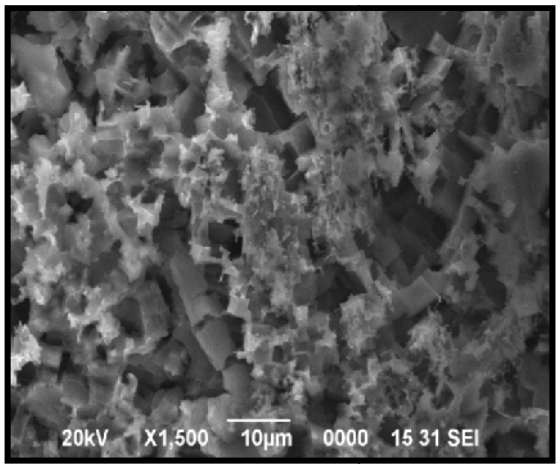

e. AA1100 /TCL/ 1M HCl

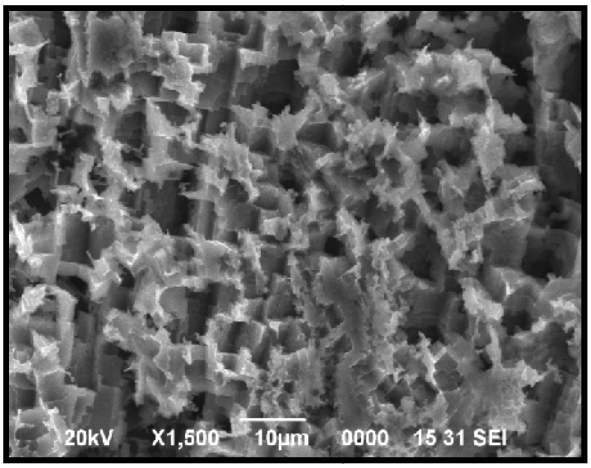

f. AA1100 /TCF/ 1M HCl

Figure 4.36 : SEM images of AA1100 corrosion in absence and presence of (c) SCL (d) SCF (e) TCL (f) TCF in 1M HCl

4.7.3.3 Scanning electron microscopy of AA1100 in the presence of SCL/ SCF Extract in 1M HCl

SEM micrographs obtained for AA1100 surface immersed in 1M HCl solution at room temperature for 3h immersion in the absence and presence of 0.7% concentration of SCL / SCF extracts are shown in Figure 4.36 c and d. It can be seen from Figure. 4.36 a that the plain AA1100 samples are smooth and some abrading scratches on the surface are noticed. After immersion in uninhibited 1.0 M HCl solution for 3 h, the AA1100 surface appears coarse and uneven due to the aggressive attack of the corroding medium. Furthermore, the corrosion products are very uneven and exhibits cube-shaped morphology, and the surface layer is rather rough (Figure 4.36 b). On the contrary, Figure. 4.36 c, d depicts that the inhibited metal surface is smoother than the uninhibited surface indicating a protective layer of adsorbed inhibitor that ultimately aids in preventing acid attack. **(Li *et al*, 2012)**

4.7.3.4 Scanning electron microscopy of AA1100 in the presence of TCL/TCF Extract in 1M HCl

The surface morphology of the AA1100 samples in 1M HCl solution in the absence and in the presence of TCL/TCF are depicted in Figure 4.36 b, e,f . The badly damaged surface obtained when the metal is kept immersed in 1M HCl solution for 3 h without inhibitor indicates significant corrosion (Figure 4.36 b). However, in the presence of 0.7% TCL/TCF (Figure 4.36 e, f), the surface improves markedly in terms of smoothness, indicating a considerable reduction of the corrosion rate. This improvement in surface morphology is due to the formation of a good protective film of inhibitor on the metal surface, which is responsible for the inhibition of corrosion. **(Mahendra yadav, 2013).**

4.7.4 Energy dispersive X-ray analysis (EDX)

4.7.4.1 EDX of SCL / SCF / TCL / TCF / MS / 1M HCl

Figure 4.37 represents the EDX profile analysis and percentage of atomic content in MS samples, respectively. The characteristic peaks of the elements constituting the MS in absence and presence of 0.7% optimum concentration of SCL / SCF / TCL / TCF extracts are displayed in tables along with the EDX Figures (Figures 4.37 a -f)

The analysis infers that the characteristic peaks of elements constituting polished MS samples comprises of major Fe peaks with Mn, Si & P as minor constituents. The presence of Si may be attributed to the mechanical abrasion of the MS surface prior to the experiment.

a.Plain MS

Element	Wt %	At %
Si	0.35	0.69
P	0.10	0.18
Mn	2.38	2.41
Fe	97.17	96.72

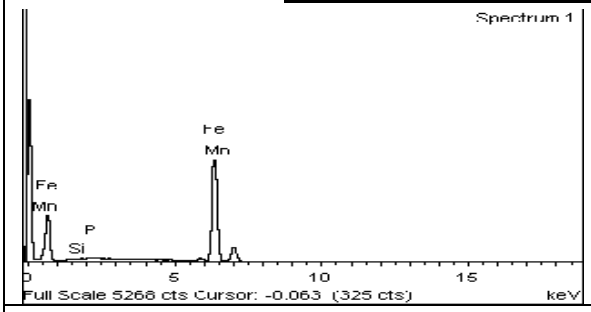

b.Blank HCl

Element	Wt %	At %
O	9.89	27.70
Fe	90.11	72.30

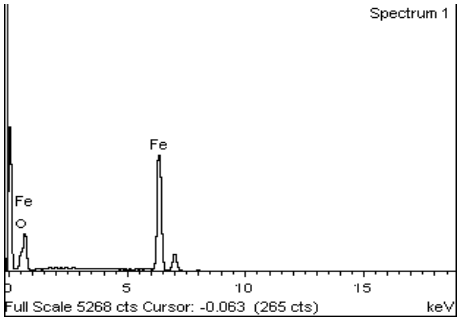

c. MS /SCL/ 1M HCl

Element	Wt %	At %
O	1.79	1.36
S	0.20	0.30
Fe	86.9	64.6

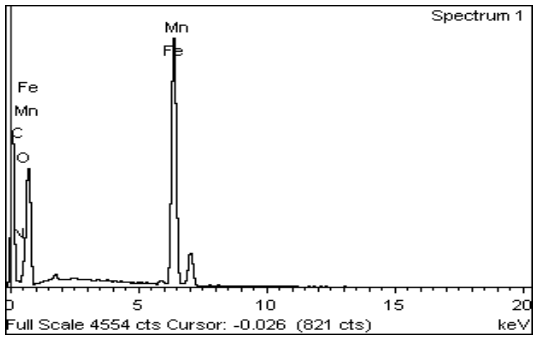

d. MS /SCF / 1M HCl

Element	Wt %	At %
O	4.47	13.27
S	0.02	0.03
Fe	91.17	77.52

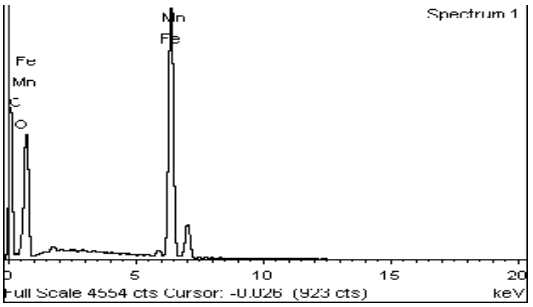

e. MS /TCL/ 1M HCl

Element	Wt %	At %
O	9.86	27.63
S	0.34	0.32
Fe	90.09	72.3

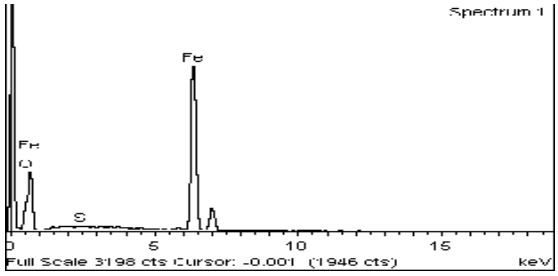

f. MS /TCF/ 1M HCl

Element	Wt %	At %
O	5.14	12.84
S	0.05	0.08
Fe	85.3	61.05

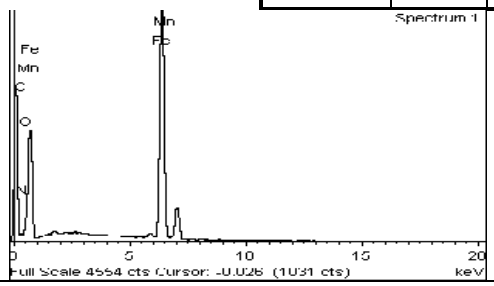

Figure 4.37: EDX images of MS corrosion in absence and presence of (c) SCL (d) SCF (e) TCL (f) TCF in 1M HCl

For MS in the presence of 1M HCl the EDX analysis reported 9.89% Fe & 90.11% Oxygen (in weight %). The detection of small peak characterizing oxygen is detected due to the formation of iron oxide layer due to the immersion of MS in 1M HCl medium. The low content of Fe when compared to the iron content in plain MS surface and the absence of Mn and the presence of high oxygen concentration indicates that the MS surface is completely covered with a thick layer of corrosion product**. (Sherif *et al,* 2011***)***

The EDX patterns in the presence of SCL / SCF / TCL / TCF gives an additional peak due to presence of S. The presence of S peaks in the EDX patterns of inhibitors on the surface indicates that the inhibitor is adsorbed on the MS surface, preventing it from being corroded. **(Quraishi *et al*, 2014)**

4.7.4.2 EDX of SCL / SCF / TCL / TCF/ AA1100 / 1M HCl

EDX survey spectra are used to determine which elements are present on the Al surface before and after exposure to the inhibitor solution. After AA1100 is immersed in 1M HCl solution in the absence and presence of 0.7% SCL / SCF / TCL / TCF for 3 hours , its surface film composition is determined by EDX. The results are displayed in Figure 4.38 a-f. For the electrode without inhibitor treatment (1M HCl) Al and oxygen are detected which indicates the presence of Aluminium oxide.Traces of S are also noticed. However, in inhibited solutions (Figures 4.38 c-f), the EDX spectra shows an additional line characteristic for the existence of C (due to the carbon atoms of the inhibitor). In addition, the O and N signal is significantly enhanced (due to the oxygen atoms present in the inhibitor). These data show that a carbonaceous material containing oxygen and nitrogen atoms covers the electrode surface. This layer is undoubtedly due to the inhibitor, because the carbon signal and the high contribution of the oxygen and nitrogen signal are not present on the electrode surface exposed to uninhibited solutions (4.38 b).

It is obvious from the spectra of Figure 4.38 c-f that the Al peaks are dramatically suppressed relative to the samples prepared in the inhibitor solution. The suppression of Al undoubtedly occurs because of the overlying inhibitor film. These results confirm the results obtained from polarisation measurements that the inhibitor surface film retards the cathodic hydrogen evolution reaction and inhibits the anodic dissolution of aluminium. These results support the results obtained from chemical and electrochemical measurements **(Amin *et al*, 2009)**

a.Plain AA1100

Element	Wt %	At %
Si	1.26	1.20
P	0.10	0.18
Mn	2.38	2.41
Al	97.87	97.34

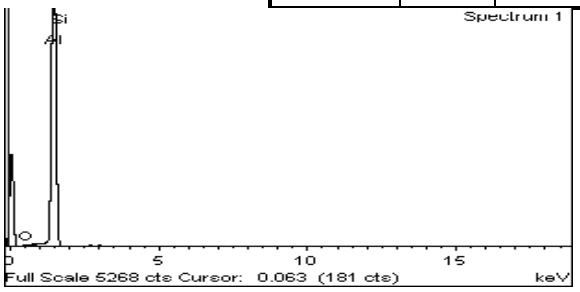

b.Blank HCl

Element	Wt %	At %
O	18.21	27.30
Al	81.68	72.62
S	0.11	0.09

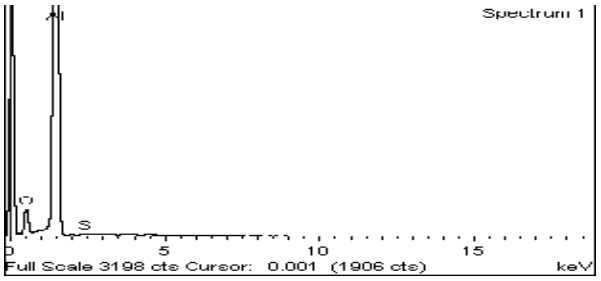

c. AA1100 /SCL/ 1M HCl

Element	Wt %	At %
O	7.20	9.94
S	0.20	0.30
Al	77.68	63.5

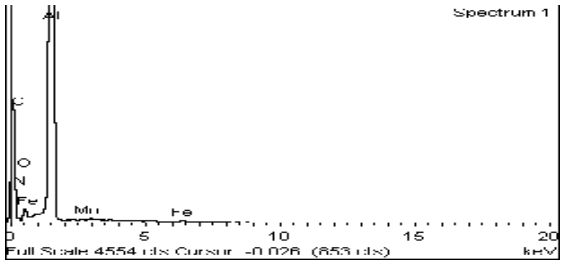

d. AA1100 /SCF / 1M HCl

Element	Wt %	At %
O	5.57	7.82
S	0.02	0.03
Al	80.14	66.74

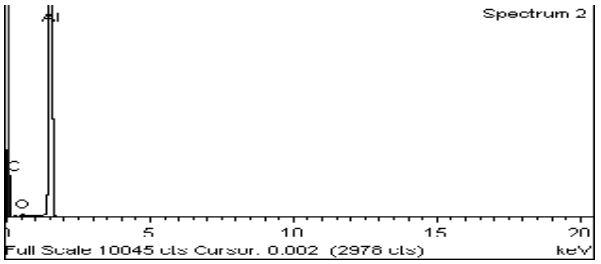

e. AA1100 /TCL/ 1M HCl

Element	Wt %	At %
O	8.04	11.17
N	0.34	0.32
Al	86.17	75.23

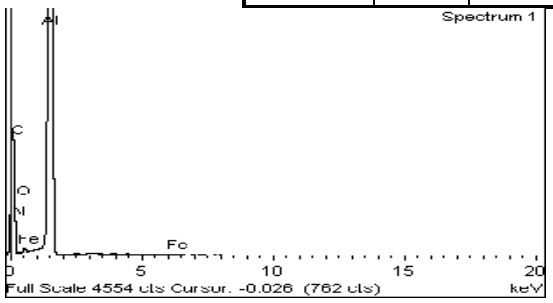

f. AA1100 /TCF/ 1M HCl

Element	Wt %	At %
O	11.97	16.6
S	0.05	0.08
Al	76	

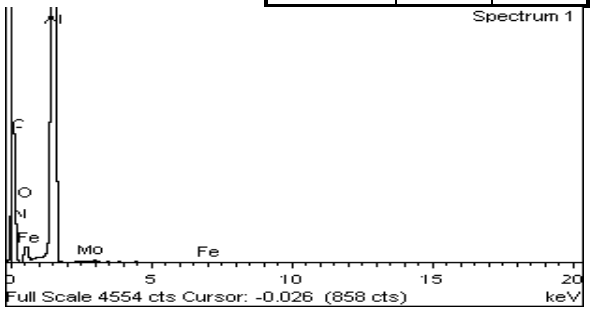

Figure 4.38 : EDX images of AA1100 corrosion in absence and presence of (c)SCL (d) SCF (e) TCL (f) TCF in 1M HCl

4.7.5 X-ray diffraction Analysis (XRD)

XRD is the method of choice for the analysis of corrosion products as it is only analysis that readily provides information about quantitative phase analysis (**Kamimura *et al*, 2002**) based on measuring the intensity of diffraction units in the pattern. In the case of MS corrosion, XRD will reveal the composition of iron oxides (magnetite, goethite and ferrihychite) while other methods will only reveal that corrosion product is iron based. The set of'd' spacing that represent the finger print of the substance can be calculate by 2θ values.

i) XRD of MS / 1M HCl / SCL / SCF / TCL / TCF

The XRD spectrum of MS in absence and presence of investigated inhibitors is depicted in the Figure 4.39 a. XRD pattern of MS immersed in corrodent solution (1M HCl) shows peaks at 45.5, 45.6 suggesting the presence of iron. The peak at 65.7 can be assigned to oxides of iron. Thus it may be observed that the surface of metal immersed in 1M HCl solution contains of Fe_3O_4 and FeOOH. (**Ramesh *et al,* 2003**). It is quite evident that peak at 45.5 is the most important product as indicated by the peak at 2θ of 45.5. This line is finger print of Fe with a maximum relative intensity.

The grazing angles XRD of the specimens immersed in the tested extracts are presented in Figure 4.39 a. This indicates the amorphous layer of surface film which is expected to be the adsorption of Fe- complex on to the surface of MS. The XRD patterns of inhibited surface shows a smooth pattern with very small peaks of iron oxide as compared with the spectral data of MS immersed in 1M HCl solution.

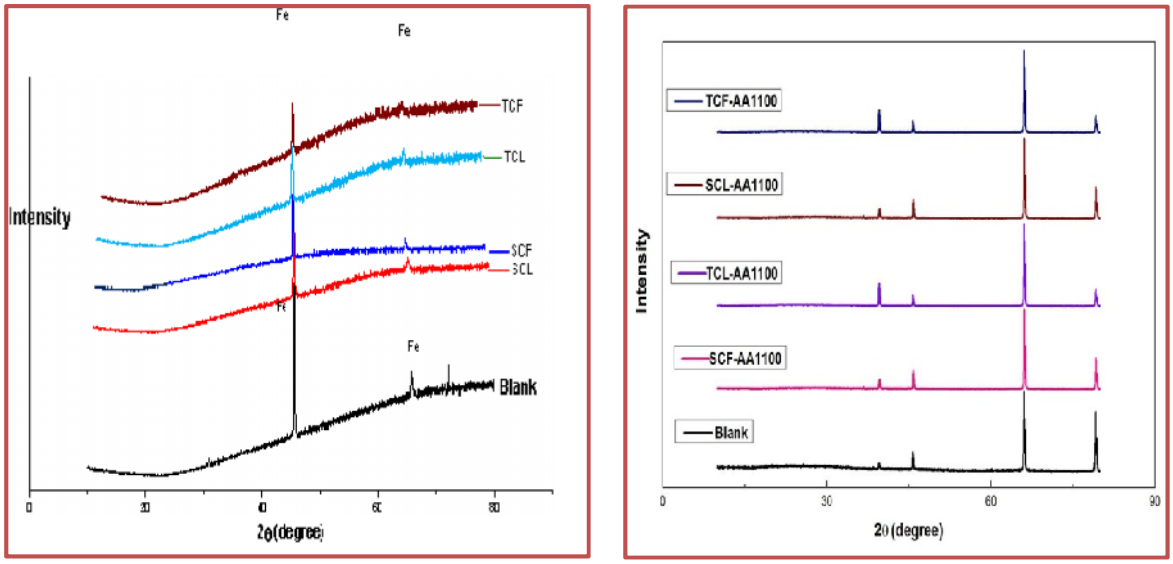

Figure 4.39: XRD spectrum of a) MS b) AA1100 corrosion in presence and absence of investigated inhibitors in 1M HCl

ii) XRD of AA1100 / 1M HCl / SCL / SCF / TCL / TCF

Figure 4.39 shows the XRD pattern of AA1100 in absence and presence of investigated inhibitors. XRD pattern of AA1100 immersed in 1M HCl revealed the several peaks associated with Al and Al_2O_3. **Khan *et al*, 2013** reported the XRD patterns of alumina and stated that the emergence of two diffraction peaks at 2θ values of 38.82° and 45.2° respectively can be correlated to Al_2O_3 H2O (111) and Al $(OH)_3$ (214) phases. **Qiang *et al*, 2014** analysed the XRD patterns of and reported 2θ values of 36.01° and 39.22° corresponding to (200) and (222) planes of aluminium oxide. In the present investigation, the XRD patterns of AA1100 in the absence and presence of investigated inhibitors could represent the occurrence of two diffraction peaks at 2θ values of 38.2

Analysing the reports given by **Khan *et al*, 2013** and **Qiang *et al*, 2014** the following conclusions can be drawn. The XRD patterns obtained in our investigation are on par with the literature reports. The XRD patterns of inhibited surface shows a smooth pattern with very small peaks of aluminium oxide as compared with the spectral data of AA1100 immersed in 1M HCl solution. Similar results were noticed in EDAX analysis also.

4.7.6 3D Optical profilometry:

It is a powerful tool to investigate the surface morphology of various samples at nano-micro scale that is currently used to study the influence of corrosion inhibitors on metal/solution interface. From the analysis, insight can be gained regarding the roughness & uniformity of the surface.

The roughness profile values play an important role in identifying / deciding the efficiency of the inhibitors under study.

4.7.6.1 Laser Profilometry of MS /AA1100/ 1 M HCl / SCL / SCF / TCL / TCF

Among the various parameters discussed R_a takes a pivotal role in providing explanation about the nature of the adsorbed film on the metal surface. Figure 4.40 shows the 3D images as well as elevation profiles of polished MS/AA1100 and MS/AA1100 in 1M HCl. Figure 40 and 41 (c),(d),(e) show that the 3D images as well as elevation profiles of MS/AA1100 / 1M HCl in the presence of investigated inhibitors.

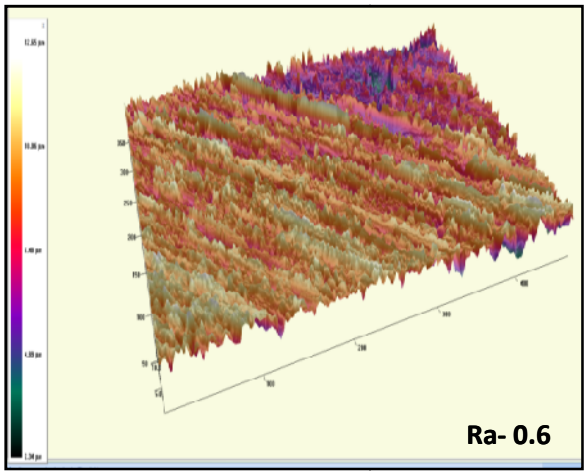

a. Plain Mild steel

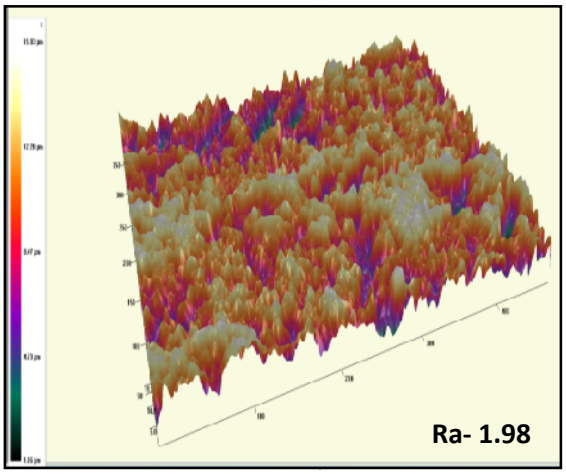

b. Blank HCl

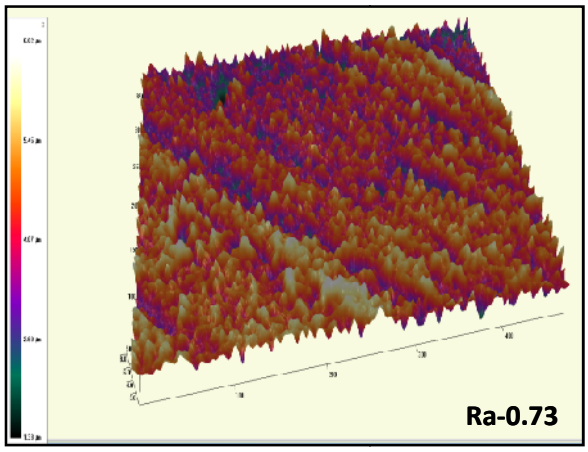

c. Mild steel /SCL/ 1M HCl

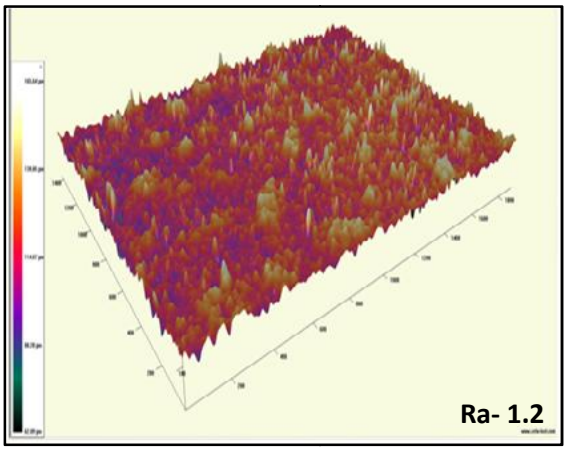

d. Mild steel /SCF/ 1M HCl

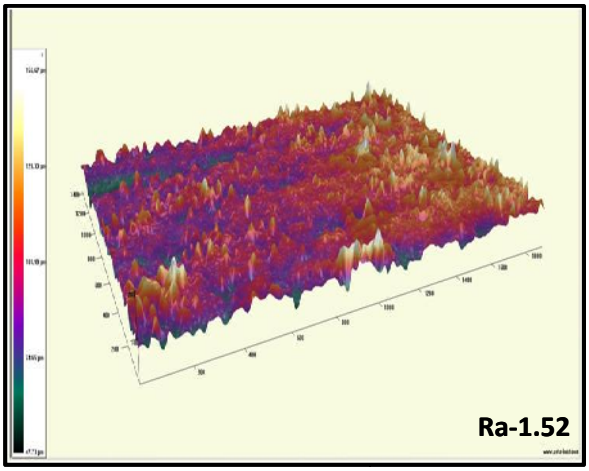

e. Mild steel /TCL/ 1M HCl

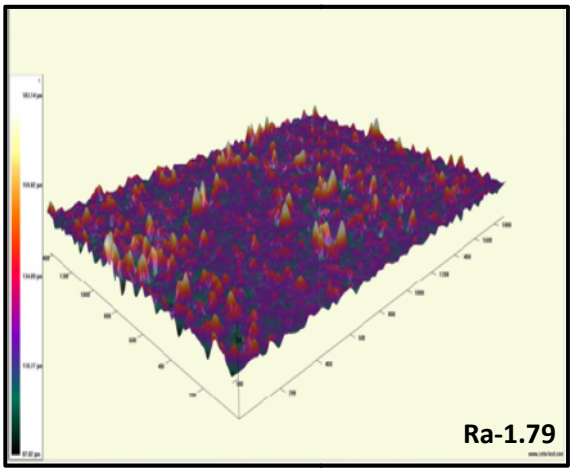

f. Mild steel /TCF/ 1M HCl

Figure 4.40: 3D Optical Profiler images of MS in absence and presence of (c) SCL (d) SCF (e) TCL (f) TCF in 1M HCl

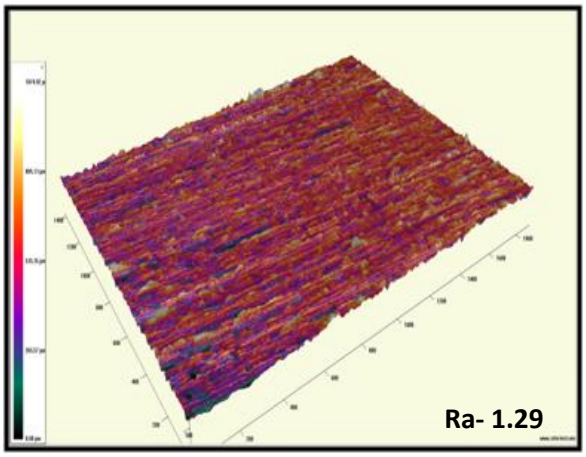

a. Plain AA1100

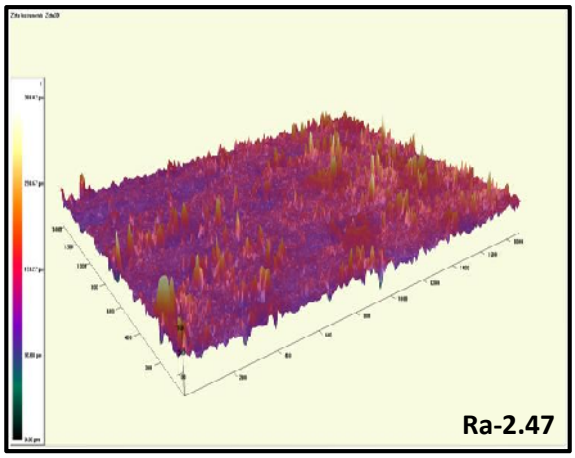

b. Blank HCl

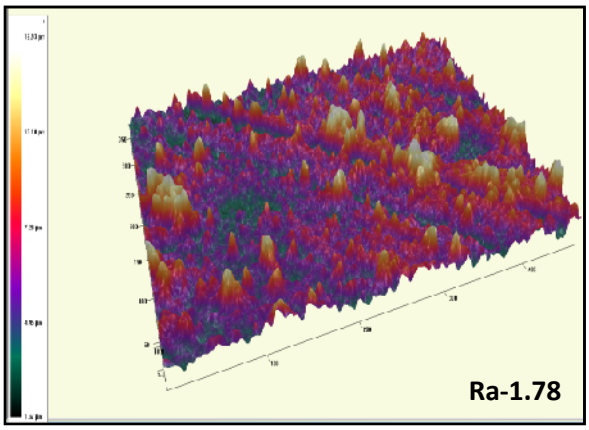

c. AA1100 /SCL/ 1M HCl

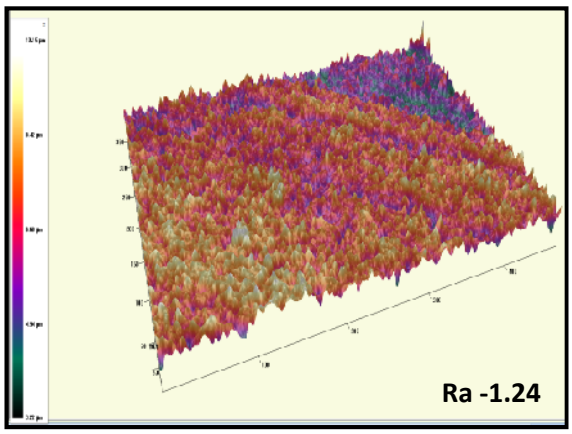

d. AA1100 /SCF/ 1M HCl

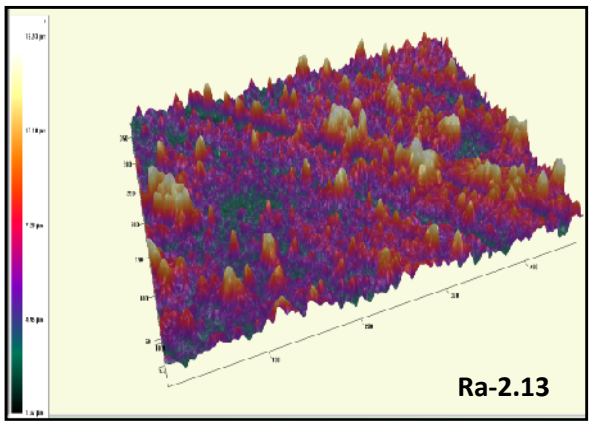

e. AA1100/TCL/ 1M HCl

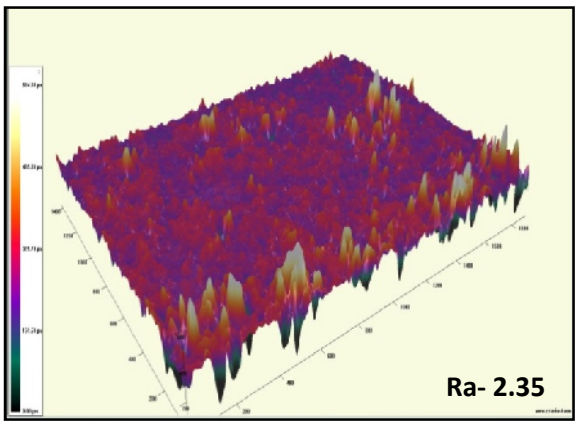

f. AA1100 /TCF/ 1M HCl

Figure 4.41: 3D Optical Profiler images of AA1100 in absence and presence of (c) SCL (d) SCF (e) TCL (f) TCF in 1M HCl

As observed in Figure 4.40 b and 4.41 b the surface of MS/AA1100 electrode exposed to corrodent solution has a considerably porous structure with large and deep pores. Figure 4.40, 4.41 c, d, e, f reveal that there is wrapping zonal film adsorbed on MS/AA1100 surface. In accordance, it can be concluded that the adsorption film can efficiently protect the MS/AA1100 from corrosion. It should be noted that laser profiler has examined only the microstructure; we focus on only the comparison of the MS/AA1100 surface corrosion before and after addition of the inhibitor. Some limitations of this study are that it could not provide the chemical composition of adsorption film (**Li *et al,* 2012**).

Analysis of the values indicate that, higher the distance, higher the values of roughness parameter reached. The mean roughness R_a is found to be 1.980 for the blank acid solution. Visualizing the Figure 4.40 ,4.41 c – f , it can be observed that the R_a of MS immersed in 1M HCl in the presence of 0.7% of inhibitors vary from 0.73 to 1.79 as compared to blank solution. Similarly in the case of AA1100, the R_a value is found to be 2.47 in 1M HCl but in the presence of inhibitors, it can be noted that the values are lower than that of the blank value of 2.47 .The decrease in the R_a value reflects the adsorption of inhibitor molecules on MS / AA1100 surface thereby reducing the corrosion rate.

In the case of MS in 1M HCl, SCL exhibits excellent behaviour in corrosion inhibition process and SCF is found to inhibit corrosion of AA1100 more effectively than the rest of the investigated inhibitors. The efficient behaviour of SCF is remarkably noticed from the R_a value. Precisely the same relationship can be noticed in mass loss method and electrochemical measurements also. This proves that SCF extract has highest efficiency among the investigated inhibitors. The same trend is substantiated by mass loss as well as SEM-EDX analysis.

Module III Quantum Chemical Studies

4.8 QUANTUM CHEMICAL CALCULATION

Theoretical explorations are proposed as a powerful tool for probing the inhibitor/surface interaction and predicting a number of molecular parameters directly related to the corrosion inhibiting property of any chemical compound **(Khaled and Hackerman, 2003; Bouayed *et al,* 1999; Kutej *et al,* 1995)**.

Frontier orbital theory is useful in predicting adsorption centers of the inhibitor molecules responsible for the interaction with surface metal atom **(Fang and Li, 2002)**. Moreover, the gap between the LUMO and HOMO energy levels of the molecules is another important factor that should be considered. It has been reported that excellent

corrosion inhibitors are usually those organic compounds that not only offer electrons to unoccupied orbital of the metal, but also accept free electrons from the metal **(Zhao *et al*, 2005)**; **(Martinez and Stagljar, 2003); (Obi-Egbedi, *et al*, 2010).**

In spite of the noted difficulties associated with precisely evaluating the individual contributions of the different constituents of SCL/SCF/TCL/TCF extract to the corrosion mitigating ability, it is nonetheless possible to identify, from molecular structure considerations, the likely contributions of individual organic entities of the extracts by taking advantage of recent advances in density functional theory-based computer simulations. The following constituents of SCL / SCF / TCL / TCF extracts namely **Tecomoside, Cornoside, Phytol, Kaempferol, Quercetin, Caffeic acid, Luteolin, Apigenin** are selected for the computational study in order to reflect how the molecules contribute to the ability of SCL / SCF / TCL / TCF extract to hinder MS / AA1100 corrosion **(Oguzie *et al*, 2014)**

Table 4.49 shows the values of some quantum chemical parameters, namely the energy of the highest occupied molecular orbital (E_{HOMO}), energy of the lowest unoccupied molecular orbital (E_{LUMO}), the energy gap (E_{LUMO}-E_{HOMO}), the total electronic energy of the molecules (EE), dipole moment (μ). The quantum chemical parameters are computed for 2 different Hamiltonians, namely, parametric method 3 (PM3), Austin model 1 (AM1) .Optimised structures of selected phytochemicals, HOMO and LUMO obtained using PM3 and AM1 are pictorially presented in Figures 4.42-4.48.The results obtained from semi empirical computations, are presented in Table 4.49

4.8.1 Frontier Orbitals

It is well established in the literature that the higher the HOMO energy of the inhibitor, the greater the trend of offering electrons to unoccupied orbital of the metal, and the higher the corrosion inhibition efficiency. In addition, the lower the LUMO energy, the easier the acceptance of electrons from metal surface; as the LUMO–HOMO energy gap decreases the efficiency of inhibitor improves.

Figures 4.42-4.48 show the optimized geometry, the HOMO density distribution, the LUMO density distribution and the Mulliken charge population analysis plots for the selected phytoconstituents of SCL / SCF / TCL / TCF with PM3 and AM1 The regions of highest electron density (HOMO) are the sites at which electrophiles attack and represent the active centers, with the utmost ability to bond to the metal surface, whereas the LUMO

orbital can accept the electrons in the orbital of the metal using antibonding orbitals to form feedback bonds . Therefore, high values of the E_{HOMO} indicate an increased tendency of the inhibitor to donate electron to the metal. Similarly, E_{LUMO} represents the ability of the molecule to accept electrons. Finally, the HOMO orbitals of the selected plant is located on the three six-membered rings containing OH groups and a C=O group. Similarly, the LUMO orbitals show the same behaviour for all the molecules studied as the HOMO orbitals. These active sites ensure strong interaction of each molecule with the metal surface. The separation energy, $\Delta E = (E_{LUMO}-E_{HOMO})$ is a parameter which determines the reactivity of a molecule towards a metallic surface and is a very important stability index. As ΔE decreases, the reactivity of the molecule increases leading to increase adsorption on the metal surface. The calculations from Table 4.49 shows the following increasing reactivity abilities of the molecules towards MS / AA1100

4.8.2 Global Descriptors

4.8.2.1: Global Softness and Hardness

The general rule as suggested by HSAB principle is that hard acids prefer to co-ordinate to hard bases and soft acids prefer to co-ordinate to soft bases. Metal atoms are known as soft acids.

As expected, there are some similarities in the trends between the quantum chemical parameters and frontier orbital molecular energies. The global softness σ for the phytochemicals is the same, suggesting that softer molecules are stronger inhibitors. Calculated values of σ and η are also presented in Table -4.50. For the easiest transfer of electrons, adsorption should occur at the part of the molecule where the softness σ, which is a local property, has the highest value **(Martinez, 2002)**.

Hard molecules have a high HOMO-LUMO gap and soft molecules have a small HOMO-LUMO gap .Thus, soft bases (organic heterocyclic molecules) are most effective for metal interactions. Analysis of the values in Table 4.50 infers that hardness of the molecules increases in the following order: Kaempferol < Quercetin < Tecomoside < Caffeic acid < Luteolin < Cornoside < Apigenin while softness which is the inverse of hardness has the opposite effect. The trend shows Apigenin is the least reactive of the compounds studied while Kaempferol is the most reactive towards MS / AA1100 surface.

Table – 4.49 Quantum chemical parameters for the selected phytoconstituents using semiempirical approach PM3 and AM1

Selected phyto constituents	Model	Total energy (Kcal/mol)	E_{HOMO} (eV)	E_{LUMO} (eV)	Change in energy - ΔE (eV)	Dipole Moment- μ (Debye)
Kaempferol	PM3	-82679.44	-8.531	-2.195	-6.336	4.147
	AM1	-89480.99	-8.704	-2.478	-6.226	3.931
Quercetin	PM3	91924.85	-8.6878	-1.0863	-7.6015	2.7777
	AM1	99163.58	-8.7086	-1.0650	-7.6436	3.007
Caffeic acid	PM3	-54521.69	-9.0513	-0.8898	-8.1615	3.062
	AM1	-58668.90	-9.0483	-0.8372	-8.2111	3.012
Tecomoside	PM3	-63936.68	-9.036871	-1.2427	-7.794	6.259
	AM1	-68920.67	-8.987648	-1.097268	-7.89	6.426
Cornoside	PM3	106711.6	-10.2975	-0.6907	-9.6068	1.595
	AM1	-99427.3046	-10.32682	-1.2095	-9.1175	1.348
Luteolin	PM3	-85153.55	-9.0652	-1.0572	-8.008	3.474
	AM1	-91772.95	-9.0976	-0.9659	-8.1317	3.016
Apigenin	PM3	78378.45	-9.1873	-0.8478	-8.3395	3.546
	AM1	84380.21	-9.1554	-0.8882	-8.2672	3.489

4.8.2.2 Ionization Potential and Electron Affinity

Values of IP and EA calculated are presented in Table 4.50. From the table it can be noticed that IP is directly related with the E_{HOMO} (Equation 3.22), while EA is related to the E_{LUMO} (Equation 3.23). High volume of IP and low volume of EA, (Table 4.50) favour the inhibiting potential of selected phytoconstituents which in turn highlight the efficiency of the investigated plant extracts.

4.8.3. Electron transfer processes

To obtain a clear picture of the interaction between the molecules studied and MS/ AA1100 surface, intermolecular parameters such as a charge transfer descriptors and the associated energy change should be taken into account. Corrosion inhibition of MS / AA 1100 by organic inhibitors (present in plant extract) in acidic media is a complex process and is mainly influenced by charge transport.

Electrophilicity (ω) is an index which measures the propensity of chemical species to accept electrons. The higher the value of ω, the higher the capacity of the molecule to accept electrons. Thus, a good nucleophile is characterized by low values of μ and ω; whereas a good electrophile is characterized by high values of μ and ω. It is clear in Table 4.50, that the molecules have low electrophilicity index values and are good nucleophiles. The amount of charge transfer, ΔN, between the molecules and the MS /AA1100 surface as calculated are given in Table 4.50. A positive value of ΔN indicates that the molecules act as an electron acceptor, while a negative value of ΔN indicates that the molecules act as electron donors. Thus, from the table, it can be seen that all the molecules studied act as electron acceptors except Quercetin which acts as electron donor. According to Lukovits, if ΔN < 3.6, the molecules can be assumed to posses charge transfer ability towards the metal surface. The molecules studied possess charge transfer abilities towards MS / AA1100.

The energy change (ΔE) associated with the charge transfer process were all negative and exothermic indicating a favourable transfer of charge process from the organic molecules onto steel surface **(Umoren, 2014)**

4.8.4 Mulliken charges:

The use of Mulliken charges to estimate the adsorption centers of inhibitors has beenwidely reported and it ismostly used for the calculation of the charge distribution over the whole skeleton of the molecule and thus aid in estimating the adsorption centres of inhibitors **(Obot *et al*, 2010)**. Appendix II depicts Mulliken atomic charges calculated for the studied molecules. It is inferred that the more negative the atomic charges of the adsorbed centre, the more easily the atom donates its electrons to the unoccupied orbital of the metal. The values presented in Appendix II show that the oxygen atoms have high charge densities, implying that the most probable reactive site for the adsorption is located on the oxygen atoms .These atoms having negative charge could offer electrons to the MS/AA 1100 surface to form a coordinate-type of bond. **(Khaled, 2010)**

Analyzing the quantum chemical parameters obtained the inhibition process can be explained as follows:

In a corrosion system containing inhibitor, the inhibitor and the metal act as a lewis base and a lewis and, respectively, therefore the frontier orbital theory may be used to determine possible modes of interaction between the inhibitor and metal **(Sastri, 1997).**

Table – 4.50 Derived Quantum chemical parameters for the selected phytoconstituents using semiempirical approach PM3 and AM1

Selected Phyto constituents	Model	IP (eV)	EA (eV)	η (eV)	σ (eV)	χ (eV)	ω	ΔN(Fe)	ΔN(Al)
Kaempferol	PM3	8.53	2.2	3.168	0.1578	5.36	2.71	0.2581	-0.3369
	AM1	8.70	2.48	3.113	0.1606	5.59	2.48	0.2263	-0.3791
Quercetin	PM3	8.69	1.09	3.8008	0.1316	8.69	1.015	-0.2234	-0.2347
	AM1	8.71	1.07	3.8218	0.1308	4.89	1.18	0.2765	-0.2168
Luteolin	PM3	9.07	1.06	4.004	0.1249	5.06	1.51	0.2421	-.0.2287
	AM1	9.09	0.97	4.0659	0.1230	5.032	1.12	0.2420	-0.2216
Apigenin	PM3	9.19	0.85	4.1698	0.1199	5.018	1.51	0.2377	-0.2144
	AM1	9.16	0.89	4.1336	0.1210	5.018	1.47	0.2398	-0.2175
Caffeic acid	PM3	9.05	0.89	4.0808	0.1225	4.971	1.15	0.2487	-0.2133
	AM1	9.05	0.84	4.1056	0.1218	4.943	1.10	0.2505	-0.2086
Tecomoside	PM3	9.04	1.24	3.897	0.1283	5.14	0.64	0.2386	-0.2451
	AM1	8.99	1.1	3.945	0.1267	5.042	5.24	0.2482	-0.2297
Cornoside	PM3	10.3	0.69	4.8034	0.1041	5.494	0.26	0.1568	-0.2357
	AM1	10.33	1.21	4.5588	0.1097	5.77	0.2	0.1351	-0.2784

If bulk metal and the inhibitor molecule are brought together, the flow of electrons will occur from the molecule of lower electronegativity to the metal that has higher electronegativity until the value of the chemical potential becomes equal

The stability of the adsorption bond may further be related to the pearson's HSAB principle **(Pearson, 1988)**. Bulk metals are soft acids, thus soft base inhibitors are most effective for metals corroding in acid solutions. **Klopman, 1968** relates the hard-hard at soft-soft bond character, respectively, to electrostatic (charge controlled) and covalent (Frontier controlled) reactions. In case of the soft-soft inhibitor-metal interaction, the bond is largely covalent in character and is accomplished by a favorable overlap of the frontier orbitals, i.e. HOMO and LUMO. The results obtained by the above analysis (Table – 4.50) imply the possibility of soft-soft interaction between metal acting as a soft acid and inhibitor acting as a soft base in the investigated system as described by **Martinez, *et al.,* 2003.**

Frontier orbital theory may also be used to predict the adsorption centers of the inhibitor molecules. For the easiest transfer of electron, adsorption should occur at the part of the molecule where the softness σ, which is a local property, has the highest value. Characterization of SC /TC reveals the presence of many phytochemical constituents (Table 4.50). The adsorption centers in the present system are found to be $–OCH_3$, -OH and phenyl ring.

Figures 4.42 -4.48 : Optimised structures and Frontier molecular orbital distribution of selected phytochemicals

FIGURE NO	OPTIMISED STRUCTURE OF KAEMPFEROL	FRONTIER MOLECULAR ORBITAL DISTRIBUTION - HOMO	FRONTIER MOLECULAR ORBITAL DISTRIBUTION - LUMO
4.42 a	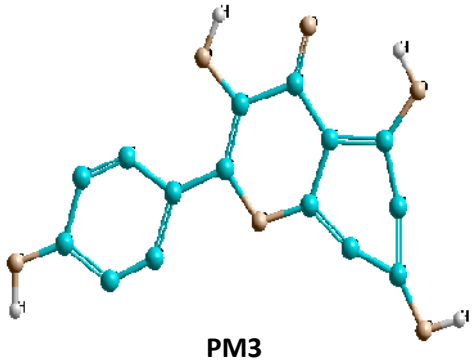 PM3	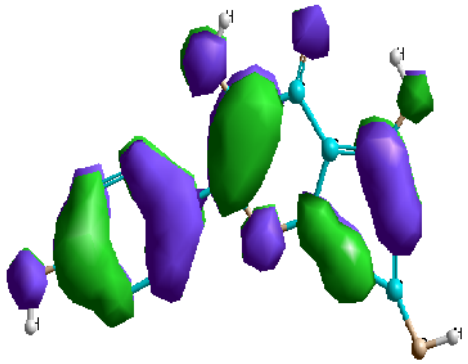	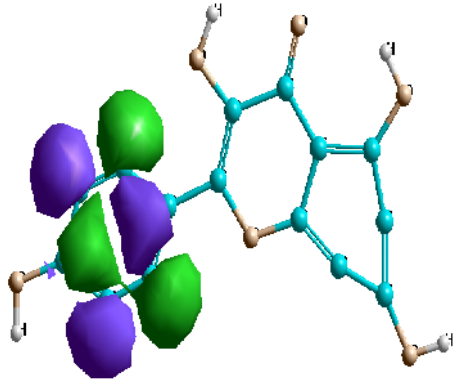
4.42 b	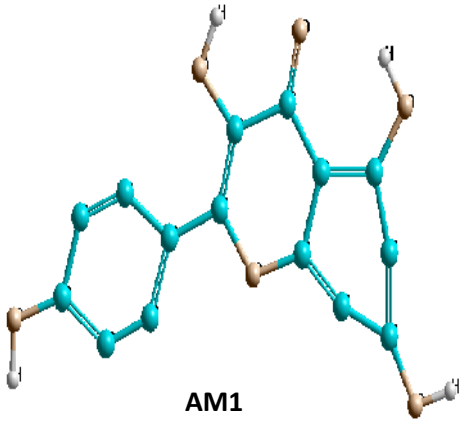 AM1	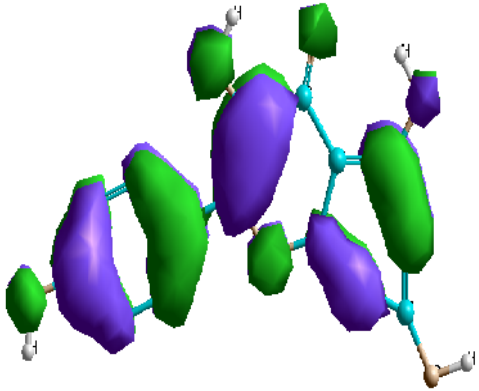	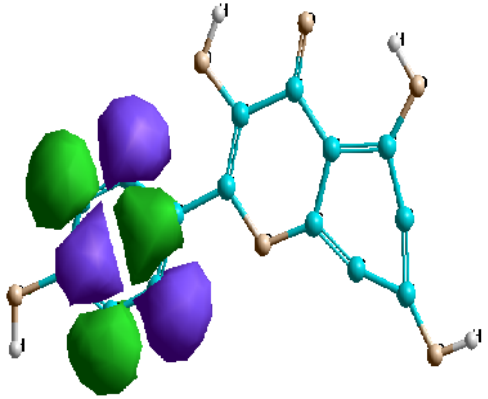

FIGURE NO	OPTIMISED STRUCTURE OF APIGENIN	FRONTIER MOLECULAR ORBITAL DISTRIBUTION - HOMO	FRONTIER MOLECULAR ORBITAL DISTRIBUTION - LUMO
4.43 a	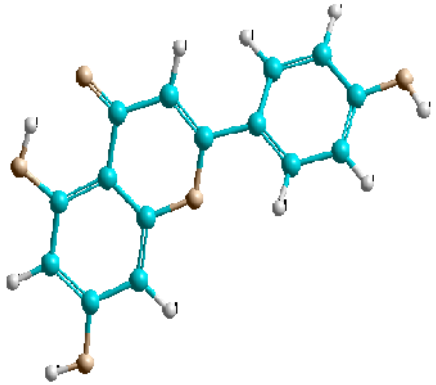 PM3	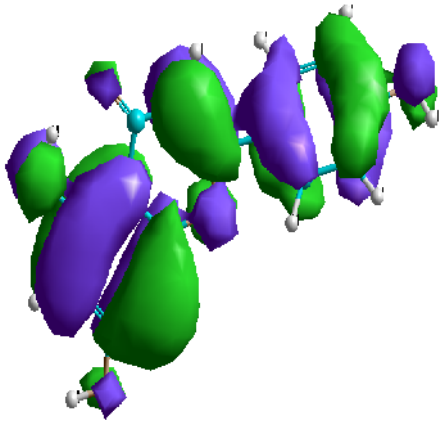	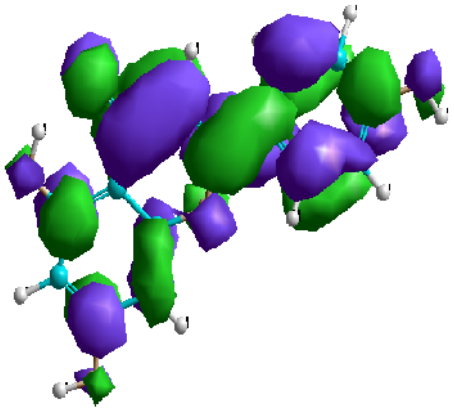
4.43 b	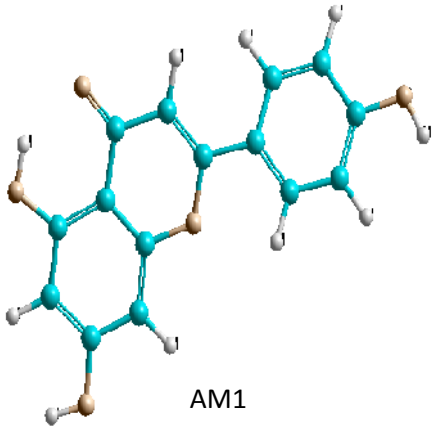 AM1	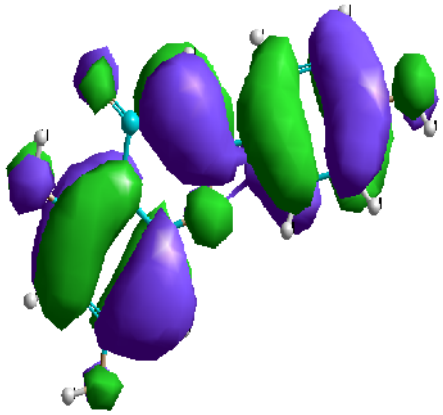	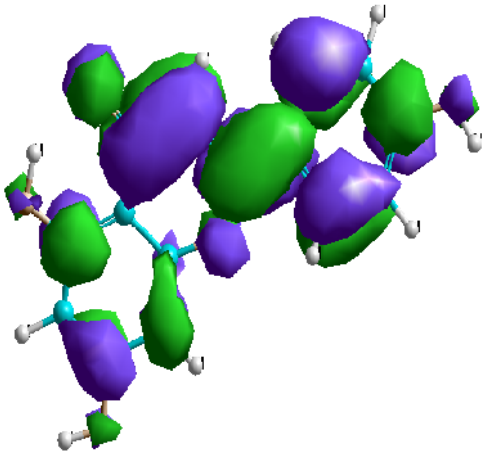

FIGURENO	OPTIMISED STRUCTURES OF LUTEOLIN	FRONTIER MOLECULAR ORBITAL DISTRIBUTION - HOMO	FRONTIER MOLECULAR ORBITAL DISTRIBUTION - LUMO
4.44 a	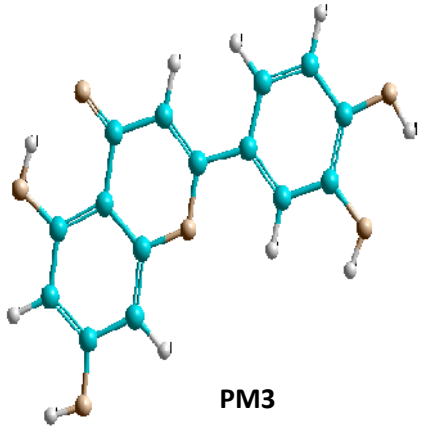 PM3	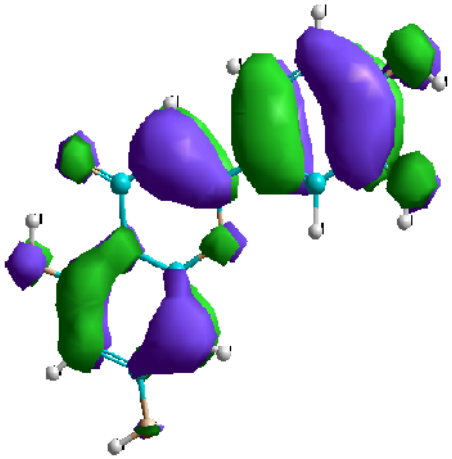	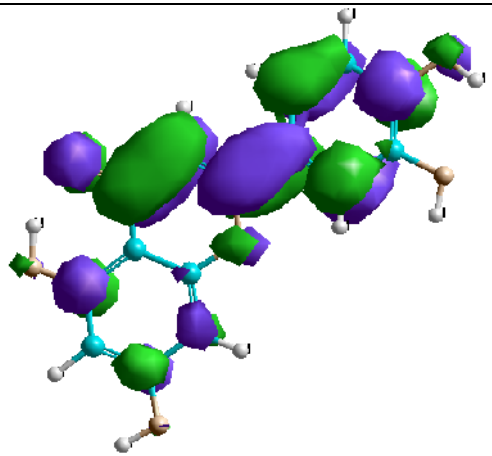
4.44 b	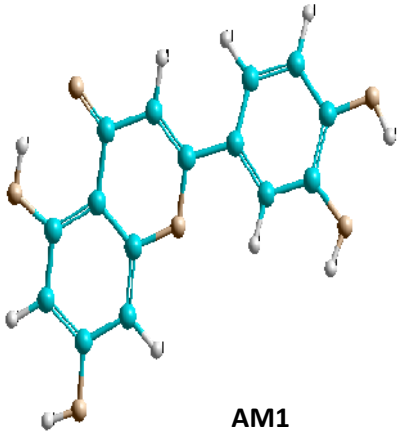 AM1	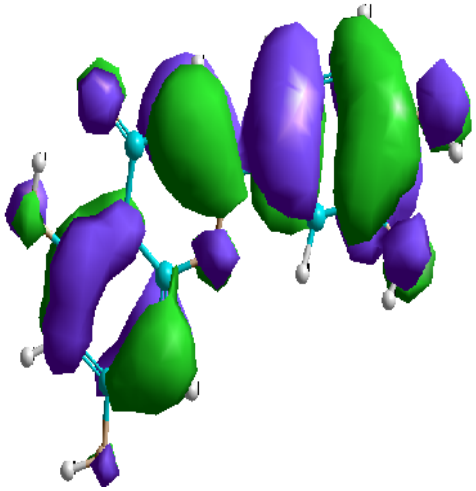	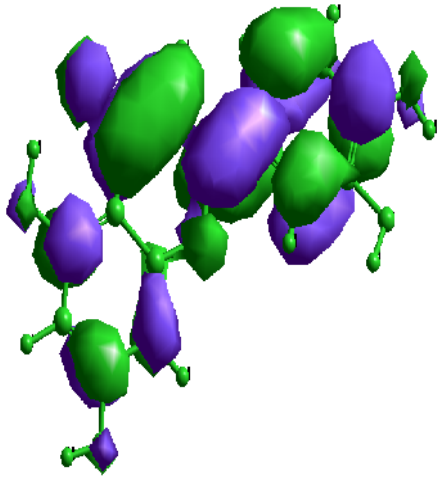

FIGURE NO	OPTIMISED STRUCTURES OF QUERCETIN	FRONTIER MOLECULAR ORBITAL DISTRIBUTION - HOMO	FRONTIER MOLECULAR ORBITAL DISTRIBUTION - LUMO
4.45 a	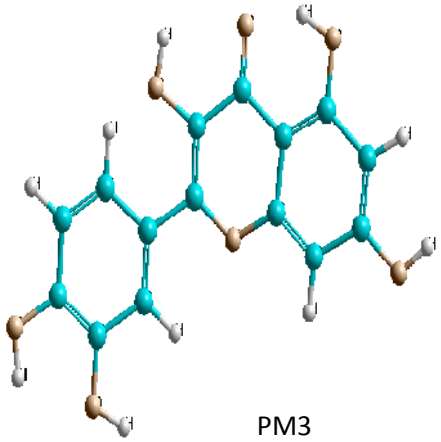 PM3	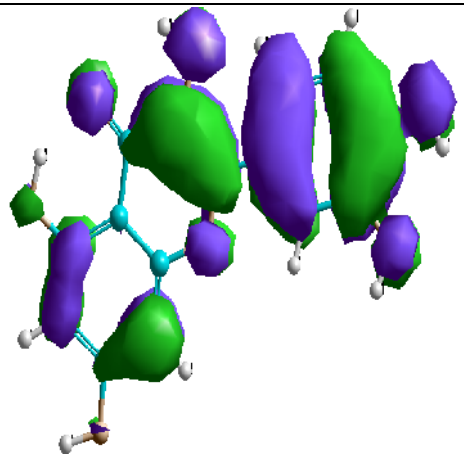	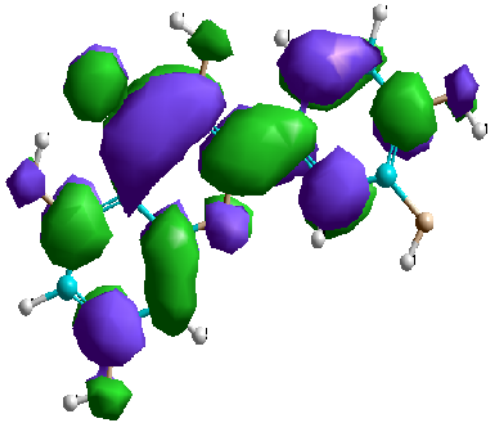
4.45 b	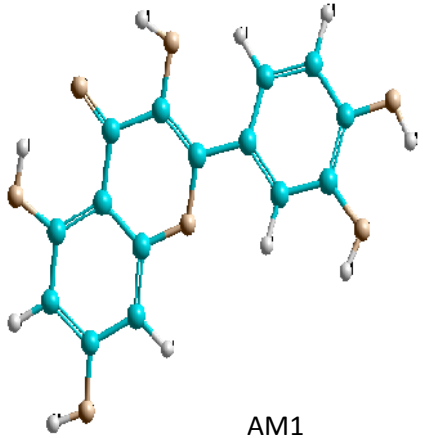 AM1	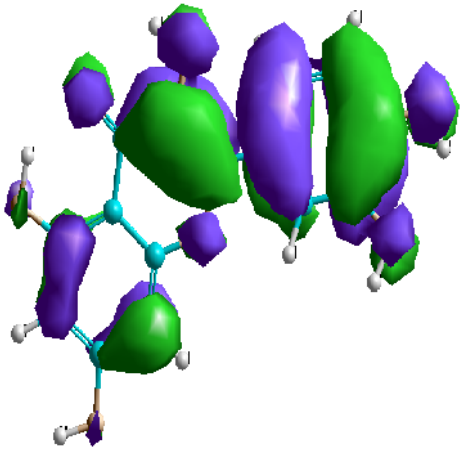	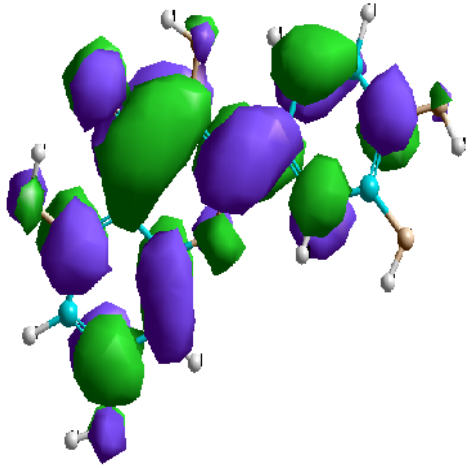

FIGURE NO	OPTIMISED STRUCTURES OF TECOMOSIDE	FRONTIER MOLECULAR ORBITAL DISTRIBUTION - HOMO	FRONTIER MOLECULAR ORBITAL DISTRIBUTION - LUMO
4.46 a	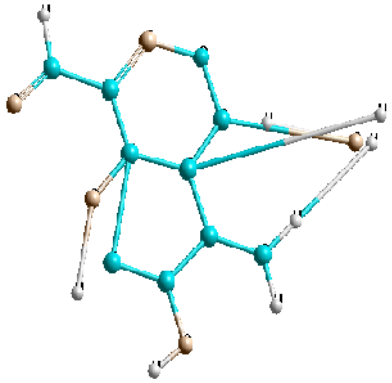 PM3	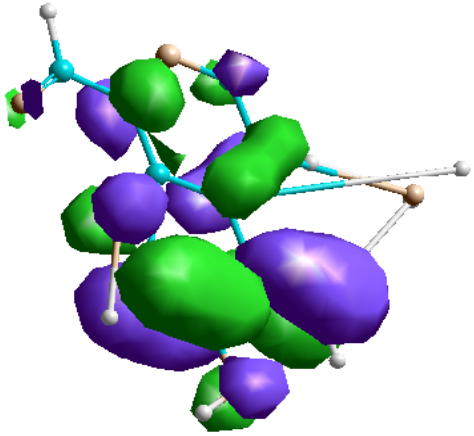	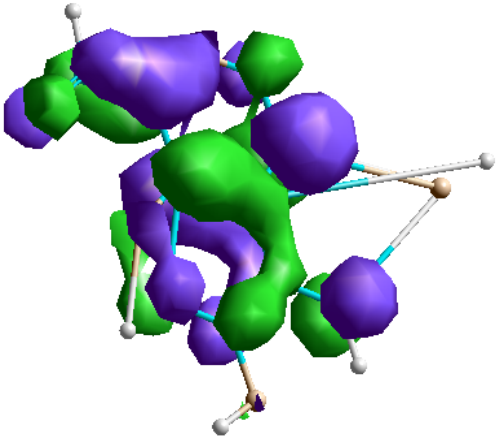
4.46 b	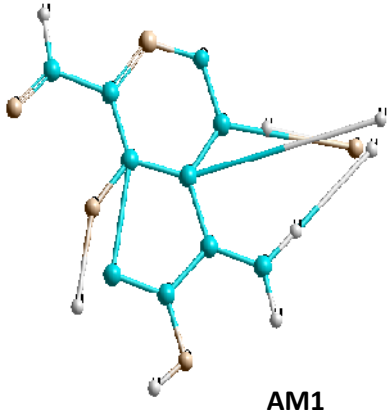 AM1	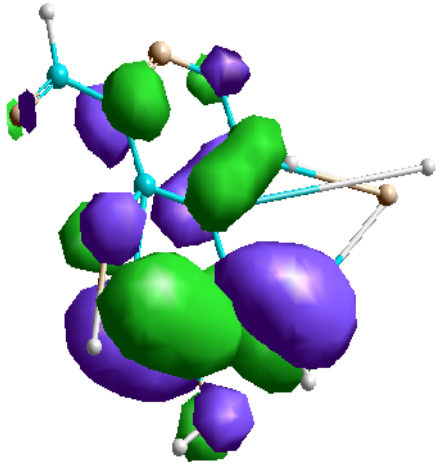	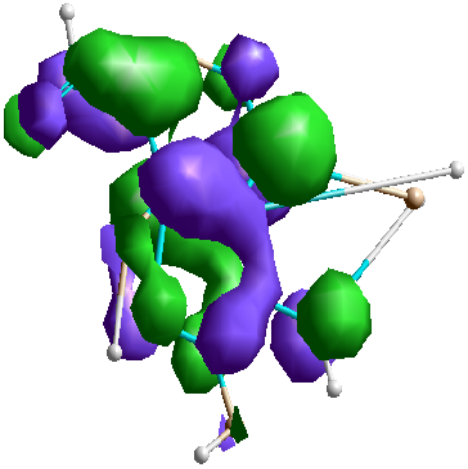

FIGURE NO	OPTIMISED STRUCTURES OF CAFFEIC ACID	FRONTIER MOLECULAR ORBITAL DISTRIBUTION - HOMO	FRONTIER MOLECULAR ORBITAL DISTRIBUTION - LUMO
4.47 a	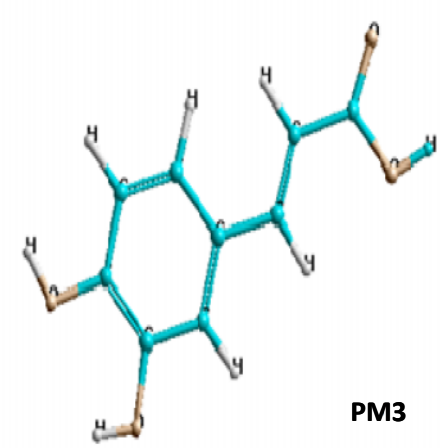 PM3	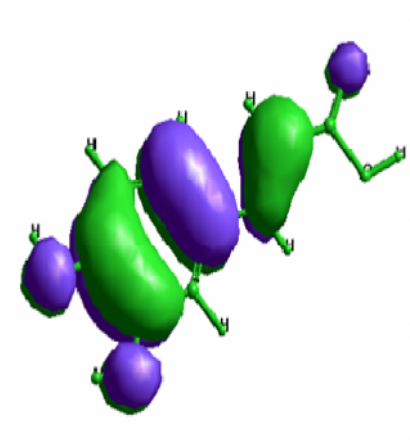	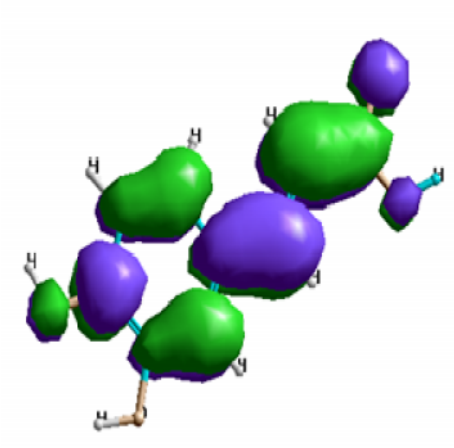
4.47 b	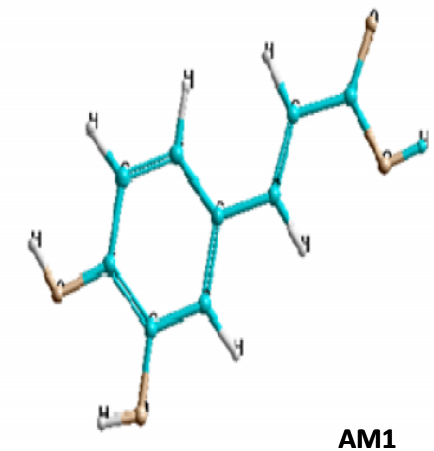 AM1	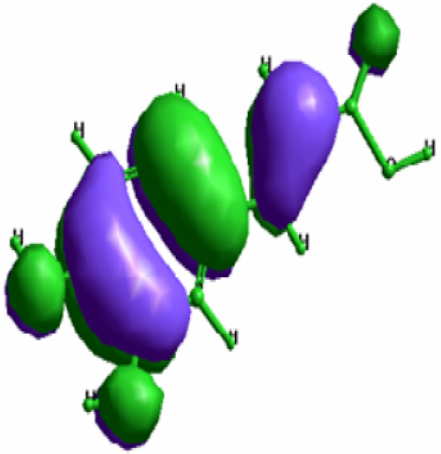	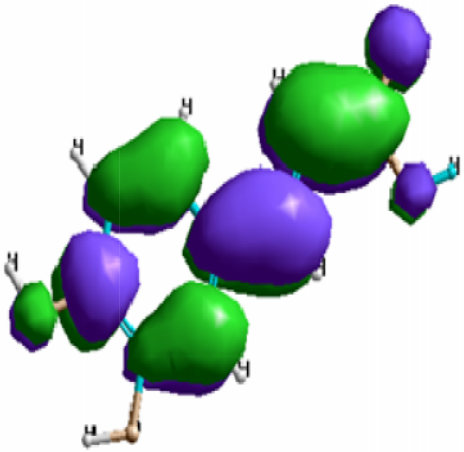

FIGURE NO	OPTIMISED STRUCTURES OF CORNOSIDE	FRONTIER MOLECULAR ORBITAL DISTRIBUTION - HOMO	FRONTIER MOLECULAR ORBITAL DISTRIBUTION - LUMO
4.48 a	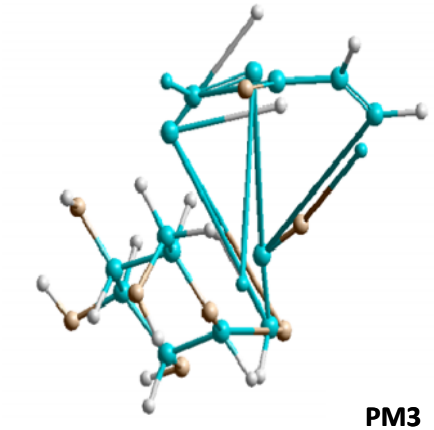 PM3	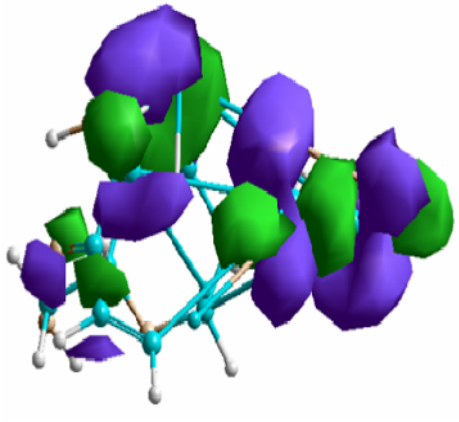	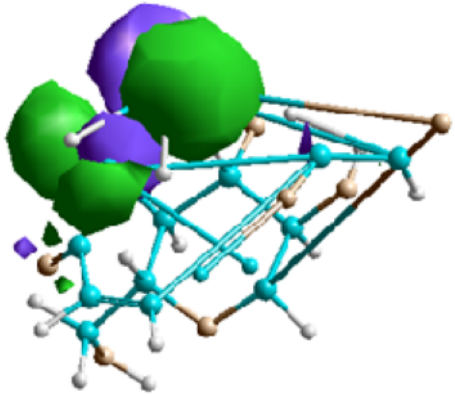
4.48 b	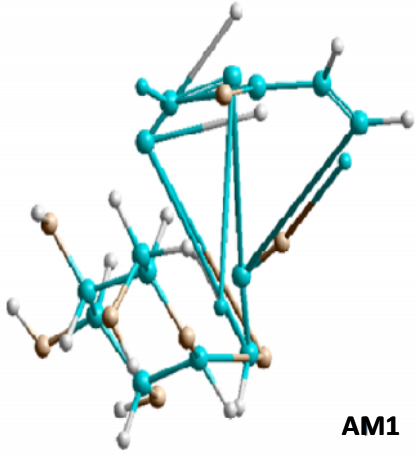 AM1	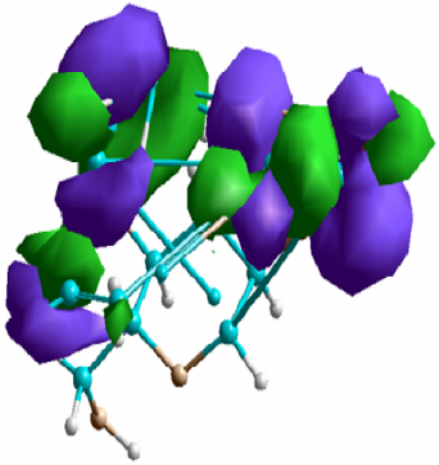	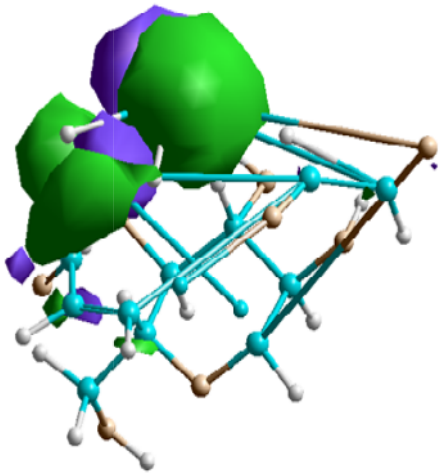

Quantum chemical studies are conducted for the main constituents present in the investigated extracts. Hence it is reasonable to assume that the higher mass fraction of SC and TC extract, not included in the present analyses would contain even more polar compounds and more complicated geometric structures. Thus the suggested adsorption mechanism would also apply to this fraction of extract **(Martinez *et al.,* 2003).**

4.9. Mechanism of inhibition process

The transition of metal/solution interface from a state of active dissolution to the passive state is attributed to the adsorption of the inhibitor molecules at the metal /solution interface forming a protective film. The rate of adsorption is usually rapid; hence, the reactive metal surface is shielded from the aggressive environment. **(Ritchie *et al*, 1999)**

Mechanism of the inhibition process for studied inhibitors can be discussed on the basis of the experimental findings - mass loss, electrochemical measurements, surface analytical techniques and theoretical studies on quantum chemical calculation using HyperChem 7.5.

In the present investigation, corrosion inhibition of MS / AA1100 in 1M HCl using SCL / SCF / TCL / TCF extracts could furnish the following results:

- All the investigated SCL / SCF / TCL / TCF extracts obey Langmuir adsorption isotherm indicating that the SCL / SCF / TCL / TCF extracts are of adsorptive type.
- The negative values of ΔG°_{ads} could confirm that the adsorption process is not merely physical adsorption or chemical adsorption but a mixed adsorption.
- Values of cathodic and anodic Tafel constant confirm that the investigated SCL / SCF / TCL / TCF extracts under study act as mixed type of inhibitors.
- Surface analytical techniques confirm the inhibitive nature of the plant extracts
- The quantum chemical computations of parameters associated with the electronic structures of specific components of the extract confirm their inhibiting potentials.
- Analyzing the optimized geometry and frontier molecular orbital density distribution of main phytochemical constituents, it is clear that the phenyl ring being plane thus helps in the interaction of C=O and -OH with the metal surface.. When the frontier molecules are analyzed, the HOMO are localized over the

oxygen, -OCH_3, -OH, C=O and the phenyl ring, consequently this is the preferred zone of the molecular interaction with the metal surface. Both the -OCH_3 and -OH can coordinate with MS / AA1100.

Based on the above facts the mechanism for corrosion inhibition for MS /AA1100 may be discussed as follows

4.9.1 PROPOSED MECHANISM FOR MILD STEEL /1M HCl / INHIBITORS

The mechanism of inhibitive action can be different, depending on metal, the medium and the structure of the inhibitor. Generally, two modes of adsorption are considered on the metal surface in acid media. In one mode, the neutral molecules may be adsorbed on the surface of MS through the chemisorption mechanism, involving the displacement of water molecules from the MS surface and the sharing of electrons between the hetero atoms and iron. The inhibitor molecules can also adsorb on the MS surface on the basis of donor-acceptor interactions between π-electrons of the aromatic ring and vacant d-orbitals of surface iron atoms.

In second mode, since it is well known that the MS surface bears positive charge in acid solution **(Mu *et al,* 1996)**, it is difficult for the protonated molecules to approach the positively charged MS surface (H_3O^+/metal interface) due to the electrostatic repulsion. Since chloride ions have a smaller degree of hydration, they could bring excess negative charges in the vicinity of the interface and favour more adsorption of the positively charged inhibitor molecules, the protonated inhibitors adsorb through electrostatic interactions between the positively charged molecules and the negatively charged metal surface. Thus, there is a synergism between adsorbed Cl^- ions and protonated inhibitors.

In aqueous acidic solutions, main constituents exist either as neutral molecules or as protonated molecules (cations).The inhibitors may adsorb on the metal / acid solution interface by one and / or more of the following ways:

- Electrostatic interaction of protonated molecules with already adsorbed chloride ions,
- Donor-acceptor interactions between the π-electrons of aromatic ring and vacant d orbital of surface iron atoms,
- Interaction between unshared electron pairs of hetero atoms and vacant d-orbital of iron surface atoms.

The corrosion of MS in aqueous acidic solutions can be inhibited by the extract of SCL / SCF / TCL / TCF. It is often not possible to assign a single general mechanism of action to an inhibitor, because the mechanism may change with experimental conditions. Thus, the predominant mechanism of action of an inhibitor in acidic solutions may vary with factors such as concentration of the extracts, the nature of the anion of the acid, the presence of other species in the solution, the extent of reaction to form secondary inhibitors and the nature of the metal **(Shreir *et al,* 1994)**.

In the present situation two modes of adsorption could be considered:

i. The neutral SCL / SCF / TCL / TCF may adsorb onto the metal surface via the chemisorption mechanism, involving the displacement of water molecules from the metal surface and sharing electrons between the O atoms and Fe. The phytochemical constituents of the selected inhibitor can also adsorb on the metal surface on the basis of donor-acceptor interactions between π-electrons of aromatic ring and vacant d-orbitals of Fe.

$$Fe \longrightarrow Fe^{2+} + 2e^{-} \qquad \textbf{(4.26)}$$

$$[SCL/SCF/TCL/TCF] + Fe^{2+} \leftrightarrow [SCL/SCF/TCL/TCF\text{ -}Fe]^{2+} \qquad \textbf{(4.27)}$$

ii. The protonated SCL / SCF / TCL / TCF extracts may adsorb through electrostatic interactions between the positively charged molecules and the negatively charged metal surface. In other words, there may be a synergism between Cl^- and SCL / SCF / TCL / TCF extract, which improves the inhibitive capability of the inhibitor.

$$[SCL/SCF/TCL/TCF\ H_x]^{x+} + Fe^{2+} \leftrightarrow [SCL/SCF/TCL/TCF\text{ -}Fe]^{(2+x)+} \qquad \textbf{(4.28)}$$

$$[SCL/SCF/TCL/TCF] + Fe^{2+} \leftrightarrow [SCL/SCF/TCL/TCF\text{ -}Fe]^{2+} \qquad \textbf{(4.29)}$$

When protonated SCL / SCF / TCL / TCF extract is adsorbed on metal surface, a coordinate bond may be formed by partial transference of electrons from polar atoms (O atoms) to the metal surface. In addition, owing to lone-pair electrons of O atom in SCL / SCF / TCL / TCF extract or protonated extracts may combine with freshly generated Fe^{2+} ions on steel surface forming metal-inhibitor complexes.

Similar type of mechanism has also been proposed by Xiang-Hong **Li *et al,* (2010)**. These complexes might be adsorbed onto steel surface by vander Waals force to form a protective film to prevent mild steel from corrosion.

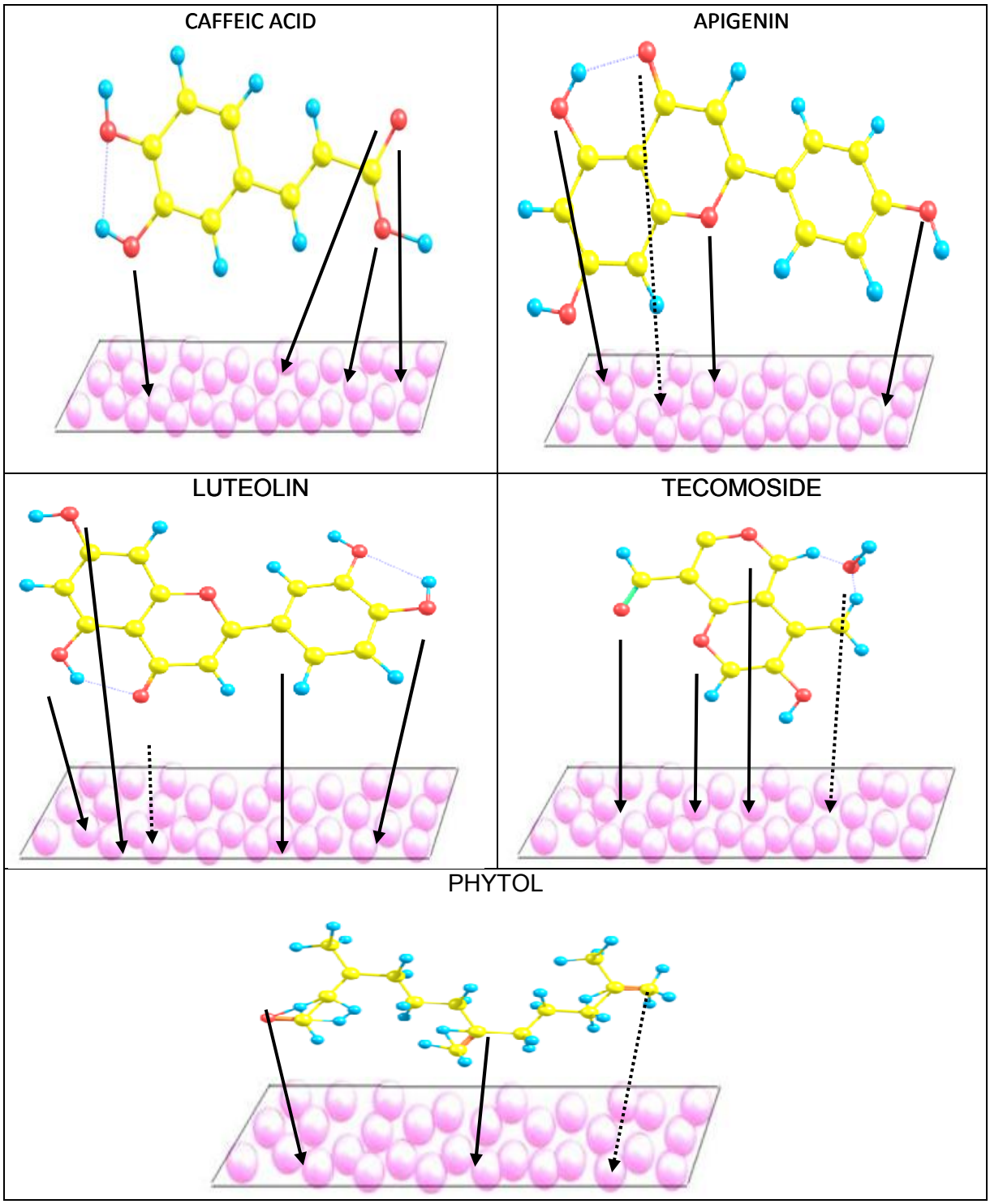

4.49 Schematic Illustration of Selected Phyto Constituents on MS Surface

LEGEND

- Charged Metal Surface
- Hydrogen atoms
- Carbon atoms
- Oxygen atoms

The main constituents of the SCL / SCF / TCL / TCF extracts are **Tecomoside, Cornoside, Phytol, Kaempferol, Quercetin, Caffeic acid, Luteolin, Apigenin** etc., Notable among them are depicted below. The effective performance of the inhibitor may also be due to the large size of the phytochemical constituents of the plant extract cover a wider area of the metal surface thus minimising the corrosion.

The inhibition efficiency afforded by selected phytoconstituents may be attributed to the presence of electron rich O and N atoms. The possible reaction centers are unshared electron pair of hetero-atoms and / or p -electrons of aromatic ring. Generally, phytoconstituents can adsorb on the MS surface on the basis of donor – acceptor interactions between π (pi) electrons of the O and aromatic ring and vacant d orbitals of surface iron. The schematic illustration of different modes of adsorption on metal is shown in Figure 4.49. Similar type of mechanism is also proposed by **Noor, 2007 and Emeka Oguzie, 2008b.**

4.9.2 PROPOSED MECHANISM FOR AA1100 /1M HCl / INHIBITORS

As discussed in standard adsorption free energy (ΔG^0), the adsorption is mainly the physical adsorption. In accordance, the following adsorption mechanisms are presented.

i) In acid solution, SCL / SCF / TCL / TCF could be protonated in the acid media due to the interaction between O atom and H^+. AA1100 surface is positively charged due to accumulation of Al- OH_2^+ species in acidic solution **(Brett *et al*, 1990)**. In HCl solution, Cl^- ions could accumulate gradually closely to the aluminum/solution interface, being specifically adsorbed; they create an excess negative charge toward the solution and favour more adsorption of the cations. Thus, the protonated SCL / SCF / TCL / TCF may adsorb through electrostatic interactions between the positively charged molecules and the negatively charged metal surface. In other words, there is a synergism between Cl^- and protonated inhibitor. **(Li *et al*, 2012)**

$$Al_{(s)} + H_2O \longleftrightarrow AlOH_{ads} + H^+ + e^- \quad \textbf{(4.30)}$$

$$AlOH_{ads} + 5\ H_2O + H^+ \longleftrightarrow Al^{3+}.6\ H_2O + 2\ e^- \quad \textbf{(4.31)}$$

$$Al^{3+} + H_2O \longleftrightarrow [AlOH]^{2+} + H^+ \quad \textbf{(4.32)}$$

$$[AlOH]^{2+} + X^- \longleftrightarrow [AlOHX]^+ \quad \textbf{(4.33)}$$

The controlling step in the metal dissolution is the complexation reaction between the hydrated cation and the anion present (Equation 4.32). In the presence of chloride ions the reaction will correspond to

$$[AlOH]^{2+} + Cl^- \longleftrightarrow [AlOHCl]^+ \quad \textbf{(4.34)}$$

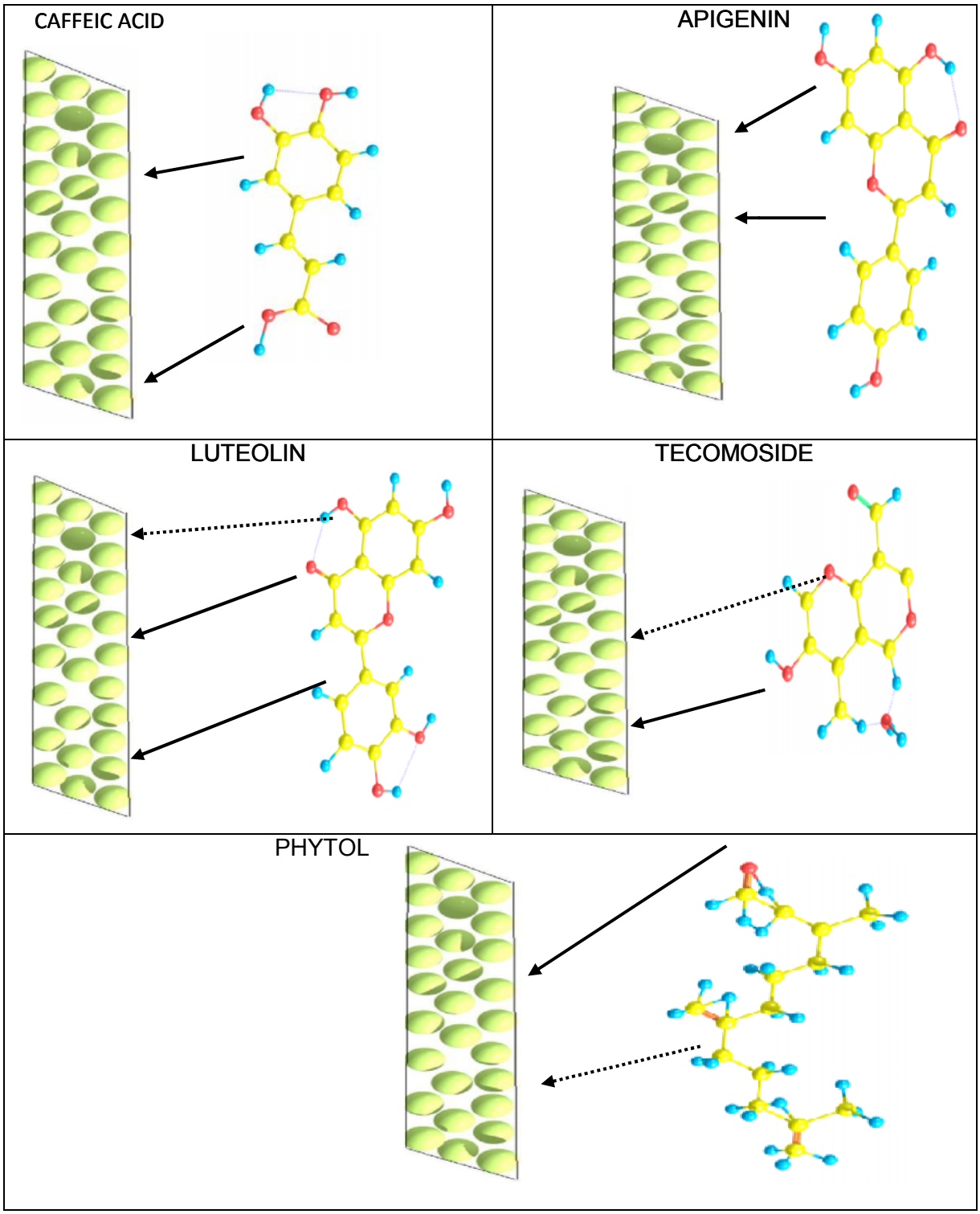

4.50 Schematic Illustration of Selected Phyto Constituents on AA1100 surface

LEGEND

- Charged Metal Surface
- Hydrogen atoms
- Carbon atoms
- Oxygen atoms

The soluble complex ion formed increases the metal dissolution rate which depends on the chloride concentration. In order to predict the adsorption mechanism of protonated SCL / SCF / TCL / TCF to positive charged AA1100 surface, corrosion mechanism of AA1100 in HCl must be known. According to this mechanism, anodic dissolution of Al follows the steps:

$$Al + Cl^- \longleftrightarrow AlCl^-_{ads} \quad \textbf{(4.35)}$$

$$AlCl^-_{ads} + Cl^- \longleftrightarrow AlCl^-_2 + 3e^- \quad \textbf{(4.36)}$$

The cathodic hydrogen evolution follows the steps:

$$H^+ + e^- \longrightarrow H_{ads} \quad \textbf{(4.37)}$$

$$H^+ + H_{ads} \longrightarrow H_2 \quad \textbf{(4.38)}$$

The protonated inhibitors electrostatically adsorb onto the anion covered AA1100 surface, through their protonated form. Thus the oxidation reaction in Equation 4.35 can be prevented. This phenomenon is attributable to the stabilisation of the adsorbed halides by the electrostatic interaction with the inhibitor molecules resulting in greater surface coverage. The protonated molecules also adsorb on the cathodic sites in competition with H^+ ions. Also the inhibitors can adsorb from the negatively charged O atoms and the pi bonds of the aromatic systems to positively charged AA1100 surface.